



HAL
open science

Preparation and characterization of bionanocomposites based on protein and cellulose nanocrystals by continuous casting

Liliane Samara Ferreira Leite

► **To cite this version:**

Liliane Samara Ferreira Leite. Preparation and characterization of bionanocomposites based on protein and cellulose nanocrystals by continuous casting. Materials Science [cond-mat.mtrl-sci]. Université Grenoble Alpes [2020-..]; Universidade federal de São Carlos, 2020. English. NNT : 2020GRALI063 . tel-03476470

HAL Id: tel-03476470

<https://theses.hal.science/tel-03476470>

Submitted on 13 Dec 2021

HAL is a multi-disciplinary open access archive for the deposit and dissemination of scientific research documents, whether they are published or not. The documents may come from teaching and research institutions in France or abroad, or from public or private research centers.

L'archive ouverte pluridisciplinaire **HAL**, est destinée au dépôt et à la diffusion de documents scientifiques de niveau recherche, publiés ou non, émanant des établissements d'enseignement et de recherche français ou étrangers, des laboratoires publics ou privés.



THÈSE

Pour obtenir le grade de

DOCTEUR DE L'UNIVERSITE GRENOBLE ALPES

**préparée dans le cadre d'une cotutelle entre la
Communauté Université Grenoble Alpes et
L'Université Fédérale de São Carlos**

Spécialité : **Matériaux, Mécanique, Génie Civil, Électrochimie et
Science et Ingénierie des Matériaux**

Arrêté ministériel : le 6 janvier 2005 – 25 mai 2016

Présentée par

Liliane Samara FERREIRA LEITE

Thèse dirigée par **Julien BRAS** et **Luiz Henrique Capparelli MATTOSO**
codirigée par **Francys Kley Vieira MOREIRA**

préparée au sein des **Laboratoire du Génie de Procédés Papetiers et
Département d'Ingénierie des Matériaux**

dans l'**École Doctorale IMEP-2 – Ingénierie, Matériaux, Mécanique,
Environnement, Énergétique, Procédés, Production**

Préparation et caractérisation de bionanocomposites à base de protéines et nanocristaux de cellulose par casting continue

Thèse soutenue publiquement le **11 décembre 2020**,
devant le jury composé de:

Pr, Naceur BELGACEM

Professeur à Grenoble INP, Président

Luiz Henrique Capparelli MATTOSO

Professeur à l'Université Fédérale de São Carlos, Directeur de thèse

Dr, Julien BRAS

Maître de Conférences à Grenoble INP, Directeur de thèse

Pr, Francys Kley Vieira MOREIRA

Professeur à l'Université Fédérale de São Carlos, Co-encadrant, Membre invité

Pr, Morsyleide de Freitas ROSA

Recherché à Embrapa Agroindústria Tropical, Rapporteur

Dr, Eric POLLET

Maître de Conférences à l'Université de Strasbourg, Rapporteur

Pr, Silvia Helena Prado BETTINI

Professeure à l'Université Fédérale de São Carlos, Examinatrice



**UNIVERSIDADE FEDERAL DE SÃO CARLOS
CENTRO DE CIÊNCIAS EXATAS E DE TECNOLOGIA
PROGRAMA DE PÓS-GRADUAÇÃO EM CIÊNCIA E
ENGENHARIA DE MATERIAIS**

**UNIVERSITE GRENOBLE ALPES - ÉCOLE DOCTORALE DE INGENIERIE -
MATERIAUX, MECANIQUE, ENVIRONNEMENT, ENERGETIQUE,
PROCEDES, PRODUCTION (IMEP2)**

**PREPARATION AND CHARACTERIZATION OF BIONANOCOMPOSITES
BASED ON PROTEIN AND CELLULOSE NANOCRYSTALS BY
CONTINUOUS CASTING**

Liliane Samara Ferreira Leite

SÃO CARLOS-SP
2020

**UNIVERSIDADE FEDERAL DE SÃO CARLOS
CENTRO DE CIÊNCIAS EXATAS E DE TECNOLOGIA
PROGRAMA DE PÓS-GRADUAÇÃO EM CIÊNCIA E
ENGENHARIA DE MATERIAIS**

**UNIVERSITE GRENOBLE ALPES - ÉCOLE DOCTORALE DE INGENIERIE -
MATERIAUX, MECANIQUE, ENVIRONNEMENT, ENERGETIQUE,
PROCEDES, PRODUCTION (IMEP2)**

**PREPARATION AND CHARACTERIZATION OF BIONANOCOMPOSITES
BASED ON PROTEIN AND CELLULOSE NANOCRYSTALS BY
CONTINUOUS CASTING**

Liliane Samara Ferreira Leite

Tese apresentada ao Programa de
Pós-Graduação em Ciência e Engenharia
de Materiais como requisito parcial à
obtenção do título de DOUTORA EM
CIÊNCIA E ENGENHARIA DE MATERIAIS

Orientador brasileiro: Dr. Luiz Henrique Capparelli Mattoso

Orientador francês: Dr. Julien Bras

Coorientador brasileiro: Dr. Francys Clay Vieira Moreira

Agência Financiadora: FAPESP, Processo nº: 2016/03080-3 e 2018/00278-2

São Carlos-SP
2020

DEDICATION

Ao meu pai, Orivaldo Leite (*in memoriam*), a minha mãe, Odelfa Marchezin e aos meus irmãos, Silvania e Henrique Leite, por sempre me apoiarem e acreditarem na educação como meio transformador para uma sociedade mais justa, inclusiva e de oportunidades.

VITAE

1. Joint Ph.D. in Science and Materials Engineering. Thesis title: "Preparation . and characterization of bionanocomposites base on protein and cellulose nanocrystals by continuous casting", 2020, UFSCAR/UGA. Supervisor: Dr. Luiz Henrique Capparelli Mattoso and Dr. Julien Bras. Co-supervisor: Dr. Francys Kley Vieira Moreira.
2. Master Degree in Chemistry. Dissertation title: "Preparação e caracterização de compósitos de acetato de celulose e nanocristais de celulose", 2015, UNICAMP. Supervisor: Dra. Maria do Carmo Gonçalves.
3. Graduation in Chemistry at the UNICAMP 2012.



UNIVERSIDADE FEDERAL DE SÃO CARLOS

Centro de Ciências Exatas e de Tecnologia
Programa de Pós-Graduação em Ciência e Engenharia de Materiais

Folha de Aprovação

Defesa de Tese de Doutorado da candidata Liliane Samara Ferreira Leite, realizada em 11/12/2020.

Comissão Julgadora:

Prof. Dr. Luiz Henrique Capparelli Mattoso (EMBRAPA)

Profa. Dra. Sílvia Helena Prado Bettini (UFSCar)

Profa. Dra. Morsyleide de Freitas Rosa (EMBRAPA)

Prof. Dr. Eric Pollet (UNISTRA)

Prof. Dr. Julien Bras (Grenoble INP)

Prof. Dr. Mohamed Naceur Belgacem (Grenoble INP)

O presente trabalho foi realizado com apoio da Coordenação de Aperfeiçoamento de Pessoal de Nível Superior - Brasil (CAPES) - Código de Financiamento 001.

O Relatório de Defesa assinado pelos membros da Comissão Julgadora encontra-se arquivado junto ao Programa de Pós-Graduação em Ciência e Engenharia de Materiais.

ACKNOWLEDGEMENTS (AGRADECIMENTOS)

No final dessa etapa, gostaria de agradecer a muitas pessoas que direta ou indiretamente contribuíram para a realização deste trabalho, que posso chamar de um sonho realizado.

Aos meus estimados orientadores Dr. Mattoso, Dr. Julien e Dr. Francys, pela orientação, dedicação, paciência e por serem exemplos de pesquisadores apaixonados pela ciência. Aos pesquisadores: Dra. Henriette Azeredo, Dr. Osvaldo Novais de Oliveira Jr. e Dr. Emily Cranston pelas parcerias e discussões científicas. Quero agradecer, em especial a todos os professores que não medem esforços para que seus alunos conquistem um futuro melhor, em especial a minha professora de literatura, Ciça Cerântola, por me mostrar que nunca devemos deixar de sonhar e que a universidade pública é um lugar para todos, e a minha professora de inglês, Debora Pollini, por me fazer acreditar que podemos ir além.

Aos colegas de laboratório e de escritório no Brasil pela amizade, descontração, conversar e aprendizados: Carla, Amanda, Larissa, Anielle, Thalita, Jéssica, Ana Carolina, Caio Moreira, Naja, Alex, Vitor, Stanley, Rafaella, Caio Gomide e Marcos. Aos colegas do LGP2 na França que me acolheram tão bem e me fizeram sentir em casa: Merci donc à Eva, Lorelei, Claire, Ardilla, Manon, Malek, Estelle, Camille, Amina, Rim, Justine, Hippolyte, Bastian, Hugo, Gabriel, Mathieu et Max. A todos os técnicos da Embrapa Instrumentação e do LGP2 que sempre estiveram dispostos a ajudar os alunos.

À minha família e em especial a minha mãe pela paciência, compreensão, incentivo e apoio, sem os quais não teria concluído este trabalho. A todos os meus amigos que tornaram essa caminhada mais leve.

À Embrapa Instrumentação, ao Laboratório Nacional de Nanotecnologia Aplicado ao Agronegócio, a Université Grenoble Alpes e ao Laboratoire Génie des Procédés Papetiers pelas facilidades concedidas para realização deste trabalho, e à rede Embrapa Agronano, ao SISNANO/MCTI pelo apoio financeiro.

À Universidade Federal de São Carlos, Programa de Pós-Graduação em Ciência e Engenharia de Materiais. Federal University of São Carlos, Graduate Program in Materials Science and Engineering (PPG-CEM)

À FAPESP – Fundação de Amparo à Pesquisa do Estado de São Paulo pelas bolsas de estudo concedidas neste período, processo n° 2016/03080-3 e processo n° 2018/00278-2. FAPESP – São Paulo Research Foundation – grant 2016/03080-3 and grant 2018-00278-2.

O presente trabalho foi realizado com apoio da Coordenação de Aperfeiçoamento de Pessoal de Nível Superior - Brasil (CAPES) - Código de Financiamento 001 .

This study was financed in part by the Coordenação de Aperfeiçoamento de Pessoal de Nível Superior - Brasil (CAPES) – Financial Code 001.

ABSTRACT

This Ph.D. thesis covers the production and characterization of gelatin-cellulose nanocrystals (CNCs) bionanocomposite films intended for multifunctional food packaging. The up-scalability of the gelatin/CNCs films was attained by continuous casting and the rheological parameters of the film-forming solutions and drying temperature required to produce 12 m film/h were established. The continuous casting processing was proven to be advantageous when compared to the bench solution casting method. Tensile test, thermogravimetric analysis, and water vapor permeability analysis showed that the continuously cast gelatin/CNCs films had exceptionally better performance than the films obtained by bench casting. The physical and structural properties of the gelatin/CNCs bionanocomposites as tailored by pH-dependent electrostatic interactions were investigated. The suitability of CNCs was successfully extended by functionalization with rosin (r-CNCs), thus giving rise to antimicrobial reinforcing agents. Tensile test and antimicrobial analysis showed that r-CNCs served as bacterial nanofillers in gelatin-based films, which otherwise would suffer from limited physical and biological properties. Plant-derived tannic acid was successfully used as an antioxidant and bactericidal additive, as another perspective of extending the potential of the gelatin/CNCs films as a packaging material. Non-oxidized tannic acid favored non-covalent interactions and intermolecular connections between gelatin, CNCs, and tannic acid. These physico chemical interactions showed to have a greater influence on the antioxidant and physical properties of gelatin/CNCs/Tannic acid films. This thesis provides a comprehensive understanding of how CNCs can be explored to develop biodegradable films based on gelatin with enhanced properties or extra functionalities. A continuous solution casting was applied for scaling up the production of gelatin/CNCs-based films making them highly desirable for packaging applications.

Keywords: Gelatin; Cellulose Nanocrystals; Packaging; Physical Properties; Continuous Casting.

RESUMO

PREPARAÇÃO E CARACTERIZAÇÃO DE BIONANOCOMPÓSITOS A BASE DE PROTEÍNA E NANOCRISTAIS DE CELULOSE POR CASTING CONTÍNUO

Esta tese de doutorado foca na produção e caracterização de filmes bionanocompósitos de gelatina-nanocristais de celulose (CNCs) destinados a embalagens multifuncionais de alimentos. A escalabilidade da produção dos filmes de gelatina/CNCs foi obtida por casting contínuo e os parâmetros reológicos das soluções formadoras de filme e a temperatura de secagem necessária para produzir de 12 m de filme/h foram estabelecidos. O processo de casting contínuo provou ser vantajoso comparado ao método de casting convencional. Testes de tração, análises termogravimétricas e análises de permeabilidade ao vapor de água mostraram que os filmes de gelatina/CNCs laminados continuamente tiveram um desempenho excepcionalmente melhor do que aqueles obtidos por casting convencional. As propriedades físicas e estruturais dos filmes de gelatina/CNCs, moduladas por interações eletrostáticas dependentes do pH foram investigadas. A função dos CNCs foi ampliada com sucesso pela funcionalização com rosina (r-CNCs), resultando em agentes de reforço antimicrobianos. Testes de tração e análises antimicrobianas mostraram que r-CNCs serviram como agente antibacteriano à filmes à base de gelatina que apresentavam propriedades físicas e biológicas limitadas. O ácido tânico foi utilizado com sucesso como aditivo antioxidante e antimicrobiano, como outra alternativa para estender o potencial dos filmes de gelatina/CNCs como material de embalagem. Ácido tânico na forma não oxidada favoreceu interações não covalentes e conexões intermoleculares entre gelatina, CNCs e ácido tânico. Essas interações físico-químicas mostraram ter grande influência nas propriedades antioxidantes e físicas nos filmes de gelatina/CNCs/ácido tânico. Esta tese fornece uma compreensão abrangente de como os CNCs podem ser explorados para desenvolver filmes biodegradáveis à base de gelatina com propriedades aprimoradas ou funcionalidades extras. Além disso, casting contínuo foi aplicado para aumentar a produção de filmes gelatina/CNCs, tornando- os altamente desejáveis para aplicações em embalagens.

Palavras-chave: Gelatina; Nanocristais de celulose; Embalagem; Propriedades Físicas; Casting Contínuo.

RÉSUMÉ

PRÉPARATION ET CARACTÉRISATION DES BIONANCOMPOSITES À BASE DE PROTÉINES ET DE CELLULOSE NANOCRISTALS PAR CASITING CONTINUE

Cette thèse étudie la production et la caractérisation de films bionanocomposites de gélatine-cellulose nanocristaux (CNCs) destinés aux emballages alimentaires multifonctionnels. L'évolutivité des films de gélatine/CNCs a été obtenue par casting continue, et les paramètres rhéologiques des solutions filmogènes et la température de séchage nécessaire pour produire 12 m de film/h ont été établis. Le processus de casting continue s'est avéré avantageux par rapport au processus de casting conventionnel. Les tests de traction, l'analyse thermogravimétrique et l'analyse de perméabilité à la vapeur d'eau ont montré que les films de gélatine/CNCs laminés produits continuellement ont eu une meilleure performance que ceux obtenus par casting conventionnel. Les propriétés physiques et structurelles des gélatine/CNCs modulé par des interactions électrostatiques changés par le pH ont été étudiées. La fonction des CNCs a été étendue avec succès par la fonctionnalisation avec rosin (r-CNCs), qui a produit des nanocharges antimicrobiennes. Des tests de traction et des analyses antimicrobiennes ont montré que les r-CNCs servent d'agent antibactériens dans les films à base de gélatine. Sans cela, les films souffriraient autrement de propriétés physiques et biologiques limitées. L'acide tannique a été utilisé avec succès comme antioxydant et additif antibactérien, comme une autre perspective pour développer le potentiel des films de gélatine/CNCs comme matériel d'emballage. L'acide tannique non oxydé a favorisé les interactions non covalentes et intermoléculaires entre la gélatine, les CNCs et l'acide tannique. Ces interactions physico-chimiques ont montré une plus grande influence sur les propriétés antioxydantes et physiques des films gélatine/CNCs-acide tannique. Cette thèse donne une compréhension globale de la façon dont la CNCs peut être exploitée pour développer des films biodégradables à base de gélatine avec des propriétés améliorées ou des fonctionnalités supplémentaires. Le casting continue a été appliqué afin d'augmenter la production de films de gélatine/CNCs, ce que rend les films hautement souhaitables pour les applications d'emballage.

Mots clés : Gélatine ; Nanocristaux de Cellulose ; Emballage ; Propriétés Physiques ; Casting Continue.

SCIENTIFIC CONTRIBUTIONS (2016-2020)

Publications in scientific journals

1. **LEITE, L.S.F.**; FERREIRA, C.M.; CORRÊA, A. C.; MOREIRA, F. K. V.; MATTOSO, L. H. C. Scaled-up production of bionanocomposite films based on gelatin and cellulose nanocrystals by continuous casting. In: CARBOHYDRATE POLYMERS, (2020), 238, 116198. <https://doi.org/10.1016/j.carbpol.2020.116198>
2. **LEITE, L.S.F.**; MOREIRA, F. K. V; MATTOSO, L. H. C; BRAS, J. Electrostatic interactions regulate the physical properties of gelatin-cellulose nanocrystals nanocomposite films intended for biodegradable packaging. In: FOOD HYDROCOLLOIDS, (2020), 106424. <https://doi.org/10.1016/j.foodhyd.2020.106424>
3. **LEITE, L.S.F.**; BILATTO, S.; PASCHOALIN, R. T.; SOARE, A. C.; OLIVEIRA JR. O. N.; MOREIRA, F. K. V; MATTOSO, L. H. C; BRAS, J. Eco-friendly gelatin films with rosin-grafted cellulose nanocrystals for antimicrobial packaging. In: INTERNATIONAL JOURNAL OF BIOLOGICAL MACROMOLECULES, (2020), 165, 2974-2983. <https://doi.org/10.1016/j.ijbiomac.2020.10.189>
4. **LEITE, L.S.F.**; PHAM, C.; BILATTO, S.; CRANSTON, E. D.; F. K. V; MATTOSO, L. H. C; BRAS, J. Active properties of gelatin films as affected by tannic acid and cellulose nanocrystals. (ACS SUSTAINABLE CHEMISTRY & ENGINEERING – submitted)

Oral presentation in international conferences

1. **LEITE, L.S.F.**, PIZA, M. A.; MOREIRA, F. K. V. L.; MATTOSO, L.H.C. Tailoring mechanical properties of biodegradable gelatin plastics obtained by continuous casting. In: 4TH INTERNATIONAL CONFERENCE ON

BIO-BASED MATERIALS AND COMPOSITES. Nantes-France. March, 2017.

Posters in scientific conferences

1. **LEITE, L.S.F.**; PIZA, M.A.; BERTOLINO, L.C.; MATTOSO, L. H. C.; MOREIRA, F.K.V. Obtaining of cationic starch/Palygorskita bionanocomposites by continuous casting. In: 5th INTERNATIONAL CONFERENCE ON MULTIFUNCTIONAL, HYBRID AND NANOMATERIALS. Lisbon-Portugal. March, 2017.
2. **LEITE, L.S.F.**; MOREIRA, F. K. V. L.; MATTOSO, L.H.C. Preparação e caracterização de bionanocompósitos à base de gelatina e nanocristais de celulose por casting contínuo. In: IX WORKSHOP DE NANOTECNOLOGIA APLICADA AO AGRONEGÓCIO. São Carlos – SP. November, 2018.
3. **LEITE, L.S.F.**; MOREIRA, F. K. V. L.; BRAS, J.; MATTOSO, L.H.C. Bionanocomposites based on gelatin and cellulose nanocrystals obtained by continuous casting. In: 4TH INTERNATIONAL CONFERENCE ON BIOINSPIRED AND BIO-BASED CHEMISTRY AND MATERIALS. Nice-France, October, 2018.
4. **LEITE, L.S.F.**; MOREIRA, F. K. V. L.; MATTOSO, L.H.C.; BRAS, J. Reinforcement of gelatin films by carboxylated cellulose nanocrystals for food packaging applications. In: 5TH INTERNATIONAL CONFERENCE ON BIO-BASED MATERIALS AND COMPOSITES. Monastir-Tunisia. March, 2019.
5. **LEITE, L.S.F.**; MOREIRA, F. K. V. L.; MATTOSO, L.H.C.; BRAS, J. Effect of the pH film-forming solution and the reinforcement ability of CNCs on properties of gelatin films for food packing. In: 3RD NANOCELLULOSE WORKSHOP. Campinas-SP. June, 2019.
6. **LEITE, L.S.F.**; MOREIRA, F. K. V. L.; BRAS, J.; MATTOSO, L.H.C. Propriedades reológicas de soluções filmogênicas de gelatina e nanocristais de celulose para produção de filmes biodegradáveis por

casting contínuo. In: SIAGRO - SIMPÓSIO NACIONAL DE INSTRUMENTAÇÃO AGROPECUÁRIA. São Carlos-SP. December, 2019.

7. **LEITE, L.S.F.**; MOREIRA, F. K. V. L.; MATTOSO, L.H.C.; BRAS, J. Scaled-up of the production of sustainable bionanocomposite films based on protein and cellulose nanocrystals for food packaging application. In: TAPPI NANO 2020 VIRTUAL CONFERENCE. July, 2020.

TABLE OF CONTENTS

	Page
APPROVAL SHEET.....	i
ACKNOWLEDGEMENTS (AGRADECIMENTOS).....	iii
ABSTRACT.....	v
RESUMO.....	vii
RÉSUMÉ.....	ix
SCIENTIFIC CONTRIBUTIONS (2016-2020).....	xi
TABLE OF CONTENTS.....	xv
INDEX OF TABLES.....	xxiii
INDEX OF FIGURES.....	xxv
SYMBOLS AND ABBREVIATIONS.....	xxxiii
GENERAL INTRODUCTION.....	3
CHAPTER I: Literature review.....	7
Introduction to chapter I.....	9
1 Food packaging: current challenges and sustainability.....	11
1.1 Impact of food losses and waste on sustainability.....	12
1.2 Plastic food packaging.....	13
1.3 Main properties of food packaging materials.....	16
1.3.1 Permeability properties.....	16
1.3.2 Mechanical properties.....	21
1.3.3 Optical properties.....	21
1.3.4 Heat sealing properties.....	22
2 Bio-based and biodegradable materials: definitions.....	22
2.1 Bio-based plastics: competition with food production.....	26
2.2 Natural polymers.....	27
2.2.1 Protein.....	28
2.2.1.1 Gelatin.....	31
2.2.1.2 Gelatin-based films for food packaging.....	34
2.2.3 Cellulose.....	38
2.2.3.1 Cellulose nanocrystals.....	39
2.2.3.2 Cellulose nanocrystals in food packaging.....	43
2.2.3.3 Functionalization of cellulose nanocrystals.....	46

2.2.3.4 Cellulose nanocrystals safety and toxicology assessment	48
3 Processing of natural polymer-based film packaging	48
3.1 Bench casting	49
3.2 Continuous solution casting.....	50
Conclusions	52

CHAPTER II: Gelatin-based films produced by continuous casting..... 53

Introduction to chapter II	55
1. Scalability of the gelatin/CNCs bionanocomposites by continuous solution casting	57
1.1 introduction	58
1.2 Materials and Methods	59
1.2.1 Materials	59
1.2.2 Preparation of CNCs.....	59
1.2.3 Preparation of gelatin/CNCs film-forming solutions (FFS)	59
1.2.4 Continuous casting	60
1.2.5 Bench casting	61
1.2.6 Transmission electron microscopy (TEM).....	61
1.2.7 Determination of Zeta potential (ζ -potentials)	61
1.2.8 Rheological study	61
1.2.9 Scanning electron microscopy (SEM).....	62
1.2.10 Attenuated total reflectance Fourier transform infrared spectroscopy (ATR-FTIR)	62
1.2.11 Color measurement.....	62
1.2.12 Light transmission and transparency	63
1.2.13 Thermogravimetric analysis (TGA)	63
1.2.14 Tensile tests	63
1.2.15 Contact angle measurements.....	64
1.2.16 Statistical analysis	64
1.3 Results and discussion.....	64
1.3.1 Characterization of CNCs.....	64
1.3.2 Characterization of gelatin-CNCs FFS.....	65
1.3.3 Production capacity of gelatin/CNCs films by continuous casting.....	70
1.3.4 Morphological characterization	71

1.3.5 Structural aspects	72
1.3.6 Optical and thermal properties	74
1.3.7 Mechanical properties	77
1.4 Conclusions	78
2 The relationship between heterogeneous CNCs and homogeneous CNCs suspensions and physical properties of gelatin-based films obtained by bench casting and continuous casting	80
2.1 Introduction	81
2.2 Materials and Methods	82
2.2.1 Materials	82
2.2.2 Hydrolyses of CNCs from eucalyptus kraft pulp	83
2.2.3 Preparation film-forming solutions (FFS)	83
2.2.4 Polarized light optical microscopy (POM)	83
2.2.5 Transmission electron microscopy (TEM)	84
2.2.6 X-ray diffraction (XRD)	84
2.2.7 Bench casting	85
2.2.8 Continuous casting	85
2.2.9 Tensile test	85
2.2.10 Scanning electron microscopy (SEM)	86
2.2.11 Field emission gun scanning electron microscopy (FESEM)	86
2.2.12 Water Vapor Permeability (WVP)	86
2.2.13 Contact angle measurements	87
2.2.14 Thermogravimetric analysis (TGA)	87
2.2.15 Statistical analysis	87
2.3 Results and discussion	87
2.3.1 CNCs isolated from eucalyptus pulp into gelatin FFS	87
2.3.2 Heterogeneous CNCs vs. homogeneous CNCs	89
2.3.3 Physical properties of gelatin-based films obtained by bench casting vs continuous casting	91
2.3.3.1 Mechanical properties of gelatin-based films	91
2.3.3.2 Structure analyses of gelatin-based films	93

2.3.3.3 Morphological analysis of gelatin-based films.....	95
2.3.3.4 Water vapor barrier analysis of gelatin-based films	96
2.3.3.5 Contact angle measurement of gelatin-based films	97
2.3.3.6 Thermostability of gelatin-based films.....	98
2.4 Conclusion.....	99

CHAPTER III: Evaluation of physical properties of gelatin-based films under the influence of electrostatic interactions..... 101

Introduction to chapter III	103
1 Evaluation of physical properties of gelatin-based films under the influence of electrostatic interactions	105
1 Introduction.....	106
1.2 Materials and methods	107
1.2.1 Materials	107
1.2.2 Preparation of gelatin/CNCs films.....	107
1.2.3 Determination of Zeta potentials (ζ -potentials)	107
1.2.4 Rheological study	108
1.2.5 Polarized light optical microscopy.....	108
1.2.6 Scanning electron microscopy (SEM).....	108
1.2.7 X-ray diffraction (XRD) analysis	109
1.2.8 Tensile tests	109
1.2.9 Water vapor permeability (WVP)	110
1.2.10 Water solubility (WS) determination.....	110
1.2.11 Thermogravimetric analysis (TGA).....	110
1.2.12 Statistical analysis	111
1.3 Results and discussion.....	111
1.3.1 Physical and rheological properties of gelatin/CNCs film-forming solutions.....	111
1.3.2 Characterization of gelatin/CNCs films	117
1.3.2.1 Morphological and structural characterization	117
1.3.2.2 Mechanical properties.....	121
1.3.2.3 Water sensitive properties	122

1.3.2.4 Thermostability	124
1.4 Conclusion	127

CHAPTER IV: Functionalization of CNCs and active gelatin-based films 129

Introduction to chapter IV	131
1 Functionalization of CNCs with natural antimicrobial rosin mixture and evaluation of their gelatin-based films	133
1.1 introduction.....	134
1.2 Materials and Methods	135
1.2.1 Materials.....	135
1.2.2 Synthesis of rosin-grafted CNCs (r-CNCs).....	136
1.2.3 Preparation of gelatin/r-CNCs bionanocomposite films.....	136
1.2.4 X-ray photoelectron spectroscopy (XPS)	137
1.2.5 Fourier Transform Infrared Spectroscopy (FTIR)	137
1.2.6 Transmission Electron Microscopy (TEM).....	137
1.2.7 X-ray diffraction (XRD)	137
1.2.8 Scanning Electron Microscope (SEM).....	138
1.2.9 Water Vapor Permeability	138
1.2.10 Oxygen Transmission Rate (OTR)	138
1.2.11 Tensile tests	139
1.2.12 Antimicrobial activity tests	139
1.2.13 Statistical analysis	140
1.3 Results and discussion.....	140
1.3.1 Functionalization of CNCs with rosin.....	140
1.3.2 Morphology of gelatin films reinforced with CNCs and r-CNCs	145
1.3.3 Contact angle of gelatin films reinforced with CNCs and r-CNCs.....	146
1.3.4 Optical properties of gelatin films reinforced with CNCs and r-CNCs....	147
1.3.5 Barrier properties of gelatin/CNCs and gelatin/r-CNCs films.....	149
1.3.6 Antimicrobial properties of r-CNCs and gelatin/r-CNCs films	152
1.3.7 Use of gelatin films reinforced with r-CNCs for actual packaging.....	154
1.4 Conclusion	156

2 Effect of tannic acid and cellulose nanocrystals on antioxidant, antimicrobial, and physical properties of gelatin-based films	157
2.1 Introduction	158
2.2 Materials and Methods.....	159
2.2.1 Materials	159
2.2.2 Film-forming solution (FFS) preparation	160
2.2.3 Film casting	160
2.2.4 Transmission electron microscopy (TEM).....	161
2.2.5 X-ray diffraction (XRD).....	161
2.2.6 Quartz crystal microbalance with dissipation (QCM-D).....	161
2.2.7 Rheological properties	163
2.2.8 Determination of crosslinking degree	163
2.2.9 Scanning electron microscopy (SEM).....	164
2.2.10 Determination of antioxidant activity	164
2.2.11 UV-Vis spectroscopy and transparency determination	165
2.2.12 Contact angle measurements.....	165
2.2.13 Tensile tests	165
2.2.14 Puncture test	166
2.2.15 Water vapor permeability and moisture content determination.....	166
2.2.16 Antimicrobial tests.....	167
2.2.17 Statistical analysis	168
2.3. Results and discussion	168
2.3.1 Cellulose nanocrystals characterization.....	168
2.3.2 Gelatin, tannic acid, and CNCs interactions	169
2.3.3 Crosslinking degree in the gelatin-based films with TA or OTA.....	176
2.3.4 Viscoelastic behavior of the gelatin-based films	177
2.3.5 Morphological characterizations of gelatin-based films with TA or OTA	178
2.3.6 Antioxidant activity of gelatin-based films with TA or OTA.....	181
2.3.7 Optical properties of gelatin-based films.....	183
2.3.8 Contact angle of gelatin-based films.....	184
2.3.9 Mechanical properties of gelatin-based films.....	186
2.3.10 Water barrier properties and water vapor absorption of gelatin-based films.....	188

2.3.11 Antimicrobial activities of tannic acid and gelatin-based films with TA	189
2.4 Conclusion	192
CHAPTER V: General conclusions and perspectives	193
General conclusions and perspectives.....	195
EXTENDED PORTUGUES ABSTRACT - Resumo Português	201
EXTENDED FRENCH ABSTRACT - Résumé Français	213
REFERENCES.....	223

INDEX OF TABLES

	Page
CHAPTER I	
Table 1.1 - Common biodegradable materials used in food packaging applications	27
Table 1.2 - Amino acid composition (expressed as no. residues/1000 residues) from various sources of gelatin.....	33
Table 1.3 - Physical-chemical properties of gelatin-based films.....	35
Table 1.4 - Physical-chemical properties of gelatin-nanocellulose bionanocomposites.....	45
	Page
CHAPTER II	
Table 2.1 - ζ -potential of gelatin and CNCs suspensions and viscosity and rheological parameters of gelatin FFS calculated by the Power Law model. ...	68
Table 2.2 - Productivity of biopolymers-based films produced by casting/evaporation.....	71
Table 2.3 - Color parameters, transparency, and thermal properties of gelatin/CNCs bionanocomposite films.....	75
Table 2.4 - Average length, diameter, aspect ratios measured by TEM, and percent crystallinity determined by XRD of CNCs and commercial CNCs.	90
Table 2.5 - Triple helix content of gelatin-based films obtained by bench and continuous casting.	95
Table 2.6 - Onset of thermal degradation, 50% weight loss, and maximum thermal degradation temperatures for CNCs powder and gelatin-based obtained by bench casting and continuous casting.	99

CHAPTER III

Table 3.1 - Apparent viscosity (η_{ap}), parameters of Ostwald de Waele model (consistency index (K), and flow index (n)) and transition temperatures of gelatin/CNCs FFS at pH 3, 6, and 8	114
Table 3.2 - Triple helix content of gelatin films obtained from FFS at different pH and CNCs amount	120
Table 3.3 - Water vapor permeability at 50% RH and 25 °C and water solubility of the gelatin films with different pH and CNCs content.....	124
Table 3.4 - TGA results of gelatin/CNCs films at different pH.....	125
Table 3.5 - Tensile, thermal properties, water vapor permeability, and triple-helix content of gelatin films with 0.5% CNCs at pH 8 as a function of different drying temperatures.	126

CHAPTER IV

Table 4.1 - X-ray photoelectron spectroscopy data of CNCs and r- CNCs.....	142
Table 4.2 - Optical properties of gelatin/r-CNCs bionanocomposite and synthetic films currently applied in food packaging	149
Table 4.3 - Transitions temperatures for gelatin-based solution with TA and CNCs.....	172
Table 4.4 - Apparent viscosity and rheological parameters of gelatin-based FFS calculated by the Power Law.	175
Table 4.5 - Light transmission and transparency of gelatin-based films with TA.	184

CHAPTER IV

Table 5.1 – Main results of this Ph.D. Work.....	196
--	-----

INDEX OF FIGURES

	Page
GENERAL INTRODUCTION	
Figure 1 - Number of papers and patents releases each year dealing with CNCs until 2020 (extracted from ACS SciFinder in September 2020, descriptors are cellulose nanocrystals, cellulose nanowhiskers, nanocrystalline cellulose, and cellulose whiskers).	4
	Page
CHAPTER I	
Figure 1.1 - Primary functions of food packaging.	12
Figure 1.2 - Food loss and waste that occur along the entire food chain.	13
Figure 1.3 - Plastic demand by segment in 2018 (adapted from [39]).	14
Figure 1.4 - General mechanism of gas or vapor permeation through a polymer packaging film.	18
Figure 1.5 - Requirements on packaging for different foods (adapted from [51])	20
Figure 1.6 - Comparison of water vapor and oxygen transmission rate of conventional plastics (grey) and biopolymers (green) at 23°C. (source: [52][51] [53] [54]).	20
Figure 1.7 - Overview of all plastics types, classified according to raw material source and functionality (adapted from EUBP [59]).	24
Figure 1.8 - Global production capacities of bioplastics by market segment in 2019 (source: https://www.european-bioplastics.org/market/ [59]).	25
Figure 1.9 - Publications extracted from ACS SciFinder in September 2020 with keywords: biodegradable and food packaging.	26
Figure 1. 10 - Advantages and disadvantages of natural polymers and applications (source: [65] [66][40] [67][68]).	28
Figure 1.11 - Amino acid residues, peptide bonds, and levels of protein organization (adapted from [70]).	30
Figure 1.12 - Conversion of insoluble native collagen into soluble gelatin (adapted from [77]).	32

Figure 1.13 - Representation of a cellulose chain showing the anhydroglucose unit, the glycosidic link, and both reducing and non-reducing ends of the polymer.	38
Figure 1.14 - Number of papers and patents releases each year dealing with CNCs until 2020 (extracted from ACS SciFinder in September 2020, descriptors are cellulose nanocrystals, cellulose nanowhiskers, nanocrystalline cellulose, and cellulose whiskers).	40
Figure 1.15 - Schematic acid hydrolysis production of CNCs resulting in sulfate half ester surface groups (adapted from [134]).	41
Figure 1.16 - Transmission electron microscopy images of CNCs suspensions obtained from (a) tunicate, (b) ramie, (c) cotton, (d) beet sugar, (e) microcrystalline cellulose, and (f) bacterial cellulose [8].	42
Figure 1.17 - Common surface functionalization of CNCs: (clockwise from top-right) sulfuric acid hydrolysis, carboxylic acid halides, acid anhydrides, epoxides, isocyanates, TEMPO oxidation, halogenates acetic acids, and chlorosilanes [127].	47
Figure 1.18 - Schematic representation of gelatin-CNCs bionanocomposite production by continuous casting [18].	51

Page

CHAPTER II

Figure 2.1 - Schematic representation of gelatin-CNCs bionanocomposite production by continuous casting.	60
Figure 2.2 - TEM micrograph of CNCs isolated from eucalyptus pulp.	65
Figure 2.3 - Structure of ionized and zwitterion forms of glycine.	65
Figure 2.4 - Power Law model fitting for the film-forming solutions as a function of gelatin concentration at 30 °C.	67
Figure 2.5 - Rheological characterization of gelatin-CNCs FFS containing different CNCs concentrations (a) apparent viscosity vs. shear rate (25 °C), (b) apparent viscosity vs. temperature curves, and (c) storage modulus (G') and loss modulus (G'') vs. temperature curves.	70

Figure 2.6 - SEM images of cross-sectional surfaces of films (a) neat gelatin and with (b) 0.5 wt% CNCs, (c) 1.0 wt% CNCs and (d) 2.5 wt% CNCs.	72
Figure 2.7 - ATR-FTIR spectra of (a) CNCs powder, (b) gelatin powder and gelatin/CNCs bionanocomposite films with (c) 0 wt% CNCs and (d) 2.5 wt% CNCs.	73
Figure 2.8 - Photography of gelatin/CNCs bionanocomposite films obtained by continuous casting.	74
Figure 2.9 - UV-Vis spectra of pure gelatin film and its bionanocomposites with CNCs.	76
Figure 2.10 - (a)TG and (b) DTG curves of the gelatin/CNCs bionanocomposites obtained by continuous casting.	77
Figure 2.11- (a) tensile strength, (b) Young's modulus (c) strain at break, and (d) stress-strain curves as a function of CNCs content in gelatin films obtained by bench casting and continuous casting.	78
Figure 2.12 - Schematic of poor and well dispersion and distribution of particles	81
Figure 2.13 - (a) Polarized light images of gelatin/CNCs film-forming solution and (b) photographs of gelatin/CNCs films obtained by continuous casting.	88
Figure 2.14 - (a) Polarized light images of CNCs isolated from eucalyptus pulp and commercial CNCs aqueous suspensions at 1.0 wt% and (b) TEM micrograph of CNCs isolated from eucalyptus pulp and commercial CNCs.....	90
Figure 2. 15 - (a) Young's modulus, (b) tensile strength, (c) strain at break, and (d) stress-strain curves as a function of CNCs content in gelatin films obtained by bench casting and continuous casting.	93
Figure 2.16 - FESEM micrograph of the cross-sectional surface of (a) pure gelatin film and SEM micrographs of (b), (c) gelatin film with 6.0 wt% CNCs obtained by bench casting. FESEM micrographs of the cross-sectional surface of (d) pure gelatin and (e) and (f) gelatin films with 6.0 wt% CNCs obtained by continuous casting.	96
Figure 2.17 - Water vapor permeability of gelatin-based films obtained by bench and continuous casting	97

Figure 2.18 - XRD patterns of gelatin films with (a) 0 wt% CNCs and (b) 6.0 wt% CNCs obtained by bench and continuous casting.	94
Figure 2.19 - Contact angle of gelatin-based films obtained by bench and continuous casting.....	98

Page

CHAPTER III

Figure 3.1 - ζ -Potential values of neat gelatin solution and CNCs suspension (0.25 wt%) at and 25 °C as a function of pH.....	112
Figure 3.2 - ζ -potential curves of gelatin/CNCs FFS at different pH as a function of CNCs concentration.	113
Figure 3.3 - Apparent viscosity (left) and shear stress (right) curves as a function of the shear rate of gelatin/CNCs films at different pH values. (—) increase in shear rate and (-----) decrease in shear rate.	115
Figure 3.4 - Viscoelastic modulus of gelatin/CNCs FFS at different pH and CNCs contents. Heating (a and c) and cooling (b and d) at 1 °C min ⁻¹	117
Figure 3.5 - (a) Photographs of gelatin/CNCs films with different CNCs contents, (b) SEM micrographs of air-drying and cross-sectional surfaces of gelatin/CNCs films with 5.0 wt% CNCs at pH 3, pH 6 and pH 8. White arrows indicate CNCs-gelatin coacervates at pH 3.	118
Figure 3.6 - XRD patterns of (a) pure gelatin films obtained from FFS films at pH 3, 6, and 8 and (b) gelatin/CNCs films obtained from pH 8 and different CNCs amount. The magnified view of the 2 θ range 3 – 12 ° is shown as an insert. .	120
Figure 3.7 - (a) Young's modulus, (b) elongation at break, (c) tensile strength, and (d) stress-strain curves of gelatin/CNCs films as a function of pH and CNCs content.....	122
Figure 3.8 - XRD spectra of the gelatin/CNCs films with 0.5% at pH 8 obtained at different temperatures.	127

Page.

CHAPTER IV

Figure 4.1 - The most representative structures found in Rosin.	135
--	-----

Figure 4.2 - Schematic representation of the rosin-functionalized CNCs.	141
Figure 4.3 - C _{1s} XPS spectra of (a) CNCs and (b) r-CNCs.....	142
Figure 4.4 - ATR-FTIR spectra of rosin, CNCs and r-CNCs.....	143
Figure 4.5 - TEM micrograph of CNCs and (e) r-CNCs. (f) schematic representation of rosin-functionalized CNCs.....	144
Figure 4.6 - XRD spectra of the CNCs and r-CNCs.	144
Figure 4.7 - SEM micrographs of the cross-sectional surface of (a) pure gelatin films and gelatin bionanocomposites with 4.0 wt% (b) CNCs and (c) r-CNCs, and with 6.0 wt% (d) CNCs and (e) r-CNCs content.	146
Figure 4.8 - Contact angle of gelatin films and gelatin bionanocomposites with CNCs and r-CNCs.....	147
Figure 4.9 - Photography of (a) gelatin/CNCs and (b) gelatin/r-CNCs bionanocomposite films.....	148
Figure 4.10 - UV-Vis spectra of gelatin films reinforced with CNCs and r-CNCs.	148
Figure 4.11 - Water vapor permeability and water vapor transmission rate (WVTR) of gelatin bionanocomposites as functions of CNCs and r-CNCs contents.	150
Figure 4.12 - (a) Young's modulus, (b) tensile strength (c) elongation at break, and (d) stress-strain curves as a function of CNCs and r-CNCs content in bionanocomposite gelatin films obtained by casting.	152
Figure 4.13 - Minimum inhibitory concentration (MIC) of CNCs and r-CNCs suspension tested on Gram-positive <i>Staphylococcus aureus</i> and Gram-negative <i>Escherichia coli</i>	153
Figure 4.14 - Agar overlay assay of gelatin film discs against <i>S. aureus</i> and <i>E. coli</i>	154
Figure 4.15 - Schematic comparison of accelerated storage for mozzarella cheese slices packed in a PVC cling film, pure gelatin film, and gelatin/r-CNCs nanocomposite (6 wt%) film over 30 days at 25 °C. The control refers to free-standing, unpacked cheese slices (The Brazilian version of mozzarella cheese can be sliced, in contrast to the Italian mozzarella). Microbial spoilage is indicated by arrows in the images.	155

Figure 4.16 - Scheme of crosslinking reaction and hydrogen bonding interactions between protein and tannic acid (adapted from [209]).....	159
Figure 4.17 - (a) TEM micrograph of CNCs and (b) XRD spectra of CNCs. .	169
Figure 4.18 - (a-d) Normalized third overtone frequency (black) and dissipation (gray) data versus time from QCM-D analysis of CNCs-coated silica sensors exposed to three different injection orders of tannic acid (TA), gelatin (GEL) and glycerol (GLYC) with water (W) rinsing steps in between each injection step	171
Figure 4.19 - Storage modulus and loss modulus vs. temperature curves of (a), (b) G-TA-CNC6, and (c), (d) G-OTA-CNC6 solutions under heating and cooling scans.	172
Figure 4.20 - (a) storage (G') and loss (G'') moduli and (b) $\tan \delta$ as a function of frequency sweep and at 35 °C of G-TA-CNC6 and G-OTA-CNC6 solutions. .	173
Figure 4.21 - (a) Free TA released and (b) UV-Vis spectra of film-forming solutions, photography of the (c) G-OTA-CNC6 and G-TA-CNC6 solutions, and (d) G-OTA-CNC6 and G-TA-CNC6 films.	174
Figure 4.22 - (a) Apparent viscosity and (b) shear stress as a function of shear rate of the gelatin-based film-forming solution at 35 °C.	176
Figure 4.23 - (a) Calibration curve of TA in water and (b) free TA extracted from gelatin-based films.	177
Figure 4.24 - (a) Storage and (b) loss modulus of the gelatin-based films with TA or OTA.	178
Figure 4.25 - SEM images of cross-section of (a) Gel, (b) G-TA (c) G-TA-CNC6, and (e) G-OTA-CNC6 films before and after swelling for 24 in water.	180
Figure 4.26 - (a) Structure of DPPH and its reduction by an antioxidant agent. (b) Intermolecular stabilization of the tannic acid radical responsible for its efficient antioxidant activity.	181
Figure 4.27 - (a) DPPH radical scavenging activity of free TA solution and bionanocomposite films with CNCs and TA and (b) stability of gelatin bionanocomposite films.	183
Figure 4.28 - Photography of gelatin and gelatin-based films with TA.	184
Figure 4.29 - Contact angle measurements of gelatin-based films.	186

Figure 4.30 - (a) Tensile strength and elongation at break, (b) puncture force and strain at puncture of gelatin-based films and (c) tensile properties compared with those of synthetic polymeric film (adapted from [22]).	187
Figure 4.31 - Water vapor permeability and water vapor absorption of gelatin-based films.	189
Figure 4.32 - Minimum inhibitory concentration (MIC) of CNCs and TA suspension tested on Gram-positive <i>Staphylococcus aureus</i> and Gram-negative <i>Escherichia coli</i>	190
Figure 4.33 - Agar overlay assay of gelatin-based film discs against <i>S. aureus</i> and <i>E. coli</i> . Inset of the growth inhibition area observed under the sample. ...	191

Page

EXTENDED PORTUGUESE ABSTRACT

Resumo Português

Figura 1.1 - Viscosidade em função da taxa de cisalhamento para (a) SFF com diferentes concentrações de gelatina e (b) viscosidade e tensão de cisalhamento em função taxa de cisalhamento para SFF 20%.	204
Figura 1.2 - Resumo esquemático dos resultados obtidos nesse trabalho de doutorado.	208

Page.

EXTENDED FRENCH ABSTRACT

Résumé Français

Figure 1.1 – Viscosité en fonction du taux de cisaillement pour (a) SF avec différentes concentrations de gélatine et (b) viscosité et contrainte de cisaillement en fonction du taux de cisaillement pour SF 20%.	216
Figure 1.2 - Résumé schématique de tous les résultats les plus pertinents et étapes développées dans ce travail.	220

SYMBOLS AND ABBREVIATIONS

Chemical and materials

0 wt% CNCs	Gelatin film with 0 wt% cellulose nanocrystals
0.5 wt% CNCs	Gelatin film with 0.5wt% cellulose nanocrystals
0.5 wt% r-CNCs	Gelatin film with 0.5wt% functionalized cellulose nanocrystals with rosin
1.0 wt% CNCs	Gelatin film with 1.0wt% cellulose nanocrystals
2.5 wt% CNCs	Gelatin film with 2.5wt% cellulose nanocrystals
4.0 wt% CNCs	Gelatin film with 4.0wt% cellulose nanocrystals
4.0 wt% r-CNCs	Gelatin film with 4.0wt% functionalized cellulose nanocrystals with rosin
6.0 wt% CNCs	Gelatin film with 6.0wt% cellulose nanocrystals
6.0 wt% r-CNCs	Gelatin film with 6.0wt% functionalized cellulose nanocrystals with rosin
CNC-OTA	CNCs with oxidized tannic acid
CNCs	Cellulose nanocrystals
CNC-TA	Cellulose nanocrystals and tannic acid
FFS	Film-forming solution
G and GEL	Pure gelatin
Gelatin/CNCs	Gelatin film with cellulose nanocrystals
GLYC	Glycerol
G-OTA-CNC6	Gelatin film with oxidized TA and 6.0 wt% cellulose nanocrystals
G-TA	Gelatin film with tannic acid
G-TA-CNC4	Gelatin film with tannic acid and 4.0 wt% cellulose nanocrystals
G-TA-CNC6	Gelatin film with tannic acid and 6.0 wt% cellulose nanocrystals
OTA	Oxidized tannic acid
r-CNCs	Functionalized cellulose nanocrystals with rosin
TA	Tannic acid

Methods

AFM	Atomic force microscopy
ART-FTIR	Attenuated total reflectance Fourier transform infrared spectroscopy
CI	Crystallinity index
DTG	Derivative thermogravimetry
EAB	Elongation at break
EM	Elastic modulus
FESEM	Field emission gun-scanning transmission electron microscopy
G'	Storage modulus
G''	Loss modulus
Ip	Isoelectric point
k	Consistency factor
L/D	Aspect ratio
n	Flow behavior index
OTR	Oxygen transmission rate
POM	Polarized light microscopy
QCM-D	Quartz crystal microbalance with dissipation
SEM	Scanning electron microscopy
TEM	Transmission electron microscopy
TGA	Thermogravimetric analysis
T_{gel-sol}	Transitions temperature from gel to solution
T_{onset}	Temperature of degradation
TS	Tensile strength
T_{sol-gel}	Transitions temperature from solution to gel
UVA	Ultraviolet A
UVB	Ultraviolet B
UVC	Ultraviolet C
UV-Vis	Ultraviolet and visible
WS	Water solubility
WVP	Water vapor permeability
WVTR	Water vapor transmission rate
X_c	Triple helix content of gelatin
XDR	X-ray diffraction analysis
XPS	X-ray photoelectron spectroscopy
$\dot{\gamma}$	Shear rate
Δa	Color parameter a
Δb	Color parameter b
ΔE	Color difference
ΔL	Color parameter L
σ	Shear stress

General introduction

GENERAL INTRODUCTION

The growing plastic production has led to a global waste disposal crisis. Nowadays, researches are focused on solving this problem by obtaining biodegradable packaging. Biopolymers, including proteins and polysaccharides, are the main natural resources employed to develop biodegradable films [1].

Proteins such as gelatin can be suitable for food packaging due to their renewability, biodegradability, low costs, film-forming ability, and edible nature [1–3]. Gelatin is a water-soluble protein produced from partial hydrolysis of collagen, one of the most used biopolymers in food and pharmaceutical fields [4]. Gelatin films have suitable properties, such as transparency, biodegradability, and low oxygen permeability [5]; but they show poor barrier properties against moisture and only moderate mechanical strength in high relative humidity conditions [6]. This drawback could be overcome by incorporating reinforcing nanoparticles, such as cellulose nanocrystals (CNCs), in gelatin films [3,9–12].

Cellulose nanocrystals are rigid rod-like crystalline particles extracted from bio-sourced cellulosic materials. Since the last two decades, interest in cellulose nanocrystals has been growing as shown in Figure 1 by the exponential number of publications per year, owing to their biodegradability, renewability, abundance, low density, and excellent mechanical properties [13].

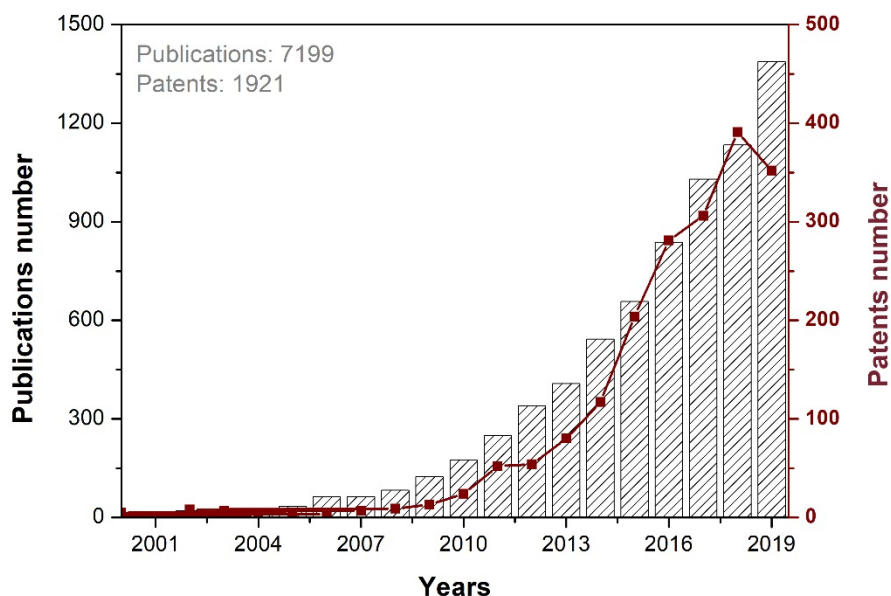


Figure 1 - Number of papers and patents releases each year dealing with CNCs until 2019 (extracted from ACS SciFinder in September 2020, descriptors are cellulose nanocrystals, cellulose nanowhiskers, nanocrystalline cellulose, and cellulose whiskers).

CNCs are one of the most studied polysaccharide-based nanomaterials in polymer nanocomposites [14] and can not only enhance the physical properties of protein films [15–18] but can also be chemically modified with various compounds to provide the ensuing nanocomposite with other functionalities [19–22], such as antibacterial activity with grafting of natural antimicrobial agents.

The last decades have been marked by intensive research on natural polymer processing as an effort to fabricate biodegradable plastics at a large scale [23]. Most studies have been focused on melt processing techniques due to technologies already established for petroleum-based polymers. However, melt processing of natural polymers, such as proteins, has been found to be challenging due to the thermomechanical instability of these macromolecules. In this project, continuous casting is proposed as a suitable approach to scale up the production of gelatin-cellulose nanocrystals bionanocomposites and produce rolls of bioplastics.

This Ph.D. proposes the production and characterization of multifunctional gelatin-cellulose nanocrystals films intended for packaging. Several objectives can be announced for this project:

- i. Investigate the parameters necessary to produce gelatin/CNCs films by pilot solution casting method (continuous casting method).
- ii. Characterize the morphological, thermal, mechanical, and barrier properties of gelatin/CNCs films obtained by continuous casting.
- iii. Functionalize the surface of CNCs and produce active gelatin films and functionalized CNCs.

In order to achieve these objectives, an active collaboration was developed during the four years with experts for nanocellulose production and functionalization at the Laboratory of Pulp and Paper Science and Graphic Arts (France) and experts for the production of bio-based materials films packaging at the Embrapa Instrumentação (Brazil). Therefore, this joined Ph.D. took place in a very international and multidisciplinary context.

The results obtained from this Ph.D. are organized in four chapters based on scientific papers.

In **Chapter I**, a literature review describes the context and objectives of this Ph.D. A focus on gelatin and cellulose nanocrystals and their potential uses as sustainable packaging is exposed. Besides, a scaled-up processing method for natural biodegradable films is provided.

In **chapter II** focuses on the parameters such as the rheological behavior of the film-forming solution and drying temperature required to produce gelatin/CNCs films by continuous casting. In addition, the physical properties of gelatin/CNCs obtained by continuous casting will be analyzed and two different types of CNCs suspensions were compared.

Chapter III describes the production of gelatin/CNCs with tunable physical properties by controlling the physical interactions between CNCs and gelatin but also checking the influence of the CNCs content. In addition, the effect of drying

temperature on gelatin renaturation triple helices and the physical properties of gelatin/CNCs films will be investigated.

Finally, **chapter IV** describes the functionalization and characterization of the surface of CNCs with rosin, a natural antimicrobial molecule, and with tannic acid, a natural antioxidant. The physical and antimicrobial properties of gelatin-based films with functionalized CNCs are investigated. Besides, the effects of various types of tannic acid, and CNCs on the physical, morphological, antioxidant, and antimicrobial properties of the gelatin-based films will be also analyzed.

Chapter I

Literature review

I Literature Review

Introduction to chapter I

This chapter aims to introduce the concepts related to this Ph.D. thesis both to “non-expert” and “expert” readers by providing them with general knowledge and relevant data through tables and schematic representations on every topic, extracted from around 200 references. The link between the Ph.D. thesis and literature review is emphasized in italic dark gray letters.

The first part of the literature review offers an overview of the importance of food packaging to the economic sector, as well as the environmental issues generated by the disordered use of plastic packaging. Besides, this part explains the main properties of food packaging materials and provides the reader with insight into the reference data of commercial plastic packaging to easily go over the next chapters.

The second part focuses on natural biodegradable materials - gelatin and cellulose nanocrystals, and their potential use as sustainable packaging. Gelatin and cellulose nanocrystals origins, chemical structure, toxicology, and application in food packaging are described.

Finally, the last part covers the processing of natural biodegradable films and introduces continuous casting as an alternative method - not yet explored for processing protein films at a pilot scale.

1 Food packaging: current challenges and sustainability

The use of packaging, throughout human history, has brought several benefits for the conservation, convenient usage, storage, and transportation of foods; contributing significantly to the development of trade markets and the growth of cities [24]. From the view of many consumers, however, packaging is often regarded as a necessary evil or an unnecessary cost, a serious waste of resources, and an environmental menace. This happens because consumers do not exactly know all the packaging functions for a product. Usually, when consumers are in contact with packaging its job is almost done [25].

Packaging has been defined as a socio-scientific discipline that operates in society to ensure the delivery of goods to the ultimate consumer in the best conditions intended for their use [26]. Other definitions of packaging include products, items, or packages in a bag, bottle, box, can, cup, tray, pouch, or another container form with the role of containing and protecting the product, as well as providing convenience and communicating to the consumer. The device or container is considered as a package if it performs one or more of these functions [27].

The packaging sector represents about 2% of the gross national product (GNP) in developed countries, and about half of all packaging is used to package food [25]. According to Guillard et al. (2018) [28], packaging has been identified as an essential element to address the key challenge of sustainable food consumption. The primary fundamental role of food packaging is to maintain the quality and safety of food products during storage and transportation, controlling gas and vapor exchanges with the external atmosphere, thus extending the food product shelf-life and avoiding unfavorable factors or conditions, such as chemical contaminants, spoilage microorganisms, oxygen, moisture, light, physical damage, etc. [29]. To perform such functions, the packaging provides a physical barrier between the outside environment and the food, creating the physicochemical conditions that are essential for obtaining a satisfactory shelf life and maintaining food quality and safety [30]. It can also be mentioned, as a secondary role, that packaging is used to attract customers while products are on the shelf. Companies spend millions of dollars every year using packaging as a

form of marketing. Figure 1.1 - shows the primary functions required for food packaging materials.

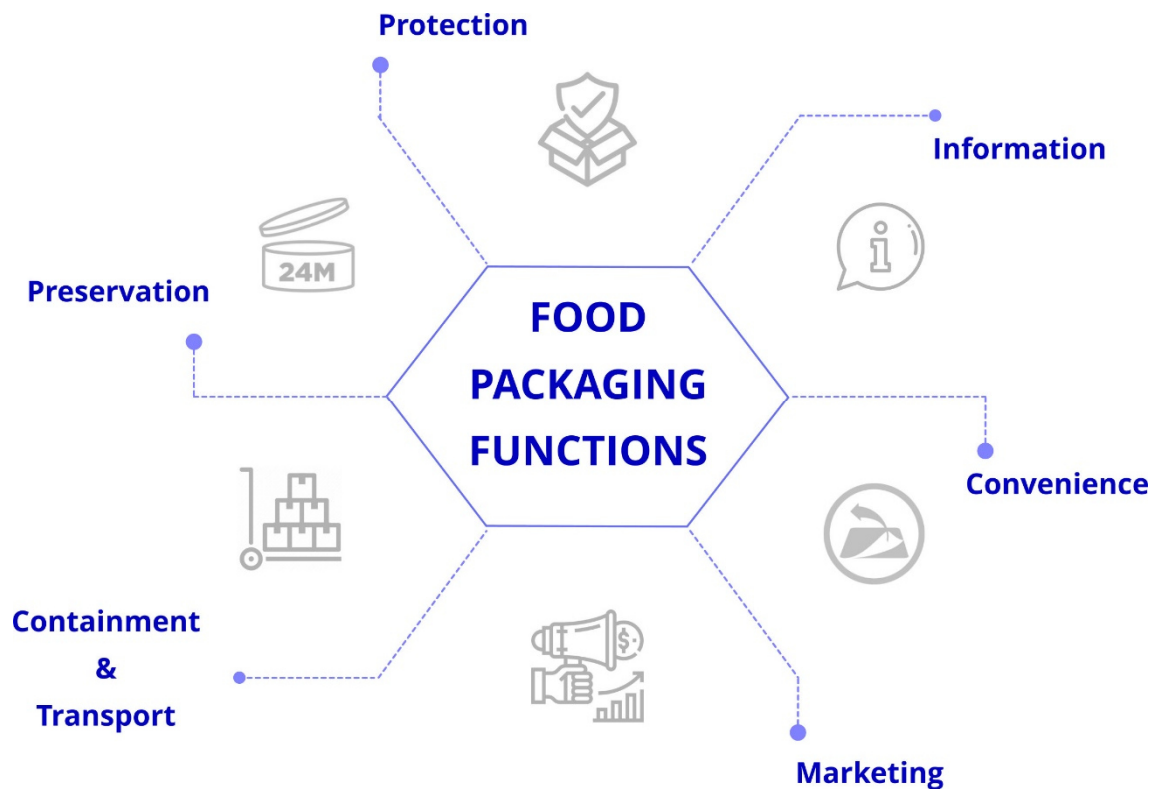


Figure 1.1 - Primary functions of food packaging.

1.1 Impact of food losses and waste on sustainability

Food packaging plays a significant role in terms of global food waste reduction thanks to reducing damage in transport and handling, as well as shelf life extension, especially by using a well-designed packaging system adapted to the food in terms of presentation [31]. According to the Swedish Institute for Food and Biotechnology, report for Food and Agriculture Organization (FAO) of the United Nations [32], almost 30 percent of all food produced for human consumption, approximately 1.3 billion tons per year, are either lost or wasted globally. In a context of uncertainties about the capacity of ecosystems and natural resources to sustain an increasing demand for foods, food losses and waste are at the same time a waste of resources and an environmental issue and represent a symbol of inefficiency, unfairness, and unsustainability of the food

chain. Therefore, reduce them is a priority to improve the sustainability of food systems.

Sustainable food systems are defined as “*food systems that ensure food security and nutrition for all in such a way that the economic, social, and environmental bases to generate food security and nutrition for the future generations are not compromise*” [32]. The subject was highlighted in the United Nations Conference on Sustainable Development (Rio+20) in 2012 [33], which connected the food loss and waste reduction to the issue of more sustainable food systems. In 2016, the European Commission set a target to reduce by 50% the food waste in Europe by 2030 [34], mobilizing a vast range of disciplines, from biology of food products and conservation technologies to organization and economics of food chains and markets, as well as consumer behavior. Figure 1.2 presents the food loss and waste that occur along the entire food chain.

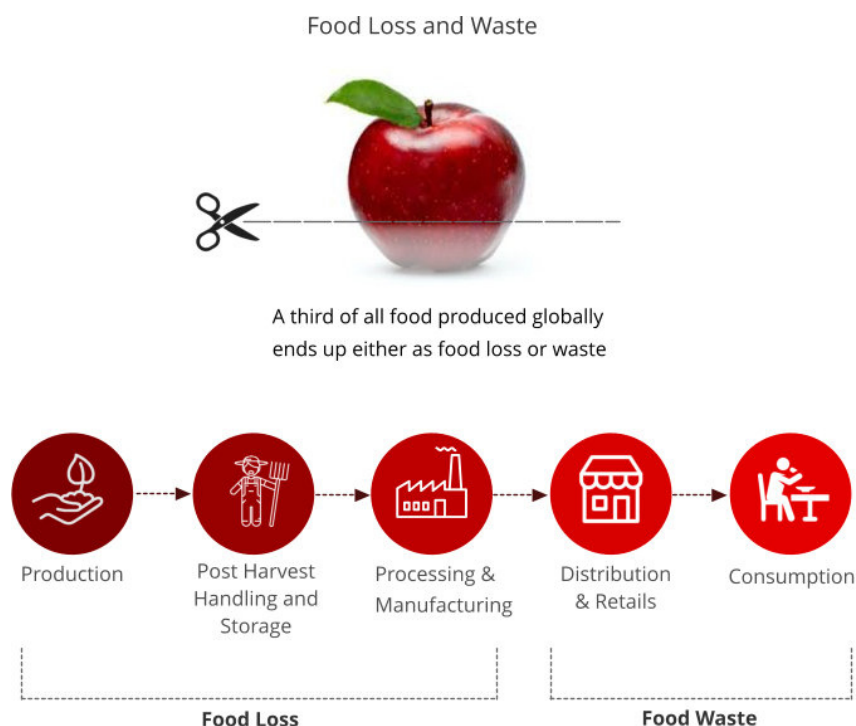


Figure 1.2 - Food loss and waste that occur along the entire food chain.

1.2 Plastic food packaging

The most common materials used for food packaging are plastic, glass, paper and paperboard, and metals. Plastic is currently the most well-known food

packaging material [24], which is a specific type of polymer, synthetic or natural, classified either as thermoset polymers (solidify into a permanent design and shape) or thermoplastic polymers (flows upon application of heat and/or pressure). Polymers are macromolecules composed of many repeating units, called meros (single units) connected by covalent bonds in a variety of ways [35]. In our plastic-based economy, plastic packaging materials are most time referred to as those made from petrochemicals.

In 2018, the worldwide annual plastics manufacturing reached 359 million metric tons, with 62 million metric tons produced in Europe only [36]. More than 40% of all plastics are used in the packaging sector, and almost half of them are used for food packaging (Figure 1.3). In Europe, 23 million tons of plastic packaging are produced each year (92 million tons expected in 2050) [32] in a wide range of forms, such as films, sheets, bottles, cups, tubs, and trays, etc. The different types of plastic packaging can provide choices with respect to transparency, color, print, footprint, and heat sealing and can offer specific features regarding durability, shelf life, lightweight, temperature range – they can be used for hot and cold filling and microwave reheating, and barrier properties against water, carbon dioxide, oxygen and nitrogen [37]. Polyethylene (PE) have been used in packaging since the late 1940s and is the most widely used plastic today, followed by poly(ethylene terephthalate) (PET), polypropylene (PP), polystyrene (PS), and poly(vinyl chloride) (PVC) [38].

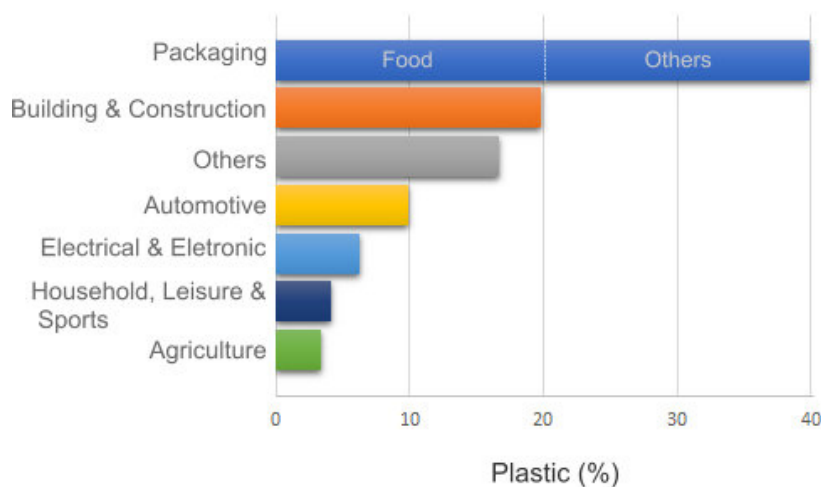


Figure 1.3 - Plastic demand by segment in 2018 (adapted from [36]).

Plastic packaging volumes are expected to continuously increasing, quadrupling by 2050, to 318 million tons annually [39]. However, plastic waste – especially from food packaging designed for single or short-term use, i.e. packaging or other consumer products that are thrown away after one brief use, results nowadays in an over-accumulation of non-degradable materials on land and seas, becoming a global threat to our environment [40]. It is estimated that 72% of plastic packaging is not recovered at all: 40% ends up in landfills, corresponding to 9 million tons of waste that are accumulates in the soil, and 32% leak out of collecting system and finally end in the soil and oceans [39]. The presence of hundreds of millions of tons of plastics and microplastics (micro- and nano-sized particles) in the ocean has caused negative impacts on the economic activities in the marine ecosystems [40]. The United Nations Environment Programme (UNEP) estimates that damage to marine environments is at least UDS 8 billion per year globally [41]. Additionally, in 2006, only 14% of plastic packaging were collected for recycling and only 5% of the original material value were retained for subsequent use, while 14% were sent to incineration and/or energy recovery process [39]. However, the recycling rate has been increasing over the years, encouraged by a favorable regulation and Circular Economy (CE) models.

CE models are described as economic systems “*where the value of products, materials, and resources is maintained in the economy as long as possible, and the generation of waste is minimal*” [42]. In this context, 42% of plastic packaging waste was recycled in the European Union (EU) in 2017, but this trend was observed at varying levels in all EU Member States, for example, only 27% of plastic waste were recycled in France [43]. The European Commission identifies plastic waste as a key priority in its Action Plan for the CE and in 2030, 65% of municipal waste and 70% of packaging waste should be recycled [42].

In the case of Brazil, according to a report published in 2019 by the World Wildlife Fund (WWF), the country ranks as the fourth global plastic waste producer, with 11.3 billion tons. Out of this total, WWF states that 91% are

collected, but only 1.28% is effectively reinserted in the production chain, which is below the global average of 9% [44].

Plastic is essential in modern economies, and also, the plastic used for packaging is almost exclusively single-use, especially in business-to-consumer applications. The current way by which plastics are produced, used, and discarded fails to capture the economic benefits and is dramatically harming the environment [45]. However, recycling is not a unique solution for the plastic economy issue. The challenges associated with the entire plastic chain can be turned into opportunities for innovation, sustainability, competitiveness, and job creation. Bio-based and biodegradable plastics can play a key role in achieving a sustainable model, as they can contribute to reduce greenhouse gas emissions and the demand for fossil resources.

1.3 Main properties of food packaging materials

Effective food packaging is designed by identifying the product requirements. The choice should take into account the product nature, use, distribution and storage, expiration date and packaging disposal, as well as environmental and waste management issues. Furthermore, ensuring food safety concerning biological risks and needs relating to flavor, color, and texture of the food is essential. In this context, the main properties evaluated in food packaging are listed below:

1.3.1 Permeability properties

The permeability properties, also called barrier properties, indicate the resistance of food packaging materials to sorption and diffusion of substances (mass transfers of gases, water vapor, aroma compounds, and other low molecular weight compounds). Barrier properties play a major role in the control of food degradation reactions by defining around the product an atmosphere whose composition is favorable to the slowing down of the reactions. Unfortunately, a single packaging material rarely fully meets all the food requirements. According to Guillard et al. (2018) [28], the barrier properties are

either too low (case of O₂ -sensitive food products for which high O₂ barrier packaging is queried) or too high. They cite, for example, the case of respiring products such as fresh fruits and vegetables, where the plastic films are perforated to compensate for their high O₂ barrier properties.

The protection of food from vapor and gas exchange with the environment depends on several factors, including food contact and environmental conditions (temperature, pH, relative humidity), film structure and permeability, thickness, area, difference in pressure or concentration gradient across the film [46]. There are two processes by which vapor and gases (permeants) may pass through materials – pore effect and solubility-diffusion effect. In the pore effect, the permeant flow through the microscopic pores, pinholes, and cracks in the material structure. The porosity falls very sharply as the thickness of the materials increases, reaching practically zero with many of the thicker types of commercially available materials. Yet in the solubility-diffusion effect, described as true permeability, the permeant dissolves in the film surface, diffuses through the film matrix, driven by the concentration gradient, and evaporates at the other film surface. The first step depends on the solubility of the specific gas in the polymer and influences the diffusivity of gases across the material, and the second step, relates to the diffusion itself, which depends on the size, and shape, and polarity of the permeant, and the crystallinity, cross-linking degree of and polymer chain segmental motion of the polymer matrix. This process is shown diagrammatically in Figure 1.4.

The true permeability is normally associated with the quantitative evaluation of the barrier properties of materials. In a material without pore defects, the primary mechanism for vapor and gases flow through a film is an active diffusion. A material that is a good barrier to gas/water vapor diffusion has a low permeability. The permeability is inversely proportional to the material thickness [47].

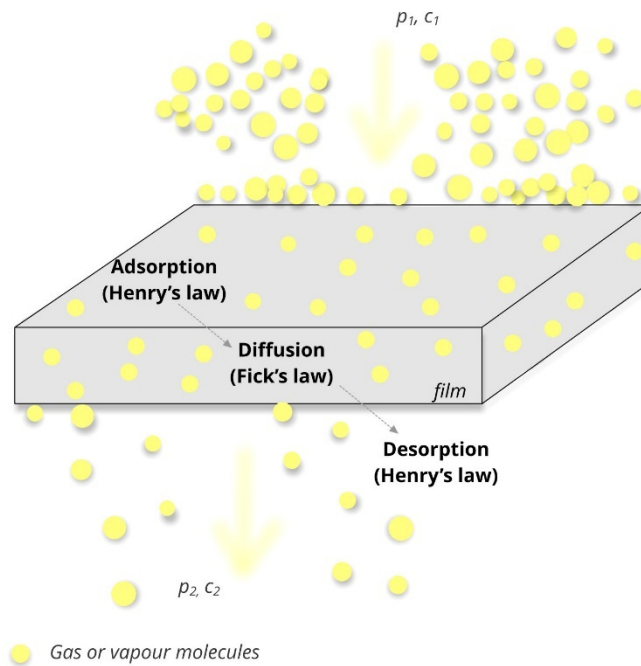


Figure 1.4 - General mechanism of gas or vapor permeation through a polymer packaging film.

The gas permeation mechanism is described by the Henry's and Fick's law by which the equations that relate the permeation rate with the area and thickness of the film are obtained [47]. The calculation of transport rate density (flux) is proportional to the permeant potential gradient, as shown in Equation 1.

$$-\frac{1}{A} \cdot \frac{dM}{dt} = K \frac{d\phi}{dx} \quad \text{Eq. 1}$$

In words: $TR = \frac{\text{amount of set}}{\text{area} \times \text{time}}$

Where A is the area, m is the amount of set, t is the time, ϕ is the potential, x is the length, K is the coefficient and TR is the transmission rate through the film and the SI units are $\text{kg} \cdot \text{m}^{-2} \cdot \text{s}^{-1}$.

The permeability coefficient (P) is calculated using the following Equation 2.

$$P = \frac{TR \times l}{\Delta p} \quad \text{Eq. 2}$$

Where l is the film thickness and Δp is the partial pressure gradient across the film. The SI units for P are $\text{kg} \cdot \text{s}^{-1} \cdot \text{m}^{-2} \cdot \text{Pa}$.

The most important barrier properties of polymer films used in food packaging are water vapor permeability and oxygen transmission rate. The water vapor barrier is quantified by the Water Vapor Transmission Rate (WVTR), which indicates the amount of water vapor that permeates a unit area of packaging film and in a time and it is expressed in $\text{cm}^3/\text{m}^2 \cdot \text{s}$ or $\text{g}/\text{m}^2 \cdot \text{day}$. The water vapor barrier properties for food packaged products are related to its equilibrium moisture content and are of great importance for maintaining or extending their shelf life. It is important to avoid dehydration in fresh food, while for bakery or delicatessen it is important to avoid water absorption.

The Oxygen Transmission Rate (OTR) indicates the amount of oxygen that permeates a packaging film per unit of area and time, expressed in $\text{cm}^3/\text{m}^2 \cdot \text{day}$. The oxygen barrier plays an important role in the oxidation of packed food (fruits, salad, ready-to-eat meals, etc.). Polymer films with low oxygen permeability rate delay the oxidation and extend the food shelf life. Figures 1.5 and 1.6 shows the packaging barrier requirements for different foods and the barrier properties of different polymers, respectively.

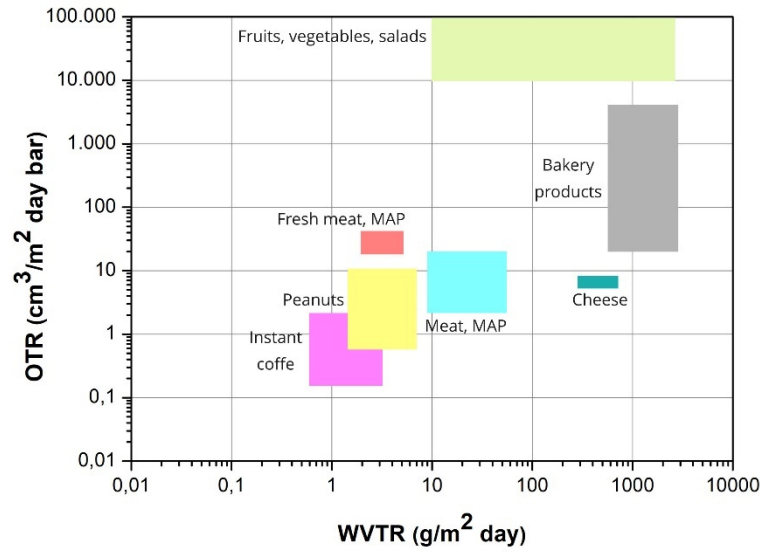


Figure 1.5 - Requirements on packaging for different foods (adapted from [48])

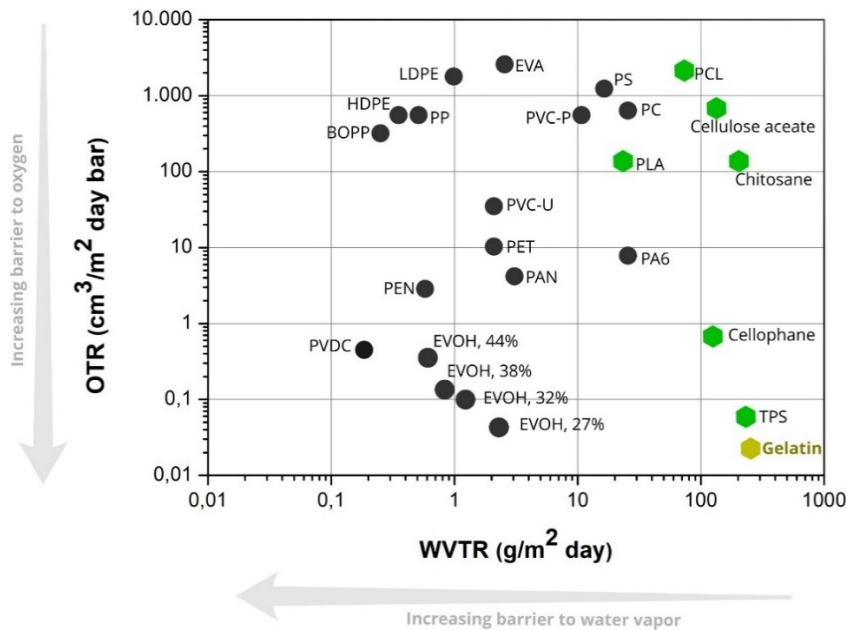


Figure 1.6 - Comparison of water vapor and oxygen transmission rate of conventional plastics (grey) and biopolymers (green) at 23°C. (source: [49][48] [50] [51]). Abbreviation: LDPE: low density polyethylene; HDPE: high density polyethylene; PET: polyethylene terephthalate; PEN: polyethylene naphthalate BOPP: biaxially oriented polypropylene; PP: polypropylene; PVDC: polyvinylidene chloride; EVOH: ethylene vinyl alcohol; EVA: ethylene-vinyl acetate; PVC-P: polyvinyl chloride plasticized PVC-U: polyvinyl chloride unplasticized; PS: polystyrene; PAN: polyacrylonitrile; PC: polycarbonate PCL: polycaprolactone; PLA: polylactic acid; TPS: thermoplastic starch.

1.3.2 Mechanical properties

The feasibility of commercial utilization of packaging films also depends on the mechanical properties. Tensile properties are composed of the reaction of the materials to resist when tensile forces are applied. Tensile properties are determined by tensile testing and provide information about the modulus of elasticity (EM), also called Young's modulus, that measure the tensile stiffness of solid material and is determined by the pulling force/area to film stretching degree ratio (Equation 3); tensile strength (TS) – maximum pulling force per film cross-sectional area that a material can support without fracture when being stretched (Equation 4); and elongation at break (EAB) – stretching ability before breaking (Equation 5) [52]. These properties are used to predict the performance of packaging films upon handling and storage.

$$TS = \frac{F}{A_0} \quad \text{Eq. 3}$$

$$EAB = \frac{(L-L_0)}{L_0} \quad \text{Eq. 4}$$

$$EM = \frac{\lim_{EAB \rightarrow 0} TS}{EAB} \quad \text{Eq. 5}$$

Where F is the maximum force supported, L_0 is the original length, L is the axial deformation at rupture and A_0 is the initial area of cross-section of the film.

1.3.3 Optical properties

The optical properties, such as color and transparency, are essential for packaging materials. These parameters are important and can provide visual evidence of the food content, which directly influences the consumer purchasing decision [53]. If films are colorless, then they are generally accepted by consumers. Besides, packaging with a high light barrier (low UV light penetration) has received special attention due to the protective effect against the oxidative rancidity catalyzed by UV light, especially for oily food [54].

1.3.4 Heat sealing properties

Heat sealing is a process of welding thermoplastic polymer surfaces together in order to produce seals or joints of sufficient strength to withstand stresses in the distribution and consumer environment. A seal can be non-peelable (tearable) or peelable (so-called easy open) [25]. The heat sealability of a packaging film is essential for maintaining the desired gas composition within the pack, avoid contamination, and have a direct impact on the food shelf life. Additionally, the seal must be strong enough to withstand the rigors of shipping and handling. Heat sealable films are those films that can be bonded together by the normal application of heat, such as by conductance from a heavy heat-resistant metal bar. A range of polymers can be heat sealed, such as PE, PP, PS, PLA, PVC, etc. [25].

2 Bio-based and biodegradable materials: definitions

Bio-based and biodegradable materials have gained attention on the food market over the last decades as alternatives for the classical petrochemical-based plastic packaging materials, especially for short-time and disposable packaging applications [55]. This is a consequence of the environmental concerns, as well as the advances in material science and processing technologies.

According to a statement of the European Bioplastics Organization (EUBP) [56], bioplastic is the word used to indicate plastics (1) that are biodegradable, (2) come from renewable resources (bio-based), or (3) that have these both features. Bio-based plastics or biopolymers are polymers produced from renewable sources: (i) natural polymers such as starch, alginate, cellulose, chitosan, proteins, etc. and, (ii) synthetic polymers such poly(lactic acid) (PLA), polyhydroxybutyrate (PHB) and its copolymers, etc. Most of bio-sourced plastics are biodegradable, such as starch, cellulose, PLA, PHB, etc. However, bio-based plastics are not always biodegradable or home-compostable, for example, the PE produced from sugar cane, also called green PE or bio-PE, and other commodities like bio-PVC, bio-PET, or bio-PP.

The International Union of Pure and Applied Chemistry (IUPAC) states that biodegradable polymers refer to “*macromolecules or polymeric substances susceptible to degradation by biological activity by lowering the molar mass of macromolecules that form the substance*” [57]. In other words, they are materials that undergo a biochemical process, in which microorganisms (yeast, bacteria, and fungi) metabolize the material into water, carbon dioxide, methane, and others [58]. This phenomenon can occur both under aerobic and anaerobic conditions and several factors such as moisture, pH, and oxygen availability, determine the rate and the final products of the biodegradation process [59]. Biodegradation leads to fragmentation or disintegration of the polymers with no toxic or environmentally harmful residues. The material biodegradability depends on its chemical structure and molecular weight, and not on its feedstock type [60]. This is the case of poly(ϵ -caprolactone) (PCL) and poly(butylene adipate terephthalate) (PBAT). These polymers are biodegradable and derived from petroleum. It should be emphasized that biodegradability is different from compostability. The term compostability refers to the aerobic process, including the level of biodegradation, timeframe, surrounding conditions, and the safety of final products (ISO 17088, EN 13432, EN 14995, or ASTM D6868) [59].

To illustrate the distinctions between the various types of plastics (bioplastic and conventional plastics), the EUBP has provided a simple two-axis model that encompasses the plastic types, classified according to the raw material source (bio-based or petrochemicals-based) and functionality (biodegradable or non-biodegradable) (Figure 1.7).

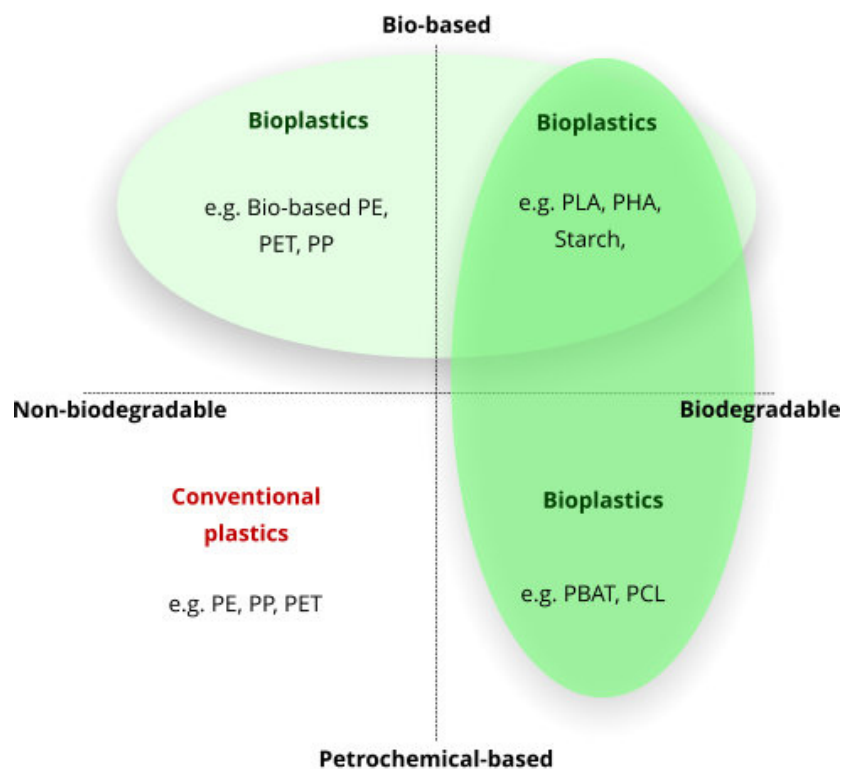


Figure 1.7 - Overview of all plastics types, classified according to raw material source and functionality (adapted from EUBP [56]).

The global bioplastic production is expected to increase from 2.11 million tons in 2019 to approximately 2.43 million tons in 2024 [56]. Compared to the annual production capacity of 359 million tons of conventional plastics [36], the bioplastics represent a very small share of the market. Nevertheless, the demand for sophisticated bioplastics, applications, and products is increasing, the bioplastics market is, therefore, expected to grow continuously.

Currently, 25% of the global bioplastic production capacity is located in Europe, but Asia continues to be the major production hub with 45% of the total bioplastics production. According to EUBP [56], biodegradable plastics as a whole, including PLA, PHA, starch blends, and others, account for over 55.5% (over one million tons) of the global bioplastic production capacity. The production of biodegradable plastics is expected to increase to 1.33 million by 2024.

It is known that not all applications should be made from bioplastic, but several key products and applications can amplify the benefits and contributions of biodegradable plastics to prevent and reduce waste. Bioplastics are used in an

increasing number of markets and the portfolio of applications continues to diversify. Segments, such as automotive, transport, and building and construction, significantly increased their share (Figure 1.8). However, packaging remains as the largest field of application for bioplastics with more than 53% (1.14 million tonnes) of the total bioplastics market in 2019, and almost half of them were made from biodegradable bioplastics [56].

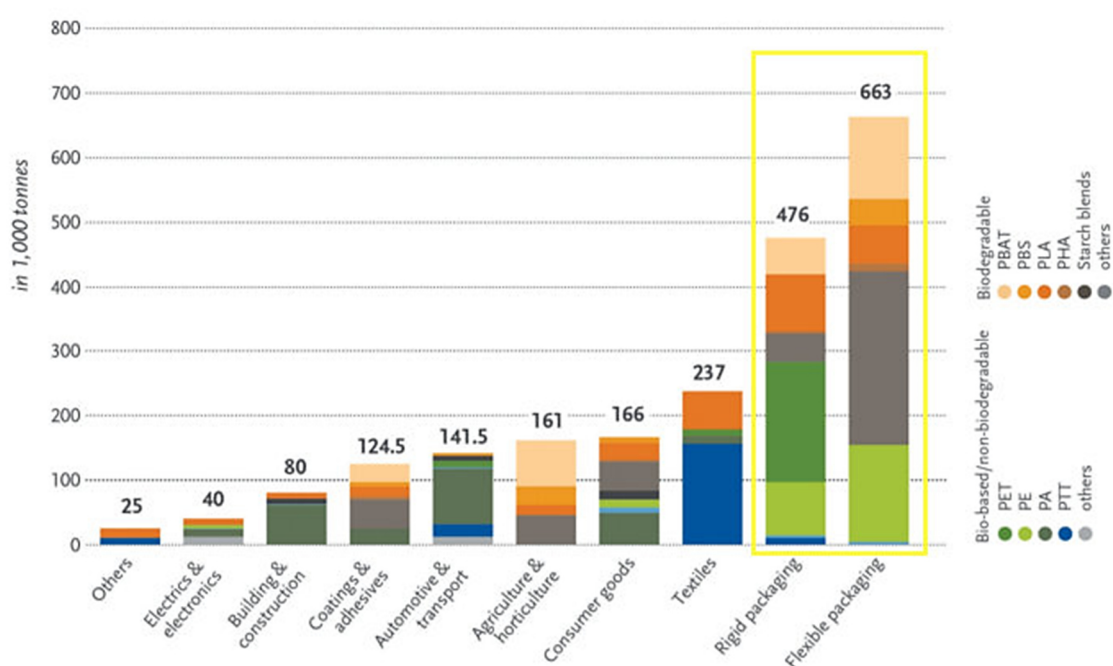


Figure 1.8 - Global production capacities of bioplastics by market segment in 2019 (source: <https://www.european-bioplastics.org/market/> [56])

Biodegradable plastics can be used as flexible or rigid packaging in the food industry. Flexible packaging such as films is applied in a variety of foods, and are particularly suitable for fresh products, such as fruit and vegetables [61]. For instance, searching on the ACS SciFinder tool concerning the last 20 years, with the following keywords: biodegradable and food packaging, 2335 articles, and 1328 patents were found (done September in 2020) proving the dynamic research in the field (Figure 1.9).

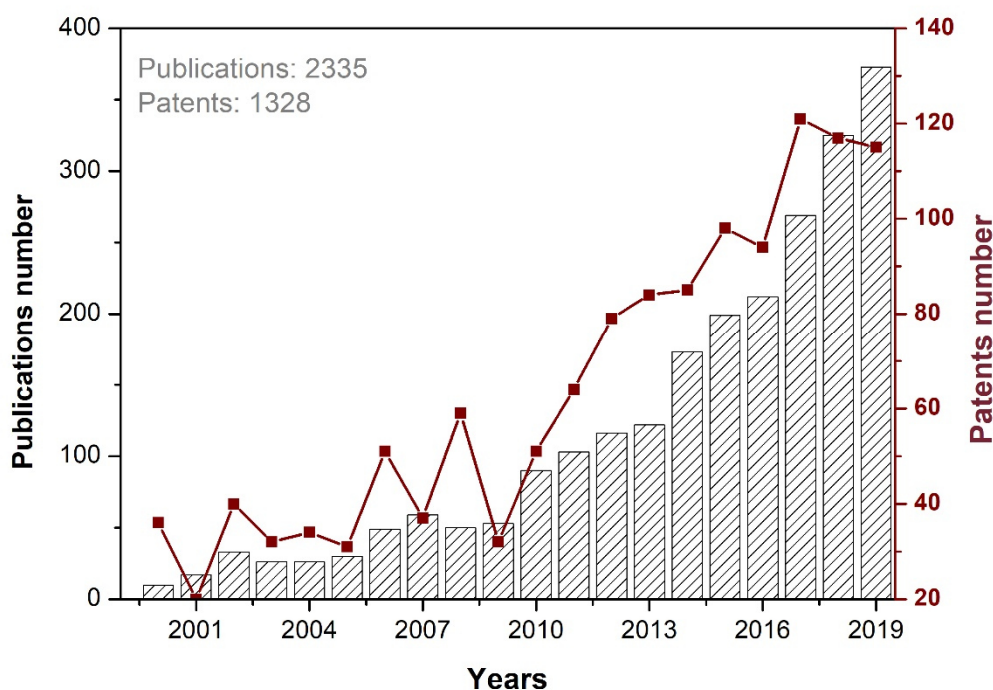


Figure 1.9 - Publications extracted from ACS SciFinder in September 2020 with keywords: biodegradable and food packaging.

2.1 Bio-based plastics: competition with food production

The land used to grow the renewable feedstock for bioplastics production, as reported by the EUBP [56], corresponds to approximately 0.79 million hectares in 2019, which represents 0.02% of the global agricultural area (4.8 billion hectares). Nowadays the area for biofuel production is equivalent to 1% of the global agricultural area. Despite the expected market growth for the next five years, the share of land use for bioplastics will remain around 0.02% (1.00 million hectares by 2024). This clearly shows that there is no competition between renewable raw materials for food, feed, and the production of bioplastics. Besides, bioplastic can use the marginal land (areas not suitable for food production), and, mainly, residual and co-products from agriculture and forestry.

2.2 Natural polymers

In general, natural polymers applied in food packaging are derived from biomass, mainly polysaccharides (starch, chitosan, cellulose, pectin, carrageenan, alginate, etc.) and proteins (collagen, soy isolate, whey, etc.). From a sustainability perspective, they are advantageous over petroleum-derived biodegradable polymers because, in principle, biomass is a vastly abundant resource on earth. A comprehensive classification of natural polymers currently used in food packaging is summarized in Table 1.1.

Table 1.1 - Common biodegradable materials used in food packaging applications (adapted from [37]).

Natural polymers	Sources	Examples
Polysaccharide	Plant/algal	Starch, cellulose, pectin, konjac, alginate, carrageenan, gums
	Animal	Hyaluronic acid, chitosan/chitin
	Fungal	Pullulan, elsinan, scleroglucan
	Bacterial	Chitin/chitosan, levan, xanthan, polygalactosamine, curdlan, gellan, dextran, bacterial cellulose
Protein	Plant	Soybean, zein, wheat gluten, resilin, polylysine, polyamino acids, poly(g-glutamic acid), elastin, fibrin gel, polyarginyl-polyaspartic
	Animal	Collagen/gelatin, casein, serum, albumin, silks whey,

In general, polysaccharide-based have selective permeability to carbon dioxide and oxygen molecules, due to their the tightly-packed network structure, but they are also highly permeable to water vapor, are water sensitive, and present moderate to low mechanical properties, especially in high relative humidity environments. Several factors should be taken into consideration for the development of bio-based packaging from natural polymers. Figure 1.10 presents some advantages and disadvantages of some natural polymers used for food packaging.




Natural Biodegradable Polymers				
	Raw material	Advantages	Disadvantages	Application (coating or films)
Polysaccharides	Starch 	Availability Relatively cheap cost	Hydrophilic character Poor mechanical properties Brittleness Retrogradation	Fresh-cut (apples and mango) Strawberries, pumpkin, papaya, walnut Frozen dough Roasted turkey Red crimson grapes Chicken breast fillets
	Chitosan 	Antimicrobial and antifungal activity Good mechanical properties	Brittleness, Low thermal stability High water vapor permeability	Cheese Semi-hard cheese Fresh-cut asparagus, baby corn Cabbage, red bell peppers, tuna fillets Shrimps Cooked pork, pork meat patties,
Protein	Gelatin 	Excellent film-forming capacity Excellent oxygen and carbon dioxide barrier Low cost	High sensitivity to moisture High water vapor permeability, Brittleness,	Fruit and vegetables (banana, fuji apples, red crimson grapes, strawberries, cherry tomatoes, red bell peppers, fresh-cut oranges) Beef, ground beef patties, microwaved beef Chicken breast fillets, chicken tenderloin, pork sausages Cold-smoked salmon, fresh smooth omelette fillets, rainbow trout slices, tuna fillets, shrimp, mackerel meat powder Brazil nut and Cashew nut

Figure 1.10 - Advantages and disadvantages of natural polymers and applications (source: [62] [63][37] [64][65]).

The two next sub-chapters are dedicated to gelatin and cellulose nanocrystals that are both naturally occurring bio-based materials of importance for this Ph.D. work. A more detailed review of their physicochemical properties and food packaging applications is thus presented.

2.2.1 Protein

Proteins are renewable natural macromolecules synthesized by animals (casein, collagen, silk fibroin, etc.) plants (soy protein, zein, wheat proteins, etc.), and bacteria (lactate dehydrogenase, chymotrypsin, fumarase, etc.). They are composed of up to twenty different amino acid residues, which can be characterized as polar, non-polar, aromatic, anionic, and cationic (Figure 1.11)

[66]. Due to the amphoteric nature of amino acids, protein can act as acids (the carboxyl group is able to lose a proton) or alkali (the amine group is able to accept a proton), or both at the same time, leading to the well-known *zwitterionic* form of amino acids [67]. The diversity of amino acid composition and sequence leads to the different structures, conformations, and functionality of proteins. The structure of proteins is organized in four levels and are distinguished from one another by the degree of complexity in the polypeptide chain conformation [67], as shown in Figure 1.11.

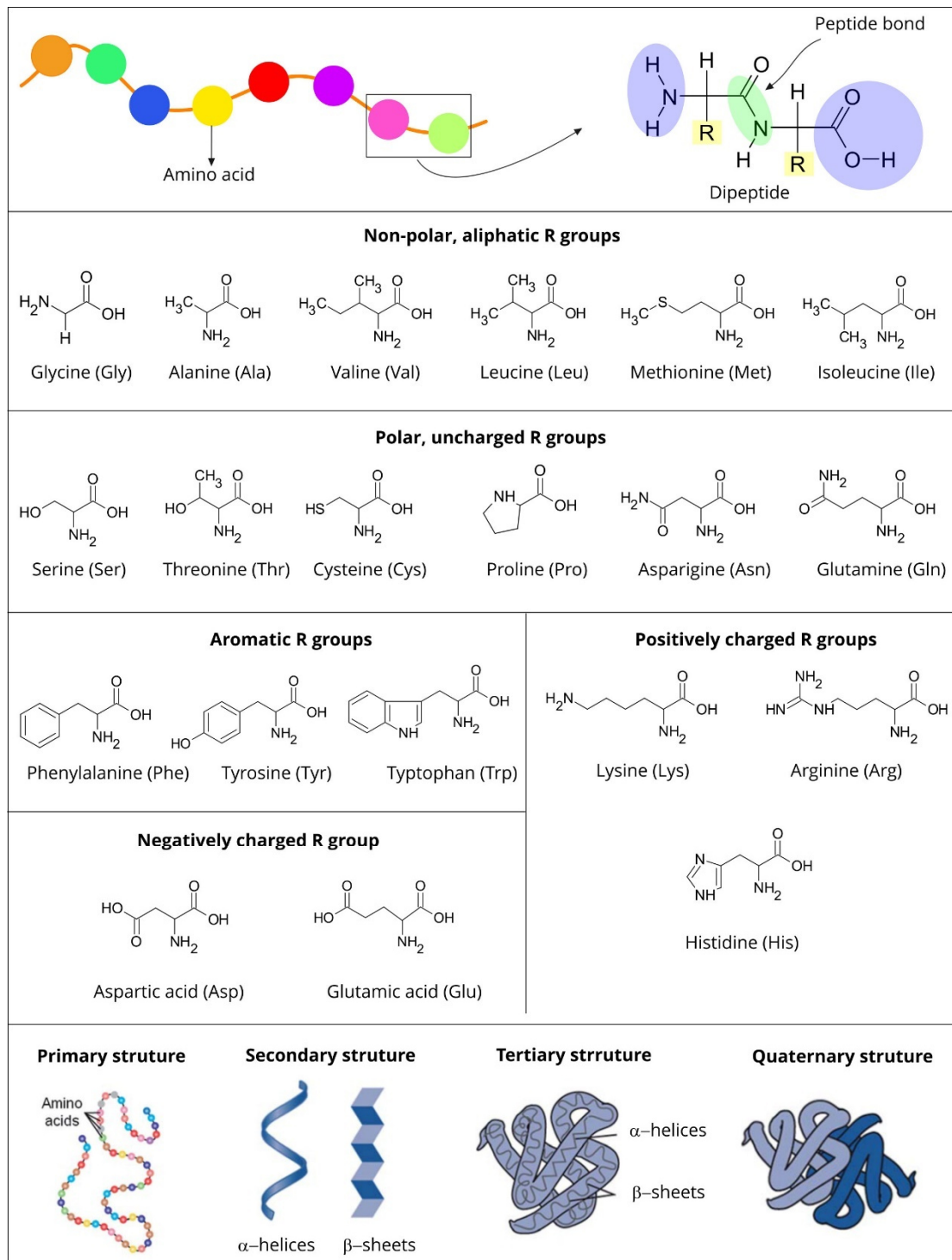


Figure 1.11 - Amino acid residues, peptide bonds, and levels of protein organization (adapted from [67]).

The primary structure is related to the linear amino acid sequence in the protein chain. This sequence is formed by linkages between the α -carboxyl group

of one amino acid and the α -amino group of another amino acid by a peptide bond (also called an amide bond). The order of amino acids in a polypeptide chain is unique and specific to a particular protein. The secondary structure of proteins refers to the spatial conformation of the primary structure. The two most important secondary structures of proteins are α -helices and β -sheets. The α -helix structure is formed by hydrogen bonding between the amino groups and the carbonyl oxygen of the fourth amino acid on the amino terminal side of the peptide bond. The β -sheets structure appears to be folded or pleated, and it is held together by hydrogen bonding between polypeptide units of the folded chain that lie adjacent to one another [67].

The tertiary structure refers to the three-dimensional structure of the polypeptide chain of a protein, which is generally stabilized by nonlocal interactions, salt bridges, hydrogen bonding, and disulfide bonds between thiol groups (-SH) from cysteine units. These tertiary structures can further associate with non-covalent bonding into more complex assemblies called quaternary structures (specific association of multiple polypeptide chains).

Proteins are currently being investigated to prepare edible and non-edible films due to their good functional properties as a food packaging material and biodegradability [68]. Proteins confer a wide range of functional properties, especially a high potential to form intermolecular bonds in different positions, due to their unique structure that can be modulated by pH [69]. Protein-based films display excellent barrier properties against carbon dioxide and oxygen, as well as moderate mechanical properties when compared with polysaccharide films [70].

2.2.1.1 Gelatin

Gelatin is a water-soluble protein derived from collagen [68]. Collagen is one of the most abundant animal proteins [71]. This protein is present in the skin, tendons, bone, cartilage, and most of the internal organs of animals, providing structural and mechanical support to the tissues. This fibrous protein is formed by individual chains held in a triple helix suprastructure by non-covalent

interactions. Collagen differs from gelatin due to the far more tertiary structures, leading to a lower aqueous solubility [6].

Converting insoluble native collagen into gelatin requires pre-treatments involving acidic or alkaline conditions, to breakdown the non-covalent bonds and disorganize the protein structure, allowing swelling and cleavage of intra and intermolecular bonds to solubilize the collagen. Subsequent heat treatment up to 45 °C cleaves the hydrogen and covalent bonds to destabilize the triple helix, resulting in helix-to-coil transition and conversion into soluble gelatin [72].

Gelatin can form homogeneous gels for concentrations in the range of about 1-50%. When a gelatin solution is cooled below the sol-gel transition temperature, the coil molecules form triple-chain helices through the renaturation of collagen-like spirals, and the solution transforms into a three-dimensional gel network (Figure 1.12). Since the transition is physical such as hydrogen and Van der Waals bonds, the gelatin process is thermoreversible [73].

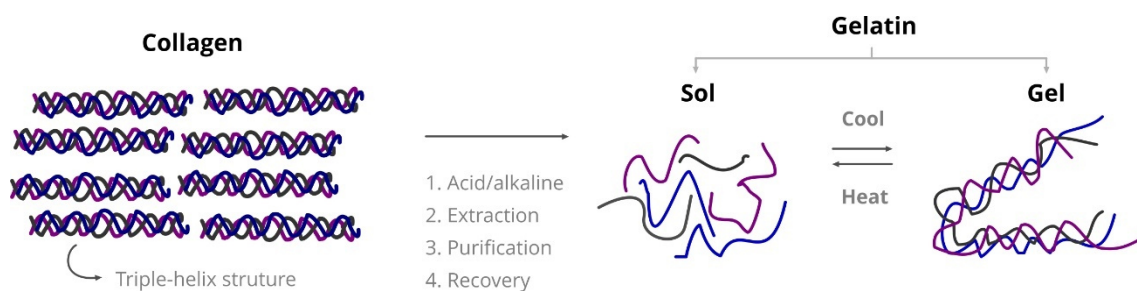


Figure 1.12 - Conversion of insoluble native collagen into soluble gelatin (adapted from [74]).

Gelatin is a combination of hydrolysate macromolecule chains with different molecular weights including α -chains (80-125 kDa), β -chains (160-250 kDa), and other low molecular substances [75]. Gelatin chains are made up of 18 specific amino acids. Table 1.2 shows the amino acid composition of different sources of gelatin. Glycine (Gly), proline (Pro), and hydroxyproline (Hyp) are the most dominant amino acids and represent almost two-thirds of the total amino acid constituents [75].

Table 1.2 - Amino acid composition (expressed as no. residues/1000 residues) from various sources of gelatin.

Amino acid	Bovine skin [76]	Pork skin [77]	Tilapia [78]
Alanine (Ala)	81	112	123
Arginine (Arg)	52	49	47
Aspartic acid (Asp)	32	46	48
Cystine (Cys)	5	0	
Glutamic acid (Glu)	54	72	69
Glycine (Gly)	365	330	347
Histidine (His)	-	4	6
Hydroxylysine (Hyl)	-	6	8
Hydroxyproline (Hyp)	102	91	79
Isoleucine (Ile)	10	10	8
Leucine (Leu)	19	24	23
Lysine (Lys)	49	27	25
Methionine (Met)	2	4	9
Phenylalanine (Phe)	16	14	13
Proline (Pro)	101	132	119
Serine (Ser)	29	35	35
Threonine (The)	8	18	24
Tyrosine (Tyr)	11	3	2
Valine (Val)	20	26	15

The gelatin quality parameters such as molecular weight, rheological properties, isoelectric point (IEP), and Bloom strength depend on the source, animal age, collagen type, and processing conditions (e.g., pH, temperature, and extraction time) [79]. Gelatins obtained under acidic and alkaline pre-treatment conditions give rise to type A gelatin (IEP at pH 8-9) and type B gelatin (IEP at pH 4.5-6.0), respectively [80]. The Bloom strength or resistance of a gel is a measure of its hardness, consistency, firmness, and compressibility at a certain temperature. Bloom strength refers to the number of grams required for a 0.5 inch diameter probe to deflect a set gel by 4 mm at 10 °C without breaking it. This property is largely dependent on (i) the amino acid composition and (ii) the molecular weight distribution [79]. The Bloom index for commercial gelatin varies from lower bloom (50-125), medium bloom (175-225), and high bloom gelatin (225-325) [81,82].

The growing applications in food and beverage, pharmaceuticals, cosmetics, and nutraceuticals industries are responsible for the growing demand for gelatin. The global gelatin market is around 300,000 tons per year and is valued at close to USD 3 billion [83]. According to Mordor Intelligence market research company, it is expected to register a compound annual growth rate (CAGR) of 4.13% during the forecast period of 2020-2025 [84]. Europe is the largest gelatin consumption region and accounted for approximately 40% of the global revenue in 2019 [85].

2.2.1.2 Gelatin-based films for food packaging

Gelatin has attracted much attention as an alternative plastic material due to its abundance, low cost, biodegradability, excellent gelling properties, ability to form films and non-toxicity that poses no hazard for food contact applications. However, gelatin films are mechanically weak and brittle [64]. To overcome this problem, plasticizers are added to gelatin films. Plasticizers are low volatility molecules that are added to polymers to increase their extensibility, flexibility, and toughness, lowering the glass transition temperature and reducing the polymer-polymer interactions and molecular cohesion [86]. Polyols such as glycerol and sorbitol are commonly applied plasticizers for gelatin-based films. These

plasticizers are added to the film-forming solution at approximately 10-60% on a dry basis [87]. Nevertheless, these plasticizers have hydrophilic groups (-OH) that are known to increase water vapor permeability and decrease the film strength, and this effect is directly related to plasticizer concentration [87].

Gelatin-based films can be made from a variety of sources with the most commonly used forms in food packaging derived from porcine [88], fish [89], and bovine [90] tissues. The physicochemical properties of gelatin films depend on the gelatin source, film manufacturing conditions (concentration, solvent, pH, temperature, drying time), and type and concentration of additives (plasticizer, reinforcement, crosslinkers). Having said this, data from the scientific literature are not readily comparable since methodologies may differ considerably from one work to another. The physical properties of gelatin-based films are shown in Table 1.3.

Table 1.3 - Physical-chemical properties of gelatin-based films.

Matrix film	Additive	TS (MPa)	EAB (%)	WVP (g mm/h m ² kPa)	Solubility (%)	Ref.
Gelatin		74.2	5.26			[91]
Gelatin/starch + 10% Gly			11.13 4.47	1.57 1.43	16.52 10.86	[92]
Gelatin/starch + 10% Sor Gly		13.62	38.89	0.873	20.85	[93]
Gelatin + 20% Glycerol	20% SPI	49.45	3.5			
Gelatin + 25% Glycerol	10% MMT	63.6	9.7	0.002		[94]
Gelatin + 30% Glycerol	7% MMT	40.2		0.43		[95]
Gelatin + 25% Glycerol		66.11	1.01	2.81		[96]
Gelatin + 10% Glycerol	30% Starch-BTCAD-NHS -N	48.54	31.3%			[97]
Gelatin + 20% Glycerol	40% CA	35	16	1.16		[98]
Gelatin + 60% Glycerol	0.15% Genipi	4.4	244%	0.88	36.3	[99]
Gelatin + 20% Glycerol	5% Gallic acid	28.34	3.62	0.064		[100]
Gelatin + 20% Glycerol	6% CA	26.35	4.92	0.048		
Gelatin + 25% Glycerol	1.8% GTA	16.13	53.34			[101]
Active packaging						
Gelatin + 20% Glycerol	1% AgNP AgNP+5%TA	3.18 8.12		0.55 0.60	4.3 1.8	[102]

Table 1.3 Continued

Gelatin + 20% Glycerol	5% nano-clay 2% SiO ₂	13.39 12.22	55.72 40.31	1.50 1.94	76 80	[103]
Gelatin/starch + 44% Glycerol	3.5% ZnO	18.69	8.02			[104]
Gelatin + 25% Glycerol	2% curcumin	1.9	176.5	0.32	20.2	[105]
Gelatin/agar + 50% Glycerol	1% nano-clay + 1.5% thymol	36.25	58.04	12.31		[106]
Gelatin + 30% Glycerol	40% chitosan	16.60	25.3	0.410	29.96	[107]
Gelatin + 40% Glycerol	10% TA	75	15.1			[108]
Gelatin + 50% Glycerol	15% TA	23.5	30.8	0.53		[109]
Gelatin + 25% Glycerol	5% carvacrol + 1% GTA	3.2	180	0.34	36	[110]
Gelatin + 30% Glycerol	5% chitin-N + 30% corn oil + 0.6% Tween-80 + 1% GTA	28.08	45.68	2.76	20.75	[111]
Commercial films						
Cellophane				0.22-0.35		[112]
Oriented PP		165	50-75			[112]
HDPE		17-35	300	0.00007		[112]
PET				0.00709	ND	[112]
LDPE		11.4	622.7	0.144	ND	[113]
PVC		44.9	254	0.108	ND	[114]

Abbreviations: WVP: water vapor permeability; TS: tensile strength; EAB: elongation at break; Sor: sorbitol; CA: citric acid; GTA: glutaraldehyde; BTCAD: 1,2,3,4-butanetetracarboxylic acid; NHS, N-hydroxysuccinimide; SPI soy protein isolate; TA: tannic acid; MC: methylcellulose; PP: polypropylene; HDPE: high-density polyethylene; LDPE: low-density polyethylene; PVC: poly(vinylalcohol); PET: poly(ethylene terephthalate).

In general, gelatin films are nearly colorless and display high transparency and excellent UV barrier properties. Gelatin-based films exhibit very low UV light transmission (200-280 nm) (0.01%-30.3% transmission), compared to commercial films such as PVC and LDPE (12.2-87.4% transmission). This is due to the light absorption ability of the disulfide bonds, aromatic amino acids, and carbonyl groups of peptide bonds [64]. Another major advantage of gelatin as a packaging material is its excellent barrier against carbon dioxide and oxygen due to its hydrophilic nature. Avena-Bustillos et al. [115] reported oxygen permeability from 0.2 to 0.7 [(cm³ mm)/(m² d bar)] at 23 °C and 55 % RH for gelatin films from different sources. The hygroscopic nature of gelatin also represents the main drawback of gelatin films. These films are moisture sensitive and exhibit low

mechanical properties and water vapor barrier at high relative humidity [87]. Therefore, new approaches are focused on enhancing the functional properties of gelatin films for augmenting their function as food packaging materials.

The mechanical and water resistance of gelatin films can be enhanced by producing blends or biocomposites with other polysaccharides, proteins, and synthetic plastic. Various types of biopolymers have been mixed with gelatin including soy protein isolate [116], starch [92], pectin [117], chitosan [107], and carboxymethyl cellulose (CMC) [1].

Crosslinking reactions can also improve the physical properties of gelatin films. The crosslinking of proteins can be induced by heating, irradiation (plasma, γ -irradiation, high energy electron beam, etc.), enzymatic (transglutaminase), and chemical crosslinkers [70]. The latter is the most used and involves the formation of covalent bonds between the gelatin chains and the crosslinking agent. Crosslinking agents, in general, increase the tensile strength and water resistance, while decreasing the elongation of the films. Several crosslinking agents including, carbodiimide [118], tannic acid [108], acid citric [100], genipin [99] were recently used to crosslink gelatin-based films, as they are significantly less cytotoxic than formaldehyde and glutaraldehyde [119].

Recently, nanotechnology has been used not only to enhance the physical properties of gelatin-based films but also to provide extra functional properties, such as antioxidant and antimicrobial functions. Polymer nanocomposite is a multiphase solid material in which at least one type of the phases domain is a continuous phase and in which at least one of the phases has at least one dimension smaller than 100 nm [120]. The development of bionanocomposite films with antimicrobial properties especially broadens the application range of gelatin in food packaging. Several metallic or inorganic nanoparticles such as silver [102], tin dioxide [103], zin oxide [104], and clay [106] have been used to improve the functional properties of gelatin. Additionally, other organic nanoparticles, such as starch [97], chitin [111], and cellulose nanocrystals [17] have been incorporated with the gelatin matrix to prepare fully biodegradable films.

2.2.3 Cellulose

Cellulose is the most abundant polymer in nature, with approximately 250 megatons produced annually through photosynthesis by green plants from carbon dioxide, water, and sunlight [121]. Cellulose is widely biosynthesized by several living organisms ranging from higher to lower plants, several marine animals (for example, tunicates), algae, fungi, bacteria, invertebrates, and even amoeba (protozoa) [13]. Cellulose is a renewable, biodegradable, biocompatible, and non-toxic material [12].

Cellulose was discovered in 1838 by the French chemist Anselme Payen, who isolated it from a plant matter and determined its chemical formula [122], and since then, multiple physical and chemical aspects of cellulose have been extensively studied. According to the work of Haworth et al. (1930) [123], cellulose is a linear homopolysaccharide composed of D-glucopyranose units linked by $\beta(1\rightarrow4)$ glycosidic bonds, resulting in anhydroglucose units ($C_6H_{10}O_5$). The repeating unit of cellulose is cellobiose that comprises two anhydroglucose units (AGU). AGU is commonly used to define the degree of polymerization ($DP = n/2$) of cellulose. According to Habibi et al. (2010) [13], the degree polymerization is up to 20,000, but shorter cellulose chains can occur and are mainly localized in the primary cell walls. Figure 1.13 shows the basic chemical structure of cellulose with three types of AGU: (i) the internal UGA, (ii) a reducing end (i.e., a hemiacetal unit), and (ii) the non-reducing end with a pendant hydroxyl group.

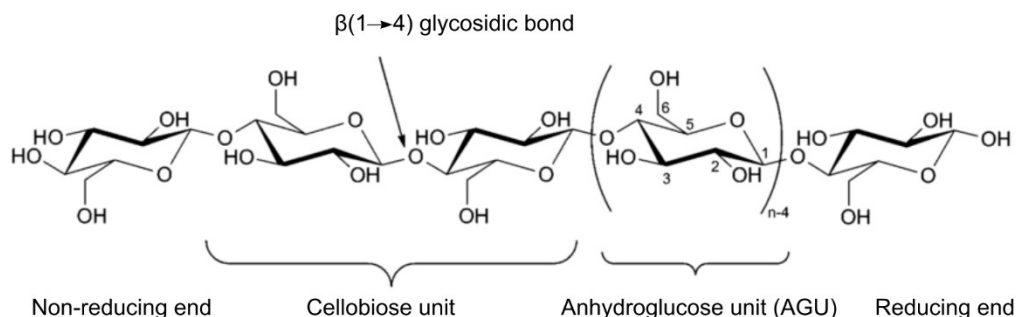


Figure 1.13 - Representation of a cellulose chain showing the anhydroglucose unit, the glycosidic link, and both reducing and non-reducing ends of the polymer.

One of the most distinguishing and useful characteristics of cellulose is the high degree of hydroxylation along the polymer chain. Each AGU has three hydroxyl groups, which form strong intra and inter hydrogen bonds in the same and neighboring cellulose chains. Intra- and inter-chain hydrogen bonding play a major role in directing the crystalline packing and also governing the physical properties of cellulose, namely, its high mechanical strength and flexibility [12].

In nature, cellulose does not occur as an isolated individual molecule. The Van der Waals and intermolecular hydrogen bonds promote parallel stacking of multiple cellulose chains forming elementary fibrils that further aggregate into large microfibrils (5-50 nm in diameter and several microns in length) [124]. The fibrils contain regions where the cellulose chains are arranged in a highly ordered structure (crystalline), and regions that they are disordered (amorphous). The organization of the amorphous and crystalline domains in the cellulose fibers is dependent on the cellulose source. According to Mariano et al. (2014) [125], for some plant species, the amorphous regions represent up to 50% of the structure, while in bacterial cellulose and celluloses extracted from some algae the crystalline domains correspond to almost 100% of the fibril.

2.2.3.1 Cellulose nanocrystals

Cellulose nanocrystals (CNCs), also referred to as cellulose whiskers, nanowhiskers, or nanocrystalline cellulose, are crystalline domains extracted from several natural sources, including wood, plants, cellulose-containing animals, and microorganisms. The main characteristics of CNCs are related to their low density, excellent mechanical properties, flexibility regarding chemical modifications, and the possible myriad applications, which explains the exponential growth interest from researchers and companies for this material over the last 20 years (Figure 1.14).

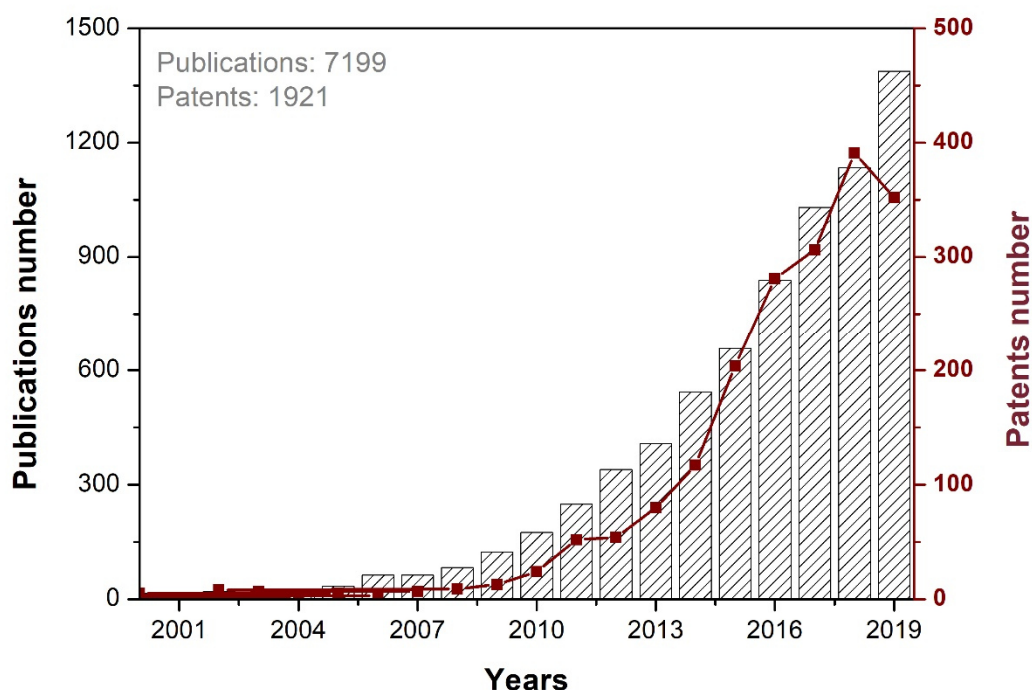


Figure 1.14 - Number of papers and patents releases each year dealing with CNCs until 2019 (extracted from ACS SciFinder in September 2020, descriptors are cellulose nanocrystals, cellulose nanowhiskers, nanocrystalline cellulose, and cellulose whiskers).

The discovery of CNCs is attributed to Rånby et al. in 1950 [126], who reported for the first time that colloidal cellulose particles with crystalline character can be obtained by controlled sulfuric acid degradation of cellulosic fibers. A typical process for the production of CNCs from fibers begins with pre-treatments (bleaching, alkaline treatment, etc.) to remove non-cellulosic components (hemicellulose, lignin, waxes, etc.), followed by isolation of CNCs, washing, centrifugation, dialysis, and ultrasonication to form a suspension which may be further subjected to lyophilization (freeze-drying) or spray-drying [12]. The methods used to release CNCs from the cellulose source include mechanical, chemical, and enzymatic processes or a combination of them. However, the main process for the isolation of CNCs is the acid hydrolysis [127–129]. According to De Souza Lima et al. (2004) [130], the acid hydrolysis mechanism involves the diffusion of hydronium ions into the amorphous domains of native cellulose,

promoting the hydrolytic cleavage of glycosidic bonds and releasing highly order cellulose in the form of rod-shaped particles. Figure 1.15 illustrates the preparation of CNCs by sulfuric acid hydrolysis.

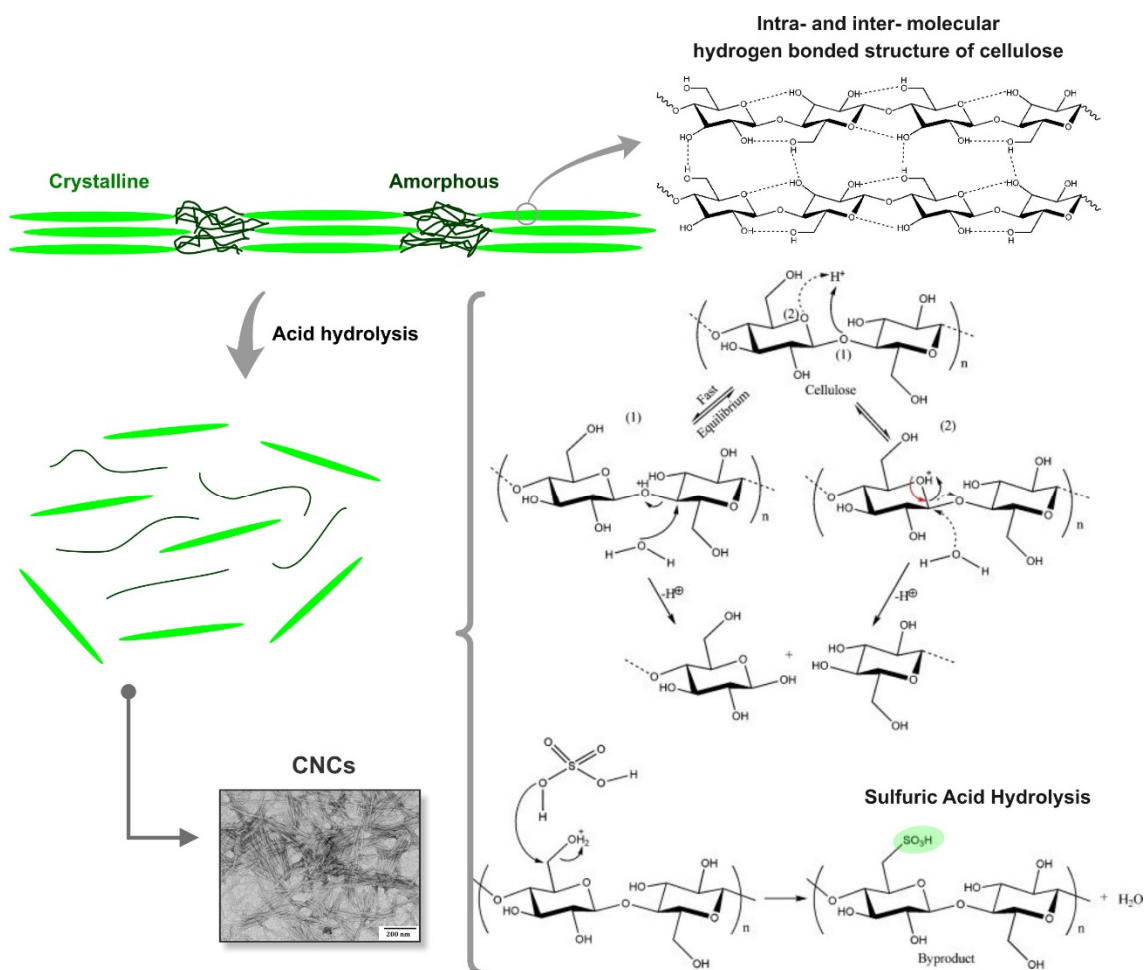


Figure 1.15 - Schematic acid hydrolysis production of CNCs resulting in sulfate half ester surface groups (adapted from [131]).

The CNCs dimensions depend on the cellulose source and hydrolysis conditions, ranging from 100 to 500 nm in length (L) and from 5 to 10 nm in width (d), resulting in high aspect ratios (L/d) [13,132]. Figure 1.16 shows transmission electron microscopy images of CNCs obtained by acid hydrolysis from different sources. Dufresne (2018) [133].reported that the stability of CNCs suspensions depends on the dimensions of their dispersed particles, size polydispersity, and surface charge. Strong mineral acids like sulfuric, hydrochloric [134], but also phosphoric [135] and hydrobromic [136] have been applied for obtaining CNCs.

However, sulfuric acid (~64 wt%) is classically used because it promotes grafting of anionic sulfate groups (OSO_3^-) onto the CNCs nanoparticles, resulting in stable aqueous dispersions [137].

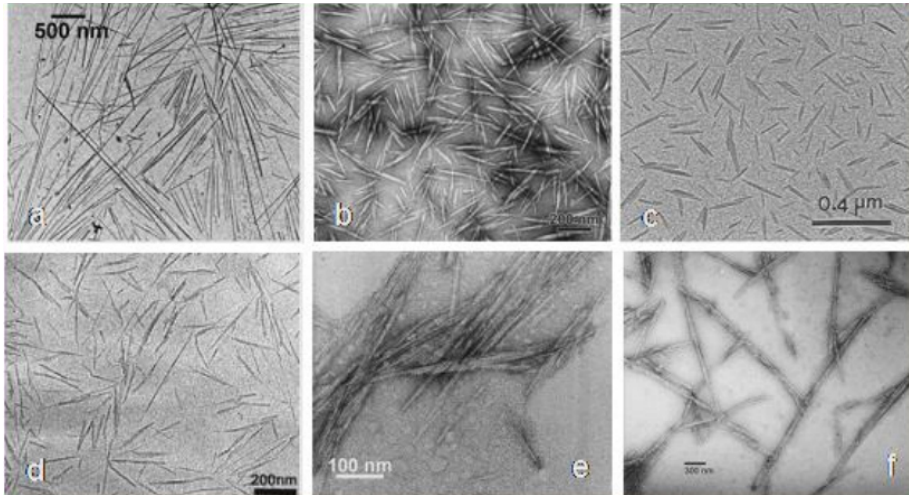


Figure 1.16 - Transmission electron microscopy images of CNCs suspensions obtained from (a) tunicate, (b) ramie, (c) cotton, (d) beet sugar, (e) microcrystalline cellulose, and (f) bacterial cellulose [8].

CNCs encompass a suitable combination of properties such as high aspect ratio (~10-70), low density ($1.5\text{-}1.6\text{ g/cm}^3$), low thermal expansion coefficient, optical transparency and anisotropy, negative diamagnetic anisotropy, and shear-thinning rheology [13,138,139]. In addition, the well-defined CNCs dimensions, their high crystallinity (70-90%), and their bond packing organization induce excellent mechanical properties such as high axial stiffness (~150 GPa), high Young's modulus (20-50 GPa) [140], and high tensile strength (~7 GPa) [138]. making them excellent candidates for the design and development of high-performance nanomaterials in several applications.

In the last decades, the interest in the use of CNCs encouraged the development of large-scale CNCs production facilities around the world. For instance, North America dominates the market with a share of almost 45 %, which is expected to grow in the coming years. The key players and their industrial capacity (tonnes per year, dry basis) are Celluforce (Canada) 300 tons, American Process Inc. (USA) 200 tons, Melodea (Sweden) 35 tons, Alberta Innovates

(Canada) 7 tons, US Forest Products Lab (USA), and Blue Goose Biorefineries (Canada), FPInnovations (Canada), University of Maine (USA) with 4 tons each.

Today, CNC-based materials are used in a wide range of applications such as security paper [141], energy & electronics [142], environment [143], biomedical [144], and composites and nanocomposites [145]. The use of CNCs in nanocomposites has been detailed in several papers that focused on demonstrating the reinforcing potential of high aspect ratio CNCs for different polymer matrixes [133].

2.2.3.2 Cellulose nanocrystals in food packaging

CNCs can provide many benefits for packaging films in terms of performance, including biodegradability, mechanical properties, and gas, and vapor barrier. According to Criado et al. (2019) [146], the improvement of polymer film mechanical properties due to CNCs addition is attributed to the good dispersion of the CNCs in the polymer matrix, effective filler-matrix interaction, and the creation of a CNC percolation network. This behavior, explained by the Halpin & Kardos percolation model (1972) [147], led to the conclusion that infinite networks of nanoparticles stabilized by hydrogen bonding were responsible for improving the mechanical properties of the polymer matrix. The percolation threshold for rod-like nanoparticles can be linked to the CNCs aspect ratio following Equation 6 [148]. The effect of adding CNCs has been explored in different types of biodegradable polymers, such as poly(butylene adipate terephthalate) (PBAT) [149], PCL [150], alginate [151], polyhydroxybutyrate (PHB) [152], gum arabic, chitosan [153] and whey protein [16].

$$\phi_c = \frac{0.7}{L/d} \quad \text{Eq. 6}$$

Parameters such as cohesive energy density, free volume, and crystallinity play a role in the oxygen barrier properties of polymers [146]. As reported by Kofinas et al. (1994) [154], gas molecules are unable to permeate the crystalline regions of polymers. Thus, gas permeation in semicrystalline polymers is confined in the amorphous regions [46]. Garcia et al. (2004) [155] described that

the presence of crystalline nanoparticles, such as CNCs, can result in a more compact material and create a large tortuous path inside the matrix, which interrupts the gas path or a gas "jump" response in diffusion. Therefore, a decreased gas permeation is expected after the CNCs are appropriately dispersed in the polymer matrix [156]. This effect has been described in detail in several papers [157–159].

A decrease in water vapor permeability in CNC-based nanocomposites has also been observed. Although the fact that CNCs are hydrophilic due to the OH groups, CNCs have shown to enhance the moisture barrier properties and decrease the WVP of several biopolymers [160–162]. This behavior is attributed to the formation of hydrogen networks that allows better cohesiveness in the nanocomposite structure. However, it is important to highlight that the addition of excessive amounts of CNCs results in aggregated and accelerate preferential paths for water diffusion, thus reducing the material barrier performance [163]. Table 1.4 shows the effect of CNCs on the physical properties of gelatin films (done September in 2020).

Table 1.4 - Physical-chemical properties of gelatin-nanocellulose bionanocomposites

Matrix (wt%)	Bloom	Plasticizer (wt%)	CNCs (wt%)	Additive	Drying Temp. (°C)	TS (MPa)	EAB (%)	WVP (g mm/m ² h kPa)	RH (%)	T _{onset} (°C)	Ref.
10% gelatin	-	-	0-5% BCNCs	-	37 °C	83.7-108.6	33.7-20.8	0.0002-0.0017	-	-	[17]
10% bovine gelatin	-	20% Glycerol	0-1.5% CNCs	-	25 °C	32-33	27.5-38.3	0.0003-0.0002	50%	-	[164]
9.6% fish gelatin	139	25% Glycerol	0-15% CNCs	-	24 °C	16.3-17	19-15	2.5-1.6	85%	-	[165]
5-10% pigskin gelatin	225-325	-	0-10% CNCs 0-10% CNF	-	24 °C	110-80 100-110	4.2-5.8 4.2-4.4	1.21-1.89 1.21-1.89	100%	-	[166]
10% gelatin	-	4% Glycerol	0-1% CNCs	-	25 °C	8.2-13.6	18-43	2.30-1.37	50%	-	[167]
10% gelatin	-	1-5% Glycerol	0-20% di-aldehyde CNCs	-	25 °C	12-38	110-38	-	-	-	[22]

Abbreviation: WVP: water vapor permeability, TS: tensile strength, EAB: elongation at break; BCNCs: bacterial cellulose nanocrystal

Regarding the objective of this Ph.D. to produce gelatin packaging with CNCs, no more than 6 papers can be cited on this date. Of this total, only one paper studied the effect of functionalized CNCs on the properties of gelatin film, being an area with many possibilities for innovation.

2.2.3.3 Functionalization of cellulose nanocrystals

The surface of CNCs can be easily modified due to the reactivity of the hydroxyl group, which makes CNCs a unique platform amenable to various surface functionalization, extending the specific applications of CNCs, particularly to alleviate difficulties in dispersing them in apolar solvent or polymers [168]. Though, it is important to keep the crystalline structure intact and avoid the degradation of CNCs during the functionalization, since their mechanical properties are important for most applications.

The functionalization of CNCs can generally be categorized into 2 distinct groups (i) non-covalent and (ii) covalent surface functionalization or direct chemical modification. Non-covalent functionalization is typically achieved *via* adsorption of molecules or macromolecules such as surfactant to the CNCs surface. These additives interact with the CNCs surface by electrostatic attractions, Van der Waals forces, or hydrogen bonding, thus improving the CNCs stability and dispersion [169]. Dispersants as stearic acid and cetyltrimethylammonium-bromide (CTAB) are the most common molecules applied for non-covalent functionalization of CNCs [170]. In the covalent functionalization, also referred to as grafting, many molecules or polymers are covalently attached to the CNCs surface. This has been achieved by reacting the hydroxyl groups using various methods such as silylation [171,172], coupling with isocyanate [173], macromolecular grafting [174,175], acetylation [176], acetylation with acetic anhydride [177], esterification [175], covalent grafting by polymer ring-opening polymerization [178], etc. Alternatively, many groups seek to change the chemistry of the hydroxyl groups by 2,2,6,6-tetramethylpiperidine-1-oxyl (TEMPO)-oxidation that converts alcohol groups to carboxylic acid moieties for better CNCs dispersibility [179]. The hydrolysis method using sulfuric acid can also be used to form sulfate esters, as mentioned before [170]. Figure

1.17 gives a wide overview of the common reactions used to modify CNCs surface.

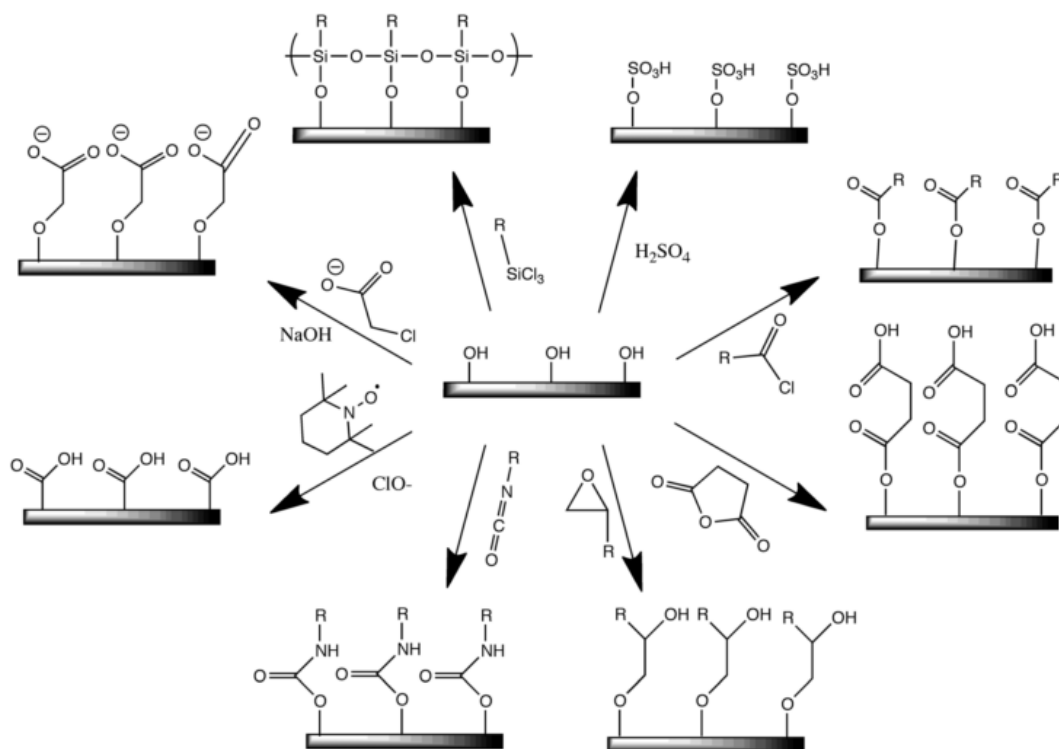


Figure 1.17 - Common surface functionalization of CNCs: (clockwise from top-right) sulfuric acid hydrolysis, carboxylic acid halides, acid anhydrides, epoxides, isocyanates, TEMPO oxidation, halogenated acetic acids, and chlorosilanes [124].

One recent strong trend is to focus on the functionalization of CNCs to develop novel active packaging with diverse advanced functionalities such as antimicrobial and antioxidant. Active packaging is an innovative concept that offers positive impacts on consumer health by integrating functional ingredients in the packaging material structure to actively enhance the shelf life of food products while ensuring their quality, safety, and integrity. The most common types of active packaging are those that release active compounds such as antimicrobial agents onto the food surface [180].

CNCs themselves have no antibacterial or antimicrobial activity [146]. Nevertheless, the CNCs have allowed for adsorption or grafting of active

compounds. Also, CNCs have been studied based on the controlling release of bioactive compounds generated by the CNCs in polymer matrices [181]. Different active packaging systems based on functionalized CNCs can be produced by different routes, as summarized in recent reviews [180,182,183]. Of particular interest are treatments with food-grade compounds such as sorbic acid [184] or bio-based cationic polymers like chitosan [185]. Also, there has been much interest in applying nanomaterials such as colloidal silver particles in combination with nanocelluloses for antimicrobial active packaging. The silver nanoparticle/CNCs-based materials showed enhanced antibacterial properties against *E. coli* and *Staphylococcus aureus* due to the metal ion reducing and chelating capacity of the modified CNCs [186].

2.2.3.4 Cellulose nanocrystals safety and toxicology assessment

Cellulose is considered as a non-toxic material. However, the particularities of CNCs, especially regarding the nanometric size and the high aspect ratio, are expected to increase their toxicity as compared to that of bulk cellulose. In-depth research has been carried out to assess the *in vitro* or *in vivo* toxicity of CNCs. According to Ventura et al. (2020) [187], in general, the CNCs uptake into cells is generally low, with no induction of oxidative stress and no significant cytotoxic and genotoxic effects. Several studies have reported that CNCs are not significantly toxic to human cells or the environment [188]. The impact of chemical modification on the toxicity of several nanocellulose materials has also been investigated [189]. Also, CNCs are currently exempted from registration in the REACH list (list of restrictions of certain hazardous substances, mixtures, and articles for their marketing and use in the European market).

3 Processing of natural polymer-based film packaging

The film-forming process plays an important role in the physical properties of polymer films. Two processes have been investigated to make packaging materials based on proteins: “dry process (extrusion)” based on the thermoplastic behavior of protein at low moisture levels, and the “wet (or solution casting)

process” based on the solubilization of the protein in a solvent medium [68]. Films can be produced by extrusion followed by thermoforming that is ordinarily higher than 80 °C [6]. This process would enhance the commercial potential of protein films. However, the extrusion/thermoforming process affects film properties.

Krishna et al (2012) [190]9, compared the properties of fish gelatin films produced either by extrusion/heat-processing or by casting and found that extruded films higher WVP values than the corresponding cast films. They explained these differences in terms of the moisture evaporation rate, which was lower in the cast films and, as a result, favored the formation of a more ordered and compact film network.

Recently, Chuaynukul et al. (2018) [96] compared the proprieties of gelatin films obtained by compression molding and solution casting. The authors found that the compression-molded gelatin films exhibited lower thermal stability and WVP than the cast films. This behavior was attributed to the higher thermal degradation of gelatin during the film thermoforming step that requires high temperatures.

The wet process is the most often use film-forming method for protein film production. In this Ph.D. work, the gelatin films were produced using this bench and continuous casting. Details on this method are described in the two next sub-chapters.

3.1 Bench casting

Bench casting is the wet process most widely used to produce gelatin films. Film production by bench casting consists of dissolving the polymer and blending it with plasticizers and/or additives to obtain a film-forming solution, which is poured on plates and then dried by driving off the solvent [191]. Film formation by solvent – water evaporation is due to increased polymer concentration in the medium, inducing the macromolecules to rearrange into a cohesive matrix stabilized by new interactions and bonds [192]. The final film thickness is controlled by the amount of solution poured on plates. The air-drying procedure is a very important step on the physical properties of the films and it is

generally carried out at room temperature or in an air circulating oven at temperatures not exceeding 30 to 40 °C and for 12 to 48 h. Indeed, the long drying times are the most remarkable disadvantage of this technique, making it not feasible for commercial production [193]. Information on parameters such as wet thickness, relative humidity, and air flow speed is critical [194].

According to Suhag et al. (2020) [195], the greatest challenge is to convert film production from laboratory to production scale because many variables, including heating, speed, and temperature, could cause quality differences and prevent the constant development for commercial scales.

3.2 Continuous solution casting

Recently, a continuous solution casting method has been proposed for the production of biopolymer films on a pilot scale. Continuous film casting is carried out on a coating line such as a tape-casting machine. In this process, solutions are continuously spread onto a moving substrate such as polyester or coated paper, with a blade whose height can be adjusted to control film thickness (Figure 1.18). The coated substrate then passes through a pre-drying infrared heater and drying chambers and at the end, the dry film is cooled to room temperature and wound on a roller while still adhered to the substrate [194]. The distance between the two drying chambers is approximately 2 meters. The continuous solution casting approach may be considered a scale-up of the previously described bench casting procedure. The main advantage of continuous casting consists in the fact that this method requires short processing times, thanks to the use of infrared radiation in the pre-drying stage, much higher temperatures, and intense air circulation. Other advantages are the high wet thickness control, no processing additives required, allows the use of aqueous solutions/dispersion, and the less need for space and labor.

Edible films based on fruits have been produced by using continuous casting in a few minutes [196]. Du et al (2008) [197], compared the properties of apple films with carvacrol produced either by continuous casting or bench casting. The authors concluded that the higher temperatures used in the continuous casting increased carvacrol evaporation and made the films thinner and denser,

probably reducing interstitial spaces for molecular diffusion, which explain the lower oxygen permeability and WVP of continuously cast films. No significant difference in tensile properties when compared to cast films was observed. Recently, Munhoz et al. (2018) [198] produced yellow passion fruit (*passiflora edulis*) packaging films by continuous casting at 120 °C. During the continuous production, the authors achieved productivity of 0.03 m² of film per minute with mechanical strength comparable to traditional PVC. These characteristics make continuous casting an attractive process for large-scale bio-based film production.

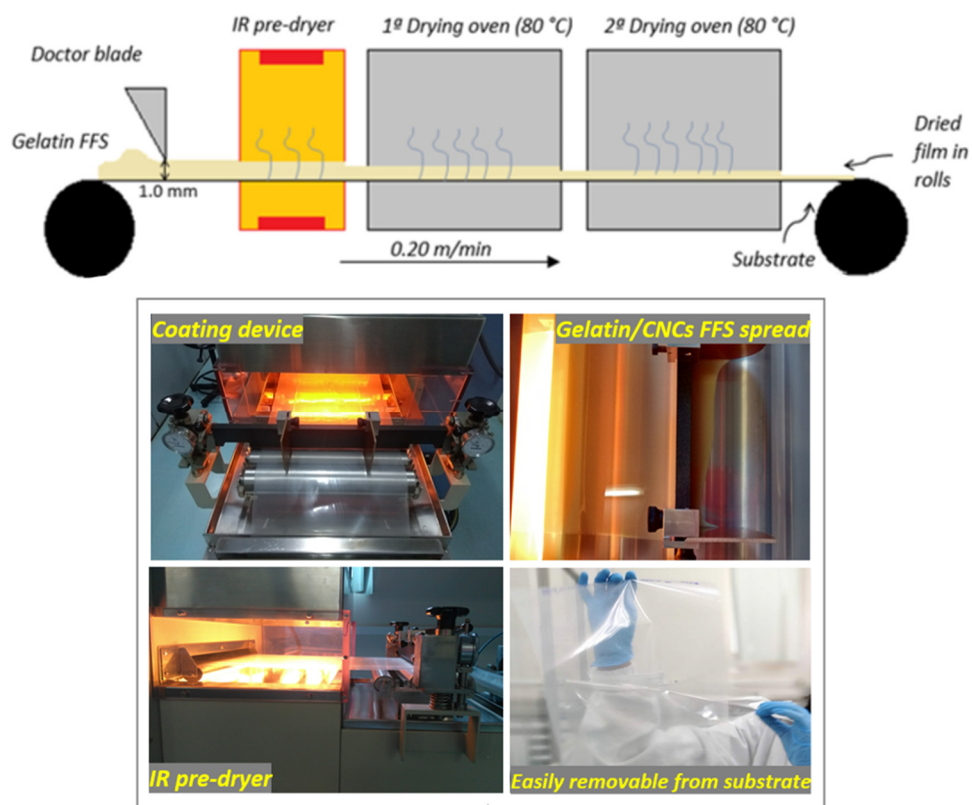


Figure 1.18 - Schematic representation of gelatin-CNCs bionanocomposite production by continuous casting [18].

Regarding the objective of this Ph.D. work to produce gelatin packaging by continuous casting, only the paper resulting from this thesis has been cited on this date.

CONCLUSIONS

Proteins are a suitable alternative for food packaging applications, replacing conventional plastics, especially those made from petrochemicals. However, using only proteins is not enough for producing films with satisfactory mechanical and barrier properties for food packaging. The excellent mechanical and barrier properties of CNCs and the fact that they can be considered as green nanomaterials because they are renewable and biodegradable, open excellent prospects for their increased use in the design of novel high performance food packaging materials. The assessment of the safety and toxicology of CNCs has been monitored and, to date, studies have shown that they had no harmful effects on human health and the environment. Besides, the functionalization of CNCs can also create other desired functions in food packaging materials, such as antimicrobial and antioxidant properties, contributing to extending food products shelf-life. Therefore, proteins and CNCs offer excellent opportunities for a new generation of bionanocomposite packaging materials. However, the processing of protein films still limits their widespread use in the food packaging industry.

In line with this context, it seems very innovative (i) to use the continuous casting as an appropriate approach to increase the production of gelatin-cellulose nanocrystalline bionanocomposites films and (ii) to functionalize the surface of CNCs with natural active molecules and to use such materials in combination with gelatin for the design of new active packaging. The strategies adopted in this Ph.D. work to achieve these objectives will be detailed in the following chapters.

Chapter II

Gelatin-based films produced by continuous casting

II. Gelatin-based films produced by continuous casting

Introduction to chapter II

As described in Chapter I, the greatest challenge is to convert the film production of natural bio-based materials from laboratory to production. Besides, the quality of the dispersion of CNCs particles in the film-forming solution also plays an important role in the physical properties of the film produced by spreading. One of the main objectives of this Ph.D. is to develop a suitable approach to scale up the production of gelatin-cellulose nanocrystals (CNCs).

In the first part of this chapter (**Chapter II.1**) will investigate the parameters such as the rheological behavior of the film-forming solution and drying temperature required to produce gelatin/CNCs films by continuous casting. In addition, the physical properties of gelatin/CNCs obtained by continuous casting will be analyzed. The results show that continuous casting is a suitable technique to hasten the production of bionanocomposites based on gelatin/CNCs from aqueous formulations.

The second part (**Chapter II.2**) will focus on the effects of the dispersion of CNCs on the properties of the gelatin-based films. We particularly examined the dispersibility of the heterogeneous CNCs and homogeneous CNCs suspensions in gelatin film-forming solutions. Based on the work realized in Chapter II.1, continuously cast gelatin/CNCs films with better CNCs dispersion and their counterparts obtained by bench casting will be analyzed. The results show that continuous casting not only allowed scaling-up the production of these bionanocomposites films but also led to films with relatively superior mechanical, barrier, and thermal performance.

1. Scalability of the gelatin/CNCs bionanocomposites by continuous solution casting

This section is adapted from Liliane S. F. Leite, Caio M. Ferreira, Ana C. Corrêa, Francys K. V. Moreira, Luiz H. C. Mattoso. Scaled-up production of gelatin-cellulose nanocrystal bionanocomposite films by continuous casting. Carbohydrate Polymers, 238 (2020) 116198.

Abstract

In this study, the continuous casting was proposed as a suitable approach to scale-up the production of gelatin-cellulose nanocrystals (CNCs) bionanocomposites. The processing conditions and bionanocomposite properties were established based on the ζ -potential and gelatin content, and CNCs concentration, respectively. Gelatin film-forming solution at 20 wt% was required for proper continuous casting processing, leading to a productivity of 0.20 m film/min, which was at least 1000-fold higher than that of classical bench casting. The gelatin-CNCs bionanocomposites displayed transparency, flexibility, and improved UV-barrier and thermal properties. Adding only 0.5 wt% of CNCs resulted in an increase of 77% and 48% in tensile strength and Young's modulus of gelatin, respectively. Comparison with previous nanocellulose-based nanocomposites pointed out the relatively superior performance of the gelatin-CNCs bionanocomposites obtained by continuous casting for various applications, including flexible food packaging.

1.1 introduction

Gelatin can be used in food packaging and biomedical applications, including coatings, wound dressing, adhesives, adsorbent materials, and drug delivery as hard or soft capsules due to its film-forming properties, low cost, biodegradability, and biocompatibility [199]. Several strategies have been reported in the literature to enhance the physical properties of gelatin films for different applications. One of these strategies is the use of nano-sized structures as reinforcing fillers in gelatin films [200–202], which usually yields nanocomposites with superior properties, compared to the corresponding micro-composites without impairing density, transparency, and film processability.

Cellulose nanocrystals (CNCs) are one of the most studied polysaccharide-based nanomaterials in polymer nanocomposites [165,203]. Reports have demonstrated that CNCs can be applied as reinforcing fillers for gelatin. George & Siddaramaiah (2012) [17] observed that the addition of 2 wt% CNCs increased the modulus and tensile strength of bench-cast gelatin films from 2190 MPa to 2273 MPa, and 84 MPa to 95 MPa, respectively. Santos et al. (2014) [165] found that gelatin nanocomposites produced by bench casting exhibited high stiffness and good ductility up to 5 wt% CNCs. After this point, the mechanical properties tended to level off or even to decrease, which was attributed to CNCs agglomeration effects. However, all these reports were based on gelatin/CNCs films obtained by bench casting, which is an important technique for small-scale studies, but fails in achieving high productivity because the drying times are relatively long (e.g. 12-24 h) [204]. In this sense, researches are still necessary to develop scaled-up routes for producing gelatin-CNCs bionanocomposites films. To the best of our knowledge, such a route has not been efficiently developed yet, neither the examination of the bionanocomposite film properties obtained in such a pilot-scale scenario.

In the present work a continuous solution casting approach was applied for scaling up the production of gelatin-CNCs bionanocomposite films. A pre-pilot labcoater machine was used to speed-up the casting drying step and to provide green and safety aspects to the films for food packaging applications. We particularly examined the effect of the CNCs concentration on the physical

properties of the bionanocomposite films. The continuously cast films were also compared for their mechanical properties to their counterparts obtained by bench casting.

1.2 Materials and Methods

1.2.1 Materials

Bovine gelatin (Bloom Strength-180) and eucalyptus kraft pulp were kindly supplied by Gelco Gelatinas do Brazil Ltda (Pedreira, SP) and Suzano Papel e Celulose Ltda (Limeira, SP), respectively. Sulfuric acid (98.08 wt%) was purchased from Sigma-Aldrich Ltd. (st. Louis, USA). Glycerol was purchased from Dinâmica Química (Indaiatuba, SP). All aqueous solutions were prepared using ultrapure water (18 M Ω .cm) obtained from a Milli-Q system (Millipore).

1.2.2 Preparation of CNCs

The CNCs were prepared by acid hydrolysis of 10 g of eucalyptus kraft pulp using 200 mL of 60% w/w sulfuric acid solution at 45 °C for 60 min with constant stirring. After hydrolysis, the suspension was diluted in 500 mL of cold water to quench the reaction and centrifuged at 10000 rpm for 10 min. The resultant pellet was rinsed, re-centrifuged, and dialyzed in water with a cellulose membrane (6-8 kDa) until neutral pH. Afterward, the suspension was sonicated for 5 min and stored in a refrigerator after adding chloroform drops to prevent microbial growth. The final solid content was 3.5% (w/w).

1.2.3 Preparation of gelatin/CNCs film-forming solutions (FFS)

FFS based on gelatin and CNCs were prepared according to the following steps: first, gelatin powder was hydrated in ultrapure water at concentrations of 10, 20, and 30 wt% (for continuous casting) and 10 wt% (for bench casting) at 24 °C for 5 min, and then heated at 60 °C under mechanical stirring for 15 min. Then, glycerol (20 wt% on a dry gelatin basis) was added to the gelatin solution, which was then homogenized with an Ultra Turrax T-25 (Ika, Staufen, Germany) at

12000 rpm for 10 min. The CNCs suspension was gradually added to the gelatin/glycerol solution over the first 2 min. Four film-forming solutions were prepared with the following CNCs concentrations (on a dry gelatin basis): 0 wt%, 0.5 wt%, 1.0 wt%, and 2.5 wt%. The solutions were allowed to rest for 60 min to eliminate bubbles before casting.

1.2.4 Continuous casting

Gelatin-based FFS were turned into monolayer films on a KTF-S labcoater casting machine (Werner Mathis AG, Switzerland), as schematically depicted in Figure 2.1. In this technique, the polymer solution is continuously spread onto a moving substrate (Mylar®, DuPont, Brazil) with a doctor blade device, which allows controlling the wet layer thickness. The wet solution layer then passes through two drying chambers with controlled temperatures. The distance between the two drying chambers is approximately 2 meters. The dried film is wound into rolls. The distance between the substrate and the doctor blade was set at 1.0 mm. The conveyor speed and the drying ovens were 12 m/h and 80 °C, respectively. All samples were conditioned in a desiccator at 50% RH and 25 ± 2 °C for at least 48 h prior to testing.

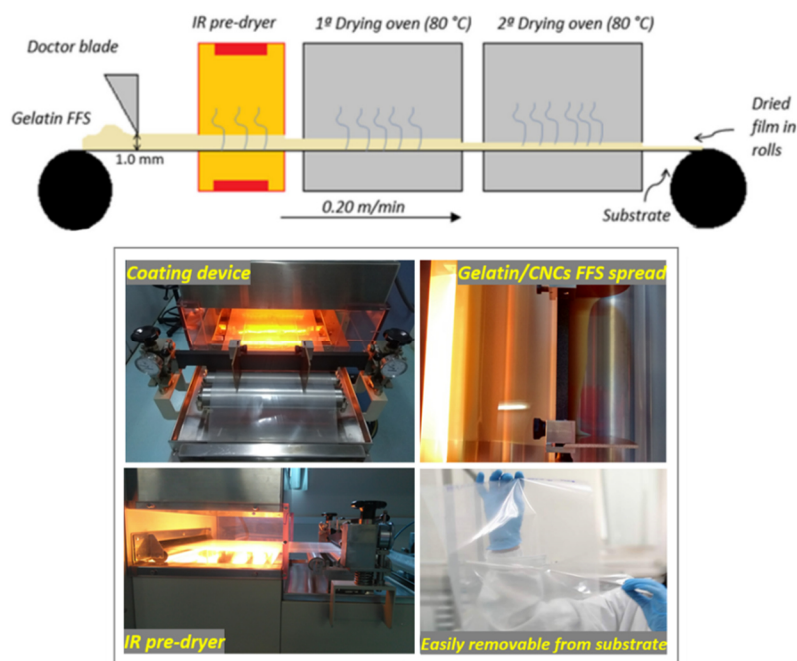


Figure 2.1 - Schematic representation of gelatin-CNCs bionanocomposite production by continuous casting.

1.2.5 Bench casting

Gelatin-CNCs FFS (60 mL) were cast on glass plates (40 cm × 25 cm) covered with a polyester film (Mylar®, DuPont, Brazil) to facilitate peeling off the films after drying at room temperature for 24 h. Film samples were conditioned in a desiccator at 50% RH and 25 °C for at least 48 h prior to testing.

1.2.6 Transmission electron microscopy (TEM)

Transmission electron microscopy was carried out on a Tecnai TM G2 F20 microscope (FEI Company, Netherlands) using the SEM (Transmission Electron Microscopy) mode. The images were acquired with a dark field (DF) detector. A droplet of diluted CNCs suspension was deposited on a carbon microgrid with formvar (400 mesh) and allowed to dry. The grid was stained with 1.5 wt% uranyl acetate solution and dried at room temperature before analysis. Average CNCs sizes were obtained from a minimum of 100 particles by using the ImageJ software.

1.2.7 Determination of Zeta potential (ζ -potentials)

ζ -potentials of aqueous CNCs and gelatin suspensions with concentration of 0.25 wt% measured at 25 °C using a Zetasizer Nano-ZS (Malvern Instruments Inc., UK). The measurements were performed in triplicate.

1.2.8 Rheological study

The apparent viscosity and flow behavior of the different FFS were evaluated on a Physica MCR101 rheometer (Anton Paar, Austria) using concentric cylinder geometries at 25 and 30 °C. The shear rate was increased from 0 to 150 s⁻¹ in 10 min. Oscillatory shear deformation tests were also carried out to determine the storage modulus (G') and loss modulus (G'') of the FFS at a constant strain of 1% and frequency of 10 rad s⁻¹ in the temperature range of 80-20 °C by cooling rate of 0.09 °C s⁻¹. Strain values were chosen to be within the linear viscoelastic region based on preliminary tests. The flow behavior was described by fitting the experimental data with the Power Law model Equation 1.

$$\sigma = k\dot{\gamma}^n \quad (1)$$

Where σ is the shear stress (Pa), $\dot{\gamma}$ is the shear rate (s^{-1}), k is the consistency coefficient (Pa s^n) and n is the flow behavior index.

Frequency sweep tests were performed in the 0.1–100 Hz range at strain 1% in the linear viscoelastic range. Storage modulus (G'), loss modulus (G'') were recorded as a function of frequency.

1.2.9 Scanning electron microscopy (SEM)

The cross-sectional surface of the film samples was investigated using a scanning electron microscope (SEM), model JMS 6510, (JEOL, Japan). Samples were first cryo-fractured in liquid N_2 and then fixed onto 90° specimen mounts. Once coated with a ca. 5-nm-thick gold layer in an argon atmosphere, the samples were analyzed using an accelerating voltage of 2 kV and a working distance of ca. 5 mm. All SEM images were taken using the secondary electron mode.

1.2.10 Attenuated total reflectance Fourier transform infrared spectroscopy (ATR-FTIR)

FTIR spectra were recorded on a FT-NIR VERTEX spectrometer (Bruker, Germany) operating in the attenuated total reflectance (ATR) mode. The ATR-FTIR spectra were registered from 400 to 4000 cm^{-1} using accumulation of 32 scans and resolution of 1 cm^{-1} .

1.2.11 Color measurement

Color parameters (L^* , a^* , b^*) were determined using a colorimeter model Miniscan XE (HunterLab, USA). Gelatin/CNCs films were placed on the surface of a white standard plate and color parameters were measured using the CIELab color scale: $L^* = 0$ (black) to $L^* = 100$ (white), $-a^*$ (greenness) to $+a^*$ (redness),

and $-b^*$ (blueness) to $+b^*$ (yellowness). The measurements were done in triplicate. Color difference (ΔE^*) was calculated using Equation 2 [205].

$$\Delta E^* = \sqrt{(\Delta L^*)^2 + (\Delta a^*)^2 + (\Delta b^*)^2} \quad (2)$$

where ΔL , Δa , and Δb are the differences between the color parameter of the samples and the color parameter of the white standard.

1.2.12 Light transmission and transparency

The barrier properties of film samples against ultraviolet (UV) and visible light were measured at selected wavelengths between 190 and 700 nm using a UV-1650 spectrophotometer (Shimadzu, Japan). Three replicates were performed for each film. Transparency values were calculated using Equation 3 [206]:

$$Transparency = \frac{A_{600}}{x} \quad (3)$$

where A_{600} is the absorbance at 600 nm and x is the film thickness (mm). Film thickness was measured using a digital micrometer (Mitutoyo Corp., Kanogawa, Japan) from Ten random measurements per film.

1.2.13 Thermogravimetric analysis (TGA)

Thermogravimetric analysis was carried out in a Q500 equipment (TA Instruments, USA). About 10 mg of each film sample was taken in a standard Pt crucible and heated from 25 °C to 700 °C with heating rate of 10 °C min⁻¹, under synthetic air atmosphere (60 mL/min). Samples before the TGA tests were conditioned in a ventilated climatic chamber at 23 ± 1 °C and 50 ± 5% RH for 48 h.

1.2.14 Tensile tests

The mechanical properties tensile strength (TS), elongation at break (EAB), and elastic modulus (EM) were measured according to ASTM standard

method D882-09 (2009). Film specimens were prepared and equilibrated at 23 °C and 50% RH for 48 h to be tested on a universal testing machine EMIC DL3000 (EMIC Equipamentos e Sistemas de Ensaio LTDA, Brazil) equipped with a 100 N load cell. Specimens were stretched using a crosshead speed of 10 mm min⁻¹ and initial distance between clamps of 100 mm. Tensile tests were performed with five replicates for each film.

1.2.15 Contact angle measurements

Contact angle measurements were conducted with CAM 101 Optical Contact Angle Meter (KSV Instruments, Finland) equipped with a CCD KSV-5000 digital camera. For each measurement, 5 µL of ultrapure water was dropped on the film surface and 100 images were automatically recorded within an experimental time of 60 s using the KSV CAM2008 software. Contact angle determinations were performed with 5 replicates as per ASTM D5725-99 (2008).

1.2.16 Statistical analysis

Data were submitted to analysis of variance (ANOVA). Mean values were compared using the Tukey's test at a confidence level of 95% ($p < 0.05$) using the software Origin (OriginLab, Northampton, USA).

1.3 Results and discussion

1.3.1 Characterization of CNCs

Figure 2.2 shows a typical TEM micrograph of the CNCs isolated from the eucalyptus fiber pulp by acid hydrolysis. The micrograph reveals the effective hydrolysis of the cellulosic fibers, giving rise to nanoparticles with needle-like morphology, as expected. The average length (L) and diameter (D) of the CNCs were 360 ± 104 nm and 16 ± 3 nm, respectively. The aspect ratio (L/D) was around 22.5. These values are in agreement with a previous report [207].

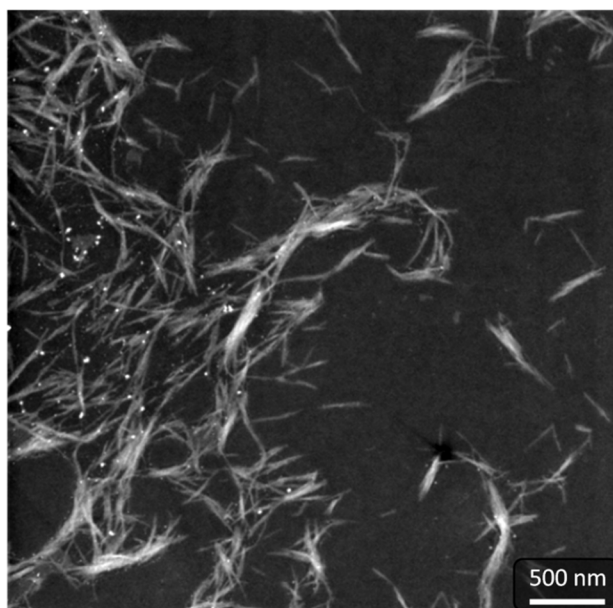


Figure 2.2 - TEM micrograph of CNCs isolated from eucalyptus pulp.

1.3.2 Characterization of gelatin-CNCs FFS

ζ -potential measurements were initially conducted to predict the best pH condition to form the gelatin-CNCs bionanocomposites. The pure gelatin solution presented an isoelectric point (Ip), that is, the pH at which the molecule exhibits an equal number of positive and negative charges, giving it a net charge zero (zwitterions), at pH 5.7, in agreement with previous reports (pH 4.8 - 5.5) [208]. At pH values lower than the Ip, the gelatin chains were positively charged, whereas, for pH values higher than the Ip, the gelatin chains exhibited predominantly negative charges (Figure 2.3).

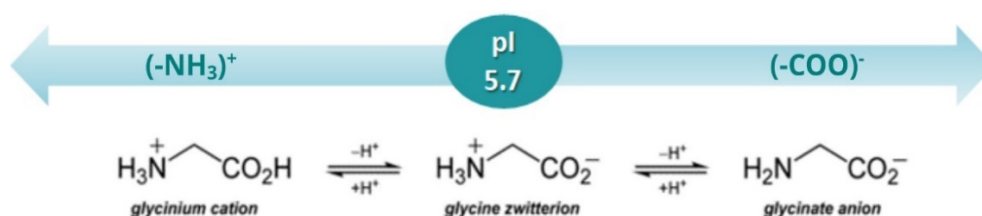


Figure 2.3 - Structure of ionized and zwitterion forms of glycine.

The presence of significant surface negative charges on CNCs was confirmed with the measured ζ -potential value of around -50 mV, which is consistent with previous reports [207,209]. This is due to the acid hydrolysis

carried out with sulfuric acid, which results in sulfate groups on the CNCs surface. This result indicates electrostatic repulsive forces between nanocrystals and good stability for the CNCs colloidal suspension [210] over an extended time, which is critical for the preparation of bionanocomposites by casting. To avoid the formation of coacervates, which may occur through electrostatic cross-linking between oppositely charged biopolymers [211], the FFS used in this study were prepared at pH 6, in which the average ζ -potentials of the CNCs and gelatin were negative.

The rheological behavior of the gelatin solutions with different polymer concentrations was studied to find the most appropriate formulation to produce the bionanocomposite films by continuous casting. Experimental shear stress vs. shear rate curves were fitted by the classical Power Law model ($R^2 \geq 0.996$) (Figure 2.4), which has been widely used for non-Newtonian fluids over the most important shear rate range [80].

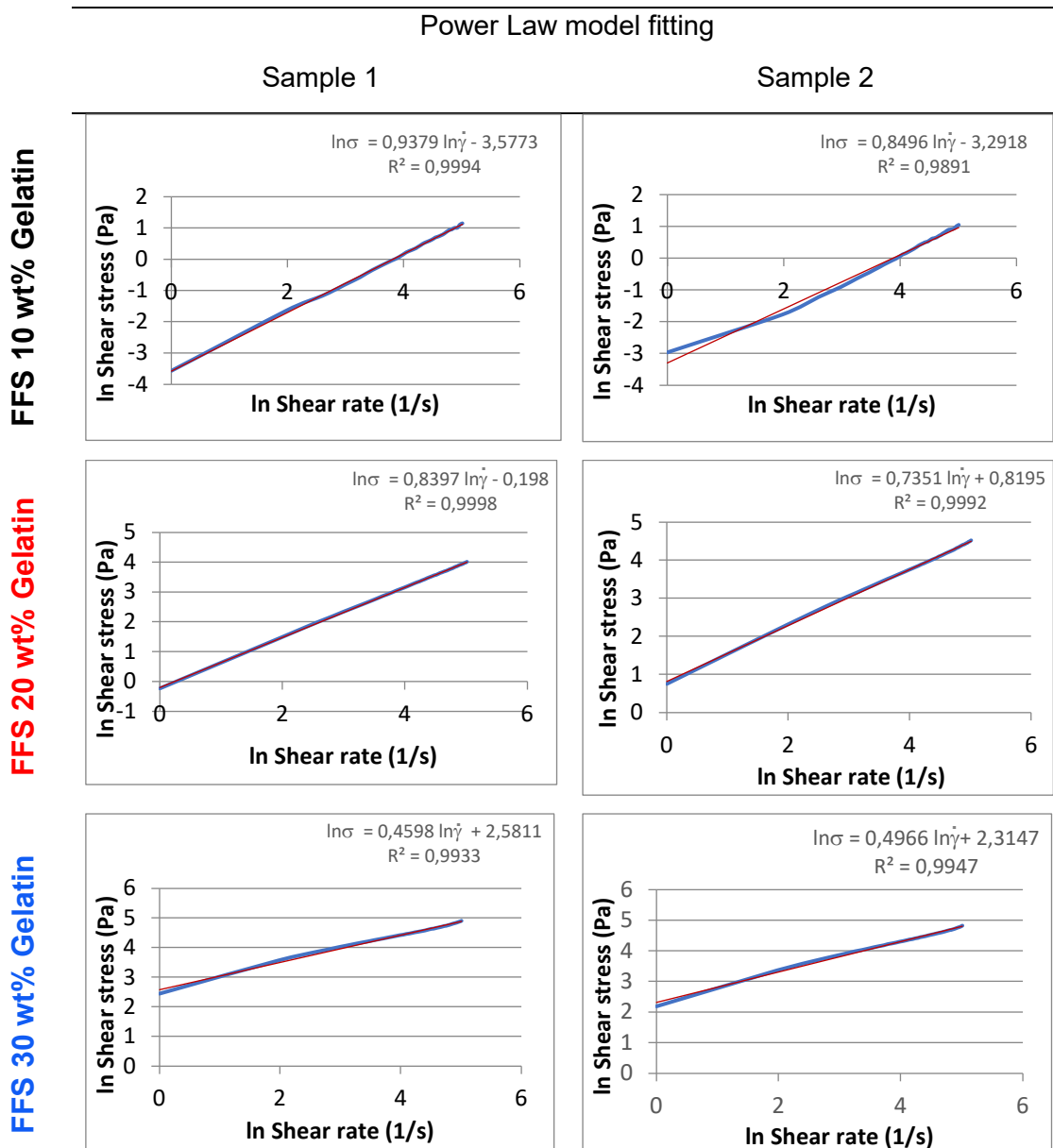


Figure 2.4 - Power Law model fitting for the film-forming solutions as a function of gelatin concentration at 30 °C.

The apparent viscosity (η) and consistency index (K) increased, and the flow index (n) was lower than 1 and decreased, with the increasing gelatin concentration (Table 2.1). This means that the gelatin solutions were pseudoplastic (shear-thinning) behavior and became progressively more viscous at high gelatin contents. This behavior is suitable for producing films by continuous casting, which required solutions that could be sheared at the low shear rates at the doctor blade ($\dot{\gamma} = 3 \text{ s}^{-1}$) of the casting process (Figure 2.1) but

also exhibit high viscosity at low shear rates to prevent undesired flow onto the moving substrate [204].

Usually, gelatin films are obtained by bench casting using solutions containing ≤ 10 wt% gelatin [166,200,212–215]. Nevertheless, this concentration was not adequate for our continuous casting technique because the solution flowed off from the substrate before the drying step due to its low viscosity. On the other hand, it was not possible to obtain homogeneous films from solutions with gelatin concentrations higher than 20 wt% due to their very high viscosity and fast gelation under cooling, which resulted in incomplete spreading on the moving substrate and discontinuous films. Therefore, the FFS containing 20 wt% gelatin, which exhibited adequate flow properties and could be spread properly on the substrate, was selected to evaluate the influence of the CNCs on the bionanocomposite film properties. The wet layer thickness was set at 1.00 mm. In this way, the continuous casting operated at a shear rate of approximately 3 s^{-1} .

Table 2.1- ζ -potential of gelatin and CNCs suspensions and viscosity and rheological parameters of gelatin FFS calculated by the Power Law model.

ζ -potential (mV)			FFS (wt%)	Viscosity (Pa s) at 3 s^{-1}	k (Pa s ⁿ)	n
pH	Gelatin	CNCs				
3	19.0 ± 1.1^a	-50.3 ± 2.2^a	10	0.04 ± 0.01^a	0.03 ± 0.01^a	0.89 ± 0.06^a
6	-0.5 ± 0.1^b	-50.4 ± 2.2^a	20	3.95 ± 0.35^b	1.54 ± 1.02^b	0.79 ± 0.07^a
8	-5.3 ± 0.1^c	-48.9 ± 0.4^a	30	169.33 ± 54.70^c	11.67 ± 2.18^c	0.48 ± 0.03^b

Values with a different superscript in the same column are significantly different ($p < 0.05$) according to Turkey's test.

Figure 2.5a shows the flow curves of the gelatin-based FFS containing different CNCs concentrations. The apparent viscosity of all FFS decreased faster at low shear rates ($< 100 \text{ s}^{-1}$), indicating their pseudoplastic behavior, regardless of the CNCs concentration. Figure 2.5b shows the influence of temperature on the rheological behavior of the gelatin/CNCs FFS. The increase of the CNCs concentration led to more viscous FFS compared to the pure gelatin

solution (0 wt% CNCs), most likely due to interactions between the CNCs and the gelatin chains. Similar behavior was observed in PLA-CNCs nanocomposites by Bagheriasl et al. (2016). The authors attributed the increase in the viscosity of all nanocomposites to the formation of a CNCs network and particle-particle interactions.

In addition, the apparent viscosity decreased with the increasing temperature at around 40 °C [217]. This behavior is typical of physical gels which present sol-gel ($T_{\text{sol-gel}}$) and gel-sol ($T_{\text{gel-sol}}$) transitions, whenever the solutions are cooled or heated, respectively [80]. The gelation of gelatin is a physical process that is mostly dependent on intermolecular interactions among protein chains through electrostatic, hydrogen bonding as well as hydrophobic interactions, which largely lead to the formation of a three-dimensional network [218].

Figure 2.5c shows the viscoelastic moduli (storage modulus G' and loss modulus G'') of the FFS with different CNCs concentrations obtained from temperature sweep tests. All samples presented a similar viscoelastic behavior: high G' and G'' and low G' and G'' moduli at temperatures below and above the $T_{\text{sol-gel}}$, respectively. The gelatin/CNCs FFS exhibited higher viscoelastic moduli compared to those of the pure gelatin solution at a fixed temperature. For the highest CNCs concentration, i.e., 2.5 wt% CNCs, the FFS still presented a gel-like behavior ($G' > G''$). Furthermore, the sol-gel transition temperature increased from 24.5 °C for the pure gelatin solution to 28.3 °C for the FFS with 0.5 wt% CNCs. These results may be due to the high stiffness of the CNCs and CNC-gelatin and CNCs-CNCs interactions, resulting in a more elastic behavior, as observed in Figure 2.5c [219,220].

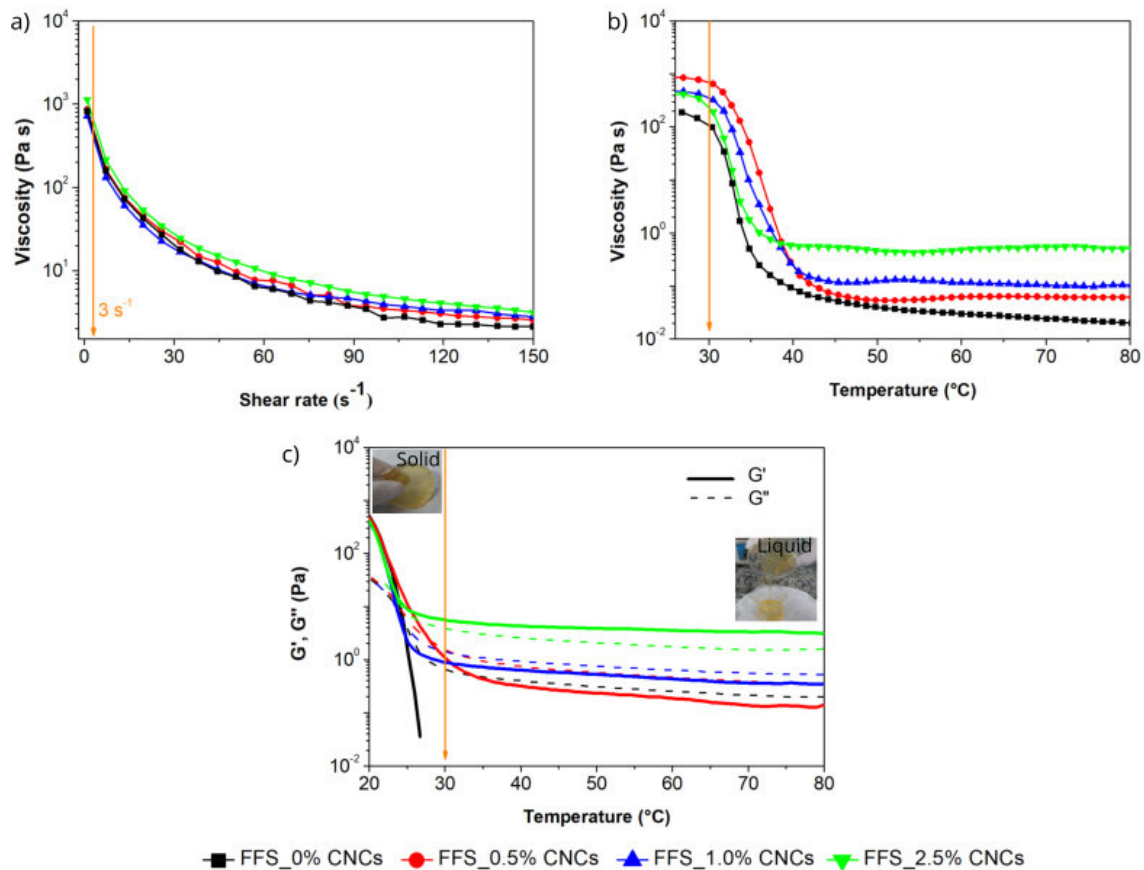


Figure 2.5 - Rheological characterizations of gelatin-CNCs FFS containing different CNCs concentrations (a) apparent viscosity vs. shear rate (25 °C), (b) apparent viscosity vs. temperature curves, and (c) storage modulus (G') and loss modulus (G'') vs. temperature curves.

1.3.3 Production capacity of gelatin/CNCs films by continuous casting

The gelatin/CNCs FFS were used at 30 °C to prevent their gelation during the continuous casting process. The major advantage of the continuous casting approach used herein is the shorter drying time due to the use of much higher temperatures concerning bench casting, and intense air circulation. Temperatures below 80 °C did not allow the efficient drying of the gelatin/CNCs FFS. On the other hand, temperatures above 80 °C led to gelatin/CNCs film degradation due to extreme fast drying (data not shown). The continuous casting produced 12 m/h of gelatin/CNCs films. The wet layer thickness of 1 mm was used to obtain dry films with a thickness of about 0.065 mm. More importantly,

the continuous casting approach used in this work had significantly higher productivity compared to nanocellulose-based nanocomposites and other films produced by bench casting reported in the literature (Table 2.2).

Table 2.2 - Productivity of biopolymers-based films produced by casting/evaporation.

Polymer	Reinforcement	Drying conditions	Productivity	Ref.
Cassava	Fibers	60 °C	0.001 m ² /min of film	[193]
k-carrageenan	CNCs	40 °C	Glass petri dish/24h	[221]
Soy protein	SNC	50 °C	Petri dishes/24h	[201]
Soy protein	-	60 °C	0.002 m ² /min of film	[204]
Soy protein	CNF	37 °C	3.3 x 10 ⁻⁶ m ² /min of film	[222]
Gelatin	CNCs	24 °C	Glass plates/24h	[165]
Gelatin	CNCs, CNF	24 °C	Petri plates/48h	[166]
Gelatin	Montmorillonite	30 °C	5.4 x 10 ⁻⁵ m ² /min of film	[95]
Gelatin	Acid citric	24 °C	Petri dishes/48h	[98]
Gelatin	-	24 °C	3.5 x 10 ⁻⁶ m ² /min of film	[96]
Gelatin	Pomegranate peel	24 °C	Petri dishes/24h	[89]
Gelatin	Melanin	23 °C	2.5 x 10 ⁻⁵ m ² /min of film	[223]
Gelatin	CNCs	80 °C	0.03 m ² /min of film	This work

1.3.4 Morphological characterization

The morphology of the gelatin/CNCs bionanocomposites was investigated by SEM. Figure 2.6 shows the micrographs of the cryo-fractured cross-sectional surface of the films. As observed in Figure 2.6a, the pure gelatin film displayed a continuous and homogeneous matrix with a smooth fractured surface. The addition of CNCs gradually promoted the formation of a rougher fractured

surface, indicating a microstructural change in the gelatin matrix. There was no clear evidence of CNCs agglomerates in all the bionanocomposite micrographs analyzed, suggesting that the CNCs were homogeneously distributed within the gelatin matrix. The presence of CNCs is typically indicated by the appearance of shiny dots, which have been related to small CNCs agglomerates embedded within the polymer matrix [224] or CNCs-Gelatin aggregates or coacervate phases [225]. In this sense, the SEM micrographs corroborate with the ζ -potentials results (Table 2.1).

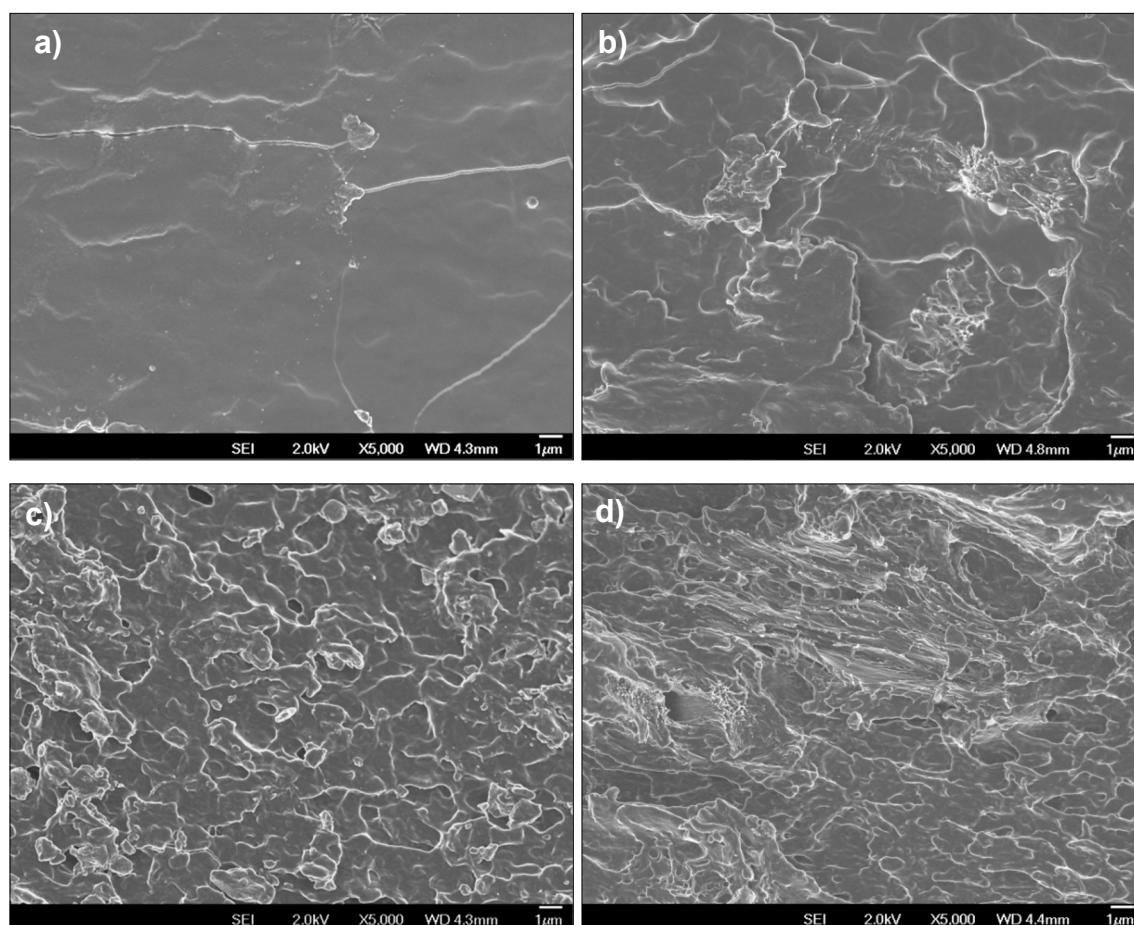


Figure 2.6 - SEM images of cross-sectional surfaces of films (a) pure gelatin and with (b) 0.5 wt% CNCs, (c) 1.0 wt% CNCs and (d) 2.5 wt% CNCs.

1.3.5 Structural aspects

Figure 2.7 shows the ATR-FTIR spectra of CNCs and gelatin powders and their corresponding bionanocomposites. The characteristic bands of gelatin are

related to -OH and NH at stretching $3600\text{-}2300\text{ cm}^{-1}$ (amide A), =C-H and -NH_3^+ stretching at $3000\text{-}3100\text{ cm}^{-1}$ (amide B), C=O stretching (amide I) at 1632 cm^{-1} , N-H bending (amide II) at 1527 cm^{-1} , and C-N stretching (amide III) at 1238 cm^{-1} , the broad band above 3000 cm^{-1} correspondings to the free and bonded hydroxyl and amino groups, and the absorption band at 1330 cm^{-1} attributable to CH_2 wagging of proline [98]. No significant changes were observed in the gelatin/CNCs bionanocomposite spectra since the characteristic bands attributed to gelatin are in similar positions. Mondragon et al. (2015) observed that the intensity of the band at 1030 cm^{-1} increased for gelatin bionanocomposites with 10 wt% CNCs and 10 wt% CNF. Such an increase was not clearly observed in the ATR-FTIR spectra of the gelatin/CNCs films.

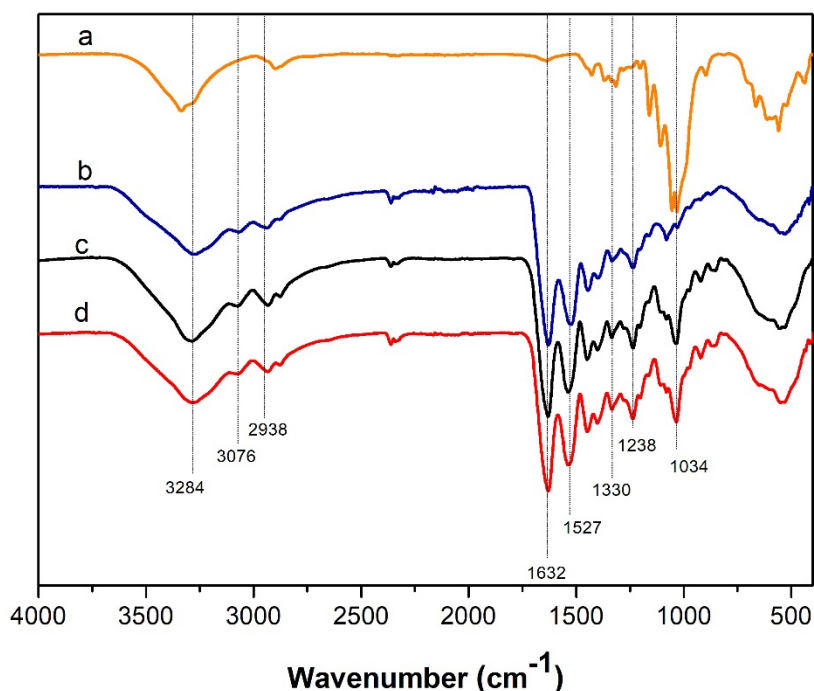


Figure 2.7 - ATR-FTIR spectra of (a) CNCs powder, (b) gelatin powder and gelatin/CNCs bionanocomposite films with (c) 0 wt% CNCs and (d) 2.5 wt% CNCs.

1.3.6 Optical and thermal properties

The gelatin/CNCs bionanocomposite films presented good macroscopic homogeneity and continuity, with no cracks or insoluble particles on the film surface as shown in Figure 2.8.

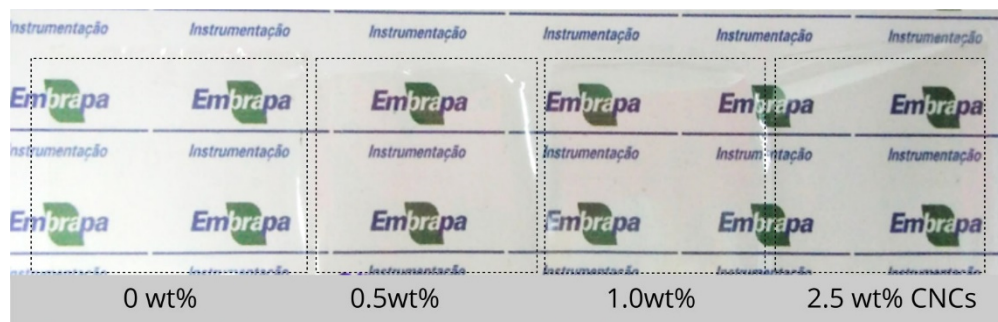


Figure 2.8 - Photography of gelatin/CNCs bionanocomposite films obtained by continuous casting.

Optical properties, such as color and transparency, were analyzed. The color parameters ΔL^* , Δa^* , Δb^* , and ΔE^* were determined and listed in Table 2.3. There were no differences between ΔE^* values of the films, indicating that the incorporation of the CNCs did not change the color of the gelatin film ($p > 0.05$). Moreover, all films were transparent with no significant differences ($p > 0.05$). Transparency is a microstructural parameter and high values of transparency suggest the absence of micrometric agglomerates that could scatter light [98]. In this case, the transparency data suggest a good macroscopic dispersion of the CNCs within the gelatin matrix of the bionanocomposites made by continuous casting.

Table 2.3 - Color parameters, transparency, and thermal properties of gelatin/CNCs bionanocomposite films.

CNCs (wt%)	ΔL^*	Δa^*	Δb^*	ΔE^*	Transparency (mm^{-1})	T_{onset} ($^{\circ}\text{C}$)
0	2.9 ± 0.4	0.8 ± 0.1	1.7 ± 0.3	3.5 ± 0.1^a	0.7 ± 0.1^a	205.9
0.5	2.4 ± 0.4	0.8 ± 0.1	1.6 ± 0.1	3.0 ± 0.4^a	0.7 ± 0.1^a	207.3
1.0	2.9 ± 0.1	0.8 ± 0.1	1.6 ± 0.2	3.4 ± 0.1^a	0.6 ± 0.1^a	214.9
2.5	2.6 ± 0.7	0.7 ± 0.1	1.9 ± 0.2	3.2 ± 0.4^a	0.7 ± 0.2^a	216.5

Mean values followed by the same letter in the same column are not significantly ($p > 0.05$) different according to the Tukey's test.

Photo-oxidation is one of the main mechanisms of food deterioration. Packaging with a light barrier has received special attention due to the protective effect against the oxidation of lipids and some other nutrients catalyzed by UV light [54]. Figure 2.9 shows the UV-Vis transmittance spectra of the gelatin/CNCs films. The bionanocomposites showed good light barrier properties, mainly in the UVC region, where they were able to block more than 99% of the radiation. This can be attributed to the chromophore groups presented in gelatin amino acid blocks, such as tyrosine and phenylalanine, which have unsaturated bonds capable of absorbing UV radiation [96]. Furthermore, the addition of 2.5 wt% CNCs slightly reduced by 10% and 6% the UVA transmittance at 320 and 400 nm, respectively ($p < 0.05$). This is due to the hydroxyl groups of cellulose, which can act as auxochrome groups. These groups when conjugated to a chromophore are capable of modifying the ability of the chromophore to absorb light [98]. In summary, all the gelatin/CNCs bionanocomposites analyzed exhibited good barrier properties against the UV light, suggesting that this type of film could be used to protect light-sensitive products, including foods and pharmaceuticals.

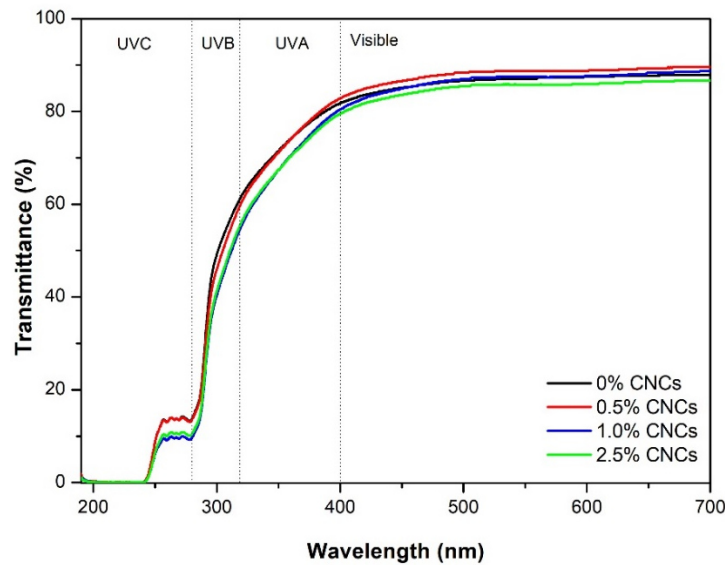


Figure 2.9 - UV-Vis spectra of pure gelatin film and its bionanocomposites with CNCs.

The thermogravimetric curves of gelatin/CNCs bionanocomposites films are illustrated in Figure 2.10 and the corresponding onset temperatures (T_{onset}) are shown in Table 2.3. The films exhibited two major mass loss stages. The first occurred at approximately 105°C, which could be attributed to the loss of free and bounded water adsorbed in the films. The second stage (T_{onset}) occurred at around 206 °C and it was mainly associated with the decomposition of gelatin molecules, as well as glycerol and CNCs. The results showed that gelatin films became more thermally stable for the highest CNCs contents, registering an increase in T_{onset} from 206 °C up to 217 °C for 2.5 wt% CNCs. Mondragon et al. (2015) observed similar increases in T_{onset} (7 and 9 °C) for gelatin films reinforced with 10% CNF and 10% CNCs, respectively. Hydrogen bonding formation between CNCs and gelatin chains can influence on protein denaturation process and formation of triple helix crystal structures, and, therefore, leading to an increase in the thermal stability of gelatin films [17]. Finally, temperatures above 600 °C are related to thermal oxidation processes and the combustion of the residues formed in the previous stages. Residual mass values after this stage were close to zero for all samples.

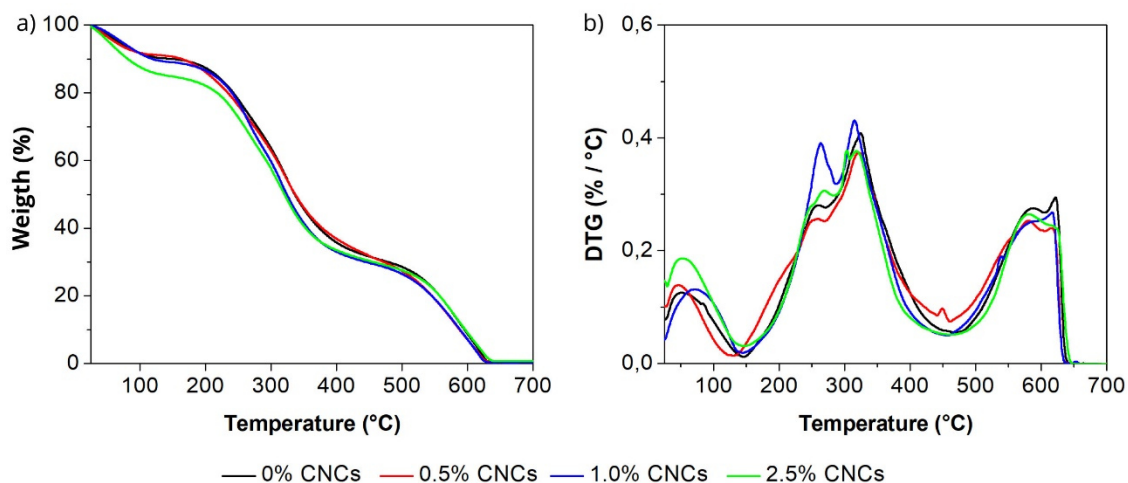


Figure 2.10 - (a) Thermogravimetric and (b) DTG curves of the gelatin/CNCs bionanocomposites obtained by continuous casting.

1.3.7 Mechanical properties

The mechanical properties of gelatin/CNCs bionanocomposite films produced by continuous casting are presented in Figure 2. 11. The results are compared with those of the corresponding films produced by bench casting. The gelatin/CNCs bionanocomposites showed higher tensile strength and Young's modulus than the unreinforced gelatin film (both produced by continuous casting), suggesting that there was stress transfer from the gelatin matrix to the CNCs. Furthermore, the addition of CNCs led to an increase of 148% in the elongation at break of the film reinforced with 1.0 wt% CNCs, if compared to the unreinforced matrix. This may be attributed to the inclusion of the stiff, nano-sized CNCs with a high aspect ratio ($L/D = 22.5$) into the soft gelatin matrix. Furthermore, the hydrophilic amino acid residues in the gelatin chains can form hydrogen bonds with the CNCs hydroxyl groups, strengthening the gelatin-CNCs interface. These interactions increased the mechanical resistance of the bionanocomposites even when the CNCs content was low. For the highest CNCs content (2.5 wt%), both tensile strength and elongation at break decreased. This may be related to morphological changes in the gelatin matrix and the formation of CNCs microscopic aggregates. Such a change might have imparted the stress transfer mechanism, and the dispersion of the CNCs within the gelatin film.

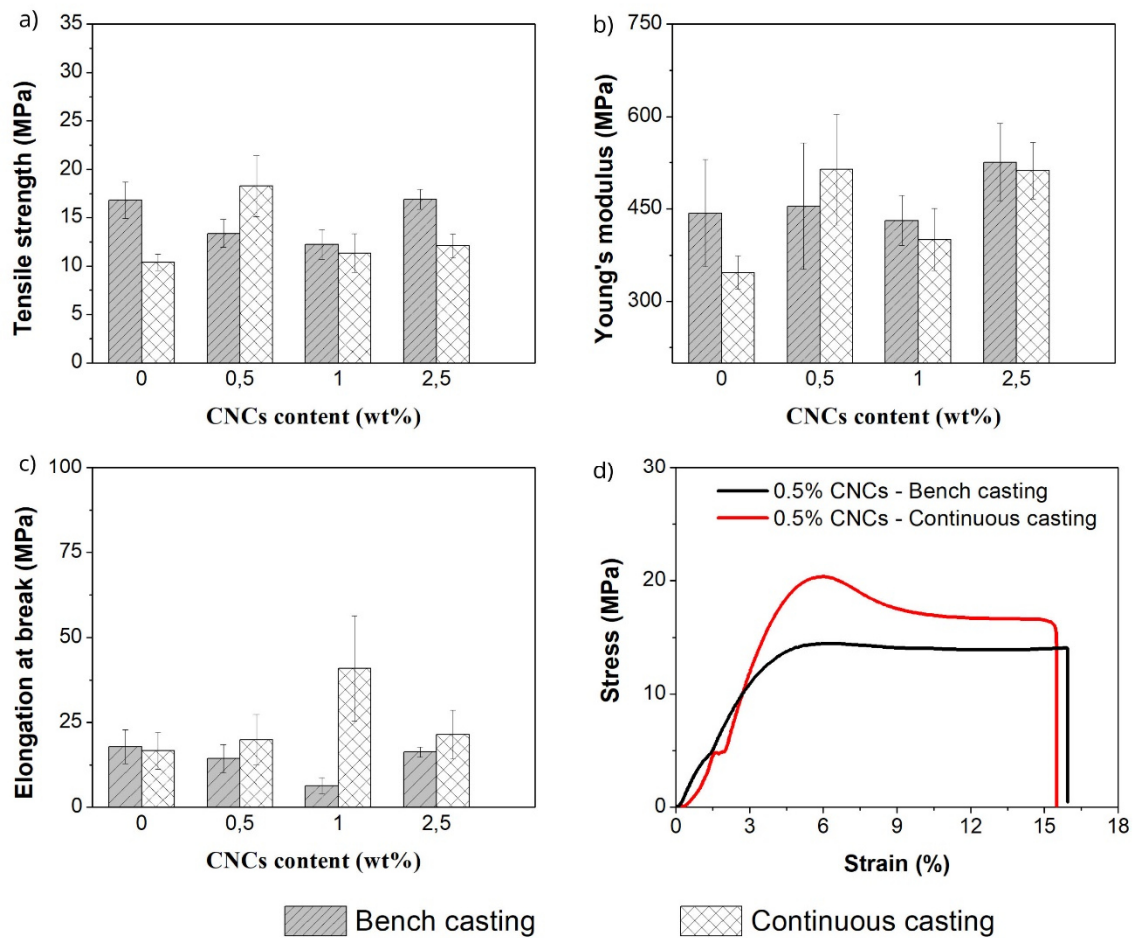


Figure 2. 11 - (a) Tensile strength, (b) Young's modulus (c) strain at break, and (d) stress-strain curves as a function of CNCs content in gelatin films obtained by bench casting and continuous casting.

1.4 Conclusions

We demonstrated that continuous casting is a suitable technique to hasten the production of bionanocomposites based on gelatin and cellulose nanocrystals from aqueous formulations. The continuous casting involved relatively low drying temperatures and allowed the production of 12 m/h of bionanocomposite film. All gelatin/CNCs bionanocomposites were highly transparent and easy to handle. More importantly, the continuously cast gelatin/CNCs films reached higher mechanical resistance at a low CNCs content (0.5 wt%) than similar nanocellulose-based nanocomposites produced by bench casting. This means that the continuous casting not only allowed scaling-up the production of these

bionanocomposites but also led to films with relatively superior mechanical performance, in addition to good thermal and UV barrier properties. It is noteworthy that improvements in such properties are of great interest to produce flexible films for food packaging, membranes for wound healing, and so on. We particularly expect that this continuous casting approach will serve as an alternative pilot-scale route to produce nanocellulose-based nanocomposites when the nanocellulose dispersion is not easily achieved through melt processing routes.

2 The relationship between heterogeneous CNCs and homogeneous CNCs suspensions and physical properties of gelatin-based films obtained by bench casting and continuous casting

Abstract

Polarized light images of gelatin/CNCs film-forming solution at different cellulose nanocrystals (CNCs) concentrations obtained in the first part of this chapter (Chapter II.1), revealed a wide range of CNCs microaggregates (ca. 5-60 μm), suggesting a poor CNCs dispersion and/or a heterogeneous CNCs suspension. Therefore, since these aggregates can influence the performance of the films, for a better evaluation of the continuous casting method on the physical properties of gelatin-based films, it is also necessary to investigate the quality of the CNCs dispersion. In this second part of chapter II, the dispersion of heterogeneous and homogeneous CNCs suspension and their morphology were analyzed. Homogeneous CNCs showed a relatively narrow distribution of length and diameter, and a higher aspect ratio and crystallinity. Therefore, they are chosen to assess the influence of CNCs on the properties of the gelatin-based films obtained by different methods. Gelatin films with 4.0 wt% homogeneous CNCs produced by continuous casting exhibited a decrease of 50% in water vapor permeability and high tensile strength (36 MPa) and Young's modulus (1.8 GPa) compared with its counterpart obtained by bench casting. In addition, gelatin/CNCs films produced by continuous casting presented hydrophilic surfaces and became more thermally stable compared with gelatin/CNCs films obtained by bench casting.

2.1 Introduction

The quality of the dispersion of CNCs particles in the film-forming solution plays an important role in the properties of the film produced by spreading. CNCs have a high specific surface area and surface energy. Consequently, these nanoparticles have a strong tendency for agglomeration (Figure 2.12a,b). CNCs agglomeration can lead to a decrease in the strength of the nanocomposites since they act as defects or stress concentrators [226]. Previous studies have demonstrated that a good dispersion and distribution of CNCs into the matrix (Figure 2.12d) can improve the thermal and mechanical properties of the films [227]. The challenge consists therefore in avoiding agglomeration and promoting the homogeneous dispersion and distribution of the CNCs, which favor CNCs-matrix interactions, and at the same time promoting CNCs-CNCs interactions to allow the beneficial formation of a percolating network of nanoparticles [125]

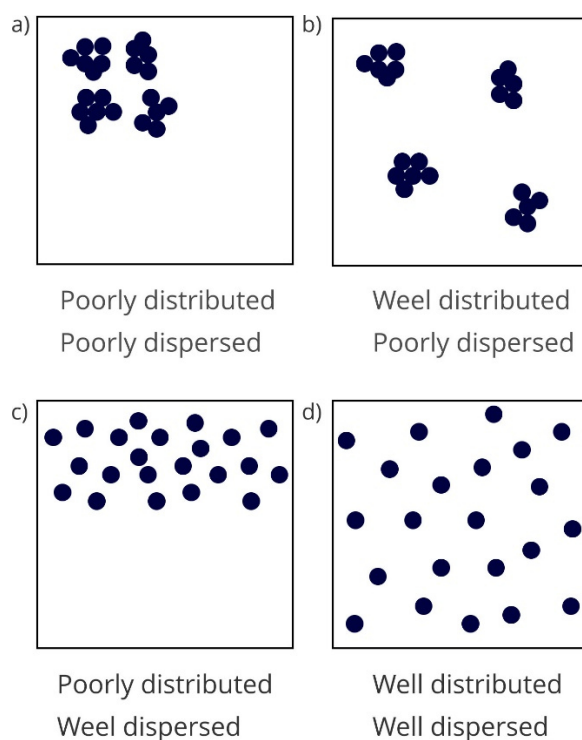


Figure 2.12 - Schematic of poor and well dispersion and distribution of particles

Two methods to disperse the agglomerated nanoparticles have been reported in the literature. The first method is to use mechanical energy to

separate the particles, and the second method consists of altering the surface energy of the particles by functionalization (covalent and non-covalent). The mechanical approach has used high shear mixing and/or ultrasonication to break agglomerates or to reduce their size. The final particle size is determined by the competition between hydrodynamic forces and cohesive forces (Van der Waals and hydrogen bond interactions). However, there is no guarantee that all agglomerated particles will separate during mixing, and some of them remain intact. This is because the hydrodynamic force (by pulling mechanism) required to fully separate two parallel CNCs particles is 115 nN, much greater than the break-up force for the C-C covalent bond (2.5-13 nN) [228]. Thus, if this amount of force is provided, the polymer chain scission and degradation can take place before particle separation.

Therefore, the separation of CNCs nanoparticles into individual nanoparticles is quite challenging. The CNCs microstructure depends highly on the employed hydrolysis conditions and drying techniques. In this study, a tip-sonication was performed to disperse the heterogeneous CNCs and homogeneous CNCs in film-forming solutions. The aggregates of both CNCs and their dispersibility in gelatin film-forming solutions were analyzed. The morphological, mechanical, thermal, and barrier properties of gelatin-based films obtained by bench casting and continuous casting were also investigated.

2.2 Materials and Methods

2.2.1 Materials

Bovine gelatin (Bloom Strength-190) and eucalyptus kraft pulp were kindly supplied by Gelco Gelatinas do Brazil Ltda (Pedreira, SP) and Suzano Papel e Celulose Ltda (Limeira, SP), respectively. Homogeneous CNCs isolated from wood pulp by sulfuric acid hydrolysis and delivered as a dried powder, were purchased from Celluforce Inc. (Windsor, Québec, Canada). Sulfuric acid and glycerol were purchased from Across Organics (USA). All aqueous solutions were prepared using ultrapure water (18 M Ω .cm) obtained from a Milli-Q system (Millipore).

2.2.2 Hydrolyses of CNCs from eucalyptus kraft pulp

The CNCs were prepared by acid hydrolysis of 10 g of eucalyptus kraft pulp using 200 mL of 60% w/w sulfuric acid solution at 45 °C for 60 min with constant stirring. After hydrolysis, the suspension was diluted in 500 mL of cold water to quench the reaction and centrifuged at 10000 rpm for 10 min. The resultant pellet was rinsed, re-centrifuged, and dialyzed in water with a cellulose membrane (6-8 kDa) until neutral pH. Afterward, the suspension was sonicated for 5 min and stored in a refrigerator after adding chloroform drops to prevent microbial growth. The final solid content was 3.5% (w/w). These CNCs were called in this work as heterogeneous CNCs.

2.2.3 Preparation film-forming solutions (FFS)

FFS based on gelatin and CNCs were prepared according to the following steps: first, gelatin powder was hydrated in ultrapure water at concentrations of 20 wt% (for continuous casting) and 10 wt% (for bench casting) at 24 °C for 5 min, and then heated at 60 °C under mechanical stirring for 15 min. Glycerol (20 wt% on a dry gelatin basis) was added to the gelatin solution under stirring. The solution obtained was mixed with the heterogeneous CNCs at various contents (0 wt%, 0.5 wt%, 1.0 wt%, and 2.5 wt%, on a dry gelatin mass basis) and stirred for 5 min. The maximum concentration of heterogeneous CNCs added was 2.5%. Above this concentration, it was observed with the naked eye aggregates in the FFS. FFS with homogeneous CNCs at various contents (0 wt%, 0.5 wt%, 4.0 wt%, and 6.0 wt% on a dry gelatin mass basis) were prepared in the same manner described above for comparison. These concentrations were chosen based on the percolation threshold calculation for homogeneous CNCs, as discussed in more detail in the results and discussion section.

2.2.4 Polarized light optical microscopy (POM)

Optical images of gelatin/CNCs FFS were taken between crossed polarizers to evaluate the dispersion of the heterogeneous CNCs within the gelatin matrix. The dispersion of 1.0 wt% of aqueous heterogeneous and

homogeneous CNCs suspensions was also analyzed. The samples were imaged by polarized optical microscopy taken at 10-fold magnification using a microscope Zeiss Axio Vert.A1 (Carl Zeiss Microscopy).

2.2.5 Transmission electron microscopy (TEM)

Transmission electron microscopy was carried out on a Tecnai TM G2 F20 microscope (FEI Company, Netherlands) using the TEM (Transmission Electron Microscopy) mode. The images were acquired with a dark field (DF) detector. A droplet of diluted heterogeneous and homogeneous CNCs suspension was deposited on a carbon microgrid with formvar (400 mesh) and allowed to dry. The grid was stained with 1.5 wt% uranyl acetate solution and dried at room temperature before analysis. Average CNCs sizes were obtained from a minimum of 100 particles by using the ImageJ software.

2.2.6 X-ray diffraction (XRD)

The crystallinity of heterogeneous and homogenous was estimated by XRD (Panalytical diffractometer, X'Pert Pro MPD-Ray, The Netherlands) with Ni-filtered Cu K α radiation ($\lambda = 1.54 \text{ \AA}$, 45 kV, 40 mA) in the 2θ range from 5° to 60° . The crystallinity index (CI) was calculated according to the method of Segal et al. [229]:

$$CI (\%) = \left(1 - \frac{I_1}{I_2}\right) \times 100 \quad (1)$$

where I_1 is the intensity at the minimum ($2\theta = 18^\circ$) and I_2 is the intensity associated with the crystalline region of cellulose ($2\theta = 22.7^\circ$).

XRD patterns of the gelatin/CNCs films were acquired from 2° to 60° (2θ). At least duplicate measurements were performed for each sample. The amount of triple helix configuration (X_c in %) in the gelatin/CNCs films was calculated using Equation. 2.

$$Xc = [A_c / (A_c + A_a)] \times 100 \quad (2)$$

where A_c is the area of the diffraction peak at $\sim 2\theta = 8^\circ$, corresponding to the triple helix configuration of gelatin chains, and A_a is the area under the hump located at $\sim 2\theta = 21^\circ$, corresponding to the fraction of amorphous domains in the gelatin films [230].

2.2.7 Bench casting

Gelatin-based FFS with homogeneous CNCs (60 mL) were cast on glass plates (40 cm \times 25 cm) covered with a polyester film (Mylar®, DuPont, Brazil) to facilitate peeling off the films after drying at room temperature for 24 h. Film samples were conditioned in a desiccator at 50% RH and 25 °C for at least 48 h prior to testing.

2.2.8 Continuous casting

Gelatin-based FFS with homogeneous CNCs were turned into monolayer films on a KTF-S labcoater casting machine (Werner Mathis AG, Switzerland). In this technique, the polymer solution is continuously spread onto a moving substrate (Mylar®, DuPont, Brazil) with a doctor blade device, which allows controlling the wet layer thickness. The wet solution layer then passes through two drying chambers with controlled temperatures. The wet solution layer then passes through two drying chambers with controlled temperatures. The dried film is wound into rolls. The distance between the substrate and doctor blade was set at 1.0 mm. The conveyor speed and the drying ovens were 12 m/h and 80 °C, respectively. All samples were conditioned in a desiccator at 50% RH and 25 ± 2 °C for at least 48 h prior to testing.

2.8.9 Tensile test

The mechanical properties were measured according to ASTM standard method D882-09 (2009). Film specimens were prepared and equilibrated at 23 °C and 50% RH for 48 h to be tested on a universal testing machine EMIC

DL3000 (EMIC Equipamentos e Sistemas de Ensaio LTDA, Brazil) equipped with a 100 N load cell. Specimens were stretched using a crosshead speed of 10 mm min⁻¹ and initial distance between clamps of 100 mm. Tensile tests were performed with five replicates for each film.

2.2.10 Scanning electron microscopy (SEM)

The cross-sectional surface of the gelatin/CNCs film samples was investigated using a scanning electron microscope (SEM), model JMS 6510, (JEOL, Japan). Samples were first cryo-fractured in liquid N₂ and then fixed onto 90° specimen mounts. Once coated with a ca. 5-nm-thick gold layer in an argon atmosphere, the samples were analyzed using an accelerating voltage of 2 kV and a working distance of ca. 5 mm. All SEM images were taken using the secondary electron mode.

2.2.11 Field emission gun scanning electron microscopy (FESEM)

The morphology of the cryogenically fractured gelatin/CNCs films was analyzed by micrographs in a field emission gun scanning electron microscopy, model JSM 6701F (JEOL®), using an accelerating voltage of 2 kV. The FEG-SEM samples were mounted on copper stubs and then coated with carbon.

2.2.12 Water Vapor Permeability (WVP)

The WVP of the gelatin/CNCs films was determined following ASTM E-96-01. The preconditioned film was sealed onto the opening of an aluminum permeation cup (28 mm internal diameter) containing dried calcium chloride. The cup was kept in a controlled chamber at 23 ± 1 °C and 50 ± 5% RH. The cup was weighed at least four times for at least 7 days under this controlled environment. For each film, three replicates were performed. WVP [(g mm)/ m² h kPa) was determined using Eq. 2:

$$\text{WVP} = \text{WVTR} \times L/\Delta p \quad (2)$$

in which WVTR is the water vapor transmission rate ($\text{g/m}^2 \text{ h}$) through the film area; L is the film thickness (mm), and Δp is the partial pressure gradient (kPa) across the film.

2.2.13 Contact angle measurements

Contact angle measurements were conducted with CAM 101 Optical Contact Angle Meter (KSV Instruments, Finland) equipped with a CCD KSV-5000 digital camera. For each measurement, 5 μL of ultrapure water was dropped on the film surface and 100 images were automatically recorded within an experimental time of 60 s using the KSV CAM2008 software. Contact angle determinations were performed with 5 replicates as per ASTM D5725-99 (2008).

2.2.14 Thermogravimetric analysis (TGA)

Thermogravimetric analysis was carried out in a Q500 equipment (TA Instruments, USA). About 10 mg of each film sample was taken in a standard aluminum cup and heated from 25 $^{\circ}\text{C}$ to 600 $^{\circ}\text{C}$ with heating rate of 10 $^{\circ}\text{C min}^{-1}$, under an inert atmosphere of nitrogen (60 mL/min). Samples before the TGA tests were conditioned at 23 ± 1 $^{\circ}\text{C}$ and $50 \pm 5\%$ RH for 48 h.

2.2.15 Statistical analysis

Data were submitted to analysis of variance (ANOVA). Mean values were compared using the Tukey's test at a confidence level of 95% ($p < 0.05$) using the software Origin (OriginLab, Northampton, USA).

2.3 Results and discussion

2.3.1 CNCs isolated from eucalyptus pulp into gelatin FFS

Polarized light images of gelatin and gelatin/CNCs FFS at different heterogeneous CNCs concentrations are shown in Figure 2.13a. As expected,

no macroaggregated was observed in the pure gelatin FFS (0 wt% CNCs). However, gelatin/CNCs FFS showed a broad range of aggregates (ca. 5-60 μm) that increased with increasing heterogeneous CNCs content, suggesting a poor dispersion. Photographs of pure gelatin and gelatin/CNCs films are shown in Figure 2.13b. All the gelatin-based films showed good continuity with no visible cracks. Nevertheless, the addition of heterogeneous CNCs into the gelatin matrix induced the formation of visible roughness on the dry surface in contact with the air. This can be attributed to the presence of CNCs aggregation. Since the increase in roughness is an indication of poor dispersion and interfacial interaction between the reinforcement phase (CNCs) and the matrix phase (gelatin) [231].

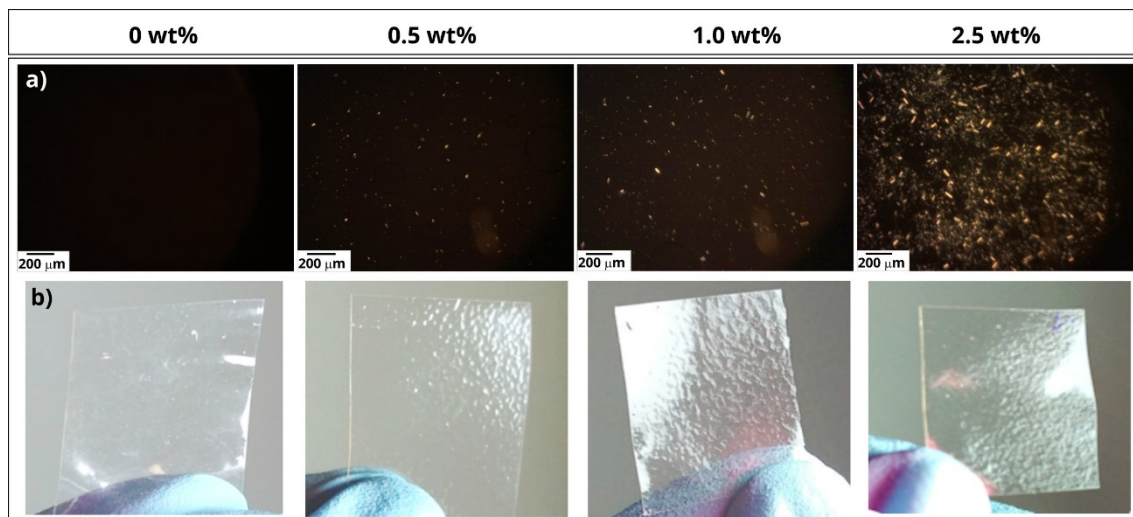


Figure 2.13 - (a) Polarized light images of gelatin FFS with heterogeneous CNCs and (b) photographs of gelatin films with heterogeneous CNCs obtained by continuous casting (Chapter II.1).

The maximum amount of CNCs incorporated in the FFS was 2.5 wt%. Above this concentration, the gelatin/CNC films obtained showed macroscopic aggregates with the naked eyes in the FFS. This is may be attributed to the presence of some partially hydrolyzed fibers (arrow in Figure 2.14). The presence of these microparticles is indicative of the lower yields attained during the sulfuric hydrolysis, which can result in a heterogeneous CNCs size distribution

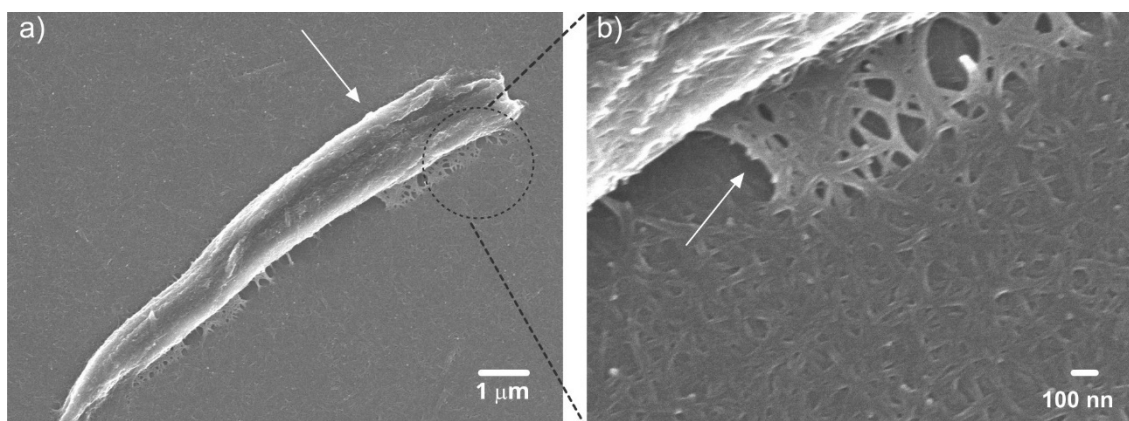


Figure 2.14 - (a) TEM micrograph of heterogeneous CNCs with partially hydrolyzed fiber (arrow) and (b) an magnified view of the image (a) showing the agglomeration of CNCs particles (arrow).

2.3.2 Heterogeneous CNCs vs. homogeneous CNCs

Polarized light images of heterogeneous and homogeneous CNCs are shown in Figure 2.15a. The aqueous suspension of heterogeneous CNCs showed more microscopic aggregates after sonication than homogeneous CNCs suspension, which suggests a better dispersion of the last nanoparticles. TEM images of both CNCs nanoparticles are shown in Figure 2.15b and their average dimensions values are presented in Table 2.4. All CNCs samples presented needle-like morphology. Heterogeneous CNCs showed the widest distribution with particles that range from 250-460 nm in length and 13-19 nm in diameter, which resulted in a lower aspect ratio. Homogeneous CNCs showed a relatively narrow distribution of length and diameter, and a higher aspect ratio. The crystallinity index was 76% for heterogeneous CNCs and 82% commercial CNCs (Table 2.4). The low crystallinity index found for heterogeneous CNCs can be attributed to the presence of amorphous components such as hemicellulose in the partially hydrolyzed fibers present in heterogeneous CNCs, as showed in Figure 2.14.

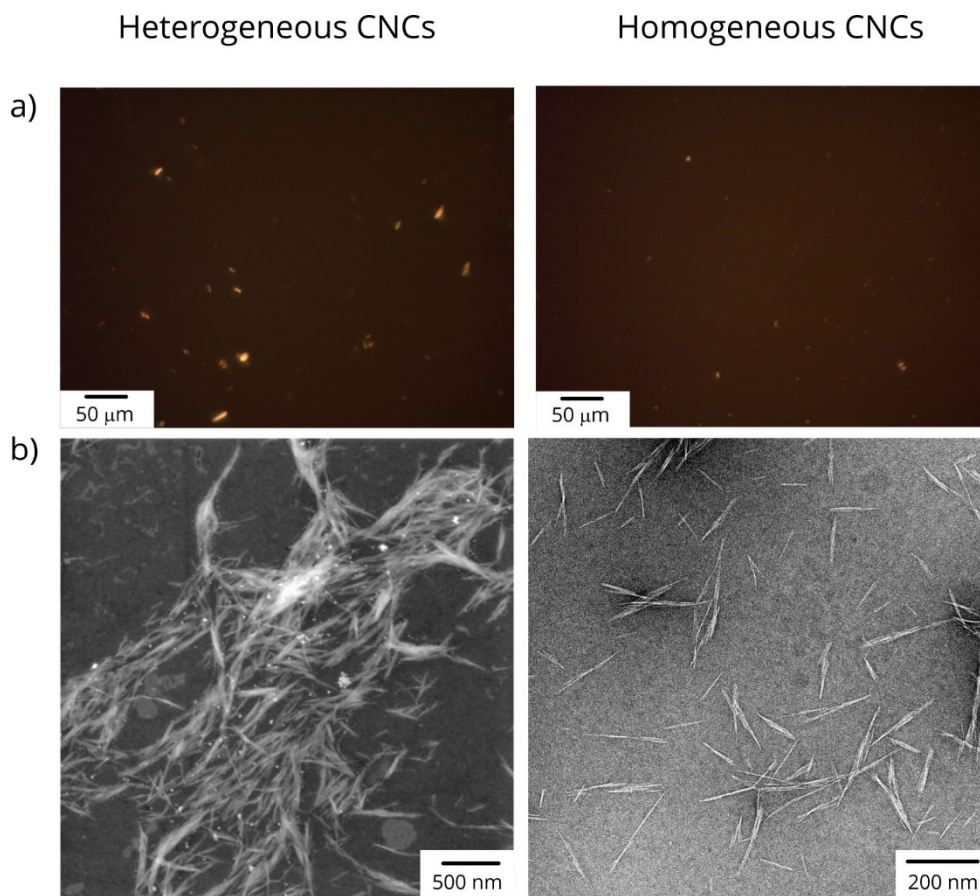


Figure 2.15 - (a) Polarized light images of heterogeneous and homogeneous CNCs aqueous suspensions at 1.0 wt% and (b) TEM micrograph of heterogeneous and homogeneous CNCs.

Table 2.4 - Average length, diameter, aspect ratios measured by TEM, and percent crystallinity determined by XRD, of heterogeneous and homogeneous CNCs.

Nanoparticles	Length (nm)	Diameter (nm)	Aspect ratio (L/D)	Crystallinity (%)
Heterogeneous CNCs	360 ± 104	16 ± 3	22.5	76
Homogenous CNCs	108 ± 33	3.8 ± 0.9	28.4	82

Therefore, as homogeneous CNCs showed the best dispersion in water, higher aspect ratio, and higher percent crystallinity compared to heterogenous CNCs, they were chosen to assess the influence of CNCs on the properties of the

gelatin-based films, and all the results presented below and in the following chapters refer to homogeneous CNCs, which will simply be called as CNCs.

2.3.3 Physical properties of gelatin-based films obtained by bench casting vs continuous casting

2.3.3.1 Mechanical properties of gelatin-based films

The mechanical properties, Young's modulus, tensile strength, and elongation at break of gelatin-based films were investigated using tensile tests and the results are shown in Figure 2.16. The Young's modulus and tensile strength of pure gelatin film obtained by bench casting were 743 and 17 MPa, respectively. The same film produced by continuous casting showed a significant increase ($p < 0.05$) of 106% for Young's modulus and 111% of tensile strength, while the elongation at break decreased to about 3%. This may be attributed to the combination of infrared radiation (IR) and higher drying temperatures applied in the continuous casting processing. The IR is a very efficient non-contact irradiation drying process that allows fast drying when containing molecules that can absorb IR as water, glycerol, and gelatin [232]. The first hypothesis is the evaporation of the plasticizer. Glycerol has a boiling point of around 290 °C. Although IR induces high temperatures in the laminated film layer, the glycerol boiling point could not be achieved without the deterioration of the gelatin matrix. Which was not the case. Therefore, it is unlikely that its evaporation could have caused the improvement in mechanical properties and this hypothesis can be eliminated.

Another hypothesis is molecular changes in the coating. According to Ortiz et al. (2017) [204], the IR applied during the casting manufacture of protein films may affect protein conformation and the protein chains can interact with each other, conditioning the physicochemical properties of the resulting materials. In addition, previous studies have shown that disulfide bridges are favored at high temperatures, presenting a major role in the stabilization of protein, which in turn influences the mechanical properties [204].[233]. The results of the mechanical properties of the pure gelatin film suggest that the film processing method

affected the level of protein interactions and molecular structure in the film matrix and will be better explored in the next section.

Gelatin/CNCs produced by bench casting showed a significant increase ($p < 0.05$) in the tensile strength and Young's modulus and decrease in the elongation at break with increasing CNCs content and reached a plateau between 4 wt% and 6 wt% CNCs, suggesting that percolation was achieved. To calculate volume fraction, Favier et al. (1997) [234] developed the following relation by using a statistical percolation theory for cylindrically shaped particles: $\phi_v = 0.7/(A)$, where A is the aspect ratio of CNCs. Therefore, considering the aspect ratio of CNCs as 28.5 (Table 2.4), the calculated volume fraction was 2.5% (v/v), which corresponds to 4 wt%, corroborating the tensile results.

Gelatin/CNCs films obtained by continuous casting showed a significant increase ($p < 0.05$) in Young's modulus with increasing CNCs content. Gelatin film with 0.5 wt% CNCs showed the highest tensile strength, compared with pure gelatin obtained by the same processing. No significant differences in the elongation at break have been detected. However, all the gelatin/CNCs produced by continuous casting became less ductile than their counterpart films obtained by bench casting, as shown in Figure 2.16d, indicating that films had a strong intermolecular interaction.

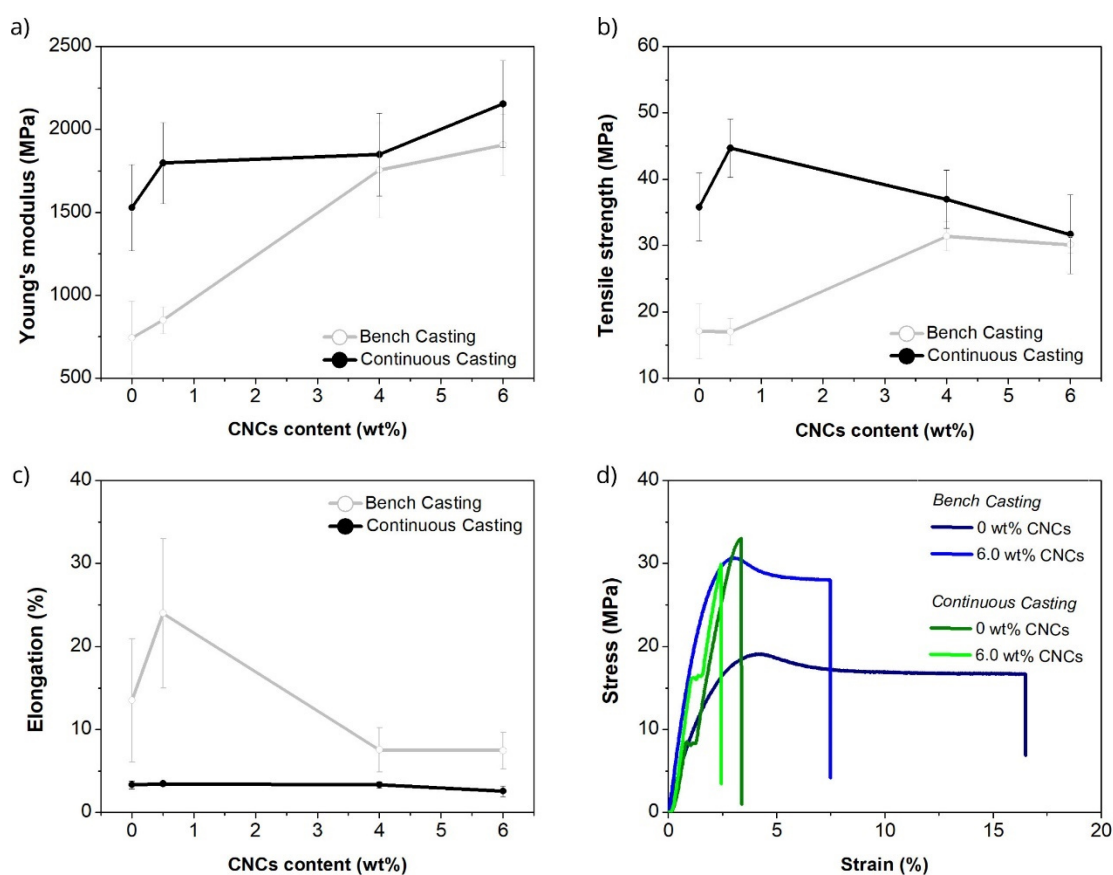


Figure 2.16 - (a) Young's modulus, (b) tensile strength, (c) strain at break, and (d) stress-strain curves as a function of CNCs content in gelatin films obtained by bench casting and continuous casting.

2.3.3.2 Structure analyses of gelatin-based films

The drying temperature used in the bench casting and also the IR used in the continuous process is a significant factor that affects the structure and physical properties of protein films. The XRD patterns of gelatin-based films are shown in Figure 2.17 and the triple helix content of them is represented in Table 2.5. The formation of gelatin film is accompanied by the partial renaturation of triple helix of the collagen structure [101], which is known to be crystalline. The XRD diffractograms showed a wide background with a band at $2\theta \sim 21^\circ$, related to the large amorphous fraction of gelatin [235]. The band at $2\theta \sim 8^\circ$ has been previously attributed to the presence of triple helix structure present in collagen and renaturated gelatin [90], and the area of this peak has been found to be directly related to the triple helix content of gelatin-based composites [235,236].

The pure gelatin film dried at 35 °C (bench casting processing) showed a higher triple helix content than pure gelatin film dried at 80 °C (continuous casting processing). This is due to the cold-dried films have a longer drying period, i.e. sufficient time for the reorganization of gelatin structures, than hot-dried films.

Surprisingly, the addition of 6.0 wt% CNCs increased the triple helix content by 60% in the gelatin/CNCs film, compared with the pure gelatin film obtained by obtained continuous casting. The CNCs contribute to the molecular reorganization of the gelatin and play an important role in the stabilization of the triple helix structure by intramolecular hydrogen bonds [237]. Though, this effect was not observed for the gelatin/CNCs film with the same amount of CNCs obtained by bench casting. This suggesting that there is a synergism between the high concentration of CNCs, IR, and high drying temperature in the formation and stabilization of the triple helix structure. However, the mechanic is still not entirely clear.

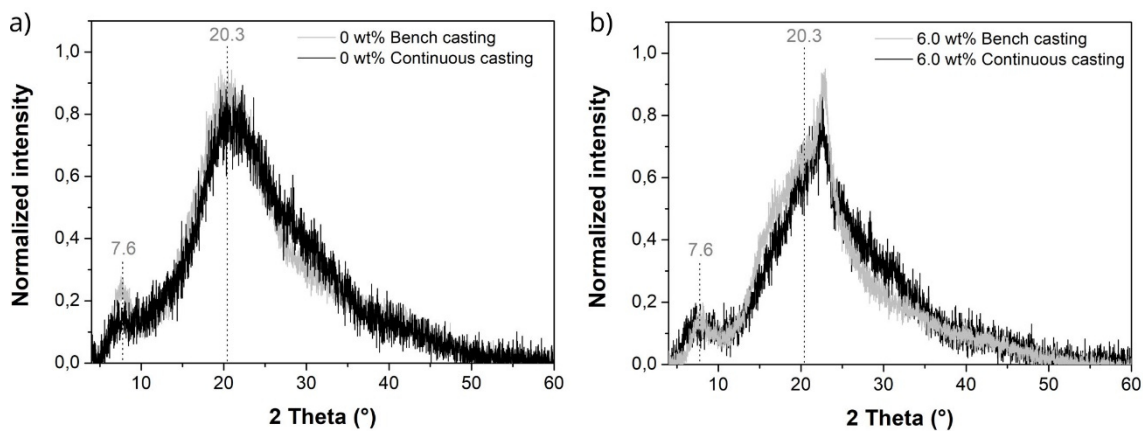


Figure 2.17 - XRD patterns of gelatin films with (a) 0 wt% CNCs and (b) 6.0 wt% CNCs obtained by bench and continuous casting.

Table 2.5 - Triple helix content of gelatin-based films obtained by bench and continuous casting.

Gelatin-based films	<i>Triple helix content (%)</i> *
Bench casting	
0 wt% CNCs	6.06
6.0 wt% CNCs	4.23
Continuous casting	
0%	4.62
0.5 wt% CNCs	4.41
4.0wt% CNCs	4.46
6.0 wt% CNCs	7.41

2.3.3.3 Morphological analysis of gelatin-based films

In an attempt to evaluate CNCs dispersion and distribution in gelatin-based films obtained by different methods, scanning electron microscope analyses were carried out. The micrographs of cryogenically fractured samples are shown in Figure 2.18. A roughness fractured surface was observed for pure gelatin obtained by both methods (Figure 2.18a, d). Gelatin films with 6.0 wt% obtained by bench casting showed a significant decrease in the fracture roughness (Figure 2.18b,c). On the other hand, gelatin/CNCs film obtained by continuous casting (Figure 2.18e,f) showed a homogenous and smooth fractured surface, suggesting a compact surface and good interfacial adhesion of CNCs to the matrix. Besides, no small CNCs aggregates were observed for gelatin/CNCs films obtained by both methods, indicating that even using high CNCs content, these nanoparticles show a good dispersion into the gelatin matrix [238].

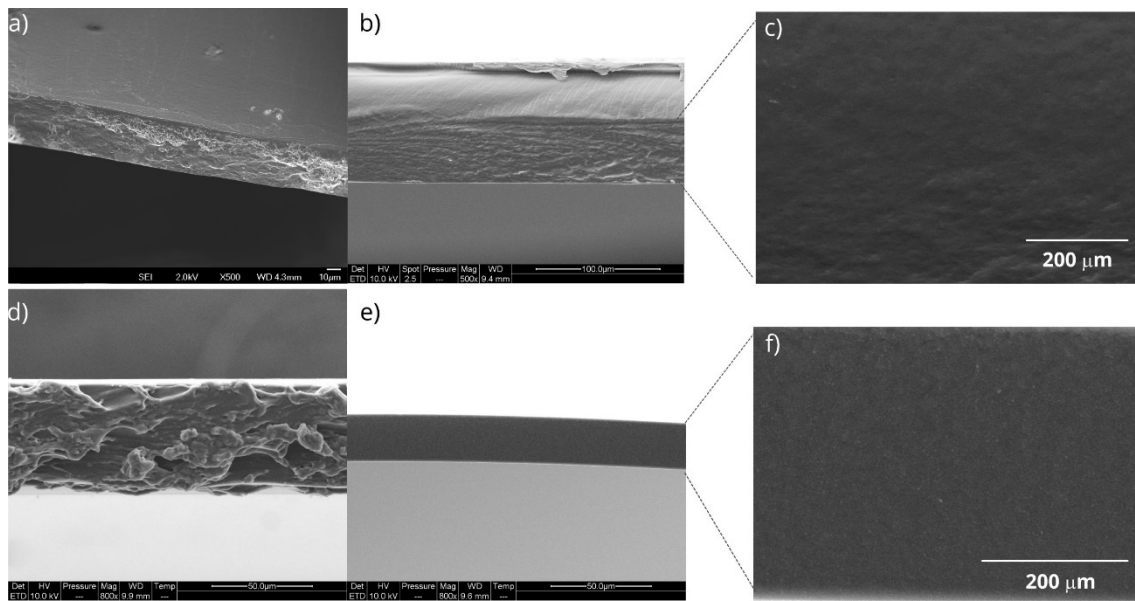


Figure 2.18 - SEM micrograph of the cross-sectional surface of (a) pure gelatin and (b) gelatin film with 6.0 wt% CNCs obtained by bench casting and (d) pure gelatin and (e) gelatin films with 6.0 wt% CNCs obtained by continuous casting. The magnified view of the image of (b) and (c) are shown in (c) and (f) image, respectively.

2.3.3.4 Water vapor barrier analysis of gelatin-based films

The water vapor barrier of gelatin-based films obtained by bench and continuous casting is presented in Figure 2.19. The addition of CNCs significantly reduced ($p < 0.05$) the WVP of the gelatin matrix for all the samples analyzed, regardless of the processing method. This phenomenon is the result of interactions between CNCs and gelatin, as well as an increased tortuosity of the pathway for vapor diffusion through the film matrix [239]. Besides, gelatin-based films obtained by continuous casting showed lower WVP value than films produced by bench casting. This can be attributed to the use of IR and higher drying temperatures in continuous casting, which contributed to better cohesiveness of the matrix resulting in more compacted films, as shown by SEM image (Figure 2.18b,e). Chiou et al. (2009) [91] reported the same behavior for fish gelatin and observed that cold-cast gelatin films had WVP values approximately two to three times higher than those of hot-cast gelatin films. Fernández-Pan et al. (2010) [240] found that chitosan films dried at 80 °C showed

WVP values twice as low as those dried at 40 °C, suggesting that films dried at a higher temperature could have more intense structural collapse, which would probably bring films with lower volume and, therefore, higher density. Higher density is generally associated with lower WVP films.

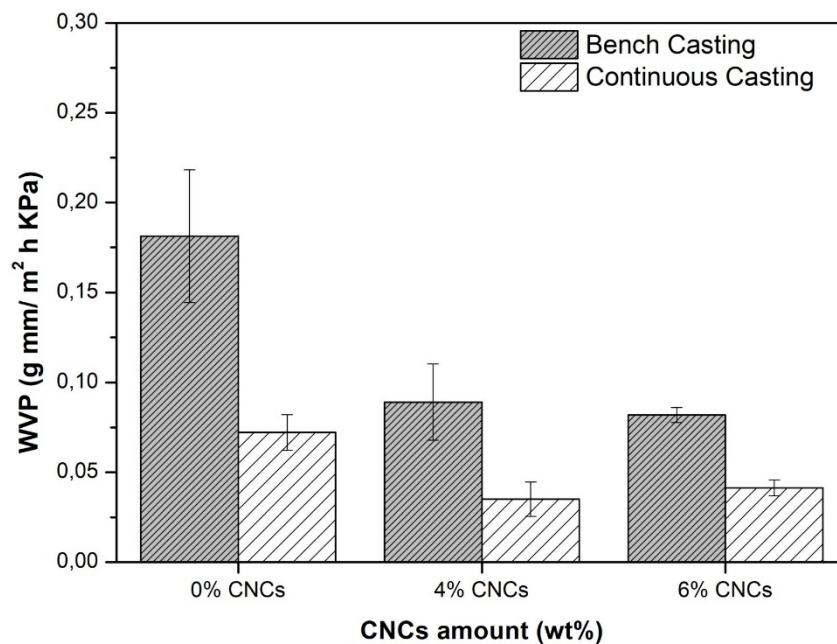


Figure 2.19 - Water vapor permeability of gelatin-based films obtained by bench and continuous casting

2.3.3.5 Contact angle measurement of gelatin-based films

Contact angle measurement is an important parameter used to investigate the surface hydrophilicity/hydrophobicity of food packaging film when in contact with water. Figure 2.20 shows the dynamic changes in the water contact angle of pure gelatin and gelatin/CNCs films obtained by bench and continuous casting. Gelatin-based films obtained by bench casting showed water contact angle values higher than 90 ° over time, which indicates that the surface analyzed was hydrophobic, except for the gelatin film with 6.0 wt% CNCs, which after approximately 45 s became hydrophilic. Gelatin has been widely known for its high hydrophilicity [241]. However, the hydrophobic surface for gelatin-based films has been reported [203,241,242] and the explanation given by the authors

is that during film drying, the randomly coiled gelatin molecules are capable of spontaneously rearranging their hydrophobic parts towards the film-air [243].

By contrast, the fast drying time used in the continuous casting did not allow this rearrangement and hydrophilic surfaces over time were observed for all the films analyzed. Besides, the increasing concentration of CNCs decreased the water contact angle value of gelatin/CNCs films obtained by continuous casting. This result demonstrated that the film was more hydrophilic due to the OH- group in the CNCs structure since the polarity around the structure could create H-bonding to react with water.

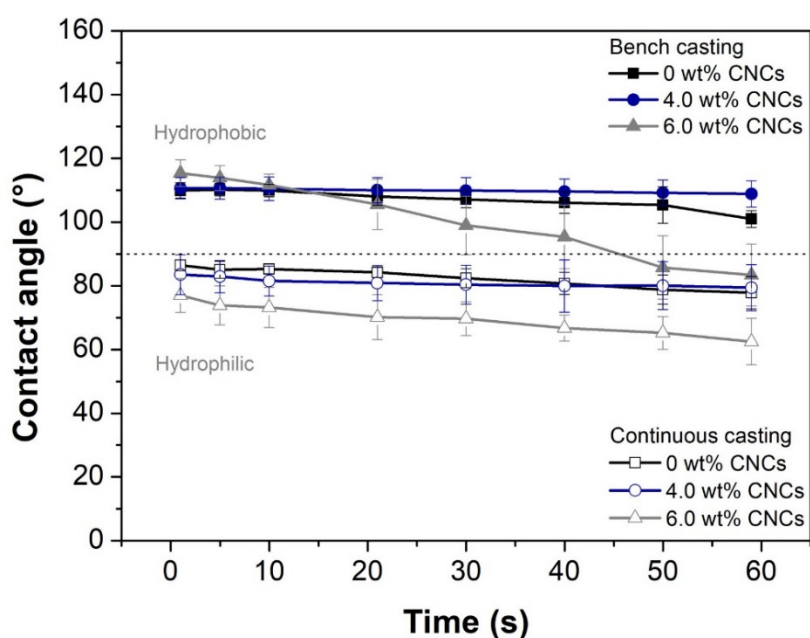


Figure 2.20 - Contact angle of gelatin-based films obtained by bench and continuous casting.

2.3.3.6 Thermostability of gelatin-based films

The decomposition temperatures of CNCs powder and gelatin-based films obtained by bench and continuous casting are reported in Table 2.6. The thermal stability is one of the main issues in the processing of natural bio-based materials. The CNCs showed onset thermal decomposition temperature at 280 °C, which was in agreement with previously reported [135]. The thermostability of gelatin-based films produced by bench casting decreased with the addition of CNCs. By

contrast, the results showed that films produced by continuous casting became more thermally stable. Pure gelatin registered an increase in onset thermal decomposition temperature by 9 °C compared to the same film obtained by bench casting. The highest thermostability was found for gelatin film with 4 wt% CNCs, which showed an increase by 24 °C compared to their counterpart films obtained by bench casting. These findings corroborate the hypothesis that the IR and the higher drying temperature applied in the continuous casting contributed to better cohesiveness of the matrix, stabilized by strong inter- and intramolecular bonds, which requires a higher temperature for breakouts. [18].

Table 2.6 - Onset of thermal decomposition, 50% weight loss, and maximum thermal decomposition temperatures for CNCs powder and gelatin-based obtained by bench casting and continuous casting.

Sample	T _{onset} (°C)	T ₅₀ (°C)	T _{max} (°C)	Residue
CNCs	281	296	293	21
Films obtained by bench casting				
0%	256	317	327	17
0.5 wt% CNCs	244	311	313	17
4.0wt% CNCs	247	310	312	18
6.0 wt% CNCs	250	314	313	19
Films obtained by continuous casting				
0%	265	331	325	20
0.5 wt% CNCs	271	333	325	21
4.0wt% CNCs	271	332	326	20
6.0 wt% CNCs	268	327	331	19

2.4 Conclusion

The results demonstrated that the good dispersion of CNCs into the matrix can improve the mechanical, barrier, and thermal properties of the gelatin films. The results obtained in this part give important insights concerning the film properties, showing that to achieve the percolation threshold the CNCs

dispersion is as important as their content. All the gelatin/CNCs films obtained by bench casting and continuous casting were highly homogeneous and easy to handle. The infrared radiation and high drying temperatures applied in continuous casting processing promoted strong intermolecular interaction and intense structural collapse, which led to the formation of more cohesive films with a better barrier, mechanical and thermal properties. Continuous casting processing has been proven to be advantageous when compared to the bench casting, as it allows not only scaling-up the production of gelatin-based films but also allows better performance of these films. This is a straightforward alternative to bench casting.

Chapter III

Evaluation of physical properties of gelatin-based films under the influence of electrostatic interactions

III. Evaluation of physical properties of gelatin-based films under the influence of electrostatic interactions

Introduction to chapter III

Chapter I was focused on the use of gelatin and cellulose nanocrystals (CNCs) as a bio-based and biodegradable material for food packaging applications. One of the main objectives of this Ph.D. is the production of gelatin-based films, which fulfill the most relevant requirements for packaging material.

The knowledge of the intermolecular interactions is crucial for understanding the structure and physical properties of gelatin-based films. Therefore, this chapter investigates the electrostatic interactions between gelatin and CNCs as a function of pH using zeta potential and rheological measurements. The physical properties such as mechanical, thermal, and water vapor permeability of gelatin-based films at different pH and CNCs amount is evaluated.

1 Evaluation of physical properties of gelatin-based films under the influence of electrostatic interactions

This section is adapted from Liliane S. F. Leite, Francys K. V. Moreira, Luiz H. C. Mattoso, Julien Bras. Electrostatic interactions regulate the physical properties of gelatin-cellulose nanocrystals nanocomposite films intended for biodegradable packaging. Food Hydrocolloids (2020), 106424.

Abstract

Cellulose nanocrystals (CNCs)-reinforced gelatin films are appealing candidates for biodegradable packaging. However, tailoring the physical properties of gelatin/CNCs films by control of pH and film-forming drying temperature continues unstudied. Here, we described the influence of pH on the physical properties of gelatin/CNCs films covering different CNCs contents. The interactions between CNCs and gelatin were studied by assessing the ζ -potential of gelatin/CNCs suspensions under acidic (pH 3) and alkaline (pH 8) conditions and at gelatin isoelectric point (pI, pH 6). pH 3 promoted the electrostatic attraction, while pH 8 favored the electrostatic repulsion in the gelatin-CNCs pair, increasing the suspension viscosity in both cases. The addition of 0.5 wt% CNCs decreased the water vapor permeability (WVP) of the gelatin/CNCs films by 68% under electrostatic attractive forces and by 39% at isoelectric point. The addition of 5 wt% CNCs at pH 3 resulted in the formation of complex coacervates, which contributed to decrease the mechanical properties and increase the WVP of gelatin/CNCs films. Increasing pH above the gelatin pI remarkably increased the gelatin renaturation as triple helices, which was found to be key for increasing by 152% and 56% in Young's modulus and tensile strength of gelatin/CNCs films with 0.5 wt% CNCs, respectively. In contrast, the film-forming drying temperatures of these films had an inverse effect on the triple helix content, and, consequently, on their physical properties. These findings can be explored to modulate the mechanical strength, permeability, and thermal stability of nanocellulose-added gelatin films for a variety of applications, including flexible food packaging.

1 Introduction

Proteins are natural polyampholytes that have attracted great interest due to their unique properties [2], in particular, their ability to form self-assembled structures, such as polyelectrolyte complexes obtained by interactions between proteins and polysaccharides carried opposite charges in aqueous medium [244]. These structures are promising for the creation of new materials applicable in pharmacy, medicine [153,245], and food packaging [246,247].

Gelatin is a protein obtained by the partial hydrolysis of collagen at controlled temperature and pH conditions [248]. The mechanical behavior of gelatin gels and films is related to the regeneration of gelatin as crystalline triple helices. Giofrè et al. (2012) [249] investigated the pH effect of film-forming solutions on the mechanical properties of pigskin type A gelatin films and observed that pH values higher than 9 and lower than 5 considerably reduced the triple helix content and, consequently, the mechanical properties of the films. These results indicate that pH can be used to modulate the mechanical behavior of gelatin-based materials.

Gelatin films have also been found to be moisture-sensitive and exhibit a reduced water vapor barrier and mechanical resistance under high relative humidity, due to the hydrophilicity of the polypeptide chains. A suitable approach to overcoming these limitations of gelatin films is the use of cellulose nanocrystals (CNCs) as nano-sized fillers [250]. The use of CNCs has been proven to enhance the mechanical and barrier properties of gelatin films. Several works have described a joint synergistic effect between gelatin and CNCs toward the formation of percolated networks stabilized by hydrogen bonding [17],[165].

To the best of our knowledge, no research has been published on the effect of reinforcing CNCs on the properties of gelatin films in function of the electrostatic interactions. The knowledge of these intermolecular interactions is crucial for understanding the structure and physical properties of gelatin/CNCs films, as well as for the development of packaging films with tunable mechanical properties. Furthermore, there is no report that examines the structure and mechanical properties of gelatin/CNCs films under the influence of drying temperature. This work aimed to investigate the effect of CNCs, pH, and drying

temperature on the triple helix content, mechanical, thermal, and barrier properties of gelatin films obtained by bench casting.

1.2 Materials and methods

1.2.1 Materials

Bovine gelatin (Bloom Strength-190) was kindly supplied by Gelco Gelatinas do Brazil Ltda (Pedreira, SP). CNCs isolated from wood pulp by sulfuric acid hydrolysis and delivered as a dried powder were purchased from Celluforce Inc. (Windsor, Québec, Canada). Glycerol and ethanol were purchased from Across Organics (USA). All chemicals were analytical grade and were used as purchased.

1.2.2 Preparation of gelatin/CNCs films

The bionanocomposite films were prepared by solvent casting. The gelatin powder was hydrated in distilled water (10 g/100 g) at 24 °C for 5 min and heated at 60 °C under stirring for 15 min. The gelatin solution pH was adjusted to 3, 6, and 8 with 3M HCl or NaOH. Glycerol (2 g/100 g of protein) was added and the gelatin solution under stirring for 5 min. The obtained solution was mixed with the CNCs suspension at desired contents (0 wt%, 0.5 wt%, and 5.0 wt%, on a dry gelatin mass basis) and stirred for an additional 5 min. The final film-forming solution (FFS) (45 mL) were cast on glass plates (40 cm × 25 cm), covered with a polyester film (Mylar®, DuPont, Brazil) to facilitate film peeling off after drying in an oven at 25, 35, and 80 °C for 24 h. Film samples were conditioned at 50% relative humidity (RH) in a ventilated climatic chamber and 25 °C for at least 24 h prior to any testing.

1.2.3 Determination of Zeta potentials (ζ -potentials)

ζ -potentials of aqueous CNCs dispersion, pure gelatin solution, and gelatin/CNCs FFS (0.5 wt% and 5.0 wt% CNCs on a dry gelatin basis) diluted to 0.25 wt% were analyzed at 25 °C using a Zetasizer Nano-ZS (Malvern

Instruments Inc., UK). Each sample was mixed with a sonicator (Branson 450 Sonifier, USA) for 5 min with a microtip before analysis. The measurements were performed in triplicate.

1.2.4 Rheological study

The apparent viscosity and flow behavior of the FFS (pure gelatin and gelatin/CNCs with 0.5, and 5 wt% CNCs at pH 3, pH 6, and pH 8) were evaluated on a Physica MCR101 rheometer (Anton Paar, Austria) using the concentric cylinder geometry at 40 °C. The shear rate was varied from 0 to 150 s⁻¹ in 10 min. Oscillatory shear deformation tests were also carried out to determine the storage modulus (G') and loss modulus (G'') of the FFS at a constant strain of 1% and frequency of 1 Hz in the temperature range of 60-20 °C, using heating/cooling rate of 0.02 °C s⁻¹. Strain values were chosen to be within the linear viscoelastic region based on preliminary measurements. The flow behavior was described by fitting the experimental data to the Power Law model (Equation 1).

$$\sigma = k\dot{\gamma}^n \quad \text{Eq. 1}$$

where σ is the shear stress (Pa), $\dot{\gamma}$ is the shear rate (s⁻¹), k is the consistency coefficient (Pa sⁿ) and n is the flow behavior index.

1.2.5 Polarized light optical microscopy

Optical images of gelatin/CNCs films were taken between crossed polarizers to evaluate the dispersion of the CNCs within the gelatin matrix. The samples were imaged by polarized optical microscopy taken at 10-fold magnification using a microscope Zeiss Axio Vert.A1 (Carl Zeiss Microscopy).

1.2.6 Scanning electron microscopy (SEM)

The film surface and the cross-sectional surface were investigated using a JEOL Scanning Electron Microscope (SEM, model Quanta200, FEI, the

Netherlands). The samples were first cryo-fractured in liquid N₂ and then fixed onto 90° specimen mounts to be coated with a ca. 5-nm-thick gold layer in an argon atmosphere. The SEM images were taken at accelerating voltages below 10 kV using the secondary electron mode. At least 10 images per sample were obtained and the most representative was used in the discussion.

1.2.7 X-ray diffraction (XRD) analysis

X-ray diffraction patterns were acquired from 2 ° to 60 ° (2θ) using a Panalytical diffractometer (X'Pert Pro MPD-Ray) with Ni-filtered Cu Ka radiation (k = 1.54 Å) generated at a voltage of 45 kV and current of 40 mA. At least duplicate measurements were performed for each sample. The amount of triple helix configuration (X_c in %) in the gelatin/CNCs films was calculated using Equation 2.

$$X_c = [A_c / (A_c + A_a)] \times 100 \quad \text{Eq. 2}$$

where A_c is the area of the diffraction peak at ~2θ = 8°, corresponding to the triple helix configuration of gelatin chains, and A_a is the area under the hump located at ~2θ = 21°, corresponding to the fraction of amorphous domains in the gelatin films [230].

1.2.8 Tensile tests

The tensile properties of the films were determined by the ASTM D882-09 standard method (2009). The film specimens (17 cm x 1 cm) were prepared and equilibrated in a ventilated climatic chamber at 23 ± 1 °C and 50 ± 5% RH for 48 h. The tests were carried out in an Instron Universal Testing Machine model 5569 (Instron Corp., USA) equipped with a 100 N load cell. The specimens were stretched using crosshead speed of 10 mm/min with clamps initially separated by 100 mm. Tensile strength, Young's modulus, and elongation at break were calculated from the stress-strain curves. Thicknesses were measured using a digital micrometer (Adamel Lhomargy) to the nearest 0.001 mm with ten random

measurements per film. The tensile tests were performed with five replicates per film sample.

1.2.9 Water vapor permeability (WVP)

WVP was determined using the ASTM E-96-01. The preconditioned film was sealed onto the opening of an aluminum permeation cup (28 mm internal diameter) containing dried calcium chloride. The cup was kept in a ventilated climatic chamber at 23 ± 1 °C and $50 \pm 5\%$ RH. The cup was weighed at least four times for at least 7 days under this controlled environment. For each film, three replicates were performed. The WVP $\text{g mm m}^{-2} \text{h}^{-1} \text{kPa}^{-1}$ was determined using Equation 3:

$$\text{WVP} = (\Delta m / \Delta t) \times (L / A \Delta P) \quad \text{Eq. 3}$$

where $\Delta m / \Delta t$ is the mass gain over time (g h^{-1}), A is the exposed film area (m^2), L is the film thickness (mm), and ΔP is the difference of partial pressure.

1.2.10 Water solubility (WS) determination

The gelatin films were cut into rectangular ($1 \text{ cm} \times 1 \text{ cm}$) specimens and pre-dried at 105 °C for 24 h. The dried specimens were accurately weighed (initial dry weight, w_0), placed in distilled water (30 mL), and stirred at 25 ± 1 °C for 24 h. Filter paper number 1 was prepared by drying at 105 °C for 24 h. Then, the film was poured onto the filter paper and dried at 105 °C for 24 h and weighed (final dry weight, w_1). WS was measured in triplicate following calculated using Equation 4.

$$\text{WS} (\%) = [(w_0 - w_1) / w_0] \times 100 \quad \text{Eq. 4}$$

1.2.11 Thermogravimetric analysis (TGA)

Thermogravimetric analysis was carried out in a Q500 equipment (TA Instruments, USA). About 10 mg of each film sample was taken in a standard Pt

crucible and heated from 25 °C to 600 °C with heating rate of 10 °C min⁻¹, under an inert atmosphere of nitrogen (60 mL/min). Samples before the TGA tests were conditioned in a ventilated climatic chamber at 23 ± 1 °C and 50 ± 5% RH for 48 h.

1.2.12 Statistical analysis

Data were subject to analysis of variance (ANOVA). The mean values were compared using the Tukey's test at a confidence level of 95 % (p<0.05) using the Origin software (OriginLab, Northampton, USA).

1.3 Results and discussion

1.3.1 Physical and rheological properties of gelatin/CNCs film-forming solutions

ζ-potentials provide evidence of the net charges on particle surfaces as a function of pH. Figure 3.1 illustrates the evolution of the ζ-potential of gelatin solution and CNCs suspension upon pH variation. The isoelectric point (pI) of gelatin solution occurred at around pH 6, at which a null ζ-potential was observed. This is in agreement with previously reported data for type B gelatins (pH 4.5-6.0) [80]. Gelatin has the ability to present different charges depending on the pH [249]. At pH < pI, the gelatin solution showed a net positive charge, which was attributed to the protonation of the amino moieties (-NH₃⁺), while at pH > pI the solution showed a net negative charge, due to the ionization of the carboxyl moieties (-COO⁻). For the CNCs suspension, the ζ-potential value was found to be negative regardless of the pH. The ζ-potential value of CNCs suspension was around -50 mV, indicating a stable suspension in water. According to Lin, Gu, & Cui (2019) [251], ζ-potentials (< -30mV and > + 30 mV) could maintain a stable colloidal system due to the repelling force between particles. This value can be attributed to the sulfate groups on the CNCs surface, agreeing with a previous study [160].

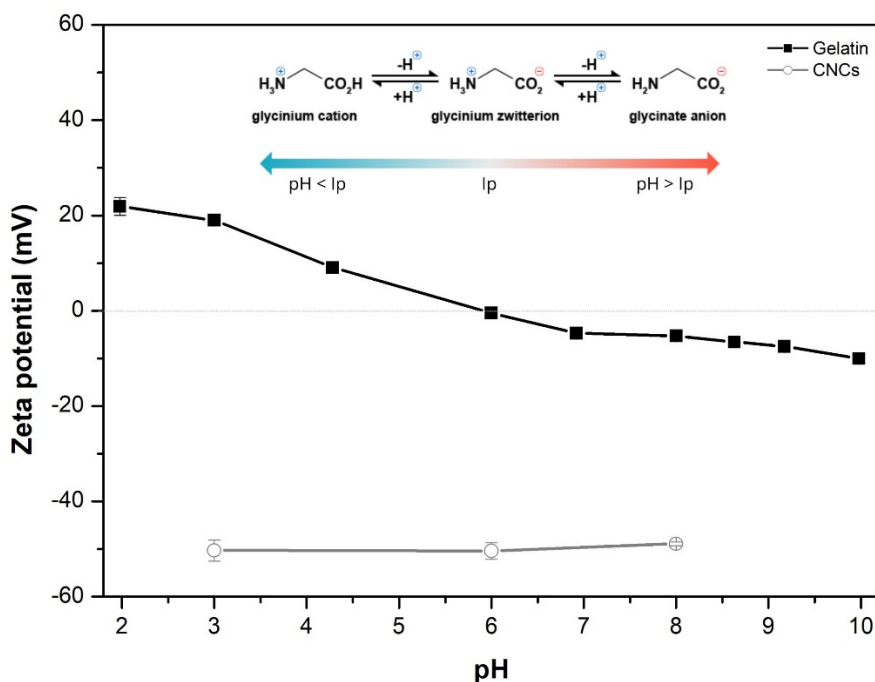


Figure 3.1 - ζ -Potential values of pure gelatin solution and CNCs suspension (0.25 wt%) at and 25 °C as a function of pH.

In aqueous solutions, the electrostatic charges are one of the main driving forces for interactions between charged biopolymers [252]. For the gelatin/CNCs FFS at $\text{pH} < \text{pI}$, the gelatin, and CNCs are expected to form complexes stabilized by electrostatic attractive interactions, while at $\text{pH} > \text{pI}$ the mixture should exhibit electrostatic repulsive interactions between the negatively charged gelatin chains and CNCs. Similar behaviors for protein-polysaccharides were recently reported [253,254].

As expected, the ζ -potential of the gelatin/CNCs FFS at pH 6 and pH 8 decreased with increasing the CNCs concentration (Figure 3.2). However, at pH 3, the addition of CNCs did not change significantly the ζ -potential values of the gelatin/CNCs FFS compared to the pure gelatin solution at the same pH, confirming that electrostatic attractive interactions occurred between the positively charged gelatin chains and negatively charged CNCs in acidic medium.

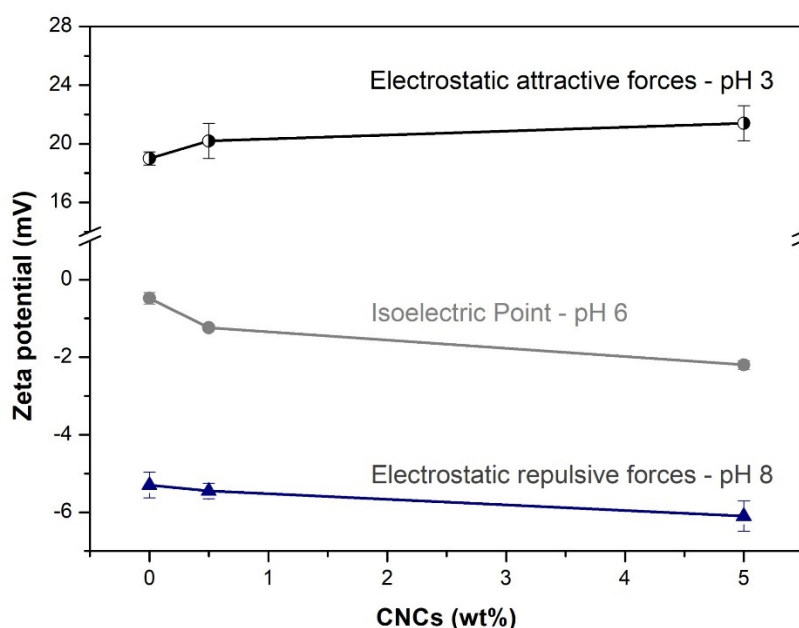


Figure 3.2 - ζ -potential curves of gelatin/CNCs FFS at different pH as a function of CNCs concentration.

The rheological behavior of the gelatin/CNCs FFS was evaluated at different pH. Apparent viscosity and parameters calculated by the Ostwald de Waele model are presented in Table 3.1. The flow curves are shown in Figure 3.3. Experimental shear stress vs. shear rate curves were fitted to the Ostwald de Waele model ($r^2 > 0.99$), which has been widely used to describe non-Newtonian fluids over the most important shear rate ranges [80]. All the FFS exhibited a shear-thinning behavior ($k > 0$; $0 < n < 1$) and their apparent viscosities (η_{ap}) decreased as the shear rate increased. This pseudoplastic behavior of gelatin/CNCs FFS became progressively more pronounced at high CNCs contents, and with electrostatic attractive (pH 3) and repulsive conditions (pH 8). As expected, the addition of CNCs increased the apparent viscosity of the gelatin/CNCs FFS. The electrostatic attraction between the CNCs and gelatin molecules at pH 3, leads to the formation of gelatin networks through physical interactions [22]. By contrast, the electrostatic repulsive forces between gelatin and CNCs at pH 8 can stretch the gelatin molecules and favor the mutual orientation of macromolecules and the creation of non-covalent interactions [253]. This could decrease the mobility of protein molecules, thus increasing the

resistance between gelatin FFS layers. In this context, the minimum viscosity was found at the gelatin isoelectric point (pH 6), where the electrostatic attractive and repulsive forces were minimized.

Table 3.1 – Apparent viscosity (η_{ap}), parameters of Ostwald de Waele model (consistency index (K), and flow index (n)) and transition temperatures of gelatin/CNCs FFS at pH 3, 6 and 8.

Gelatin/CNCs film-forming solution									
CNCs (wt%)	Electrostatic attractive forces pH 3			Isoelectric point pH 6			Electrostatic repulsive forces pH 8		
	0	0.5	5.0	0	0.5	5.0	0	0.5	5.0
Parameters of Ostwald de Waele model									
k (mPa s ⁿ)	0.01	0.03	1.03	0.01	0.03	0.01	0.01	0.02	2.25
n	0.92	0.83	0.32	0.97	0.97	0.90	0.90	0.96	0.24
r ²	0.993	0.998	0.997	0.999	0.999	0.992	0.999	0.999	0.990
η_{ap} (mPa) at 1 s ⁻¹	10.1	25.0	887.3	10.9	17.5	12.7	7.79	14.0	1788
Transition temperature (°C)									
Gel-sol	32.1	32.0	Nd	34.6	35.1	35.0	35.6	35.1	37.8
Sol-gel	19.4	22.7	Nd	22.7	22.8	22.6	22.4	22.6	Nd

Nd: not detected.

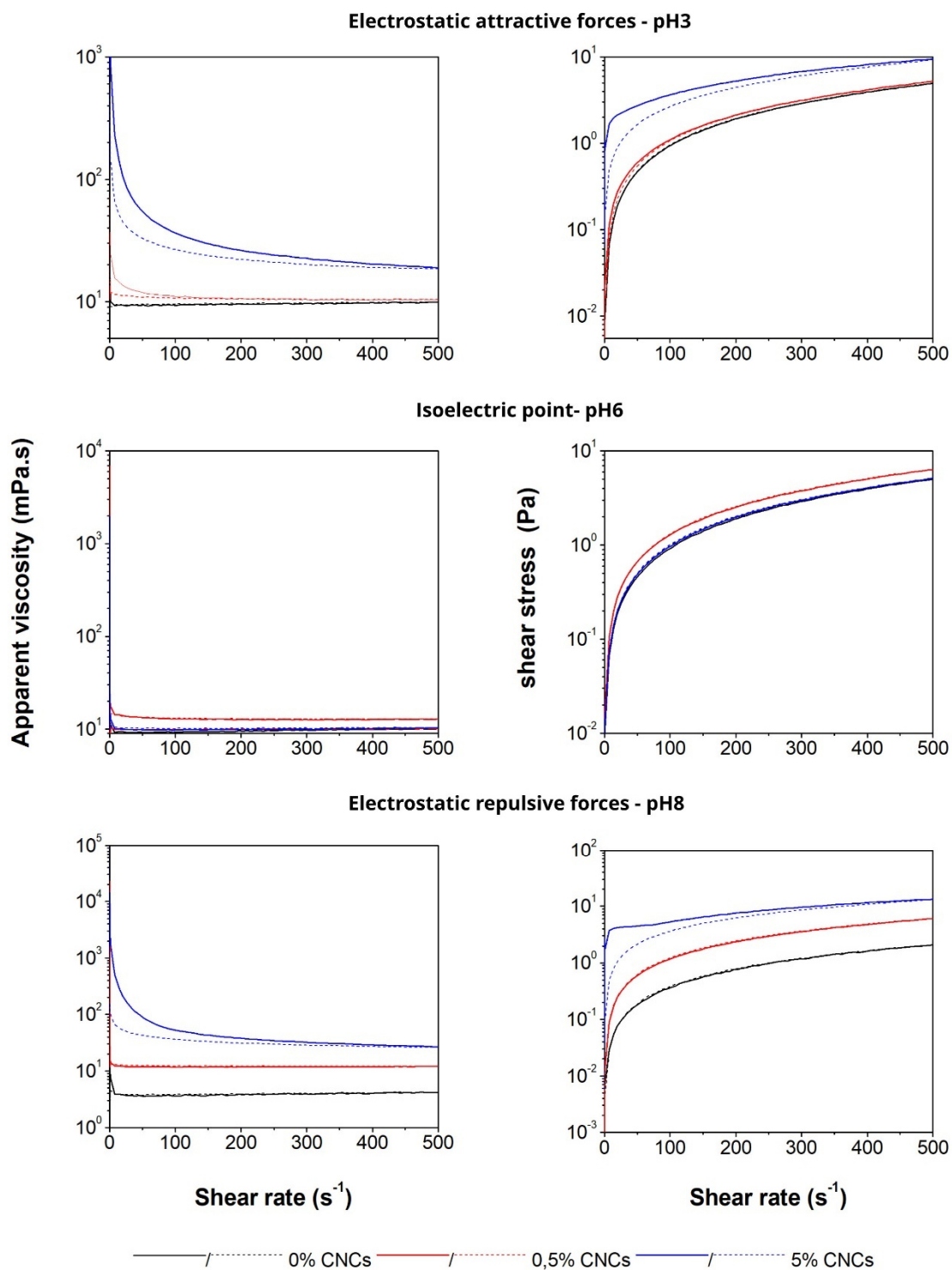


Figure 3.3 - Apparent viscosity (left) and shear stress (right) curves as a function of the shear rate of gelatin/CNCs films at different pH values. (—) increase in shear rate and (- - - -) decrease in shear rate.

Dynamic rheological measurements can be used to monitor structures in weak gels or viscoelastic fluids [255]. These measurements provide key information for gelatin processability in continuous solvent casting or 3D printing. Figure 3.4 shows the storage (G') and loss (G'') modulus of the gelatin/CNCs FFS with 0 and 5 wt% CNCs at different pH obtained from heating and cooling scans. All the samples presented a similar rheological behavior, regardless of the pH or CNCs content. The viscoelastic modulus (G' , G'') were higher at lower temperatures (gel-like domain) than at higher temperatures (sol-like domain), with a well visible inflection between both domains ($G' = G''$). This inflection is typical of physical gels and on the heating and cooling curves is defined as the gel-sol transition (Figure 3.4a,c) and sol-gel transition (Figure 3.4b,d), respectively. Similar profiles have been observed in gelatin-based systems by several authors [256,257]. The temperatures of sol-gel (cooling curves) and gel-sol (heating curves) of the gelatin/CNCs FFS were slightly affected by the electrostatic interactions, which was more pronounced for the gel-sol transitions (Table 1). Furthermore, the addition of 5.0 wt% CNCs to the gelatin solution at pH 3 resulted in an elastic gel-like behavior ($G' > G''$) even above the gel-sol temperature. According to Qiao et al. (2016) [210], proteins can form complex coacervates through interactions of oppositely charged particles, as previously indicated by the ζ -potential values of the gelatin and CNCs solutions at pH 3 (Figure 3.1). Complex coacervation can lead to precipitation of polymer complexes through the formation of a dense media that can be treated as being composed of interconnected gel-like network structures, consistent with the assumption that the CNCs are electrostatically "cross-linked" along the macromolecules. Consequently, the gel-sol and sol-gel transitions of the gelatin/CNCs FFS due to electrostatic attractive forces were not observed. Besides, the gelatin/CNCs FFS with 5% CNCs at pH 8 also did not exhibit the sol-gel transition and presented a viscoelastic solid-like behavior, indicating the existence of physical crosslinks by hydrogen bonding as mentioned before.

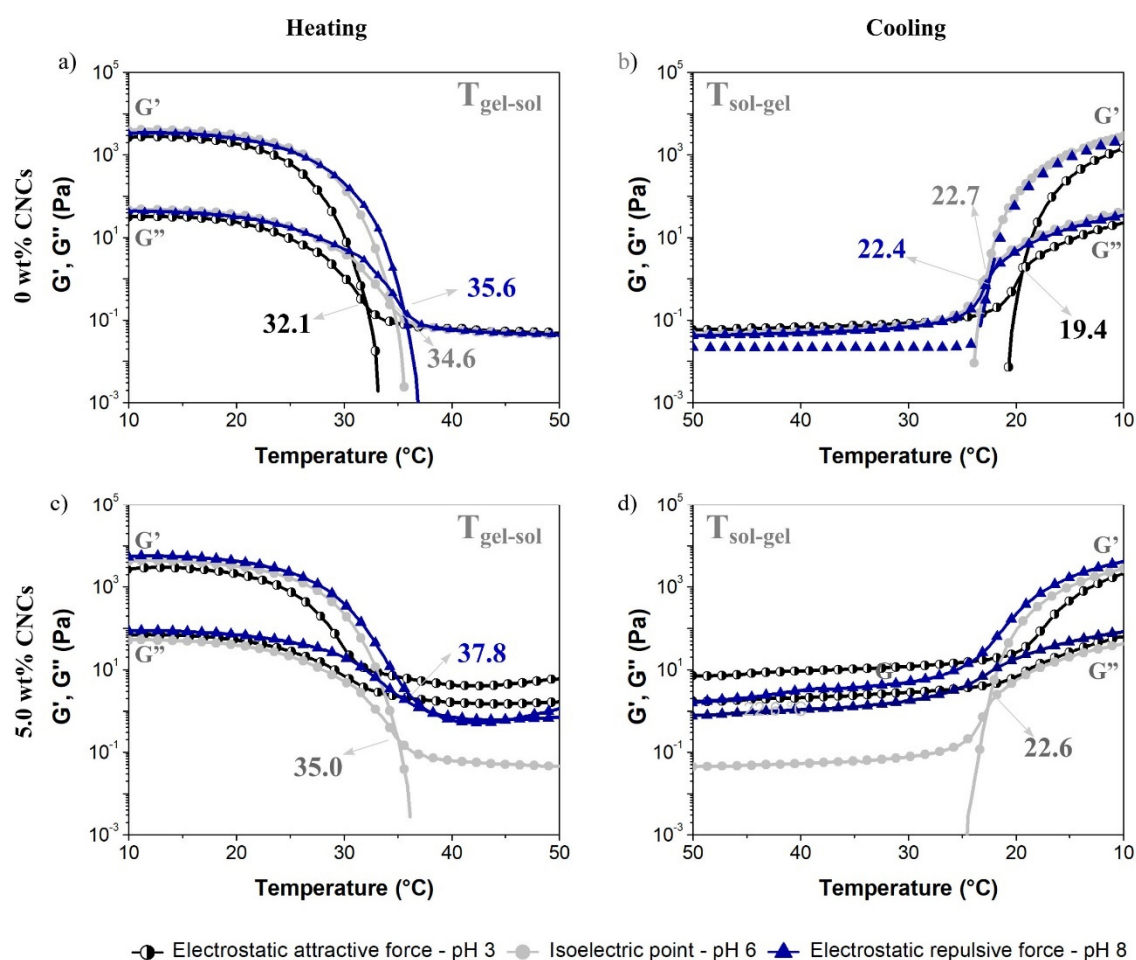


Figure 3.4 - Viscoelastic modulus of gelatin/CNCs FFS at different pH and CNCs contents. Heating (a and c) and cooling (b and d) at $1\text{ }^{\circ}\text{C min}^{-1}$.

1.3.2 Characterization of gelatin/CNCs films

1.3.2.1 Morphological and structural characterization

The photographs of the gelatin/CNCs films are shown in Figure 3.5a. All the films displayed good macroscopic homogeneity and transparency. Cracks on their surface were also absent. The morphologies of the surface and cross-sectional surface of the gelatin/CNCs films obtained from different pH were investigated by SEM (Figure 3.5b). The gelatin film with 5.0 wt% CNCs at pH 3 showed aggregates (white arrows), on both cross-sectional and air-drying surfaces, suggesting the formation of CNCs-gelatin coacervates. The same effect was observed by Li et al. (2018) [211] for gelatin/gum arabic mixtures at pH 3.5.

They found that complex coacervates were spontaneously formed between gelatin and gum arabic at low pH, where gelatin and gum arabic presented opposite surface charges. By contrast, the electrostatic attraction between gelatin and CNCs is weakened by increasing the pH, and the coacervates disappeared at pH 6 and 8 (Figure 3.5b). The gelatin/CNCs films showed homogeneous and continuous surface with no white dots, suggesting that the CNCs were homogeneously distributed throughout the film structures [224]. This indicates a uniform dispersion of CNCs within the gelatin matrix.

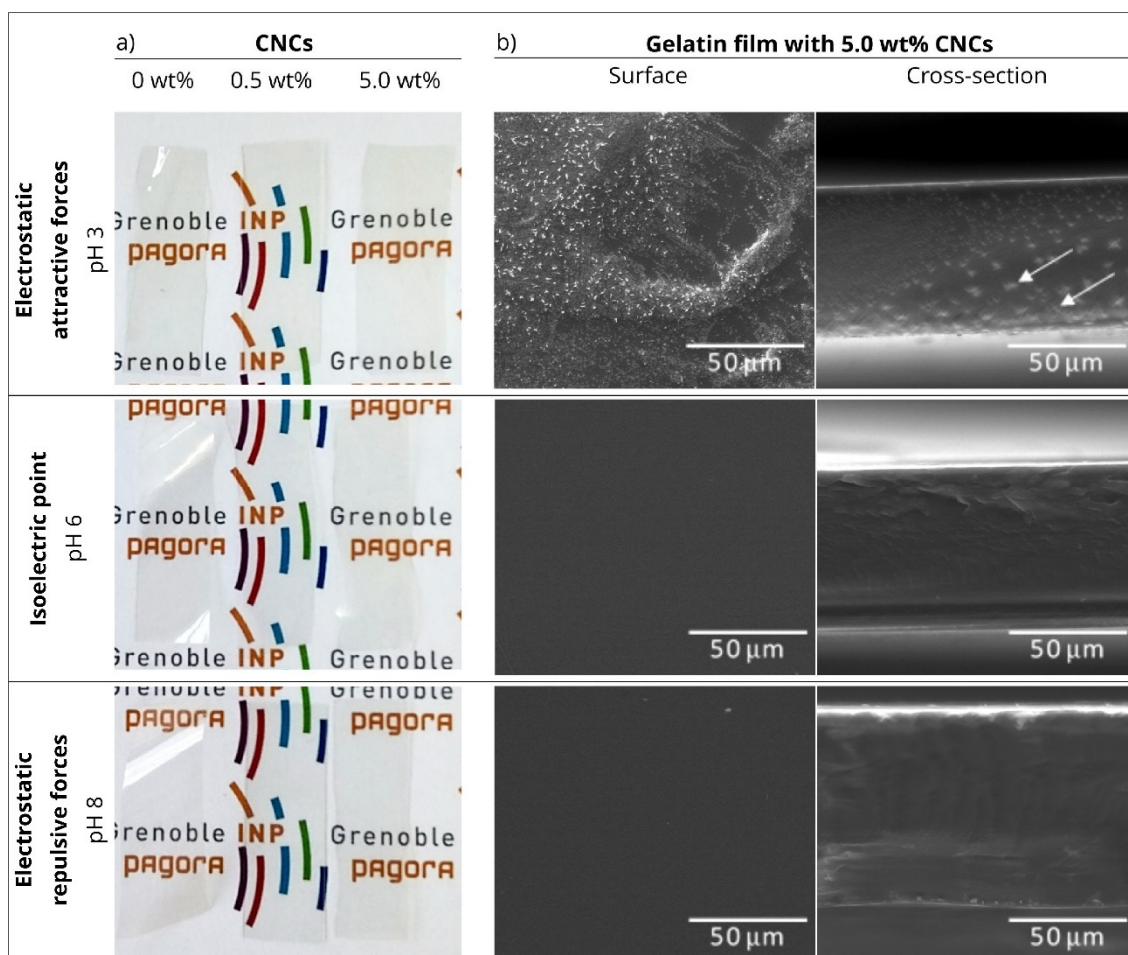


Figure 3.5 - (a) Photographs of gelatin/CNCs films with different CNCs contents, (b) SEM micrographs of air-drying and cross-sectional surfaces of gelatin/CNCs films with 5.0 wt% CNCs at pH 3, 6 and 8. White arrows indicate CNCs-gelatin coacervates at pH 3.

The XRD patterns of the gelatin-based films obtained at different pH and CNCs contents are shown in Figure 3.6. The formation of gelatin film is accompanied by the renaturation of triple helical structures of protein molecules [101]. The XRD diffractograms showed a wide background with a band at $2\theta \sim 21^\circ$ [235] and band at $2\theta \sim 8^\circ$, which has been previously attributed to the presence of triple helix structure present in collagen and renaturated gelatin [90]. The area of this peak has been found to be directly related to the triple helix content of gelatin-based composites [235–237]. As seen in the insert in Figure 3.6a,b the band area at $2\theta \sim 8^\circ$ of gelatin/CNCs, changed with the pH and CNCs content. The triple helix content of gelatin/CNCs films is presented in Table 3.2. The triple helix content of pure gelatin film decreased with decreasing pH. According to Ahsan & Rao (2017) [258] reported the same behavior for type B gelatin, which was attributed to most likely due to the structural changes in gelatin to mild denaturation, which was complete at around pH 2.5.

The highest content of triple helix (13.5%) was observed in the gelatin films with 0.5 wt% CNCs at pH 8. This behavior may result from deprotonation of the gelatin molecules at alkaline pH, favoring the formation of hydrogen bonding [80], which are essential to stabilize the gelatin triple helices. In addition, the formation of hydrogen bonds between the CNCs and proteins (both inside and outside helical fragments), also favors the regeneration and stabilization of triple helix structures [235,249]. However, the addition of 5.0 wt% CNCs amount markedly contributes to the reorganization of the gelatin molecular order and diminished the triple helix content, suggesting an increase in random coil conformation of gelatin chains. Similar behavior was observed Yakimets et al. (2005) [237] who found changes in the structural and molecular level of gelatin films induced by water content. These results also suggest that the process of folding the random coil to the triple helix is influenced by not only the pH but also by the interactions with CNCs and by the amount of nanoparticles added.

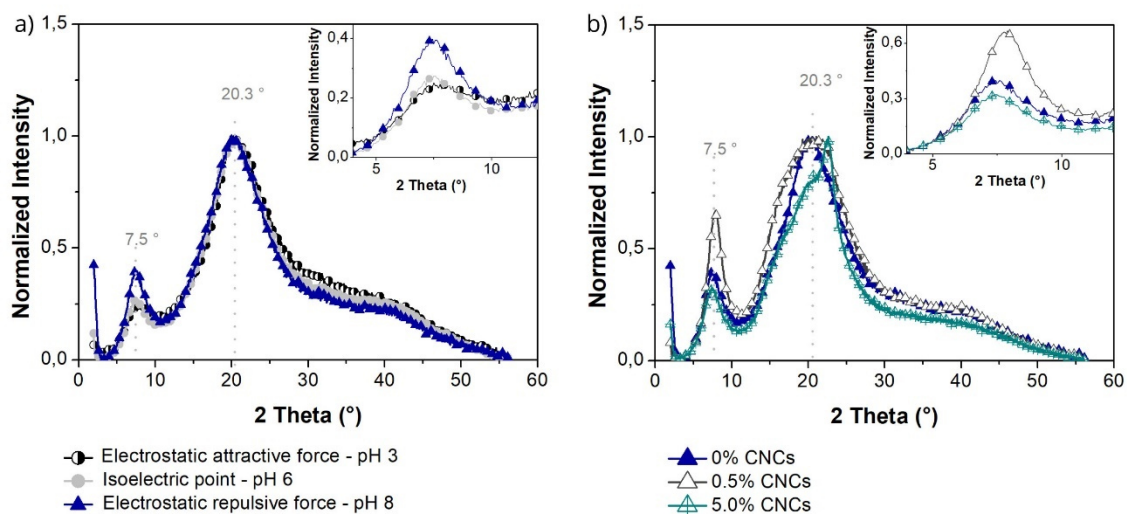


Figure 3.6 - XRD patterns of (a) pure gelatin films obtained from FFS films at pH 3, 6, and 8 and (b) gelatin/CNCs films obtained from pH 8 and different CNCs amount. The magnified view of the 2θ range 3 – 12 ° is shown as an insert.

Table 3.2 - Triple helix content of gelatin films obtained from FFS at different pH and CNCs amount.

Films		CNCs (wt%)	Triple helix content (%)*
Electrostatic attractive force pH 3	Gelatin	0	6.9
	Gelatin/CNCs	0.5	5.5
	Gelatin/CNCs	5	7.4
Isoelectric point pH 6	Gelatin	0	6.3
	Gelatin/CNCs	0.5	4.7
	Gelatin/CNCs	5	5.4
Electrostatic repulsive force pH 8	Gelatin	0	9.4
	Gelatin/CNCs	0.5	13.5
	Gelatin/CNCs	5	8.8

*Triple helix content of gelatin films was calculated using Equation 1 from X-ray diffraction spectra.

1.3.2.2 Mechanical properties

The Young's modulus, elongation at break, and tensile strength of gelatin/CNCs films are presented in Figure 3.7. The gelatin films containing 0.5 wt% CNCs at pH 3 and 8 showed significantly increased Young's modulus and tensile strength and decrease elongation at break compared to the pure gelatin films ($p < 0.05$). This effect was more pronounced at pH 8, whose Young's modulus and tensile strength increased by 152% and 56%, respectively, compared to those of the pure gelatin film ($p < 0.05$). The mechanical properties of gelatin films are related to the regeneration of triple helices, which represent crystalline domains within the film matrix and may act as reinforcing fillers in these films [235]. Similar behavior was reported by Quero et al. (2018) [90] that attributed the improved mechanical performance of microfibrillated cellulose (MFC)-salmon gelatin films at a MFC fraction of 15% w/w to the high content of triple-helix configurations present in these nanocomposites compared to the MFC-bovine gelatin nanocomposites. Gioffrè et al. (2012) [249] investigated the pH effect on the mechanical properties of pigskin type A gelatin films and observed that pH values higher than 9 and lower than 5 considerably reduced the triple helix content and consequently Young's modulus and elongation at break of the films.

The Young's modulus and tensile strength of the gelatin/CNCs films reached a maximum value with the addition of 0.5 wt% CNCs and then decreased after the addition of 5.0 wt% CNCs, at both acidic and alkaline conditions. This behavior can be attributed to high concentrations of aggregates formed by the coacervates at pH 3 [259], which provide a heterogeneous distribution of CNCs within the gelatin matrix, as revealed by SEM (Figure 3.5b). These aggregates can lead to a decrease in the strength of the nanocomposites since they act as defects or stress concentrators [226]. At pH 8, the electrostatic repulsion in alkaline gelatin/CNCs film can increase the free volume and flexibility of the gelatin matrix [101]. The moderate but gradual increases in Young's modulus and tensile strength at pH 6 may relate to the lower triple helix content compared to pH 8. These lowered effects also led the gelatin/CNCs bionanocomposites obtained from the gelatin pl to show a more ductile mechanical behavior, as

illustrated in Figure 3.7d. Overall, these results denote that pH and CNCs can be used to modulate the mechanical properties of gelatin films.

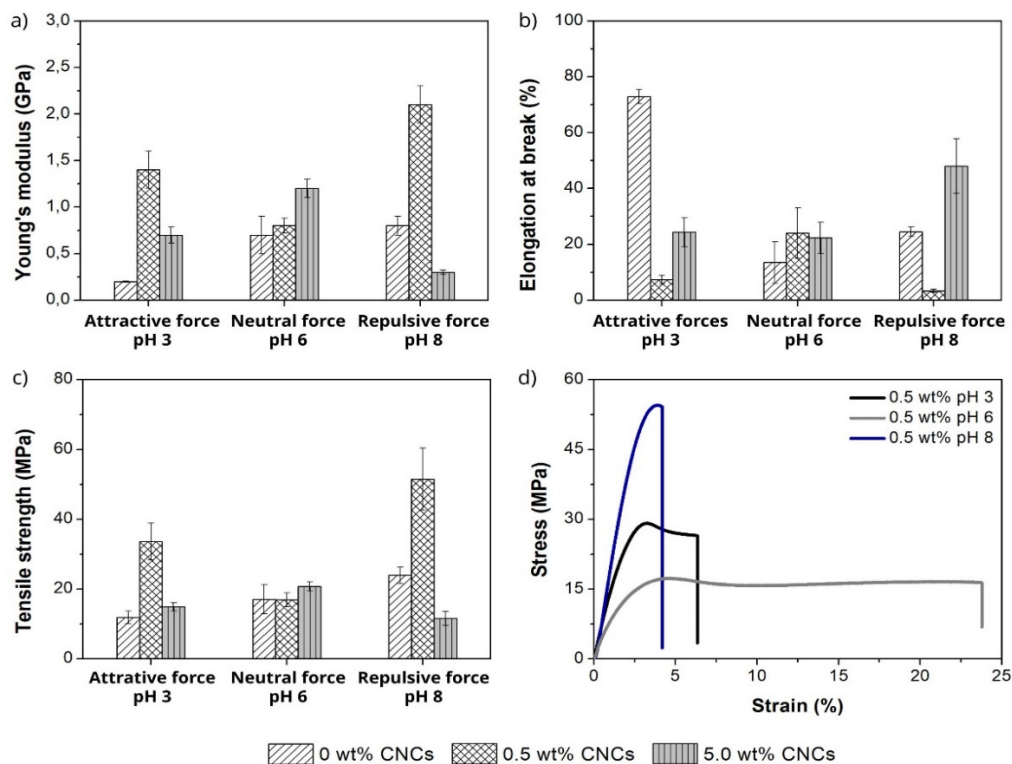


Figure 3.7 - (a) Young's modulus, (b) elongation at break, (c) tensile strength, and (d) stress-strain curves of gelatin/CNCs films as a function of pH and CNCs content.

1.3.2.3 Water sensitive properties

The WVP of the gelatin films with different pH and CNCs content are presented in Table 3.3. No significant differences ($p > 0.05$) among the WVP for gelatin films with 0% CNCs were observed concerning the pH variations. These results agree with previous findings on fish myofibrillar protein films [53], but differ from those previously reported for soy protein isolate films, which showed lower WVP at pH values above the isoelectric point [260]. However, the WVP of the gelatin/CNCs films obtained in this work at 50% RH were lower than those reported for other films based on gelatin at 0% RH [215], the results found were close to 1.8 g mm/m² h kPa (25 °C at 0% RH) for bovine and porcine gelatin films.

The addition of 0.5 wt% CNCs to gelatin at pH 3 and pH 6, significantly decreased ($p < 0.05$) the WVP of by 68% and 39%, respectively the resulting films. According to Qiao et al. (2013) [261], the addition of counterions screens the electrostatic repulsions between charges in the polymer, which, in turn, allows the chains to collapse and assume a more compact conformation. In a previous study, Santos et al. (2014) [165] reported that the WVP of protein films decreased by increasing the CNCs loading. They found that fish gelatin films with 15 wt% CNCs exhibit WVP values of approximately 2 g mm/m² h kPa (25 °C at 85% RH). George & Siddaramaiah (2012) [17] reported that 4 wt% of bacterial cellulose nanocrystals reduced the WVP of gelatin and attributed this to the low hygroscopicity of the highly crystalline cellulose nanocrystals. They found WVP values around 0.175 g mm/m² h kPa (25 °C at 50% RH). By contrast, as expected, the addition of CNCs to the gelatin matrix at pH 8 increased the WVP since the electrostatic repulsion in alkaline gelatin/CNCs films can increase the free volume, which resulted in greater gas diffusion. Overall, the WVP values of the gelatin films in the present study were lower than those of previous gelatin films reinforced with CNCs reported above.

The water solubility results are summarized in Table 3.3. No film fully dissolved or broke apart after 24 h at 25 °C, suggesting that they were formed by a stable network. The solubility of the gelatin films decreased by increasing the pH since higher pH favors the increase of protein-protein interactions and the exposition of hydrophobic groups that increase surface hydrophobicity gelatin and decrease the water solubility [262], the addition of CNCs at pH 6 and pH 8 did not significantly ($p < 0.05$) change the film solubility. However, a drastic decrease in water solubility was observed at 0.5 wt% CNCs and pH 3. This improvement in the water resistance can be attributed to the formation of the gelatin-CNCs complex coacervates, as shown in the SEM image (Figure 3.5b). These results are in agreement with Esteghlal et al. (2018) [1], who suggested that the decrease in solubility is due to charge reduction after complexation and formation of cross-linked gelatin-CMC films. Yin et al. (2005) [263] also found similar behavior for chitosan/gelatin polyelectrolyte complexes.

Table 3.3 - Water vapor permeability at 50% RH and 25 °C and water solubility of the gelatin films with different pH and CNCs content.

CNCs content (%)	WVP (g mm/ m ² h KPa)		
	Electrostatic attractive force	Isoelectric point	Electrostatic Repulsive force
	pH 3	pH 6	pH 8
0	0.204 ± 0.085 ^{aA}	0.180 ± 0.027 ^{aA}	0.131 ± 0.020 ^{aA}
0.5	0.065 ± 0.013 ^{bA}	0.111 ± 0.022 ^{bB}	0.158 ± 0.022 ^{aB}
5.0	0.189 ± 0.009 ^{aA}	0.109 ± 0.019 ^{bB}	0.262 ± 0.034 ^{bC}
	Water solubility (%)		
0	65.3 ± 2.55 ^{aA}	31.7 ± 4.81 ^{aB}	15.7 ± 3.30 ^{aC}
0.5	14.6 ± 1.24 ^{bA}	21.5 ± 6.55 ^{aA}	16.9 ± 4.97 ^{aA}
5.0	42.1 ± 2.52 ^{cA}	32.4 ± 1.30 ^{aB}	17.1 ± 9.46 ^{aB}

Mean ± standard deviation. Lowercase letters (a, b, c) - Mean values in the same column bearing the same letter are not statistically different according to the Tukey's test ($p > 0.05$). Capital letters (A, B, C) - Mean values in the same row bearing the same letter are not statistically different according to the Tukey's test ($p > 0.05$).

1.3.2.4 Thermostability

The gelatin/CNCs films were further characterized by TGA and the decomposition temperatures are reported in Table 3.4. All samples followed a similar decomposition profile. The first mass loss was due to moisture and volatiles evaporation [203]. Pure gelatin films at pH 8 showed the lowest moisture content (3%) and the addition of 5.0 wt% CNCs increased the weight loss at this stage, except the gelatin/CNCs film at pH 6, which may be due to less availability of free hydroxyl groups of the gelatin matrix to hydrogen bonding with CNCs. This result is in line with the increase in Young's Modulus (Figure 3.7) and reduction in the WVP of the gelatin/CNCs films with 5.0 wt% at pH 6 (Table 3.3).

A significant mass loss occurred at temperature (T_{onset}) above 200 °C, mainly associated with the decomposition of gelatin and glycerol molecules. The thermal stability of gelatin films increased near the gelatin isoelectric point, which is the result of a more compact form of gelatin [264]. This result is in agreement with Giofrè et al. (2012) [249], who reported a reduction in the thermal stability of gelatin films prepared at relatively high and low pH. The higher thermal stability was found for the gelatin/CNCs films with 0.5% CNCs at pH 3 and pH 8, which

showed increases of 14.4 and 15.3 °C in the T_{onset} , respectively, compared to pure gelatin films at the same pH. This improvement might be attributed to the formation of more rigid structures, like the gelatin-CNCs coacervate complexes formed at pH 3. This may also be related to the high concentration of triple helix structures present in gelatin/CNCs films at pH 8, as shown by XRD (Figure 3.6). In addition, the formation of hydrogen bonds between CNCs and gelatin can also influence the protein denaturation process and, as a consequence, lead to an increased thermal stability, as justified by George & Siddaramaiah, (2012) [17]. Previous studies found an increase of 9 °C for gelatin films with 10 wt% CNCs [166], 10.6 °C for gelatin films with 2.5 wt% [18], and a decrease of around 6 °C for gelatin films with 1.5 wt% CNCs, when compared to pure gelatin films [164].

Table 3.4 -TGA results of gelatin/CNCs films at different pH.

Films	1° Stage		2° Stage	
	T (°C)	Weight (%)	T_{onset} (°C)	Weight (%)
Electrostatic attractive forces – pH3				
0% CNCs	105	6.1	253.9	23.7
0.5% CNCs	105	7.1	268.3	19.7
5.0% CNCs	105	12.9	259.5	24.0
Isoelectric point – pH6				
0% CNCs	105	9.8	258.6	25.3
0.5% CNCs	105	8.5	248.3	23.5
5.0% CNCs	105	7.1	252.6	24.1
Electrostatic repulsive forces – pH8				
0% CNCs	105	3.0	251.2	17.4
0.5% CNCs	105	8.7	266.5	18.7
5.0% CNCs	105	7.1	253.4	23.7

The gelatin films with 0.5 wt% CNCs obtained from pH 8, which had the highest triple helix content, were chosen to evaluate the effect of the drying temperature on the mechanical, thermal, and barrier properties of gelatin/CNCs

films. The obtained results for film samples dried at 25 °C (“cold-dried”), 35 °C (gelation temperature), and 80 °C (“hot-dried”) are listed in Table 3.5. The gelatin films dried at 25 °C showed the highest Young’s modulus and tensile strength. This was likely due to the fact that cold-dried films had a longer drying time, i.e. sufficient time for the reorganization of gelatin structures as triple helices, than the hot-dried films. Chiou et al. (2009) [91] observed that gelatin films dried below their gelation temperature contained triple-helix structures, whereas films dried above their gelation temperature displayed lower crystallinity degree or amorphous structure. It has been previously reported that films with helical structures exhibit higher tensile strength and Young’s modulus than amorphous films [236].

Furthermore, the thermal stability of gelatin films increased when the drying temperature was decreased. These results might be explained by the larger amount of energy needed to break the hydrogen bonds in the triple helix structures formed in the cold-dried gelatin films (Figure 3.8). The WVP results showed no statistical difference concerning the drying temperature ($p > 0.05$). Bor Sen Chiou et al. (2008) [215] showed that mammalian gelatin films had higher levels of renaturation than fish gelatin films. However, the authors observed that this greater amount of helical structures did not lead to better water barrier properties, proving that WVP is not proportional to the renaturation level in gelatin films. The mechanical, thermal, and barrier results suggest that the drying temperature used in the casting process and the addition of CNCs are significant factors that affect the structure and physical properties of gelatin/CNCs films.

Table 3.5 - Tensile, thermal properties, water vapor permeability, and triple-helix content of gelatin films with 0.5% CNCs at pH 8 as a function of different drying temperatures.

Drying temperature (°C)	Young’s modulus (GPa)	Tensile strength (MPa)	Elongation at break (%)	T _{onset} (°C)	WVP (g mm/ m ² h kPa)	Triple helix content (%)
25	2.1 ± 0,2 ^a	51.5 ± 8,95 ^a	3.31 ± 0.53 ^a	266.5	0.16 ± 0.02 ^a	13.5
35	1.0 ± 0,2 ^b	20.9 ± 5,01 ^b	3.57 ± 0.71 ^a	252.6	0.23 ± 0.08 ^a	8.7
80	1.2 ± 0,1 ^b	19.1 ± 0,45 ^b	2.98 ± 0.29 ^a	251.4	0.24 ± 0.16 ^a	0.3

Mean ± standard deviation. Mean values in the same column bearing the same letter are not statistically different according to the Tukey’s test ($p > 0.05$).

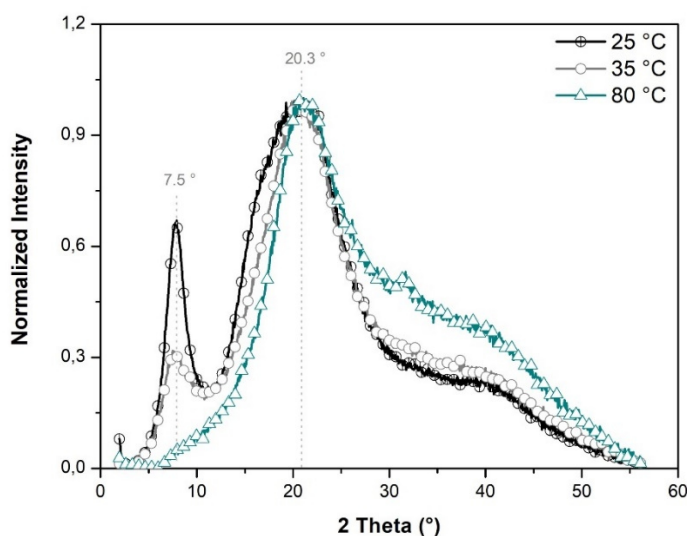


Figure 3.8 - XRD spectra of the gelatin/CNCs films with 0.5% at pH 8 obtained at different temperatures.

1.4 Conclusion

Transparent gelatin films reinforced with CNCs were successfully developed over a broad pH range. A comprehensive understanding of pH role in the properties of gelatin/CNCs films obtained by bench casting was provided by examining the possible electrostatic interactions and film structure involved. At pH 3, the electrostatic attractive forces between gelatin and high CNCs content resulted in the formation of complex coacervates, which contributed to decrease the mechanical properties and increase the WVP of gelatin/CNCs films. At pH 8, the electrostatic repulsive forces between gelatin and small CNCs amount favored the formation of triple helix structure, resulting in a significant improvement in the mechanical properties. At the isoelectric point, the addition of CNCs favored a significant increase in mechanical properties and a decrease in WVP of gelatin/CNCs films. Furthermore, the film drying temperature significantly affected the triple helix content, and consequently the physical properties of the gelatin/CNCs films. Controlling the pH, CNCs amount, and drying temperature allow gelatin/CNCs films with tunable physical properties to be obtained, thereby fulfilling requirements of packaging materials for different food products.

Chapter IV

Functionalization of CNCs and active gelatin-based films

IV Functionalization of CNCs and active gelatin-based films

Introduction to chapter IV

As described in Chapter I, the presence of a large number of reactive hydroxyl groups makes CNCs a unique platform amenable to various types of surface functionalization, extending their specific applications. One of the main objectives of this Ph.D. is the production of active packaging based on protein and CNCs.

Indeed, the first part of this chapter (**Chapter IV.1**) describes the functionalization and characterization of the surface of CNCs with rosin (r-CNCs) - a natural antimicrobial molecule. The physical and antimicrobial properties of gelatin-based films with r-CNCs are investigated. Accelerated storage tests with cheese samples are carried out to prove the antimicrobial ability of gelatin/r-CNCs films in practical applications. The results suggest that the incorporation of r-CNCs as active agents in gelatin films may be highly suitable for producing antimicrobial packaging materials.

The second part (**Chapter IV.II**) will focus on the effects of tannic acid (non-oxidized and oxidized forms), and CNCs amount on the physical, antioxidant, and antimicrobial properties of the gelatin-based films. The results show that the gelatin-based films with CNCs and TA fulfill the most relevant requirements for a natural antioxidant and antimicrobial food packaging material.

1 Functionalization of CNCs with natural antimicrobial rosin mixture and evaluation of their gelatin-based films

This section is adapted from Liliane S. F. Leite, Stanley Bilatto, Rafaella T. Paschoalin, Andrey C. Soares, Francys K. V. Moreira, Osvaldo N. Oliveira Jr., Luiz H. C. Mattoso, Julien Bras. Eco-friendly gelatin films with rosin-grafted cellulose nanocrystals for antimicrobial packaging. International Journal of Biological Macromolecules, 165 (2020) 2974-2983.

Abstract

We report on gelatin films incorporating rosin-grafted cellulose nanocrystals (r-CNCs), which fulfill the most relevant requirements for an antimicrobial food packaging material. The gelatin/r-CNCs bionanocomposites (0.5 – 6 wt% r-CNCs) were obtained by water-based casting and displayed UVA- and UVB-barrier properties (over 95% for UVB, and 59.0% for UVA) which are superior to the most used plastics while keeping the optical transparency. The films exhibited a moderate water vapor permeability (0.09 g mm/m² h kPa), lower than bio-based materials, and high tensile strength (40 MPa) and Young's modulus (1.9 GPa). These favorable properties should be attributed to Van der Waals interactions with the gelatin matrix in addition to hydrogen bonding. Grafting of rosin on CNCs resulted in a nanocellulose that inhibits *Staphylococcus aureus* and *Escherichia coli* growth, including in films as demonstrated in proof-of-principle experiments with the prevention of microbial spoilage of cheese samples.

1.1 introduction

Sustainability related to food plastic packaging has worldwide relevance owing to the need for safe disposal of post-consumer plastic wastes [2]. These problems can be mitigated if natural biodegradable polymers are employed as a packaging material, for which biopolymers have to exhibit suitable physical properties and increase the quality and safety of food [265,266]. Desirable properties of a packaging material include adequate mechanical strength, thermal stability, recyclability, biodegradability, and barrier against water vapor [267]. Recently, several researches focused on incorporating antimicrobial agents in packaging films to delay microbial growth [268], which is the major cause of deterioration of foods [269], causing off-flavor development, textural changes, loss of nutritive value, shelf-life reduction, increased risk of foodborne illnesses [55], rendering the product unacceptable for human consumption [270].

Rosin is an abundant natural product of pine resins, which is produced in more than 1 million tons annually [271,272], and contains a mixture of acids (ca. 90%) with hydrogenated phenanthrene ring structures (Figure 4.1) [273]. These acids are used in numerous applications as renewable feedstocks for polymer synthesis due to their biodegradability and nontoxicity [271,272,274]. Cellulose nanocrystals grafted with natural rosin mixture (r-CNCs) showed the antimicrobial activities for Gram-negative bacteria and Gram-positive bacteria [275]. Recently, rosin-based bionanocomposites have been studied for the production of active films [276,277]. However, these rosin-based bionanocomposites in previous works require the use of chloroform or dichloromethane to disperse the polymer, limiting their application in the food industry.

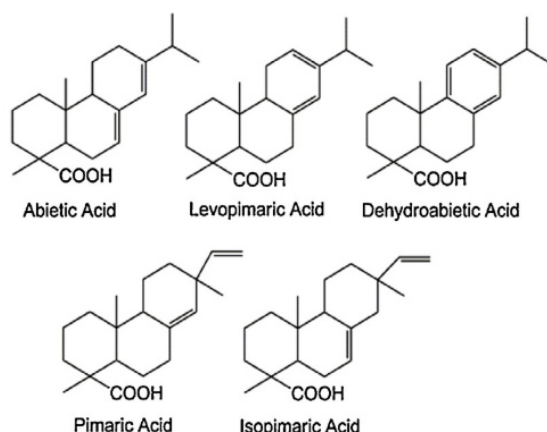


Figure 4.1 - The most representative structures found in Rosin.

Herein, rosin was grafted onto the surface of CNCs and incorporated in gelatin film to create an antimicrobial packaging material with enhanced mechanical and barrier properties. To the best of our knowledge, the concomitant modification of gelatin with r-CNCs is an interesting issue for food packaging technology that remains still unexplored. The gelatin/r-CNCs bionanocomposite films were characterized for their antimicrobial activity and physical, chemical, and barrier properties. The results were compared with those from conventional CNCs-based gelatin bionanocomposites.

1.2 Materials and Methods

1.2.1 Materials

Bovine gelatin powder (Bloom Strength-190) was kindly supplied by Gelco Gelatinas do Brazil Ltda (Pedreira, SP). CNCs, isolated from wood pulp by sulfuric acid hydrolysis and delivered as a dried powder, were purchased from Celluforce Inc. (Windsor, Québec, Canada). Rosin was purchased from Aldrich Chemical (USA). Glycerol and ethanol were purchased from Across Organics (USA). All chemicals were of analytical grade and were used as purchased. *Staphylococcus aureus* (*S. aureus*, Gram-positive, ATCC 25923) and *Escherichia coli* (*E. coli*, Gram-negative, ATCC 25922) were supplied by Cefar Diagnostica (Brazil). Distilled water was used in all experiments.

1.2.2 Synthesis of rosin-grafted CNCs (r-CNCs)

The CNCs were functionalized with rosin by a SolReact process adapted from Castro et al.[275]. The CNCs were dispersed in water at 1.0 wt% and ultrasonicated for 2 min using a Branson sonicator, and the pH was adjusted to 4.0 with HCl (0.1 mol/L). The CNCs dispersion was placed in a closed distillation system in an oil bath at 130 °C. After 10 min, an excess of rosin (10 equiv. according to the CNCs dry weight) was added slowly to ensure its melting and adsorption on the CNCs surface. The system was kept under stirring for 9 h at 130 °C. After the reaction, the rosin-grafted CNCs (r-CNCs) were purified from unreacted rosin by six dispersion-centrifugation cycles (10000 rpm at 4 °C for 10 min) with a large excess of ethanol, until no more rosin was detected by FTIR in the supernatant. Afterward, the r-CNCs were recovered by centrifugation and washed thoroughly with water, and then sonicated for 5 min and stored in a refrigerator. The final solid content was 3.5% (w/w).

1.2.3 Preparation of gelatin/r-CNCs bionanocomposite films

The bionanocomposite films were prepared by solvent casting. The gelatin powder was hydrated in distilled water (10 g/100 g) at 24 °C for 5 min and then heated at 60 °C under stirring for 15 min. Glycerol (20 wt% on a dry gelatin basis) was added to the gelatin solution under stirring. The solution obtained was mixed with the r-CNCs suspension at various contents (0 wt%, 0.5 wt%, 4.0 wt% and 6.0 wt%, on a dry gelatin basis) and stirred for 5 min. The suspensions (45 mL) were then cast on glass plates (40 cm × 25 cm) covered with a polyester film (Mylar®, DuPont, Brazil) to facilitate film peeling off after drying at room temperature for 24 h. Film samples were conditioned at 50% RH and 25 °C for at least 24 h prior to testing. Non-grafted gelatin/CNCs films were prepared at the same concentrations described above for comparison.

1.2.4 X-ray photoelectron spectroscopy (XPS)

The functionalization of CNCs with rosin was characterized by XPS (XR3E2, Vacuum Generator, UK) equipped with monochromated Mg K α X-ray source (1253.6 eV) operated at 15 kV and 20 mA.

1.2.5 Fourier Transform Infrared Spectroscopy (FTIR)

CNCs and r-CNCs were characterized by FTIR (FT-NIR VERTEX spectrometer, Bruker, Germany) in the attenuated total reflection (ATR) mode. Spectra were recorded between 4000 and 400 cm⁻¹ with a resolution of 1 cm⁻¹ and 32 spectral accumulations. The FTIR measurements of gelatin and PVC films were carried out with five repetitions for each film sample.

1.2.6 Transmission Electron Microscopy (TEM)

The morphology of CNCs and r-CNCs was investigated using TEM (TecnaiTM G2 F20 microscope, FEI Company, USA) with an accelerating voltage of 80 kV. The samples were prepared by depositing a 0.1 wt% suspension droplet on a carbon microgrid with formvar (400 mesh) stained with 1.5 wt% uranyl acetate solution. A minimum of 10 images was recorded and the most representative one was used for discussion. The CNCs and r-CNCs sizes were determined from the analysis of a minimum of 100 particles using the ImageJ software.

1.2.7 X-ray diffraction (XRD)

The crystallinity of CNCs and r-CNCs was estimated by XRD (Panalytical diffractometer, X'Pert Pro MPD-Ray, The Netherlands) with Ni-filtered Cu K α radiation ($k = 1.54 \text{ \AA}$, 45 kV, 40 mA) in the 2θ range from 5° to 60°. The crystallinity index (CI) was calculated according to the method of Segal et al. [229]:

$$CI (\%) = \left(1 - \frac{I_1}{I_2}\right) \times 100 \quad (1)$$

where I_1 is the intensity at the minimum ($2\theta = 18^\circ$) and I_2 is the intensity associated with the crystalline region of cellulose ($2\theta = 22.7^\circ$).

1.2.8 Scanning Electron Microscope (SEM)

The film cross-sectional surface was studied using a JEOL (SEM, model Quanta200, FEI, the Netherlands). The samples were first cryo-fractured in liquid N_2 and then fixed onto 90° specimen mounts to be coated with a ca. 5-nm-thick gold layer in an argon atmosphere. The SEM images were taken at accelerating voltages below 5 kV using the secondary electron mode.

1.2.9 Water Vapor Permeability

The WVP of the films was determined following ASTM E-96-01. The preconditioned film was sealed onto the opening of an aluminum permeation cup (28 mm internal diameter) containing dried calcium chloride. The cup was kept in a controlled chamber at $23 \pm 1^\circ C$ and $50 \pm 5\% RH$. The cup was weighed at least four times for at least 7 days under this controlled environment. For each film, three replicates were performed. WVP [(g mm)/ $m^2 h kPa$] was determined using Eq. 2:

$$WVP = WVTR \times L / \Delta p \quad (2)$$

in which WVTR is the water vapor transmission rate ($g/m^2 h$) through the film area; L is the film thickness (mm), and Δp is the partial pressure gradient (kPa) across the film.

1.2.10 Oxygen Transmission Rate (OTR)

The OTR of the films was determined in duplicate at 0%, 50%, and 80% RH according to the ASTM D3985 method (2002a) using an oxygen transmission rate analyzer (Systech Illinois 8500, USA).

1.2.11 Tensile tests

The mechanical properties of the films were determined as per the ASTM D882-09 standard method (2009). Film specimens were prepared and equilibrated at 23 ± 1 °C and $50 \pm 5\%$ RH for 48 h. The tests were carried out on an Instron Universal Testing Machine (model 5569, Instron Corp., USA) with a 100 N load cell. The specimens were stretched using crosshead speed of 10 mm/min with clamps initially separated by 100 mm. Tensile strength, Young's modulus, and elongation at break were calculated from the stress-strain curves. The tests were performed with five replicates for each film. Film thickness was measured with a digital micrometer (Mitutoyo Corp., Kanogawa, Japan) to the nearest 0.001 mm. At least 10 specimens of each composition were analyzed.

1.2.12 Antimicrobial activity tests

The bacterial strains to evaluate the effectiveness of CNCs- and r-CNCs-loaded gelatin solutions were *Staphylococcus aureus* and *Escherichia coli*, which are foodborne pathogens [278,279]. The inoculum cultures were prepared inoculating a selected single colony in 15 mL of Muller-Hinton Broth medium (MHB), followed by overnight incubation at 35 °C. The optical densities at 625 nm were measured by UV-Vis absorption spectroscopy and compared with the turbidity of a 0.5 McFarland standard at the same wavelength, equivalent to 1.5×10^8 colony forming units per mL (CFU/mL). The overnight cultures were diluted in MHB until reaching 10^6 CFU/mL. The antimicrobial activity of the CNCs and r-CNCs suspensions was assessed by determining the minimum inhibitory concentration (MIC) in a 96 flat-bottomed-well tissue culture microplate. Briefly, 100 μ L of sterile Mueller Hinton were added to all wells. In the first column, the wells were filled with 50 μ L of CNCs ($50 \text{ mg}\cdot\text{ml}^{-1}$) and r-CNCs ($22 \text{ mg}\cdot\text{ml}^{-1}$) suspensions. Then, 50 μ L of each antimicrobial substance were serially transferred from the well to the corresponding wells. Then, 50 μ L of the culture suspension were added to all wells. Positive and negative controls (streptomycin and culture medium – data not shown) were included in each assay plate. Afterward, the inoculated plates were incubated in a wet chamber for 24 h at 35

°C and then chlorinated with 50 µL of 2,3,5-Triphenyltetrazolium chloride (0.1%). The lowest sample concentration with an inhibition effect on microbial growth was considered as the MIC for each tested microorganism.

In the antimicrobial film test, all films were cut into discs of 10 mm diameter and both sides were sterilized by UV treatment in a laminar flow hood for 30 min. The discs were placed on Muller-Hinton Agar (MHA) plates that had been previously seeded with 100 µL of inoculums containing *S. aureus* or *E. coli* at a concentration of 1×10^6 CFU/mL. The plates were then incubated at 35 °C for 24 h. Two independent experiments were performed in triplicate.

The antibacterial activity of the gelatin/r-CNCs films on mozzarella cheese was also investigated. Fresh mozzarella samples (20 mm x 20 mm x 10 mm; four replicates) were wrapped with gelatin and gelatin/r-CNCs films. All samples were packaged, sealed by heating and stored at room temperature for 1 month. Cheese samples without film and wrapped in PVC cling film were used as control.

1.2.13 Statistical analysis

All data were subjected to analysis of variance (ANOVA). Mean values were compared using the Tukey's test at a confidence level of 95% ($p < 0.05$).

1.3 Results and discussion

1.3.1 Functionalization of CNCs with rosin

The functionalization of the surface of CNCs occurred by the esterification reaction between the –OH groups on the CNCs and the –COOH groups on the Rosin. A schematic representation of the rosin-functionalized CNCs is shown in Figure 4.2.

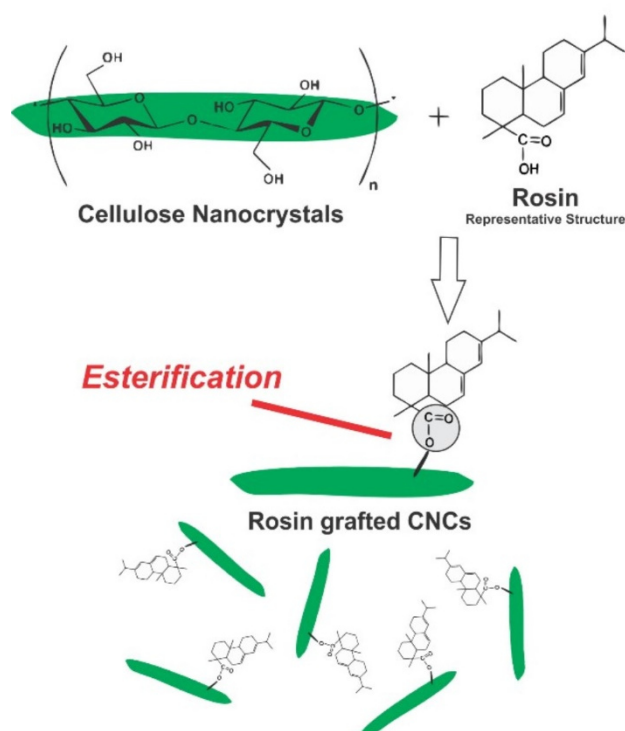
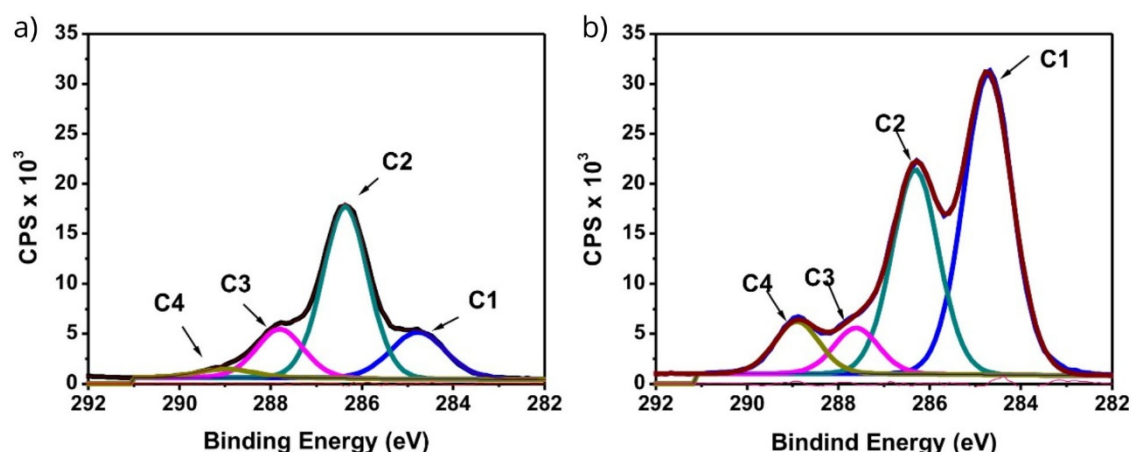


Figure 4.2 - Schematic representation of the rosin-functionalized CNCs.

The surface functionalization of CNCs with rosin was confirmed by XPS (Figure 4.3). The full spectra of CNCs and r-CNCs show that the surfaces of both samples contain mainly carbon and oxygen atoms (signals at 248 and 532 eV, respectively). The C1s signal was deconvoluted to quantify the relative abundance of the carbon atom types, which displayed 4 peaks attributed to C1 (C-C at 285.0 eV), C2 (C-O at 286.6 eV), C3 (O-C-O at 288.0 eV), and C4 (-O-C=O at 289.1 eV) [280]. The esterification of CNCs surface with rosin changed the relative proportion of C4 and C1 peaks due to the higher amount of aliphatic carbon from rosin. Furthermore, the O/C ratio decreased from 0.61 to 0.33 (Table 4.1), also confirming the successful grafting of rosin onto the CNCs. Niu et al. [277] found similar behavior for rosin-modified cellulose nanofiber.

Table 4.1 - X-ray photoelectron spectroscopy data of CNCs and r- CNCs.

Cellulose nanoparticles	O/C	Binding energy, eV			
		C1: C-C 285.0	C2: C-O 286.6	C3: O-C-O 288.0	C4: O=C-O 289.1
CNCs	0.61	16.4	62.6	17.2	3.8
r-CNCs	0.33	52.1	32.5	7.3	8.1

Figure 4.3 - C_{1s} XPS spectra of (a) CNCs and (b) r-CNCs.

The chemical grafting of CNCs with rosin was also analyzed by ATR-FTIR (Figure 4.4). Typical vibration bands of cellulose were observed in CNCs and r-CNCs spectra, including O-H stretching at 3340 cm⁻¹, C-H symmetrical stretching at 2895 cm⁻¹, H-O-H bending of absorbed water molecules at 1647 cm⁻¹, CH₂ symmetrical bending at 1427 cm⁻¹, and C-O-C vibration on glycosidic linkages at 1165 cm⁻¹ [275,277]. After chemical grafting, a new band at 1740 cm⁻¹ was observed in the spectrum of r-CNCs, assigned to ester carbonyl groups from the reaction between CNCs OH groups and -COOH groups of rosin. Likewise, the increased intensity of the 1647 cm⁻¹ band can be related to C=C stretching from rosin cyclic alkene rings. There was no significant reduction in the intensity of the O-H band at 3340 cm⁻¹, indicating that esterification occurred mainly with hydroxyl groups accessible at the CNCs surface, as reported by Castro et al. [275]. The absence of a band at ~1700 cm⁻¹ from rosin carbonyl groups indicates that the residual rosin was completely removed after the purification step.

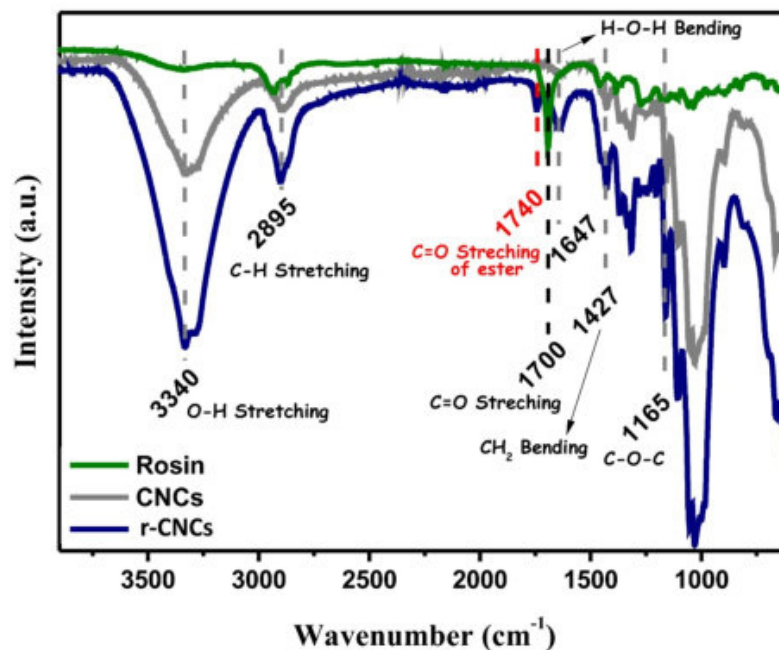


Figure 4.4 - ATR-FTIR spectra of rosin, CNCs, and r-CNCs.

The TEM images of CNCs and r-CNCs in Figure 4.5 show that the needle-like shape of the nanocrystals was unchanged after functionalization with rosin, as expected. The average lengths for CNCs and r-CNCs were 108.0 ± 33 and 122.0 ± 50 nm, and the average diameters were 3.8 ± 0.9 and 7.5 ± 2.2 nm, respectively. The largest dimensions of r-CNCs are attributed to the small aggregates of CNCs crystals. This is consistent with Espino-Pérez et al. [21] who observed the largest length for octadecyl isocyanate-grafted CNCs (179.0 nm) compared with non-grafted CNCs (155.0 nm).

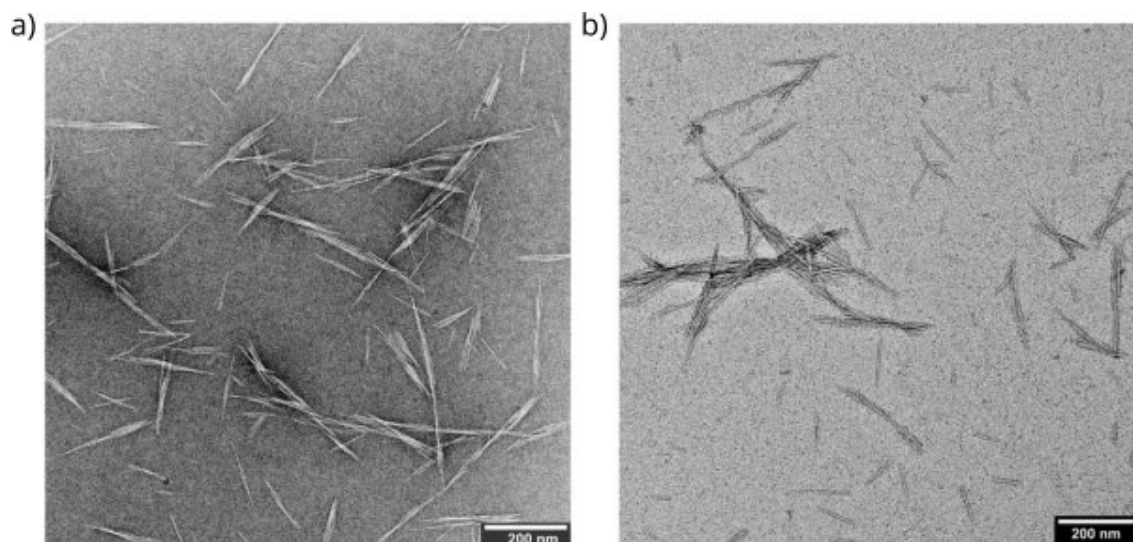


Figure 4.5 - TEM micrograph of CNCs and (e) r-CNCs. (f) schematic representation of rosin-functionalized CNCs.

The XRD patterns of CNCs and r-CNCs are displayed in Figure 4.6. Both samples exhibited typical diffraction peaks at $2\theta = 16.5, 22.7, \text{ and } 34.8^\circ$, related to cellulose I polymorph [275]. This confirms that rosin grafting did not convert cellulose I into cellulose II. The crystallinity index slightly increased from 82% to 84% after functionalization. Similar behavior was reported by Niu et al. [277], who found crystallinity indexes of 59.91 and 63.42% for CNF and rosin-CNF, respectively. The increased crystallinity was attributed to the partial hydrolysis of the CNF amorphous phase due to the acidic condition used in the reaction with rosin [277].

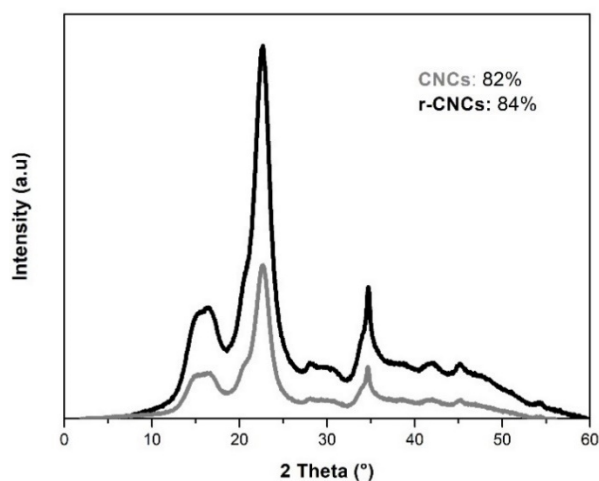


Figure 4.6 - XRD spectra of the CNCs and r-CNCs.

1.3.2 Morphology of gelatin films reinforced with CNCs and r-CNCs

Pure gelatin and bionanocomposite films of different CNCs and r-CNCs contents were obtained with solvent casting. The thickness of the free-standing films was similar ($\sim 85 \mu\text{m}$) for all compositions with standard deviations lower than 20%. The dispersion of CNCs and r-CNCs in the gelatin matrix was studied with SEM, whose images are shown in Figure 4.7. The gelatin films with low CNCs contents had smooth and more regular surfaces. The absence of agglomerates for the 4.0 wt% r-CNCs content is suggested from the SEM image in Figure 4.7b, indicating a good dispersion of r-CNCs [224] within the gelatin matrix. Nevertheless, agglomerates appeared when 6.0 wt% r-CNCs were added to the gelatin film (Figure 4.7e). This is probably due to the increased hydrophobicity of r-CNCs after functionalization with rosin, which decreased chemical compatibility with the hydrophilic gelatin matrix. The evidence of increased hydrophobicity in gelatin/r-CNCs films is provided in contact angle measurements (Figure 4.8 -).

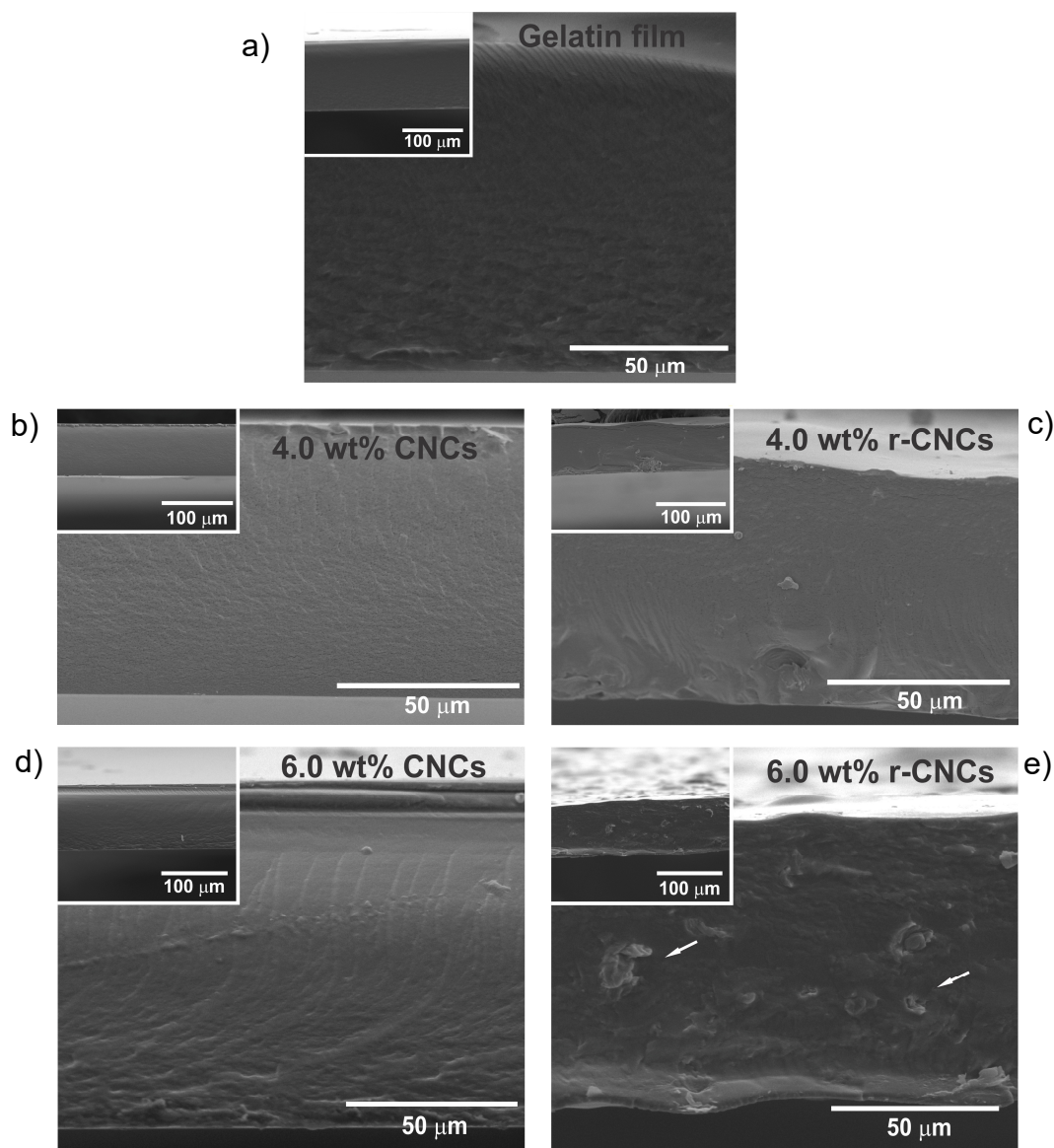


Figure 4.7 - SEM micrographs of the cross-sectional surface of (a) pure gelatin films and gelatin bionanocomposites with 4.0 wt% (b) CNCs and (c) r-CNCs, and with 6.0 wt% (d) CNCs and (e) r-CNCs content.

1.3.3 Contact angle of gelatin films reinforced with CNCs and r-CNCs

Figure 4.8 - displays the dynamic changes in the water contact angle of pure gelatin, gelatin/CNCs, and gelatin/r-CNCs films. Gelatin films presented water contact angle values higher than 90° over time, which indicates that the surface studied was hydrophobic. This behavior is attributed to the hydrophobic parts of the gelatin that are able to spontaneously rearrange towards the air-film [203,241–243]. Nevertheless, the increasing concentration of CNCs decreased

the water contact angle value of gelatin/CNCs films. This result demonstrated that the film was more hydrophilic due to the OH- group in the CNCs structure. The polarity around the structure could create H-bonding to react with water. This phenomenon was not observed for r-CNCs reinforced films, strongly indicating a more hydrophobic surface for the modified CNCs. The same results are observed by Castro et al. (2017) for r-CNCs [275]. These results suggest the less water-susceptible surface of the gelatin/r-CNCs film.

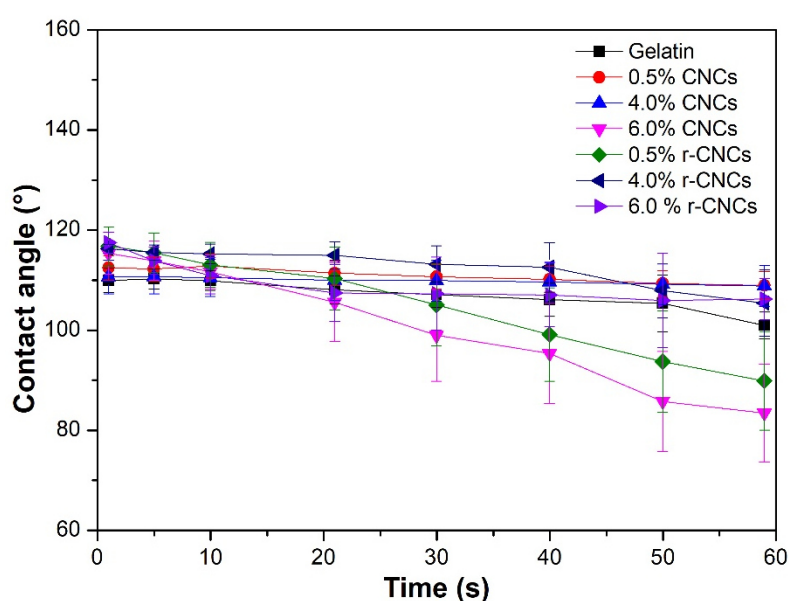


Figure 4.8 - Contact angle of pure gelatin, gelatin/CNCs, and gelatin/r-CNCs films.

1.3.4 Optical properties of gelatin films reinforced with CNCs and r-CNCs

All gelatin/CNCs and gelatin/r-CNCs bionanocomposites were flexible, and exhibited good macroscopic homogeneity and high transparency, as displayed in Figure 4.9 and the UV-Vis transmittance spectra in Figure 4.10. Gelatin films exhibited a high barrier against UV radiation, nearly 100% for UVC, over 93.3% for UVB, and 54.0% for UVA, due to chromophore groups such as tyrosine and phenylalanine [96]. The addition of r-CNCs led to a significant reduction in the transmittance over all the UV regions compared to the pure gelatin and gelatin/CNCs film samples. The gelatin film with 0.5 wt% r-CNCs

showed a reduction of 20.8 and 29.1 in the UVB and UVA transmittance, compared to the gelatin/CNCs films, respectively. Narayanan et al. [274] observed a reduction of 1% and 6% for UVB and UVA, respectively, in PLA bionanocomposites with 20 wt% rosin. The authors attributed this reduction to the absorbance by rosin which prevents light transmission through the films. However, gelatin films with 6.0 wt% r-CNCs showed a significant reduction in the visible light range, which may indicate the light scattering by r-CNCs aggregates, as shown by the SEM images (Figure 4.7e).

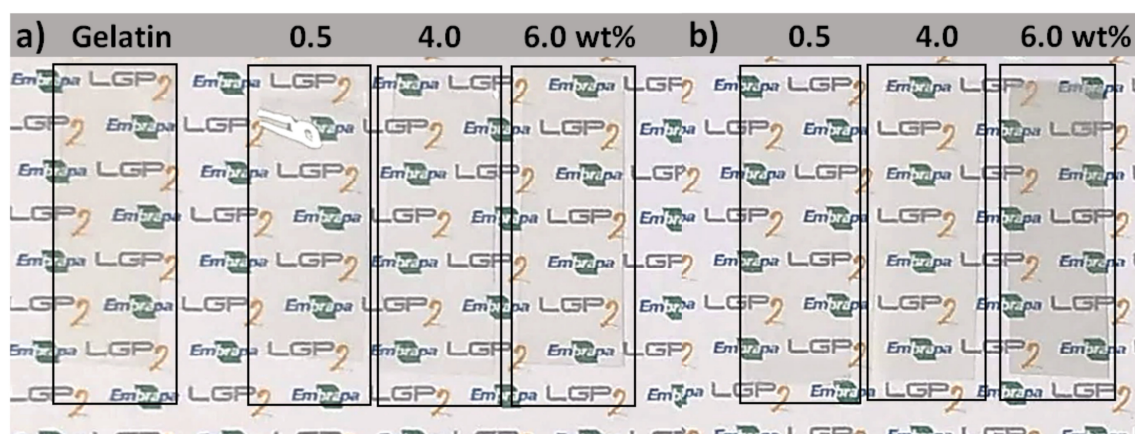


Figure 4.9 - Photography of (a) gelatin/CNCs and (b) gelatin/r-CNCs bionanocomposite films.

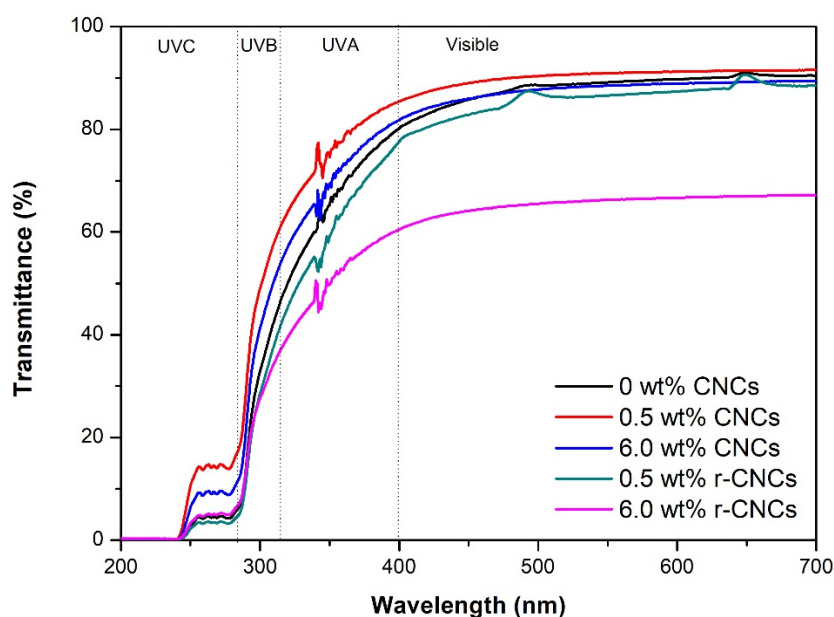


Figure 4.10 - UV-Vis spectra of pure gelatin, gelatin/CNCs, and gelatin/r-CNCs films.

Table 4.2 presents a comparison of light transmission of the gelatin/r-CNCs bionanocomposites films with some synthetic packaging films. The gelatin/r-CNCs films had low transmittance over the entire spectral range, indicating that they absorb light much more efficiently than several synthetic polymer films. These results suggest that the gelatin/r-CNCs bionanocomposites are suitable for packaging to protect light-sensitive food products.

Table 4.2 - Optical properties of gelatin/r-CNCs bionanocomposite and synthetic films currently applied in food packaging.

Film	Light transmission (%)			
	200 nm	280 nm	400 nm	600 nm
0.5 wt% gelatin/r-CNCs	0.0	4.5	77.3	87.4
6.0 wt% gelatin/r-CNCs	0.0	5.4	60.5	66.7
Synthetic films currently applied in food packaging ^a				
LDPE ^a	13.1	67.5	83.4	86.9
OPP ^a	4.6	80.0	87.9	89.1
PVC	20	83.9	87.9	88.7

LDPE: low-density polyethylene; OPP: oriented polypropylene; PVC: polyvinyl chloride.

^a adapted from [281].

1.3.5 Barrier properties of gelatin/CNCs and gelatin/r-CNCs films

Water vapor permeability (WVP) and oxygen transmission rates (OTR) are barrier properties that determine the ability of bio-based films to protect food products from moisture transfer, oxygen uptake, lipid oxidation, and loss of volatile aromas and flavors. Gelatin films generally display good barrier against oxygen at low and intermediate relative humidity [30]. Our results show that the OTR of gelatin films with 0.5 and 6.0 wt% CNCs and r-CNCs at 0% and 80% RH were $< 0.01 \text{ cm}^3/\text{m}^2 \text{ day}$, indicating that the addition of CNCs or r-CNCs did not change significantly the already high oxygen barrier of gelatin.

The values of WVP and WVTR of the gelatin bionanocomposites with CNCs and r-CNCs at 25 °C and 50% RH are presented in Figure 4.11. Pure gelatin film exhibited a WVP of $0.20 \pm 0.03 \text{ g mm/m}^2 \text{ h kPa}$. The incorporation of CNCs or r-CNCs reduced the WVP of the gelatin films. The addition of 0.5 wt% r-CNCs significantly decreased WVP of the gelatin matrix by 55% ($p < 0.05$). According to Ooi, Ahmad, & Amin [282], nanoparticles can reduce WVP by

increasing the biopolymer crystallinity or by reducing the free hydrophilic groups (OH, NH) in the gelatin matrix, thereby creating a tortuous pass for water vapor diffusion through the film. Santos et al. [165] reported decreased WVP of protein films with increasing CNCs contents. They found that fish gelatin films with 15 wt% CNCs had WVP values of approximately 2 g mm/m² h kPa (25 °C at 85% RH). George & Siddaramaiah [17] reported that 4.0 wt% bacterial cellulose nanocrystals reduced WVP of gelatin, and attributed this outcome to the low hygroscopicity of highly crystalline CNCs. They found WVP values around 0.175 g mm/m² h kPa (25 °C at 50% RH), which were higher than those of our gelatin films reinforced with CNCs or r-CNCs.

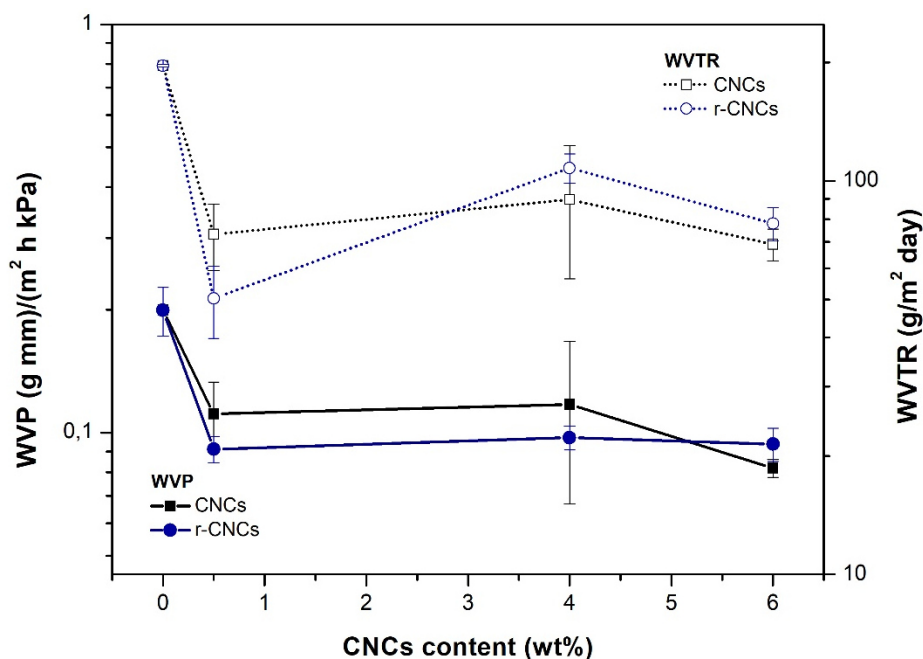


Figure 4.11 - Water vapor permeability and water vapor transmission rate (WVTR) of gelatin bionanocomposites as functions of CNCs and r-CNCs contents.

The mechanical properties, Young's modulus, tensile strength, and elongation at break of bionanocomposite films were investigated using tensile tests. The Young's modulus and tensile strength of pure gelatin film were 743 and 17 MPa, respectively, as shown in Figure 4.12. For gelatin/CNCs bionanocomposite films, the tensile strength and Young's modulus increased

significantly with increasing CNCs content. These increases can be attributed to the CNCs reinforcing effect through effective stress transfer from the gelatin matrix to CNCs [14]. For the same filler content of 4.0 wt%, the gelatin film with r-CNCs exhibited tensile strength ~30% higher than that of the film with CNCs. This improvement is likely due to the intermolecular interactions such as hydrogen bonds and Van der Waals forces between the rosin graphitized onto CNCs and gelatin matrix. Besides, the slightly increased crystallinity of r-CNCs may have contributed to the higher stiffness of the bionanocomposites. However, for gelatin/r-CNCs films with 6.0 wt% r-CNCs, a reduction in Young's modulus and tensile strength was observed. In addition, there was an increase in elongation at break, which can be attributed to the formation of aggregates, as revealed by SEM. Furthermore, the gelatin film with 6.0 wt% r-CNCs showed an elongation at break ~145% higher than that of gelatin film, indicating that the gelatin/r-CNCs films were much more ductile and flexible. The interaction formed between the gelatin and r-CNCs weakened the protein-protein interactions, which were effective in stabilizing the gelatin network, as described by Zhuang et al [15]. Therefore, it is clear that r-CNCs play an effective role in enhancing the mechanical properties of gelatin, with promising features for flexible food packaging.

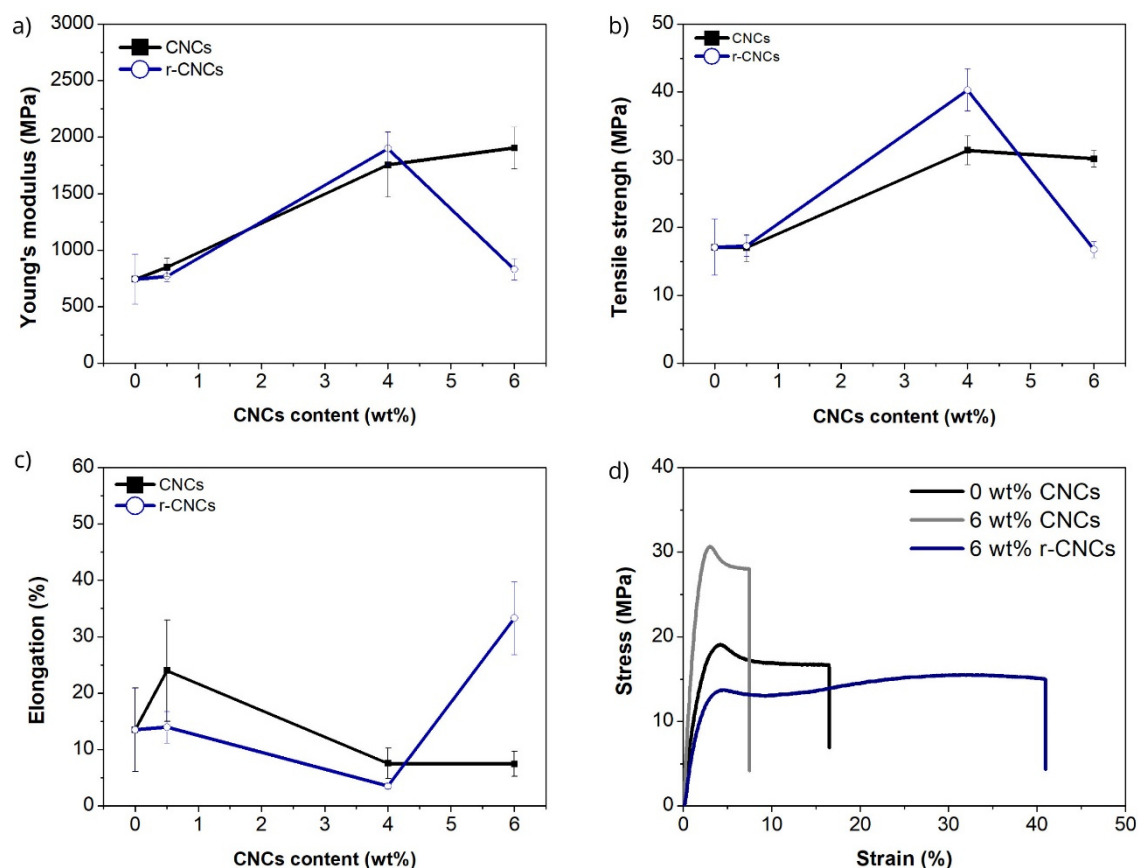


Figure 4.12 - (a) Young's modulus, (b) tensile strength (c) elongation at break, and (d) stress-strain curves as a function of CNCs and r-CNCs content in bionanocomposite gelatin films obtained by casting.

1.3.6 Antimicrobial properties of r-CNCs and gelatin/r-CNCs films

The minimum inhibitory concentration (MIC) value was determined as the lowest concentration of r-CNCs suspension that inhibited the growth of tested microorganisms. The results in Figure 4.13 show the highest bactericidal effect against Gram-positive *Staphylococcus aureus* and Gram-negative *Escherichia coli* with the r-CNCs suspension. As expected, there was no inhibitory effect for the CNCs suspension. A low concentration of r-CNCs (5.5 mg/mL) inhibited the growth of *S. aureus*, whereas for *E. coli* inhibition required 22 mg/mL. This may be due to the external lipopolysaccharide layer of the cell membrane of Gram-negative bacteria, which restricts the diffusion of hydrophobic compounds [283]. The proposed mechanism for r-CNCs antimicrobial activity is based on its interaction with the phospholipid cell membrane, which causes increased

permeability and leakage of cytoplasm, or its reaction with enzymes located at the cell wall [284]. This is consistent with findings that rosin-derived cationic compounds have antimicrobial activity against many bacteria due to the hydrophobicity and structure of resin acids [285].

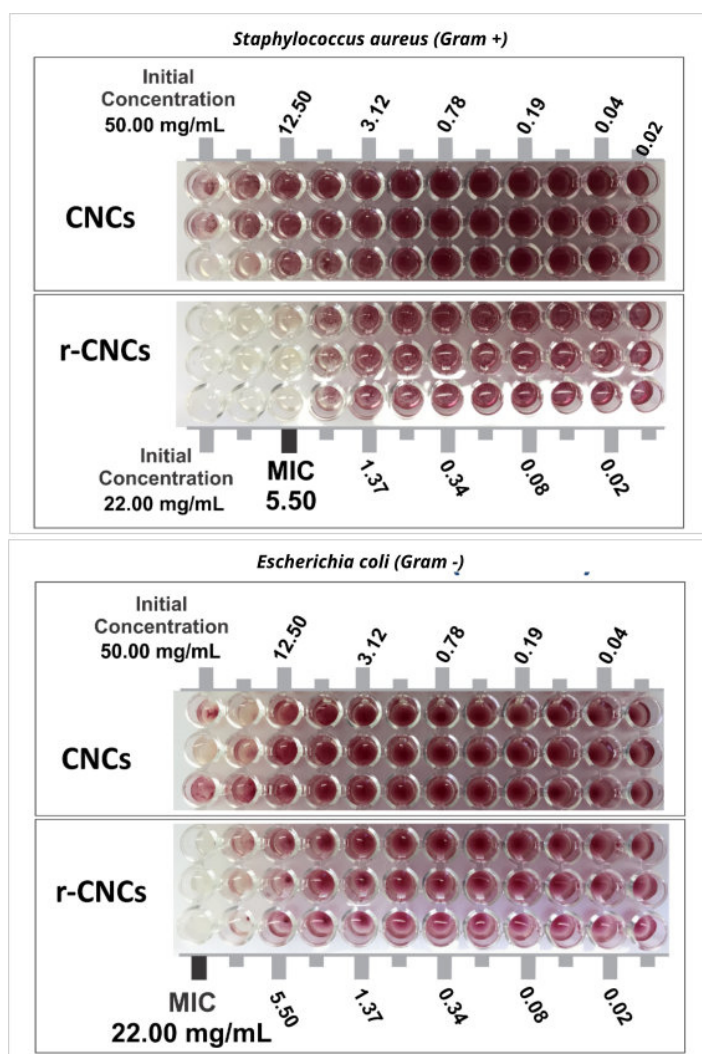


Figure 4.13 - Minimum inhibitory concentration (MIC) of CNCs and r-CNCs suspension tested on Gram-positive *Staphylococcus aureus* and Gram-negative *Escherichia coli*.

Gelatin/r-CNCs films were also tested against *S. aureus* and *E. coli* as demonstrated with agar overlay assays depicted in Figure 4.14. The control films made with neat CNCs in gelatin did not display any inhibitory effect, with bacteria observed underneath. On the other hand, gelatin/r-CNCs films showed an

effective antibacterial property, especially against *E. Coli*, since these strains did not grow in the inhibition area covered with gelatin/r-CNCs films. Neither of the tested films yielded a halo or a surrounding clearing zone, which shows that r-CNCs do not diffuse through the adjacent agar media and their antimicrobial effect is only by contact. The lack of diffusion is related to the hydrophobic nature of rosin molecules grafted onto the r-CNCs. Indeed, migration is linked to factors such as molecule size, polarity, shape, and quantity of water in the agar, in addition to the chemical structure and crosslinking in the films [286].

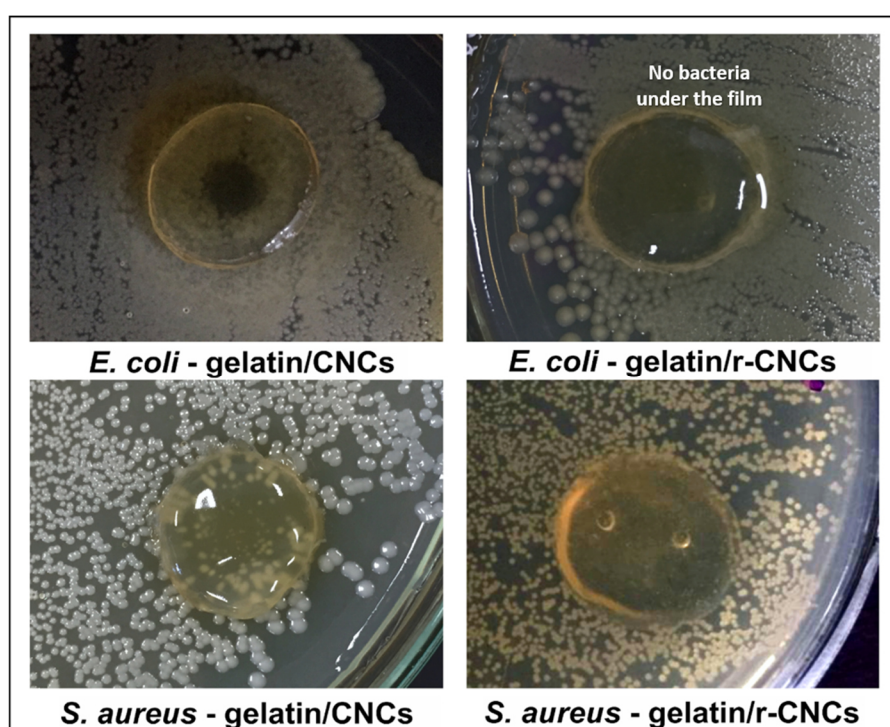


Figure 4.14 - Agar overlay assay of gelatin film discs against *S. aureus* and *E. coli*.

1.3.7 Use of gelatin films reinforced with r-CNCs for actual packaging

Accelerated storage tests were carried out at 25 °C for one month to prove the antimicrobial ability of gelatin/r-CNCs films in practical applications. The tests were conducted with mozzarella cheese samples packed with pure gelatin, 6 wt% r-CNCs gelatin film, and a PVC film. Mozzarella cheese is perishable and suffers either from fungal or bacterial spoilage depending on the storage conditions. Figure 4.15 shows evident microbial spoilage in the control and gelatin-packed cheese samples, and especially in the sample packed in PVC. In contrast, there

was no microbial growth in the sample packed in 6 wt% r-CNCs-loaded bionanocomposite films. As a proof of concept, we illustrated that the gelatin/r-CNCs bionanocomposite films can extend the shelf-life of mozzarella cheese, also providing a direct indication of the antibacterial activity of r-CNCs even after forming bionanocomposites with gelatin. However, it is possible that r-CNCs migrated towards the cheese surface in contact with the film, but this has to be confirmed with further quantitative studies.

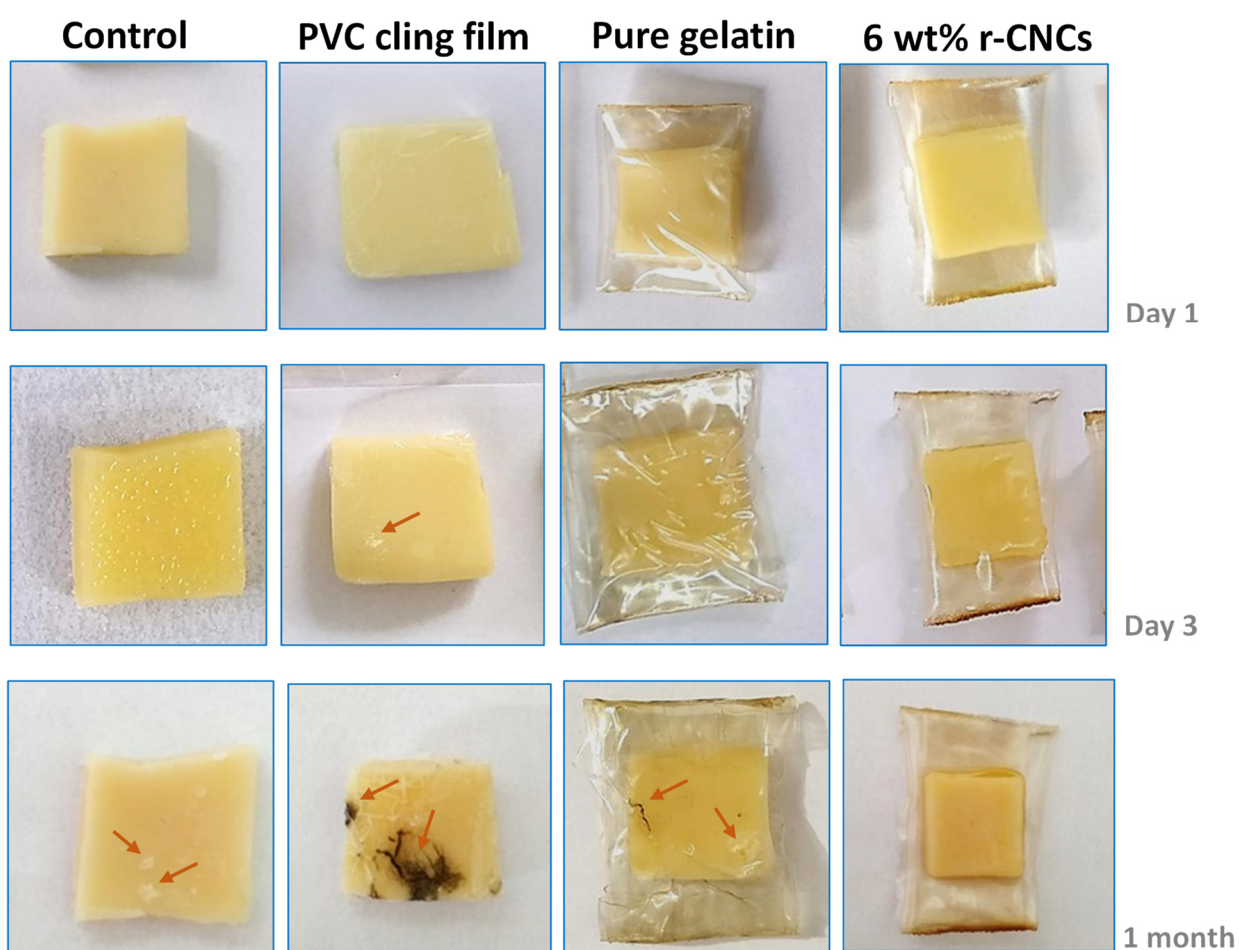


Figure 4.15 - Schematic comparison of accelerated storage for mozzarella cheese slices packed in a PVC cling film, pure gelatin film, and gelatin/r-CNCs bionanocomposite (6 wt%) film over 30 days at 25 °C. The control refers to free-standing, unpacked cheese slices (The Brazilian version of mozzarella cheese can be sliced, in contrast to the Italian mozzarella). Microbial spoilage is indicated by arrows in the images.

1.4 Conclusion

CNCs were successfully functionalized with rosin and used as a bactericidal nanofiller in gelatin for achieving multifunctional packaging. In particular, the r-CNCs consistently improved the optical, and water vapor barrier properties of gelatin films as compared to conventional CNCs. Besides, the mechanical strength of the gelatin matrix was increased and could be tuned by varying the r-CNCs content. This study demonstrates how grafting reactions can extend the functionalities of nanocelluloses for use in flexible packaging materials, which otherwise would suffer from limited physical and biological properties, as well as microbial counting assays to assess the performance of the gelatin/r-CNCs bionanocomposites as antimicrobial packaging materials for cheese and other food items stored at different conditions. These results suggest that the incorporation of low amounts of r-CNCs as active agents in gelatin films may be highly suitable for producing antimicrobial packaging materials.

2 Effect of tannic acid and cellulose nanocrystals on antioxidant, antimicrobial, and physical properties of gelatin-based films

This section is adapted from Liliane S. F. Leite, Cynthia Pham, Stanley Bilatto, Emily D. Cranston, Henriette M.C. Azeredo, Francys K. V. Moreira, Luiz H. C. Mattoso, Julien Bras. Active properties of gelatin films as affected by tannic acid and cellulose nanocrystals. Submitted in October 2020.

Abstract

In this work, we explored gelatin (G) films incorporated with tannic acid (TA) and cellulose nanocrystals (CNCs), which fulfill the most relevant requirements for a natural antioxidant and antimicrobial food packaging material. The effects of non-oxidized TA, oxidized TA (OTA), and CNCs on the physical, morphological, antioxidant, and antimicrobial properties of the films were investigated. QCM-D and rheological measurements confirmed the interactions of the gelatin with TA and the formation of hydrogen bonds between CNCs and gelatin. The decreased crosslinking effect in the G/TA film obtained from non-oxidized TA increased the antioxidant capacity of the film by 52% due to the higher TA availability as an antioxidant. This also allowed the gelatin groups to form hydrogen bonds with CNCs to a larger extent, which resulted in a substantial increase in the viscosity (410%) and mechanical stability (G' 1697%) of the films. The addition of 6 wt% CNCs resulted in films with a denser structure, with reduced interlayer space and low porosity, as revealed by SEM. As a result, the bionanocomposite displayed lower WVP (67%) and greater tensile strength (79%) compared to the G-TA films. The G-TA-CNCs films also demonstrated an inhibitory effect against *Staphylococcus aureus* and *Escherichia coli* growth.

2.1 Introduction

A new generation of multifunctional bionanocomposites based on eco-friendly polymers has emerged as a new trend in food packaging. In this context, researches have been focused on incorporating antimicrobial and antioxidant agents in packaging films to extend food shelf life [268], especially concerning lipid oxidation and microbial spoilage, which are the major causes of deterioration in a great variety of foods [269,270].

Traditionally, synthetic antioxidants such as butylated hydroxytoluene (BHT), butylated hydroxyanisole (BHA), and tertiary butylated hydroquinone (TBHQ) are used in food products. However, the potential toxicity of these compounds [287] has made natural antioxidants like plant essential oils [288] and extracts [289] to become increasingly valuable among consumers. Tannic acid (TA) is an inexpensive plant-derived polyphenol that has received considerable attention due to its multifunctionality, including antioxidant [290], antimutagenic [291], anticarcinogenic and antimicrobial properties [292]. TA is also classified as a Generally Recognized as Safe (GRAS) ingredient by the Food and Drug Administration (FDA), meaning that it can be directly used in food products [293].

Tannic acid has been used to develop multifunctional films and coatings, and as a natural crosslinker for gelatin [294]. Crosslinking of proteins with polyphenols has been found to enhance film performance, depending on the type of polyphenol-protein interaction (covalent or non-covalent). For instance, oxidation of polyphenols produces quinone compounds, which react with amino acid residues of gelatin chains *via* covalent bonds (C-N or C-S), generating crosslinked films [295]. By contrast, non-covalent bonds, such as hydrogen bonding and hydrophobic interactions, can be formed between gelatin and polyphenols at acidic or neutral pH, and are reversible in their nature [108] Figure 4.16.

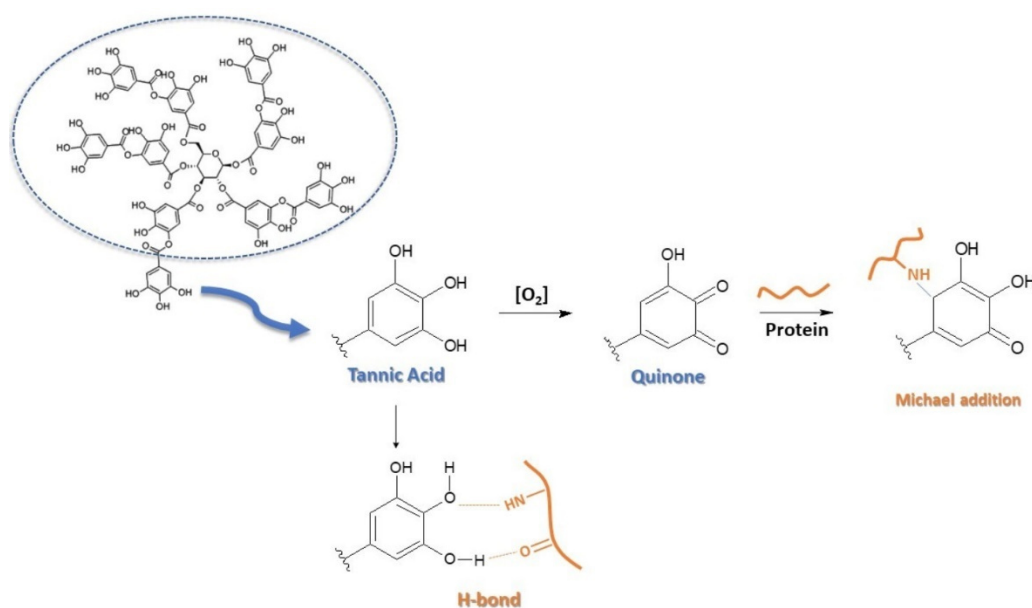


Figure 4.16 - Scheme of crosslinking reaction and hydrogen bonding interactions between protein and tannic acid (adapted from [209]).

Tannins, particularly TA in its oxidized form, have been reported to improve the mechanical and rheological properties of gelatin films and gels [108] [108]. To the best of our knowledge, however, the use of non-oxidized TA, which shows remarkable *in vitro* antioxidant activity [293], to provide functional properties to gelatin films has not been previously reported. Moreover, the concomitant modification of gelatin films with TA and CNCs is a relevant topic for food packaging technologies that remains still unexplored.

In this study, gelatin/CNCs bionanocomposite films added with non-oxidized TA were produced to explore the individual and combined effects of both agents on the antioxidant, antimicrobial and physical properties of the films aiming at multifunctional food packaging applications. The films were also compared with their counterparts obtained with oxidized TA.

2.2 Materials and Methods

2.2.1 Materials

Bovine gelatin powder (Bloom Strength-190) was kindly supplied by Gelco Gelatinas do Brazil Ltda (Pedreira, SP). Cellulose nanocrystals (CNCs) were

purchased as a spray-dried powder from CelluForce Inc. (Windsor, Québec, Canada) and used as received. Tannic acid (TA) was purchased from Roth (France). Glycerol and ethanol were purchased by Across Organics (USA). 1,1-diphenyl-2-picrylhydrazyl (DPPH) was purchased by Sigma Chemical Co. (USA). All chemicals were analytical grade and were used as purchased. *Staphylococcus aureus* (*S. aureus*, Gram-positive, ATCC 25923) and *Escherichia coli* (*E. coli*, Gram-negative, ATCC 25922) were supplied by Cefar Diagnostica (Brazil). Distilled water was used in all experiments.

2.2.2 Film-forming solution (FFS) preparation

A 10 wt% gelatin solution was prepared by first hydrating the gelatin powder in distilled water at 24 °C for 5 min, followed by heating at 60 °C under mechanical stirring for 15 min. Glycerol (20 wt% on a dry gelatin mass basis) was added to the gelatin solution under stirring at 60 °C for 5 min. Afterward, 10 mL of a TA solution (1.8 wt% in water) were slowly added to the gelatin solution and stirred for 1 h at 60 °C. The obtained solution was mixed and stirred for 1 h at 60 °C with 10 mL of CNCs dispersion at designed CNCs contents (4.0 wt% and 6.0 wt% on a dry gelatin mass basis) previously sonicated for 5 min. Pure gelatin (without TA and CNCs) and gelatin-TA solution (without CNCs) solutions were prepared likewise for comparison purposes. The samples were codified as Gel, G-TA, G-TA-CNC4, and G-TA-CNC6. The latter formulation (G-TA-CNC6) was also produced using a different mixing sequence, namely, the TA solution was first stirred with the CNCs suspension for 1 h at 25 °C to oxidize the TA molecules into quinone, followed by the addition to the plasticized gelatin solution under stirring for 1 h at 60 °C. This sample was codified as G-OTA-CNC6. All the solutions were allowed to rest for 60 min to eliminate bubbles before casting.

2.2.3 Film casting

The FFS samples (45 mL) were cast on leveled glass plates (40 cm × 25 cm) covered with a polyester film (Mylar®, DuPont, Brazil), to facilitate film

peeling off after drying at 35 °C for 24 h. The film samples were conditioned at 50% RH and 24 °C for at least 24 h prior to testing.

2.2.4 Transmission electron microscopy (TEM)

The CNCs morphology was investigated by transmission electron microscopy (Tecnai™ G2 F20 microscope, FEI Company, USA) using the STEM (Scanning Transmission Electron Microscopy) mode with an accelerating voltage of 80 kV. The samples were prepared by depositing a 0.1 wt% CNCs dispersion drop on a carbon microgrid with formvar (400 mesh) stained with 1.5 wt% uranyl acetate solution. The CNCs sizes were determined from a minimum of 100 particles using the ImageJ software.

2.2.5 X-ray diffraction (XRD)

The crystallinity of the CNCs was analyzed by X-ray diffraction (Panalytical diffractometer, X'Pert Pro MPD-Ray, The Netherlands) with Ni-filtered Cu Ka radiation ($\lambda = 1.54 \text{ \AA}$, 45 kV, 40 mA) by using 2θ range from 5° to 60°. The crystallinity index (CI) was calculated according to the Segal method [229] as shown in Eq. 1:

$$CI = \left(1 - \frac{I_1}{I_2}\right) \times 100 \quad (1)$$

where I_1 is the intensity at the minimum ($2\theta = 18^\circ$) and I_2 is the intensity associated with the crystalline region of cellulose ($2\theta = 22.7^\circ$).

2.2.6 Quartz crystal microbalance with dissipation (QCM-D)

Preparation of solutions and CNCs dispersions for QCM-D experiments

A 2 wt% aqueous CNCs dispersion was prepared by sonication (Branson Sonifier SFX 550) with a ½ inch titanium tapped horn probe at 60% amplitude, sonicated for two 2-min steps interspersed with 1-min interval. The sonication

was performed in an ice bath to avoid CNCs dispersion heating. A 0.1 wt% CNCs dispersion for the QCM-D experiments was prepared by diluting the 2 wt% CNCs dispersion with ultrapure water and sonicating again for 2 min twice. After sonication, the dispersion was filtered using a glass fiber syringe filter with 1 μm pore size (Acrodisc) and checked for apparent size and aggregation using dynamic light scattering (DLS) with a Malvern Panalytical Zetasizer Nano-ZS. DLS size for CNCs was considered an apparent size since it assumes the particles to be spherical, whereas CNCs are rod-shaped. TA and glycerol (GLYC) were both dissolved in water at room temperature at 0.1 wt% and used immediately for the QCM-D experiments. Gelatin (Gel) was added to water to achieve a 0.1 wt% solution and heated to 50 °C for full solubilization. The ensuing Gel solution was cooled down to room temperature prior to use.

Preparation of CNC-coated QCM-D sensors

Silicon dioxide-coated QCM-D sensors (QSX 303) were purchased from Biolin Scientific (batch 19030) and spin-coated with the 2 wt% CNCs dispersion. The sensors were first cleaned by blowing N_2 gas over them followed by UV/ozone treatment (Compact UV-ozone Cleaner – EQ-PCE-44-LD) for 15 min. The sensors were spin-coated with the WS-650-23B Spin Coater (Laurell Technologies). A pre-spin step with water at 4000 rpm for 30 s was done followed by depositing the 2 wt% CNCs dispersion and spinning at 4000 rpm for 30 s. The CNCs films on spin-coated sensors were annealed at 80 °C overnight in an oven [296]. The nominal CNCs film thickness is estimated to be 30-40 nm [296,297].

QCM-D experiments

QCM-D monitoring using an E4 QSense Analyzer (Biolin Scientific) was carried out to investigate the interactions between the active film components. QCM-D monitors the frequency and energy dissipation response of the sensor to obtain information regarding the adsorption of the flowing material to the sensor surface where the change in the oscillating surface frequency is inversely proportional to the mass per unit area change. All QCM-D runs used 0.1 wt%

solutions/suspensions at 25 °C. Briefly, the CNC-coated silica sensors were equilibrated overnight in water (flowed at 10 $\mu\text{L}/\text{min}$) in the QCM-D instrument to achieve a stable baseline. The samples were then injected at a flow rate of 100 $\mu\text{L}/\text{min}$, allowed to adsorb for 50 min, followed by 30 min of rinsing with water. The order of injections varied for each run while keeping constant the time of each injection (TA solution, gelatin solution, glycerol solution, or CNC dispersion). For the QCM-D measurements, 13 overtones were monitored and representative curves from 3 replicates of the third overtone were used.

2.2.7 Rheological properties

The rheological measurements were carried out on a Physica MCR101 rheometer (Anton Paar, Austria) using the concentric cylinder geometry. The apparent viscosity of FFS was measured within the shear rate range 0-500 s^{-1} at 35 °C. The flow behavior was described by fitting the experimental data to the Power Law model (Eq. 2).

$$\sigma = k\dot{\gamma}^n \quad (2)$$

Where σ is the shear stress (Pa), $\dot{\gamma}$ is the shear rate (s^{-1}), k is the consistency coefficient (Pa s^n) and n is the flow behavior index.

Oscillatory shear testing was carried out to determine the storage modulus (G'), loss modulus (G'') and $\tan \delta$ (G'/G'') of the FFS at a constant strain of 1% and frequency of 1 Hz with heating from 10 to 50 °C and then cooling down to 10 °C using constant rate of 0.02 °C/s. Frequency sweep tests were performed in the 0.1–100 Hz range at strain 1 %. The films were cut into 11-mm discs and the frequency sweep tests were conducted from 0.1 to 100 Hz at a fixed strain of 0.1%, using a 25-mm plate-plate geometry. Amplitude sweep experiments were previously carried out to determine the linear viscoelastic region of each sample.

2.2.8 Determination of crosslinking degree

The tannic acid-gelatin crosslinking degree in FFS and films was determined by UV/VIS spectrophotometry at $\lambda = 275$ nm (Model PC, Shimadzu, Kyoto, Japan), as described by [298]. TA was added to the FFS at 3×10^{-5} mol/L. The TA extraction from the gelatin films was done through several washing cycles with 50 mL of water until the phenolic compound was not observed in the UV spectrum. The amount of free TA was then calculated for each washing cycle using an absorbance vs concentration calibration curve. The crosslinking degree was estimated as the difference between the initial TA amount added to the FFS and the amount of free TA extracted from the samples.

2.2.9 Scanning electron microscopy (SEM)

The cross-sectional surface of films before and after swelling in water for 24 h was investigated using a JEOL Scanning Electron Microscope (SEM, model Quanta200, FEI, The Netherlands). The film samples were first cryo-fractured in liquid N_2 . Swollen films were freeze-dried for 24h. The films were, fixed onto 90° specimen mounts and then coated with a ca. 5-nm-thick gold layer in argon atmosphere. The SEM images were obtained from the secondary electron mode at accelerating voltages below 5 kV.

2.2.10 Determination of antioxidant activity

Antioxidant capacity was determined in triplicate using the DPPH (2,2-diphenyl-1-picrylhydrazyl) free radical scavenging method. The samples were cut into small pieces (45 mg) and immersed into 10 ml of DPPH* solution (0.003 % in ethanol 95%). The mixtures were then stirred at $23^\circ C$ and 100 rpm in the dark. The absorbance of the resulting solution was measured at 517 nm by UV/Vis spectrophotometry (Model PC, Shimadzu, Kyoto, Japan) at different times. The DPPH radical scavenging activity (RSA) was determined according to Eq. 3.

$$RSA(\%) = \left[\frac{(A_{sample} - A_{blank})}{A_{blank}} \times 100 \right] \quad (3)$$

where A_{sample} is the absorbance of DPPH* solution containing the film sample and A_{blank} is the absorbance of DPPH* solution. For each film, three replicates were performed.

2.2.11 UV-Vis spectroscopy and transparency determination

UV-Vis transmittance spectra were acquired on a UV-1650 spectrophotometer (Model PC, Shimadzu, Kyoto, Japan) at $\lambda = 190 - 800$ nm. Three replicates were performed for each film. Film transparency was calculated using Eq. 4 [206]:

$$\text{Transparency} = \frac{A_{600}}{x} \quad (4)$$

where A_{600} is the absorbance at 600 nm and x is the film thickness (mm). Film thickness was measured with a digital micrometer (Mitutoyo Corp., Kanogawa, Japan) to the nearest 0.001 mm.

2.2.12 Contact angle measurements

Contact angle measurements were conducted with CAM 101 Optical Contact Angle Meter (KSV Instruments, Finland) equipped with a CCD KSV-5000 digital camera. For each measurement, 5 μL of ultrapure water was dropped on the film surface and 100 images were automatically recorded within an experimental time of 60 s using the KSV CAM2008 software. Contact angle determinations were performed with 5 replicates as per ASTM D5725-99 (2008).

2.2.13 Tensile tests

The mechanical properties were measured according to ASTM D882-09 (2009). Film specimens were prepared and equilibrated at 23 ± 1 °C and $50 \pm 5\%$ RH for 48 h. The tests were carried out on an Instron Universal Testing Machine (model 5569, Instron Corp., USA) equipped with a 100 N load cell. The specimens were stretched at a crosshead speed of 10 mm/min with clamps

initially separated by 100 mm. Tensile strength and elongation at break were calculated from the stress-strain curves. At least five specimens of each film were tested.

2.2.14 Puncture test

The puncture test was performed according to EN 14777 (2005). The films were cut into a tape of 20 mm by at least 250 mm and perforated to the breaking point using a Multitest-xt Mecmesin machine (Mecmesin, UK) with a round-ended stainless-steel plunger 0.88 mm in diameter at a crosshead speed of 10 mm/min and a 12 N load cell. All determinations were done at least five replicates.

2.2.15 Water vapor permeability and moisture content determination

Water vapor permeability (WVP) was determined as per ASTM E-96-01. Briefly, the preconditioned film sample was used to seal an aluminum permeation cup (28 mm in internal diameter) containing dried calcium chloride. The cup was kept in a controlled chamber at 23 ± 1 °C and $50 \pm 5\%$ RH and weighed every 4 h until 7 days. For each film, three replicates were performed. The WVP [(g mm)/m² h kPa)] was determined using Eq. 5:

$$WVP = \frac{WVTR \times L}{S \Delta P} \quad (5)$$

where WVTR is the water vapor transmission rate (g/h) obtained as the slope of the mass vs time curve, S is the effective film area; L is the film thickness (mm), and ΔP is the difference of partial pressure (kPa) across the film.

The moisture absorption of the films was analyzed using the method described by Zhuang et al. (2017) [15] with slight modifications. Rectangular (20 mm x 10 mm) film specimens were conditioned at 24 °C and $50 \pm 5\%$ RH for 2 days until achieving constant weight (m_i). The samples were transferred to desiccators at $90\% \pm 5\%$ RH (supersaturated CuSO₄.5H₂O solution) at 24 °C for 2 days and then they were gently blotted and weighed (m_f). The moisture

absorption was calculated using Eq. 6. Three measurements were done for each film.

$$\text{Moisture absorption}(\%) = \frac{m_f}{m_i} \times 100 \quad (6)$$

2.2.16 Antimicrobial tests

The bacterial strains to evaluate the effectiveness of CNCs- and TA-loaded solutions were *Staphylococcus aureus* and *Escherichia coli*, which are foodborne pathogens [278,279]. The inoculum cultures were prepared inoculating a selected single colony in 15 mL of Muller-Hinton Broth medium (MHB), followed by overnight incubation at 35 °C. The optical densities at 625 nm were measured by UV-Vis absorption spectroscopy and compared with the turbidity of a 0.5 McFarland standard at the same wavelength, equivalent to 1.5×10^8 colony forming units per mL (CFU/mL). The overnight cultures were diluted in MHB until reaching 10^6 CFU/mL. The antimicrobial activity of the CNCs and TA suspensions was assessed by determining the minimum inhibitory concentration (MIC) in a 96 flat-bottomed-well tissue culture microplate. Briefly, 100 µL of sterile Mueller Hinton were added to all wells. In the first column, the wells were filled with 50 µL of CNCs (50 mg/ml) and TA (50 mg/ml) suspensions. Then, 50 µL of each antimicrobial substance were serially transferred from the well to the corresponding wells. Then, 50 µL of the culture suspension were added to all wells. Positive and negative controls (streptomycin and culture medium – data not shown) were included in each assay plate. Afterward, the inoculated plates were incubated in a wet chamber for 24 h at 35 °C and then chlorinated with 50 µL of 2,3,5-Triphenyltetrazolium chloride (0.1%). The lowest sample concentration with an inhibition effect on microbial growth was considered as the MIC for each tested microorganism.

The antibacterial activity of the film samples Gel, G-TA, G-CNC6, and G-TA-CNC6 was assessed by the disk diffusion method using the pathogenic microorganisms *Staphylococcus aureus* and *Escherichia coli*, as model Gram-positive and Gram-negative bacteria, respectively. Briefly, the bacteria were cultured in Muller-Hinton Broth medium (MHB) and incubated overnight at 35 °C.

The ensuing inoculum of each bacterium was diluted in MHB to 1×10^6 CFU/mL (turbidity = 0.5, McFarland barium sulfate standard), and further spread (100 μ L) over solid Muller-Hinton Agar (MHA) Petri dishes. Dried and sterile film sample disks (10 mm) were placed onto the inoculated Petri dishes and incubated overnight at 35 °C for optimum bacterial growth. The antibacterial activity was investigated by the presence of inhibition zones (colony-free area) surrounding the film disks.

2.2.17 Statistical analysis

The results were expressed as mean value \pm standard deviation and were subjected to analysis of variance (ANOVA). The mean values were compared using the Tukey's test at a confidence level of 95% ($p < 0.05$).

2.3. Results and discussion

2.3.1 Cellulose nanocrystals characterization

TEM revealed that the CNCs used in this work presented needle-like morphology with average length (L) and diameter (D) of 108 ± 33 nm and 3.8 ± 0.9 nm, respectively, resulting in an aspect ratio (L/D) of around 28.4 (Figure 4. 17a). These values were in accordance with Reid, Villalobos, & Cranston, (2017). The L/D value can be used to estimate the critical CNCs volume fraction required to achieve the CNCs percolation network (percolation threshold) using the equation $\phi_v = 0.7/(L/D)$ Favier et al. (1997) [234]. According to the experimental L/D, the calculated volume fraction was 2.5 % (v/v), which corresponds to 4 wt%.

The XRD pattern of CNCs exhibited typical diffraction peaks at around 16.5° , 22.5° , and 34.5° of 2θ , assigned to the planes (110), (200), and (004), respectively, representing the cellulose I polymorph (Figure 4. 17b) [13]. The crystallinity index was 82%. This result was in agreement with Hu et al. (2017) [299].

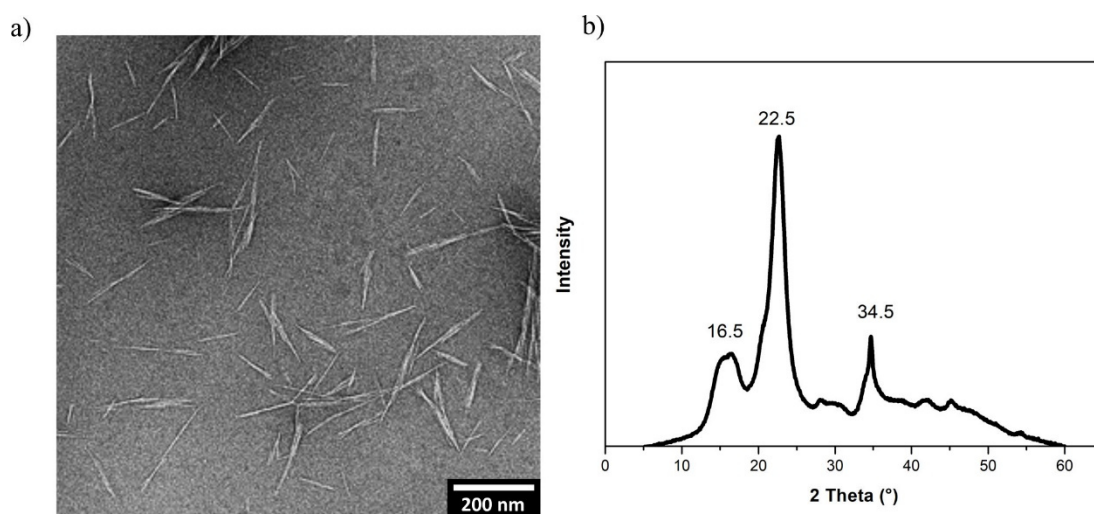


Figure 4. 17 - (a) TEM micrograph and (b) XRD spectra of CNCs.

2.3.2 Gelatin, tannic acid, and CNCs interactions

The QCM-D experiments allowed us to predict the interactions between the film components Figure 4.18. As reported by Rodahl et al (1995) [300], the change in resonance frequency is related to the mass added to the crystal, and thus adsorption or desorption of material induces a frequency shift. From the frequency and dissipation data, it can be suggested that TA adsorbed weakly to the CNCs surface (Figure 4.18a). This minimal adsorption is depicted as a minor decrease in frequency (-8 Hz) along with a minor increase in the dissipation when TA is injected over the CNCs-coated sensor. However, this interaction was found to be reversible since the water rinse brought the frequency back to the baseline, indicating that TA was washed off the sensor surface. This is in contrast to past studies [299,301] that have shown that TA can modify the nanocellulose surface by forming a “primer” layer. However, the interaction/reaction between components was promoted through conditions that allowed for oxidative processes to occur, and by increasing the pH, which is different from the neutral pH and closed flow cell conditions used herein.

Unlike the gelatin-TA interaction, the gelatin-CNCs interaction was seen to be strong (Figure 4.18a-c). with a normalized decrease in frequency of about -500 Hz. This was seen most directly when the gelatin FFS flowed over the neat CNCs surface (Figure 4.18b). This was also apparent if the gelatin adsorption

step came after the TA or glycerol injection (since these two components do not bind irreversibly to CNCs). The large frequency change after gelatin injection and the lack of frequency change after the water rinse supports the interactions between cellulose and gelatin reported previously [17]. The largest frequency shifts were seen for TA adsorbing to gelatin (-1900 Hz) (Figure 4.18b,c). The frequency shift was larger when gelatin was adsorbed to the CNCs surface prior to TA, in comparison to when TA was added first to CNCs followed by gelatin. The adsorption of TA to gelatin may be explained by the physical interaction and/or cross-linking reaction that occurs between the amine groups of gelatin chains and the catechol groups of TA [117]. This large frequency shift was accompanied by a spike in dissipation upon injection of TA, indicating that the TA-gelatin interaction results in a “soft” binding and, consequently, some TA molecules are washed off during the rinsing step (Figure 4.18b,c).

To further investigate the nature of the cross-linking between TA and gelatin, a longer water rinsing step followed by CNCs injection was tested (Figure 4.18d). It was observed that CNCs do not adsorb onto the outer cross-linked gelatin-TA layer. The CNCs injection step was likely to continue the rinsing step, the same trend of slightly increasing frequency occurred during water rinsing and CNCs flow. The QCM-D data showed that glycerol does not adsorb to any of the components (i.e., no decrease in frequency was observed upon glycerol injection), regardless of the previous layer adsorbed to the sensor. Thus, glycerol is most likely acting as a chemically inert plasticizer in the film.

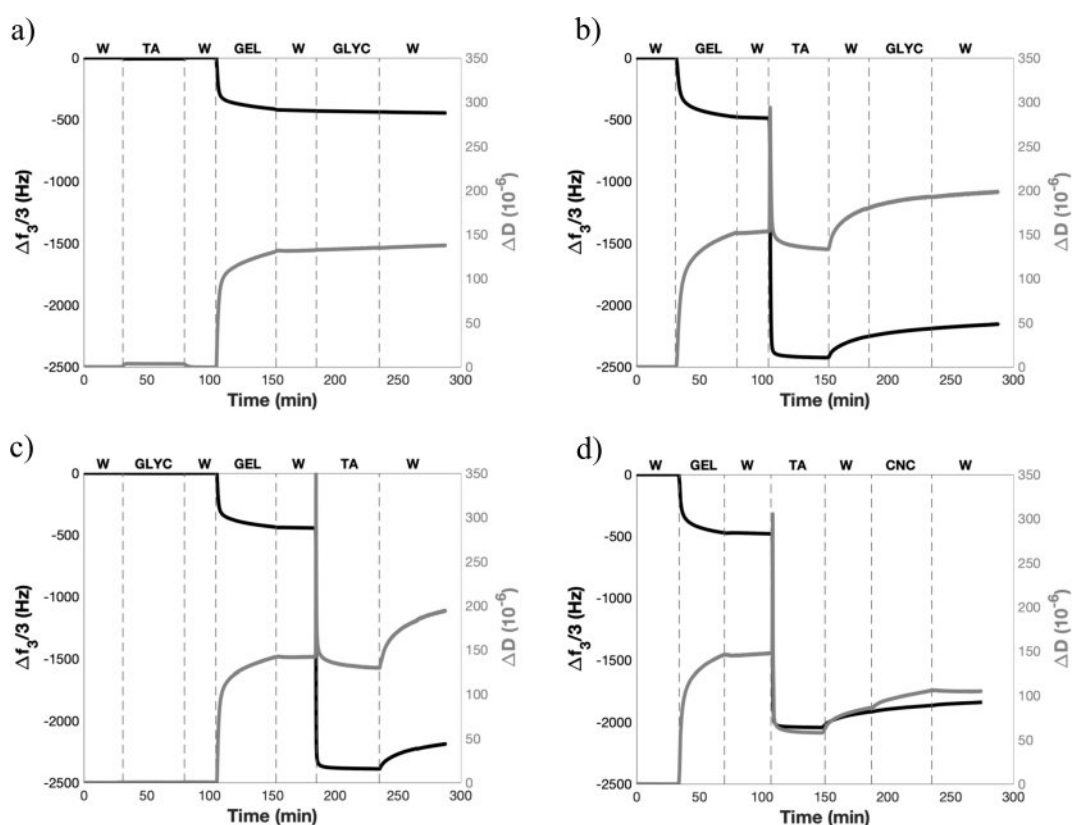


Figure 4.18 - (a-d) Normalized third overtone frequency (black) and dissipation (gray) data versus time from QCM-D analysis of CNCs-coated silica sensors exposed to three different injection orders of tannic acid (TA), gelatin (GEL), and glycerol (GLYC) with water (W) rinsing steps in between each injection step

The storage modulus (G') and loss modulus (G'') of the gelatin-based FFS were monitored by heating and cooling scans. Representative G' , G'' vs Temperature curves are shown in Figure 4.19. Cooling or heating of gelatin can result in a geometric point where G' and G'' are in equilibrium ($G' = G''$). This crossover point detected under cooling and heating is defined as gelling ($T_{\text{sol-gel}}$) and melting ($T_{\text{gel-sol}}$) points of gelatin, respectively [302]. The $T_{\text{sol-gel}}$ and $T_{\text{gel-sol}}$ of the FFS are shown in Table 4.3. As expected, the transition temperatures increased with the addition of CNCs. This tendency was more pronounced for the G-TA-CNC6 FFS, which did not show crossover point on the cooling or heating curves (Figure 4.19a,b), behaved as a viscoelastic solid ($G' > G''$), indicating the existence of an infinite connected network formed by well-dispersed CNCs that interact with each other by hydrogen bonds [220]. These results suggest that

percolation occurred with 6.0 wt% CNCs, above the percolation threshold calculated (4.0 wt% CNCs), which also is in accordance with previous studies on CNCs-based systems [219].

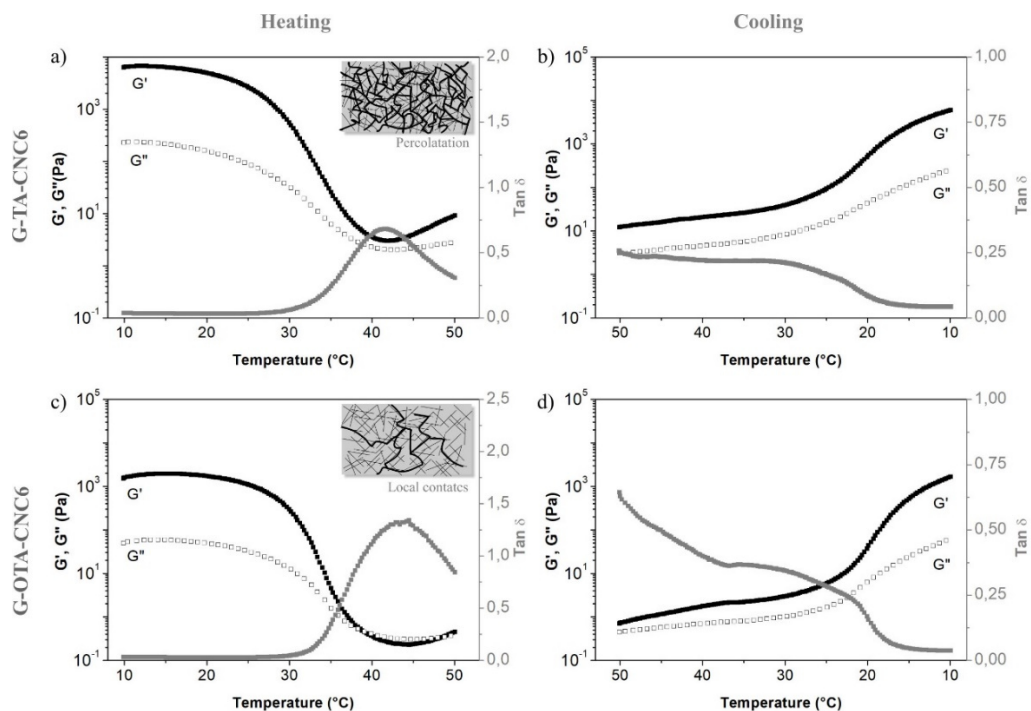


Figure 4.19 - Storage modulus and loss modulus vs. temperature curves of (a), (b) G-TA-CNC6, and (c), (d) G-OTA-CNC6 FFS under heating and cooling scans.

Table 4.3 - Transitions temperatures for the gelatin-based FFS with TA and CNCs.

Film-forming solution	Transitions temperatures	
	Cooling $T_{\text{sol-gel}}$ (°C)	Heating $T_{\text{gel-sol}}$ (°C)
Gel	22.7	34.5
G-TA	22.4	32.1
G-TA-CNC4	-	38.0
G-TA-CNC6	-	-
G-OTA-CNC6	-	38.9

Nevertheless, the $T_{\text{gel-sol}}$ was observed for the G-OTA-CNC6 FFS (Figure 4.19c), indicating that the addition of oxidized TA (OTA) disrupted the hydrogen bonds in the CNCs network. This is in line with the oscillatory frequency measurements and $\tan \delta$ (G''/G') values shown in (Figure 4.20). The $\tan \delta$ values were < 1 for the G-TA-CNC6 FFS (solid-like behavior) and > 1 to the G-OTA-CNC6 FFS (viscous liquid-like behavior) at low angular frequency. These results suggested that non-covalent interactions from TA molecules seemed to play an important role in the modification of gelatin and are in agreement with Anvari & Chung (2016) [302] who found that fish gelatin/gum arabic systems with non-oxidized TA presented a higher degree of intermolecular connectivities in comparison with those containing OTA.

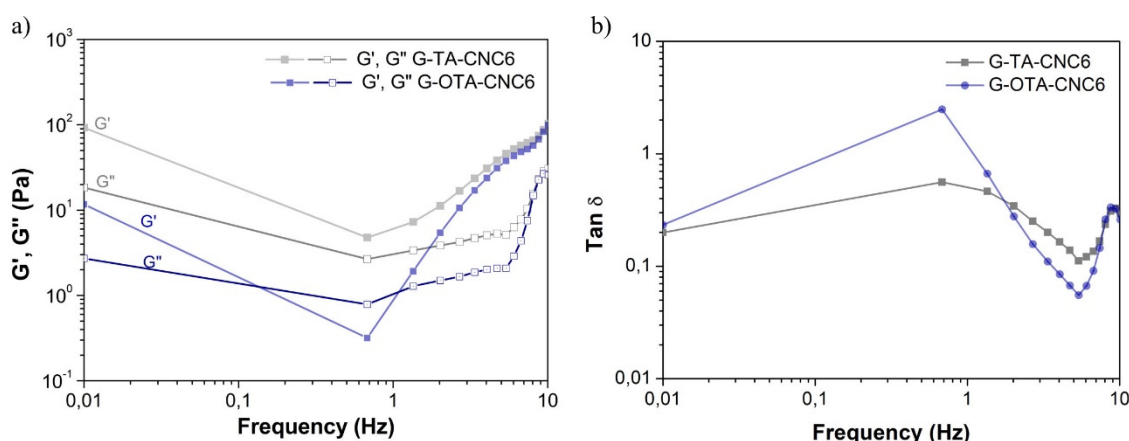


Figure 4.20 - (a) storage (G') and loss (G'') moduli and (b) $\tan \delta$ as a function of frequency sweep at 35 °C of G-TA-CNC6 and G-OTA-CNC6 FFS

The oxidation of tannic acid in the G-OTA-CNC6 FFS was confirmed by the reduction in the free TA content, as shown in Figure 4.21a,b. G-TA-CNC6 FFS showed that 74.1% of the initial amount of TA added to the FFS was released as free TA. By contrast, in the G-OTA-CNC6 FFS this value was reduced to 49.8%. This difference is attributed to the presence of OTA molecules, which reacted irreversibly with nucleophilic groups of gelatin by covalent bonds. This is in line with the color change toward dark brown on the G-OTA-CNC6 FFS and its film, compared with its counterparts by the addition of non-oxidized TA (G-TA-CNC6) as shown in Figure 4.21c,d. This color darkening is a characteristic of

covalent linkage between polyphenols and protein, as demonstrated for chitosan films crosslinked with tannic acid [303].

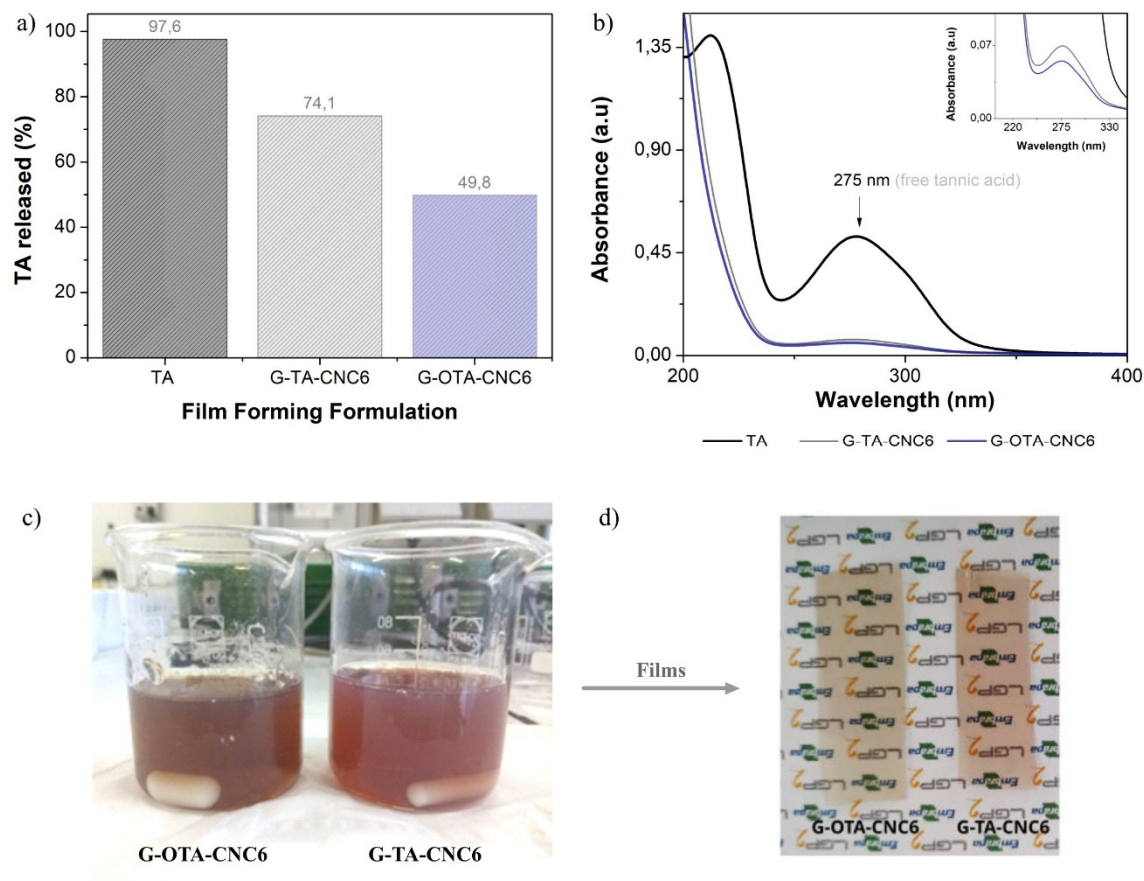


Figure 4.21 - (a) Free TA released from FFS and (b) UV-Vis spectra of FFS and photography of the (c) G-OTA-CNC6 and G-TA-CNC6 FFS, and (d) G-OTA-CNC6 and G-TA-CNC6 films.

The addition of OTA also decreased considerably the viscosity of the gelatin/CNCs FFS, even at the CNCs content above the CNCs percolation threshold (G-OTA-CNC6), as shown in Table 4.4 and Figure 4.22. The oxidation of TA molecules led to the formation of quinones. These molecules may have reacted with amino or sulfhydryl groups of gelatin to form covalent C-N or C-S bonds [304], reducing the hydrogen interaction of CNCs with gelatin and tannic acid, and as a result, decreasing the FFS viscosity. The highest viscosity was found to G-TA-CNC6 FFS, which increased by a factor of 180 and 4 compared to the G-TA and G-OTA-CNC6 FFS, respectively. Sun et al. (2018) [305]

observed similar behavior for gelatin-encapsulated tea polyphenols dispersion added with sulfated CNCs, which exhibited a positive effect on viscosity, increasing from 67 mPa s to 122 mPa s. This is in agreement with the formation of a percolation CNCs network, as previously discussed, which can result in high resistance to flow. The lower viscosity was found to G-TA FFS, which could be attributed to the plasticizing effect of TA at high concentrations [306].

Besides, all the FFS exhibited a shear-thinning behavior ($n < 1$), and the non-Newtonian index (n) decreased and the consistency coefficient (k) increased upon the addition of CNCs. This means that the viscosity is more dependent on the shear rate [217] and gelatin-based films became more viscous. For all the samples, r^2 was greater than 0.99, confirming that the Power Law model was very suitable to describe the rheological property of the gelatin/CNCs FFS containing TA and OTA.

Table 4.4 - Apparent viscosity and rheological parameters of gelatin-based FFS calculated by the Power Law.

Film-forming solution	Rheological parameters and transitions temperatures			
	Viscosity (mPa s) at 1 s ⁻¹	n	k (mPa s ⁿ)	r ²
Gel	10.9	0.90	31.1	0.9930
G-TA	9.2	0.94	7.6	0.9987
G-TA-CNC4	288	0.58	288.3	0.9995
G-TA-CNC6	1690	0.32	1735.3	0.9905
G-OTA-CNC6	334	0.59	338.1	0.9994

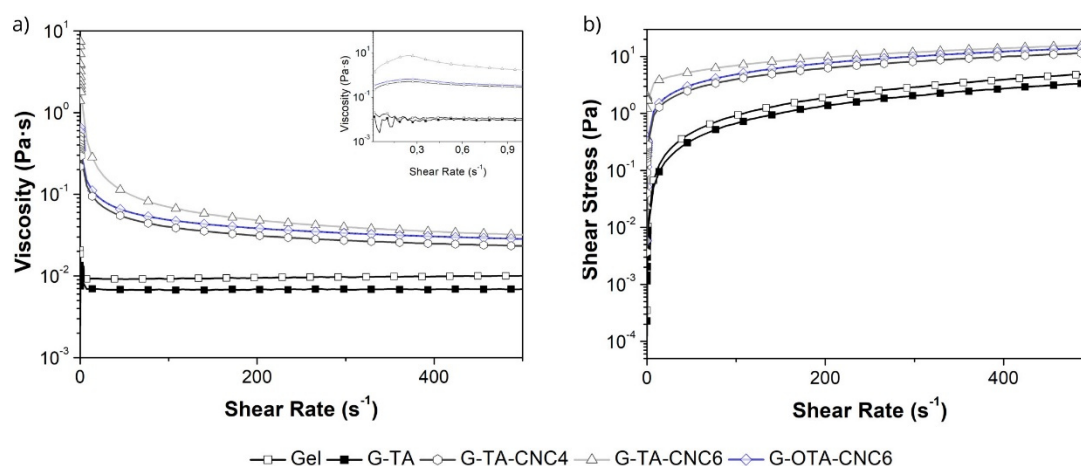


Figure 4.22 - (a) Apparent viscosity and (b) shear stress as a function of shear rate of the gelatin-based FFS at 35 °C.

2.3.3 Crosslinking degree in the gelatin-based films with TA or OTA

The amount of free TA released from the gelatin-based films was calculated for each washing cycle using a concentration curve that correlates concentration with absorbance (Figure 4.23a). Finally, the crosslinking degree was estimated by the difference between the initial amount of TA added to the FFS and the amount extracted in the washing water of each film. The amount of TA released from all the film samples is shown in Figure 4.23b. The amount of crosslinked TA in the G-TA film was around 45% and decreased to 36% when the CNCs were added at 6 wt% to the gelatin-TA FFS, indicating that the G-TA-CNC6 film had a higher free TA content (not covalently bonded to gelatin). This was probably because hydrogen bonding and electrostatic interactions between sulfate groups of CNCs and the cationic amine groups of gelatin decreased the gelatin-TA interactions, as previously observed for CNCs and chitosan [307,308].

The crosslinking degree in the G-TA-CNC6 films was lower than the previous results. Picchio et al. (2018) [298] found that 97% of phenolic compounds were crosslinked to casein at pH 9. In this case, the alkaline conditions favored the TA oxidation and crosslinking with proteins. The G-OTA-CNC6 film showed 53% TA crosslinked, due to the oxidation of TA molecules to quinones, as previously mentioned, which favors the crosslinking reaction between quinones and amino acid groups [117,165].

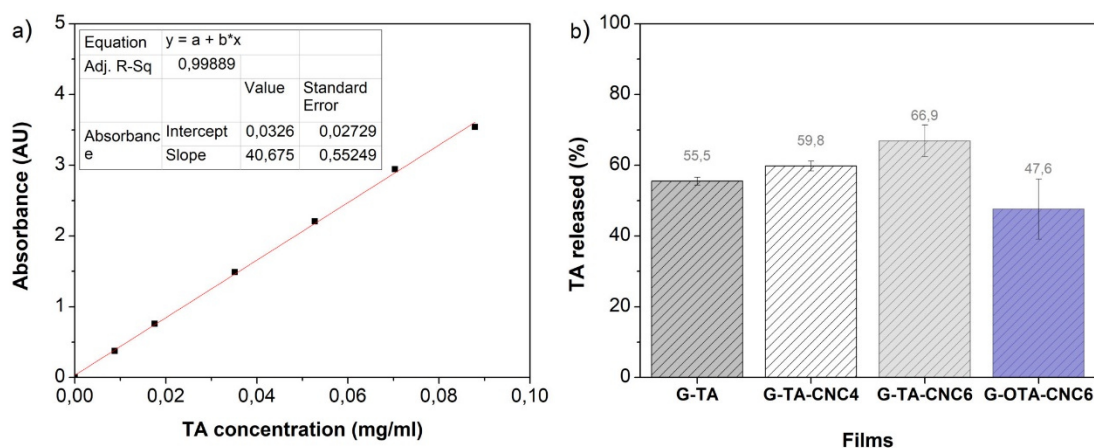


Figure 4.23 - (a) Calibration curve of TA in water and (b) free TA extracted from gelatin-based films.

2.3.4 Viscoelastic behavior of the gelatin-based films

Figure 4.24 shows the storage modulus (G') and loss modulus (G'') of the Gel, G-TA G-TA-CNC6, and G-OTA-CNC6 films at room temperature. It can be observed that the G'' component was considerably smaller than G' , exhibiting the formation of an elastic network. Besides, there was a significant increase in the G' of chemically crosslinked TA in the G-TA, G-TA-CNC6, and G-OTA-CNC6 films, compared to the physical Gel film. This result confirms that gelatin was effectively crosslinked by TA. Furthermore, both G' and G'' exhibited a plateau over all the frequency range analyzed, which is indicative of a stable crosslinked network. Similar results were observed for gelatin films crosslinked with oxidized CNCs [309]. The highest G' was found for the G-TA-CNC6 films, which increased by a factor of 15 to G-OTA-CNC6 films. This is most likely due to the decrease in the crosslinking degree between the gelatin chains and TA molecules in the G-TA-CNC6 films, which favored the non-covalent interactions between the CNCs, gelatin matrix, and TA. corroborating with the results from the rheological analysis (Table 4.4 and Figure 4.19). This also indicates that a higher degree of non-covalent intermolecular connectivities led to a significantly higher mechanical stability to the gelatin films than the covalently crosslinked films with OTA (G-OTA-CNC6).

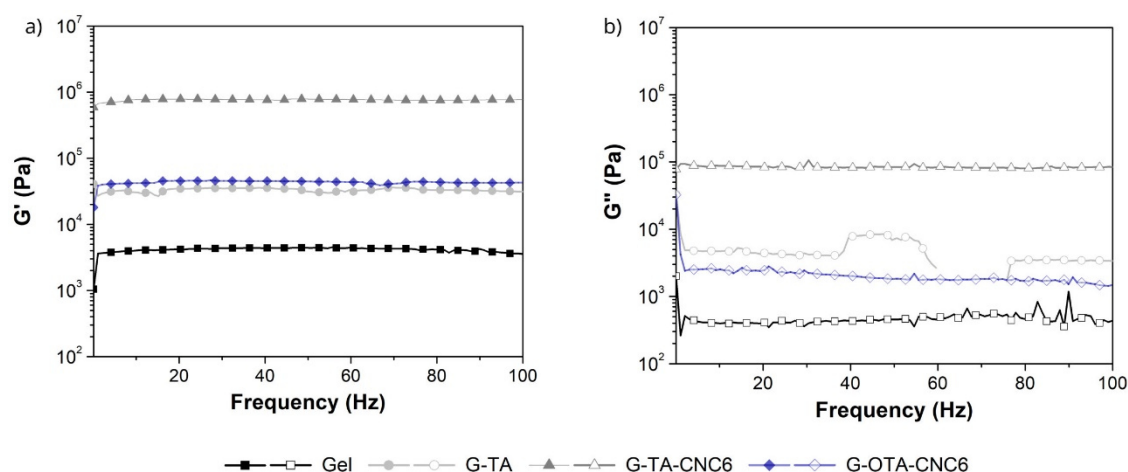


Figure 4.24 - (a) Storage and (b) loss modulus of the gelatin-based films with TA or OTA.

2.3.5 Morphological characterizations of gelatin-based films with TA or OTA

The microstructure of the gelatin/CNCs film with TA or OTA was examined by SEM. To further assess the effect of the TA crosslinking and CNCs percolation network on the stability of the gelatin matrix, the samples were also characterized after swelling in water for 24 °C at room temperature. Figure 4.25 shows the SEM images of the fractured cross-sectional surface of the films before and after swelling for 24h in water. The Gel film (Figure 4.25a) presented a homogenous and smooth surface with good structural integrity, before and after swelling. By contrast, the G-TA film before swelling (Figure 4.25b) showed an irregular and compact surface, with particulate-like structure without any phase separation. [303] also found a similar morphology for TA-crosslinked chitosan films. Nevertheless, the swollen G-TA film presented an open network structure with interconnected pores of regular sizes. Similar findings were reported by Bertolo et al. (2020) [310], who attributed this morphology to the chemical protein/phenolic crosslinking, which offers more intermolecular association and junction points to the film structure.

The G-TA-CNC6 film (Figure 4.25c) had a more regular and compact surface before swelling, and the related swollen film had a denser structure than that of G-TA, with decreased interlayer space and low porosity. This is due to the greater number of covalent and non-covalent bonding, which is supported by the

higher viscoelastic modulus observed for the G-TA-CNC6 film (Figure 4.24). However, the addition of OTA, consequently, increased the crosslinking degree and decreased the hydrogen bonding the G-OTA-CNC6 film (Figure 4.25d), which affected the swollen films, which presented an open network with irregular shape and large pores and discontinuous zones, compared to the G-TA and G-TA-CNC6 films.

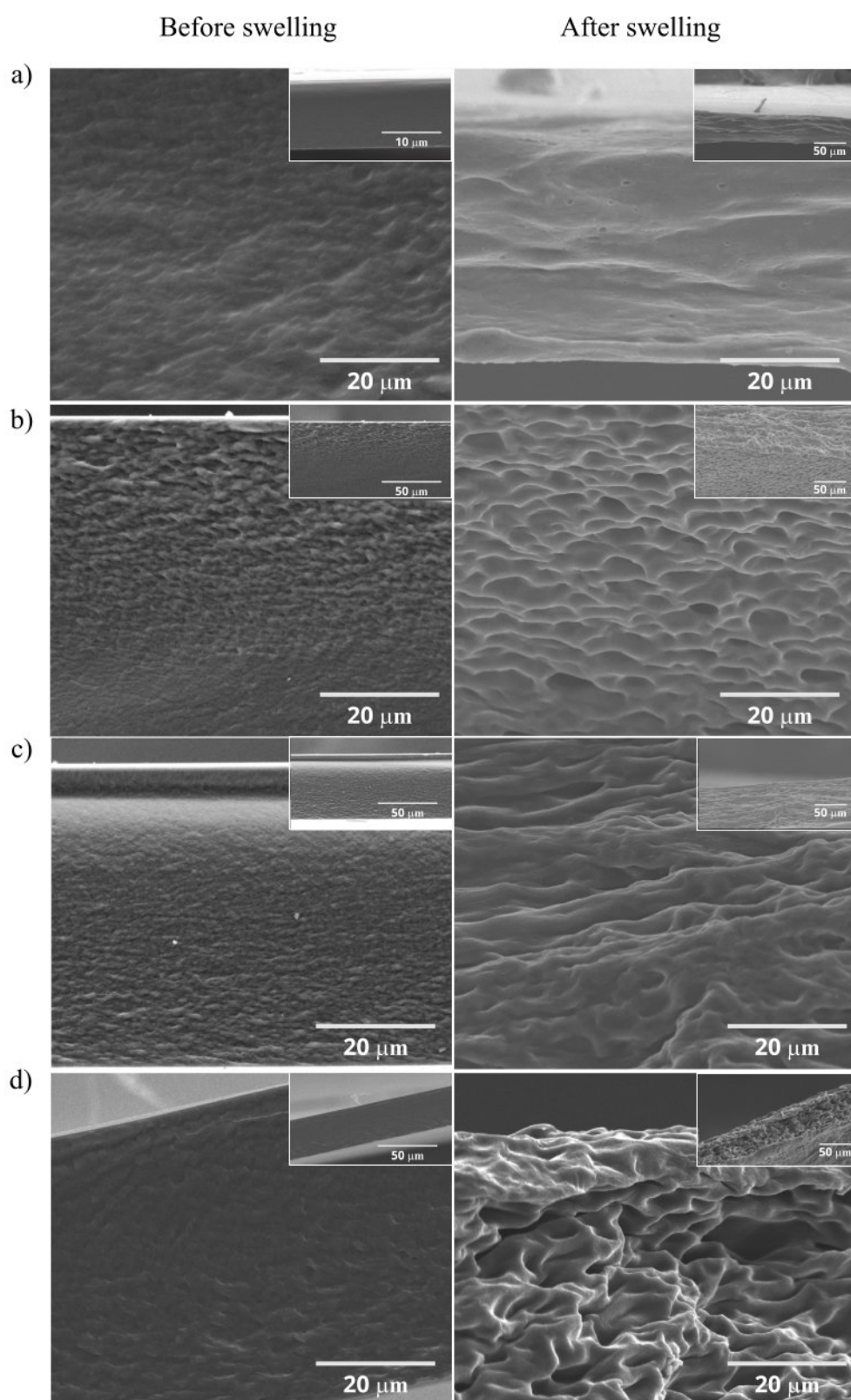


Figure 4.25 - SEM images of cross-section surface of (a) Gel, (b) G-TA (c) G-TA-CNC6, and (e) G-OTA-CNC6 films before and after swelling in water for 24. The low-magnified view of the film is shown as an insert.

2.3.6 Antioxidant activity of gelatin-based films with TA or OTA

The free radical chain reaction is extensively accepted as a common mechanism of lipid peroxidation. Assays based upon the use of DPPH^{*} radicals are the most popular spectrophotometric method for the determination of the antioxidant capacity of different samples, such as pure compounds, plant extracts, fruit, vegetables, lignocellulosic agro-waste, etc. [311]. In the DPPH assay, the purple-colored DPPH^{*} is a stable free radical, which is reduced to the yellow non-radical form DPPH-H (diphenyl-picrylhydrazine) by reacting with a hydrogen-donating antioxidant [89] (Figure 4.26a). Antioxidant as TA is a substance that inhibits or delays the free radical chain oxidation by donating hydrogen from hydroxyl groups to form a stable end product, which does not initiate or propagate further oxidation of lipid (Figure 4.26b) [290].

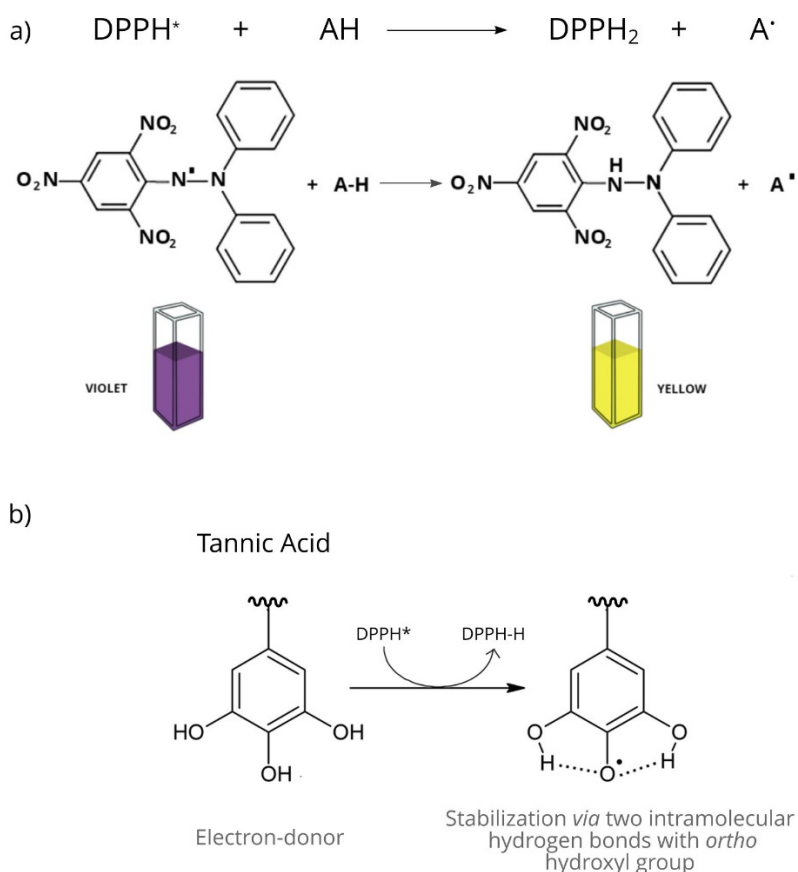


Figure 4.26 - (a) Structure of DPPH and its reduction by an antioxidant agent. (b) Intermolecular stabilization of the TA radical responsible for its efficient antioxidant activity.

Figure 4.27a shows DPPH radical scavenging activities of free TA solution and TA-loaded gelatin films. The antioxidant effect on the DPPH radical scavenging was substantially increased with the addition of CNCs, and the maximum activity was observed for the G-TA-CNC6 film (85%). Choi et al. (2018) [295] reported that an active compound is usually released from a swollen polymeric matrix by hydration, followed by diffusion of the active compound through the expanded polymeric matrix. The gelatin-TA crosslinking through covalent bonds leads to a lower TA release from the crosslinked films, consequently, a lower hydrogen donor ability, which results in a reduction of antioxidant activity when compared with free TA (89%). This was in accordance with Aewsiri, Benjakul, Visessanguan, Wierenga, & Gruppen, (2010) [293] who found similar results for gelatin-TA complexes. Accordingly, the G-TA-CNC4 and G-TA-CNC6 films showed higher antioxidant activity in comparison with the G-OTA-CNC6 (56%) and G-TA (56%) films, which presented the highest crosslinking degrees [305].

Furthermore, the addition of CNCs sustained the enhanced antioxidant capacity of the gelatin films over three months (Figure 4.27b). This trend was similar to that observed by [305], which demonstrated that the antioxidant capacity of gelatin-tea polyphenols (G-TPP) dispersions were dependent on storage time and temperature, and also that the addition of sulfated cellulose nanocrystals (SCNC) resulted in improvement in their antioxidative stabilities. The decrease in the antioxidative stabilities was only 8.9% for SCNC-G-TPP against 17.2% for G-TPP suggesting that there is a strong effect of matrix interactions, and the presence of SCNC increases the physical strength of gelatin-based capsules by hydrogen bonding.

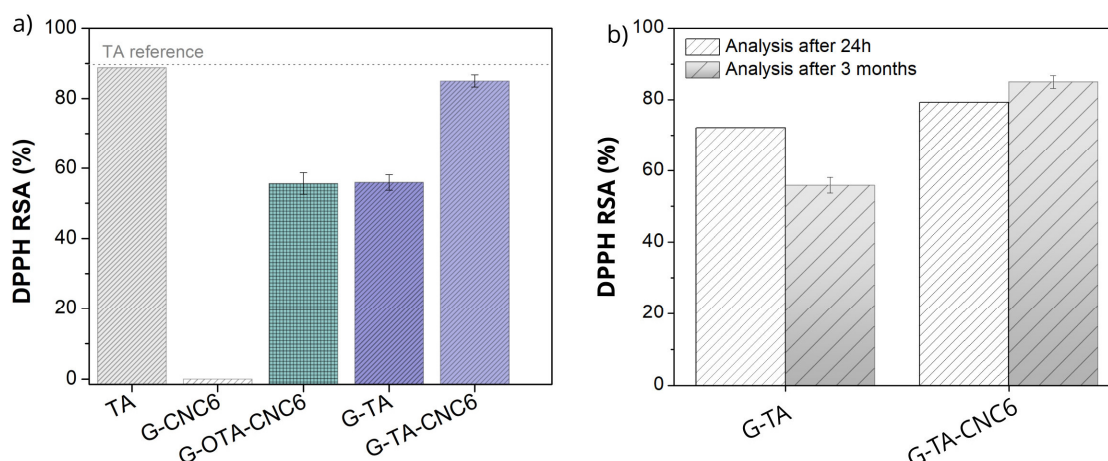


Figure 4.27 - (a) DPPH radical scavenging activity of free TA solution and gelatin-based films with CNCs and TA and (b) stability of gelatin-based films.

Therefore, as the gelatin-based films with non-oxidized TA showed the best antioxidant properties, they were chosen to evaluate the influence of CNCs and TA on the physical properties of the gelatin nanocomposite films, which will be presented below.

2.3.7 Optical properties of gelatin-based films

Photographs of the gelatin-based films are presented in Figure 4.28. All the gelatin films showed good macroscopic homogeneity and continuity, with no cracks or visible aggregates on the surface. Table 4.5 shows the light transmission at different wavelengths and the transparency value of the samples. The Gel film exhibited a high barrier against UVC (200-280 nm), due to the chromophore groups present in the amino acid residues of gelatin chains, such as tyrosine and phenylalanine [96]. After the addition of TA, the UVC transmission became negligible, due to the presence of the TA polyphenol groups, which are well-known as sensitive chromophores concerning the absorption of light at wavelengths below 300 nm. Halim et al. (2018) [109] also found similar results for G-TA films.

The addition of CNCs reduced the UV light transmission through the films. This is attributed to the hydroxyl groups of cellulose, which act as auxochrome groups [98]. As presented in Table 4.5, the gelatin films had improved light barrier

properties, while still showing high transparency after the addition of TA and CNCs. Overall, all the G-TA-CNC films analyzed exhibited excellent barrier properties against UV light (200 – 400 nm) and high transparency to visible light. This is particularly suitable for food applications since blocking UV light is more effective in reducing oxidative reactions than blocking visible light, whereas high transparency to visible light is usually required for food packaging materials.



Figure 4.28 - Photography of gelatin-based films with TA.

Table 4.5 - Light transmission and transparency of gelatin-based films with TA.

Gelatin-based film	Light transmission (%) at different wavelength (nm)							Transparency value (A/mm)
	200	280	350	400	500	600	700	
Gel	0.04	6.9	66.3	81.2	89.0	90.2	90.9	0.5 ± 0.1 ^a
G-TA	-	-	24.2	60.5	76.8	81.4	85.0	0.9 ± 0.1 ^b
G-TA-CNC4	-	-	16.1	57.6	75.5	81.8	86.9	0.9 ± 0.1 ^b
G-TA-CNC6	-	-	22.3	63.2	79.0	84.0	87.6	0.7 ± 0.1 ^{ab}

Mean values followed by the same letter in the same column are not significantly ($p > 0.05$) different according to the Tukey's test.

2.3.8 Contact angle of gelatin-based films

Figure 4.29 displays the dynamic changes in the water contact angle of Gel, G-TA, G-TA-CNC4, and G-TA-CNC6 films. Gelatin has been widely known for its high hydrophilicity [241]. However, unexpectedly, gelatin films presented

water contact angle values higher than 90° over time, which indicates that the surface studied was hydrophobic. According to Białopiotrowicz & Jańczuk (2001) [243], during film drying the randomly coiled gelatin molecules are capable of spontaneously rearranging their hydrophobic parts towards the film-air. Many other researchers have also obtained very high contact angle values on a gelatin surface [203,241,242].

Nevertheless, the addition of TA and 4 wt% CNCs decreased the water contact angle value of G-TA-CNC4 film to $70.6 \pm 2.2^\circ$. This result demonstrated that the film was more hydrophilic due to the OH- group in the TA and CNCs structure. The polarity around the structure could create H-bonding to react with water. However, adding 6 wt% of CNCs to gelatin-TA matrix increased significantly the water contact angle value to $90.0 \pm 5.9^\circ$, which can be attributed to the higher degree of hydrogen bonding between the CNCs, TA, and gelatin, which is in agreement with rheological results. These results suggest the less water-susceptible surface of the G-TA-CNC6 film. Mahajer et al. (2017) [93] observed the same effect on the surface of gelatin films after the addition of agar. The authors attributed the decrease in surface hydrophilicity of the gelatin films due to the formation of intermolecular hydrogen bonds between hydroxyl groups of agar and amino groups in the gelatin chains, reducing their ability to form hydrogen bonds with water molecules.

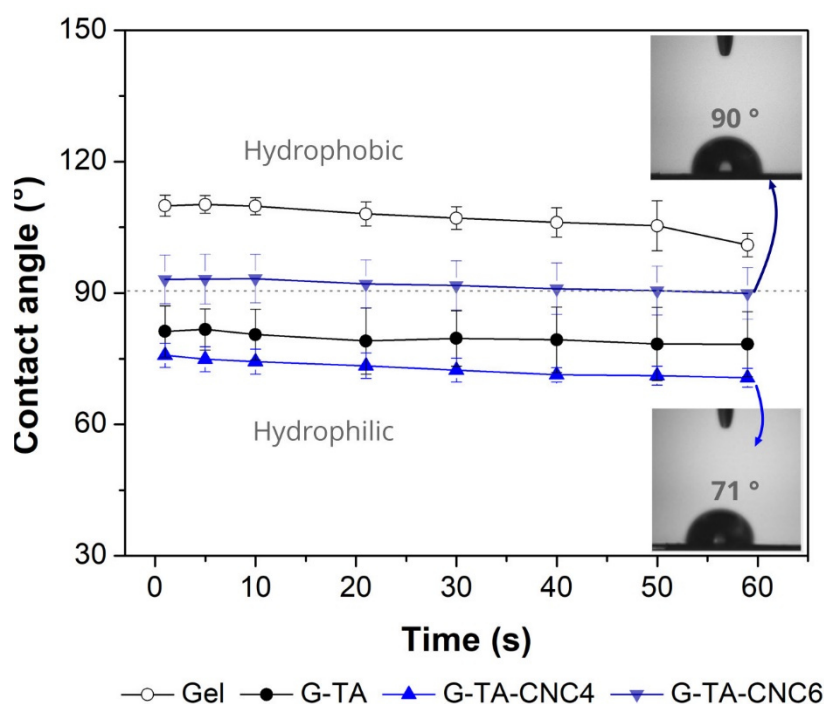


Figure 4.29 - Water contact angle measurements of gelatin-based films.

2.3.9 Mechanical properties of gelatin-based films

Figure 4.30a presents the tensile strength (TS) and elongation at break (EAB) of gelatin-based films. After reaction with TA, the TS value decreased significantly ($p < 0.05$) from 17 MPa to 10 MPa, and the EAB value increases from 13% to 19%, as similarly observed in a previous report [109]. This was due to the plasticizing effect of TA on the gelatin matrix. Nevertheless, the addition of CNCs to the gelatin matrix caused a significant increase ($p < 0.05$) by 79% in TS compared to the G-TA films. This effect is mainly due to the formation of a rigid percolated network with a large amount of hydrogen bond interactions between the hydroxyl groups of CNCs and TA with polar groups of gelatin. In a previous study, the contact percolating network of 7 wt% CNCs had a considerable impact on the mechanical properties of collagen-CNCs nanocomposites [312]. These interactions can also lead to the enhancement of mechanical properties even if the volume fraction of CNCs is low, as demonstrated in Chapter II.

The resistance of the films to be perforated was determined by puncture tests and the results for the gelatin-based films are shown in Figure 4.30b. Comparing the values of the puncture force of the G-TA and G-TA-CNC6 films,

no significant difference ($p > 0.05$) was noticed concerning the addition of CNCs. However, the puncture deformation of the G-TA-CNC films was significantly reduced ($p < 0.05$) by 38% compared with that of the G-TA films, which may be attributed to the CNCs reinforcing effect. These results are in agreement with Nazimi et al. (2017) [313] who found 6.31 N of puncture force for bovine gelatin blended with carboxymethyl cellulose films.

Figure 4.30c compares the tensile properties of synthetic polymeric films [22] with the gelatin-based films developed in this work. As reported by Hosseini et al. (2015) [247], the TS value of conventional standards for food packaging film must be > 3.5 MPa. Therefore, the obtained results suggest that gelatin films can be applied as food packaging materials.

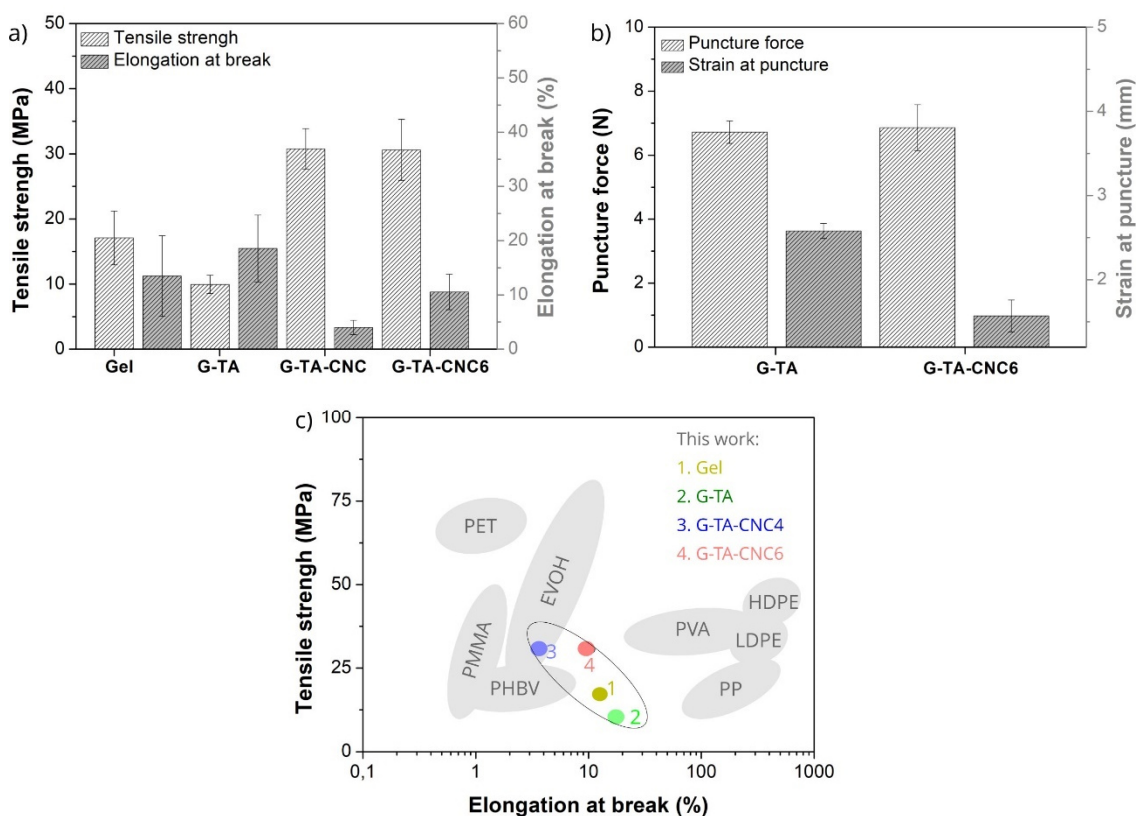


Figure 4.30 - (a) Tensile strength and elongation at break, (b) puncture force and strain at puncture, and (c) tensile properties of gelatin-based films compared with those of synthetic polymeric film (adapted from [22]).

2.3.10 Water barrier properties and water vapor absorption of gelatin-based films

The water vapor barrier is an important property for packaging films since moisture exchanges are a major cause of quality loss in foods, especially those with low water activity. As presented in Figure 4.31 the films containing CNCs had a lower water vapor permeability (WVP) value than the other samples. The gelatin films showed a WVP of 0.18 g mm/(kPa h m²). WVP values in the range of 0.17-2.0 g mm/(kPa h m²) have been reported for gelatin films [87,102,165]. The addition of TA, as a crosslinking agent, significantly decreased ($p < 0.05$) by 28% in WVP of these films, as presented in Figure 4.31. A previous study [314] had also found that incorporating glyoxal and formaldehyde as crosslinkers to bovine gelatin films decreased the WVP of the films by 12% and 22%, respectively, in comparison with pure gelatin films. An advantage of this thesis work is that TA is a nontoxic crosslinker, in contrast to the high toxicity of compounds such as formaldehyde, which may not be tolerable in many applications, including food contact materials. Furthermore, the addition of 4.0 wt% and 6.0 wt% CNCs in the G-TA film significantly reduced ($p < 0.05$) the WVP of the gelatin matrix by 83% and 67% respectively. This phenomenon is the result of interactions between CNCs and gelatin, as well as an increased tortuosity of the pathway for vapor diffusion through the film matrix [239].

The swelling properties of gelatin films were also evaluated from their moisture uptake value at 90% RH. All the films attained equilibrium in 2 days. As shown in Figure 4.31, the moisture content did not change significantly after crosslinking the gelatin films with TA. However, the addition of CNCs to the gelatin matrix decreased the moisture content, which is attributed to the formation of a rigid network, as observed by rheological experiments, which consequently has less ability to uptake water. The moisture uptake value decreased from 136% (for Gel) to 129% (for G-TA-CNC6). These results and WVP are in line with the compact structures observed by SEM (Figure 4.25c).

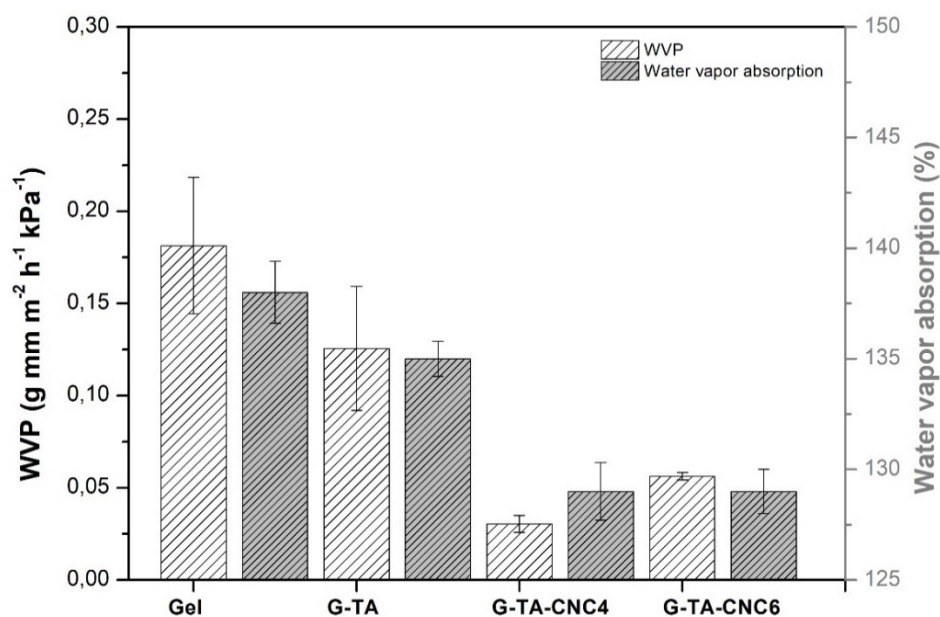


Figure 4.31 - Water vapor permeability and water vapor absorption of gelatin-based films.

2.3.11 Antimicrobial activities of tannic acid and gelatin-based films with TA

The minimum inhibitory concentration (MIC) value was determined as the lowest concentration of TA suspension that inhibited the growth of tested microorganisms. The results in Figure 4.32 show the highest bactericidal effect against *Staphylococcus aureus* (Gram-positive) and *Escherichia coli* (Gram-negative) with the TA suspension. As expected, there was no inhibitory effect for the CNCs suspension. The lowest concentration of TA that inhibited the growth of *S. aureus* was 0.39 mg/mL, whereas *Escherichia coli* inhibition required 0.78 mg/mL. The MICs found for both bacteria are much smaller than the concentration of TA used in the films (30 mg/g). These results are consistent with findings that polyphenols extracted from plants such as tannins have effective antibacterial action against pathogens like *Escherichia coli*, *Staphylococcus aureus*, among others [315]. As reported by Collazo-Bigliardi et al. (2019) [311], the antimicrobial nature of polyphenols is associated with their capacity to inhibit extracellular microbial enzymes, to destabilize the cytoplasmic membrane and to

provoke a deficit of the substrates required for microbial growth, e.g. TA complexation with cell wall protein and membrane disruption metal ions [292].

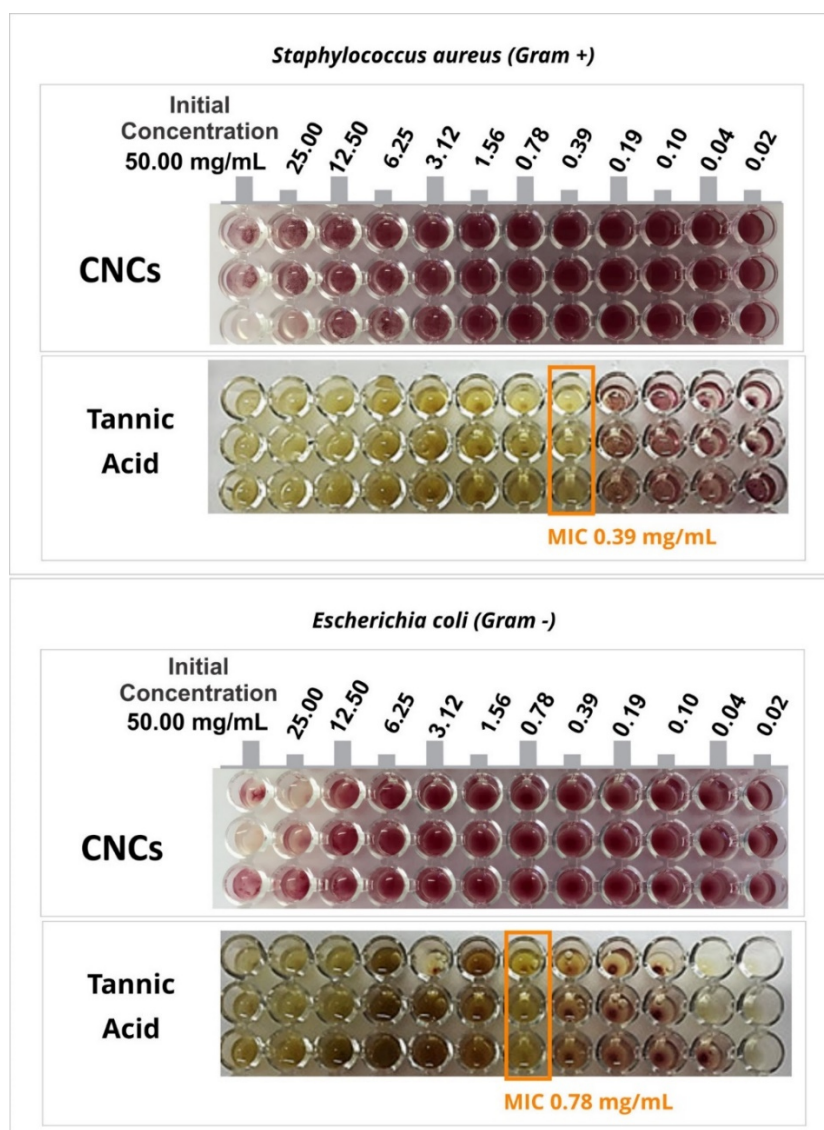


Figure 4.32 - Minimum inhibitory concentration (MIC) of CNCs and TA suspension tested on Gram-positive *Staphylococcus aureus* and Gram-negative *Escherichia coli*.

The antibacterial activity of gelatin-based films was performed by the disk diffusion method (Figure 4.33). The results indicate that the samples containing TA showed antimicrobial activity against *Staphylococcus aureus* *Escherichia coli* bacteria, with a growth inhibition area, observed under the sample (Figure

4.33c,d, g, h, and *insets*). The control films made with pure gelatin or gelatin/CNCs displayed no inhibitory effect, being totally covered by bacteria as well as the area under the film (Figure 4.33a,b, e, and f). According to the Standard SNV 195920-1992 [316], the antibacterial property of a material may be classified as “good” when resulting in an inhibition zone around and under the sample, “sufficient” when the growth inhibition area is only under the sample, and “not sufficient” when the sample, as well as the area under the sample, is totally covered by bacteria. It is important to point out the higher film stability with CNCs (Figure 4.33b, f, d, and h) compared with ones without CNCs (Figure 4.33a, e, c, and g). The last one presented a drained path after the gelatin melting or diffusion, probably due to the similarities between the gelatin and the agar.

This result also reinforces the antimicrobial activity of TA, showing the absence of bacteria across this pathway. Therefore, the antibacterial property of these films can be classified as “sufficient” for antimicrobial packaging applications. However, future quantitative studies may provide more accurate information about the susceptibility of these organisms to the antibacterial action of the film G-TA-CNC6.

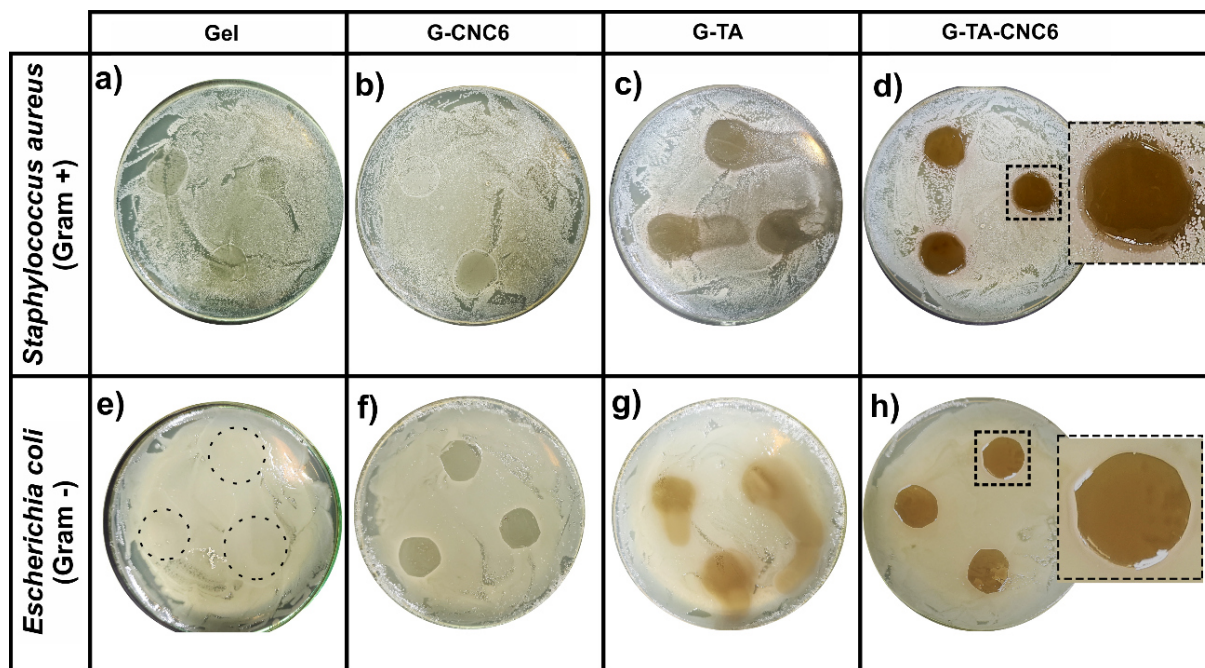


Figure 4.33 - Agar overlay assay of gelatin-based film discs against *S. aureus* and *E. coli*. Inset of the growth inhibition area observed under the sample.

2.4 Conclusion

Plant-derived TA was successfully used as an antioxidant and bactericidal compound in gelatin for achieving multifunctional active packaging. Significant interactions between the components (gelatin, TA, and CNCs) were evidenced and shown to depend on the TA type interactions. The addition of non-oxidized TA favored non-covalent interactions and intermolecular connectives, improving the mechanical stability and increased the antioxidant capacity of the film by 52% compared with gelatin film with OTA. Besides, the addition of 6 wt% CNCs formation of percolate network and resulted in films with denser structure, low porosity, and lower WVP and greater tensile strength compared to the with gelatin-TA films. Gelatin-TA-CNCs films also demonstrated an inhibitory effect against *S. aureus* and *E. coli* growth. For food applications, especially when antioxidant and antimicrobial activity is important, the use of such treatment is the most suitable.

Chapter V

General conclusion and perspectives

General conclusions and perspectives

This Ph.D. work investigated the production and characterization of multifunctional gelatin-cellulose nanocrystals films intended for food packaging. The up-scalability of the gelatin/CNCs films by continuous casting has been developed. Furthermore, active film packaging with antibacterial and antioxidant properties have been produced by bench casting. The axes of our research have been defined following the state of the art as:

- i. Develop an alternative material made from bio-based and biodegradable materials intended for food packaging.
- ii. Convert natural bio-based film production from laboratory to production scale
- iii. Develop novel active film packaging with diverse advanced functionalities such as antimicrobial and antioxidant.

As a conclusion, the results presented in this work have been demonstrated that well-dispersed CNCs into the gelatin matrix act as excellent reinforcing agents and can lead to the formation of a percolating network of CNCs when incorporated into the gelatin matrix. The electrostatic interactions (induced by pH of gelatin FFS) between CNCs and gelatin molecules as well as the drying temperature allowed to produce gelatin/CNCs films with tunable physical properties. Continuous casting processing had been proven to be advantageous when compared to the bench casting. This processing method allowed scaling-up the production of gelatin-based films. The continually casted gelatin films have shown to have exceptionally better performance than gelatin/CNCs films obtained by bench casting. Besides, the CNCs were successfully functionalized with a natural compound (rosin) and used as an antimicrobial nanofiller in gelatin for achieving multifunctional packaging. This study demonstrated how grafting reactions can extend the functionalities of CNCs for use in flexible packaging materials, which otherwise would suffer from limited physical and biological properties. Plant-derived tannic acid was successfully used as an antioxidant and antimicrobial compound in gelatin/CNCs films. This study demonstrated that the

use of oxidized TA hindered the formation of hydrogen bonds between gelatin, tannic acid, and CNCs, which showed to have a greater influence on the physical properties of gelatin/CNCs-TA films. The main results of this Ph.D. work are summarized in Table 1.

Table 1 – main results of this Ph.D. work.

Chapter	Scientific challenges	Key results
II.1	Scale up the production of gelatin-CNCs films	A roll at 12 m/h of gelatin/CNCs films was produced by continuous casting
II.2	Avoid the formation of CNCs aggregates	High dispersion of CNCs was achieved using homogenous CNCs
	Gelatin films show moderate mechanical strength and poor barrier properties against moisture	Gelatin film 4.0 wt% CNCs obtained by continuous casting exhibited high thermal and mechanical properties and its WVP decreased by 50% compared with its counterpart obtained by bench casting.
III.1	Produces gelatin/CNCs with tunable physical properties by controlling the pH and the CNCs content	pH modulated the electrostatic interactions in the CNCs-gelatin pair and physical gelatin/CNCs films
		High CNCs contents at pH3 and pH8 decreased the mechanical properties and increased WVP of films
		Lower WVP of films was attained at pH 3, however, a drastic reduction in their ductility was observed
		Gelatin/CNCs at pH 6 showed a significant increase in mechanical properties and a decrease in WVP at high CNCs content.
IV.1	Active films packaging with antimicrobial properties using a natural agent	Functionalized CNCs with rosin showed antimicrobial activity against <i>S. aureus</i> and <i>E. coli</i> bacteria
		Functionalized CNCs consistently improved the optical, and WVP properties of gelatin films as compared to conventional CNCs
		The antimicrobial activity of rosin in the gelatin films with high r-CNCs contents was demonstrated in a proof of concept test using mozzarella cheese
IV.2	Active films packaging with antioxidant and antimicrobial properties using a natural agent	The addition of non-oxidized tannic acid favored non-covalent interactions and intermolecular connections, improving the mechanical stability and increased the antioxidant capacity of the film by 52% compared with gelatin film with oxidized tannic acid.

Table 1 continued

IV.2	Active films packaging with antioxidant and antimicrobial properties using a natural agent	<p>The addition of 6% CNCs in Gelatin-TA films resulted in a denser structure, low porosity, and lower WVP (67%), and greater tensile strength (79%) compared to the gelatin-TA films.</p> <p>Gelatin-TA-CNCs films also demonstrated an inhibitory effect against <i>S. aureus</i> and <i>E. coli</i> growth.</p>
------	--	--

We believe that our research work provides important contributions to the field of biobased food packaging materials. The results presented here make gelatin-based films with CNCs and functionalized CNCs highly desirable for food packaging applications with aims to replace commercial fossil-based packaging materials that are damaging the environment. For future work, we suggest the following ideas or experiments that could to be tested:

- Evaluation of gelatin/CNCs-based films' biodegradability
Although all components used for film production are known to be biodegradable, biodegradation and composting tests should be carried out for gelatin/CNCs films to prove their effectiveness.
- Improve the elongation of the gelatin-based film
The increase in the elongation of gelatin-based films may expand its applicability to different types of food packaging.
- Expand the use of continuous casting to vegetal proteins
Although gelatin is considered a by-product of the meat industry, a culture of continuous improvement must be adopted to improve sustainability. The use of protein such as soybean can be an alternative to gelatin.
- Scale-up the production of active gelatin films using the parameters set in section 4.1 and 4.2.
- Investigate the infrared radiation effects on the physical properties of active gelatin films.

The use of infrared may especially influence film crosslinking with tannic acid crosslinking agent.

- Produce multilayer gelatin-based films intended for food packaging
Gelatin films have excellent oxygen barrier properties and, in this work. The use of gelatin films to produce multilayered packaging can combine the benefits of gelatin with other layers in terms of enhanced barrier properties, mechanical integrity, and functional properties.

Extended Portuguese Abstract
Resumo Português

Resumo Português

Extended Portuguese Abstract

A crescente produção de plástico levou a uma crise global de eliminação de resíduos. Atualmente, as pesquisas se concentram em solucionar esse problema por meio da obtenção de embalagens biodegradáveis. Biomateriais, incluindo proteínas e polissacarídeos, são os principais recursos naturais empregados para desenvolver filmes biodegradáveis [1].

Gelatina é uma proteína solúvel em água derivada do colágeno, a qual é uma das proteínas animais mais abundantes [68] [71]. Essa proteína está presente na pele, tendões, ossos, cartilagens e na maioria dos órgãos internos dos animais, fornecendo suporte estrutural e mecânico aos tecidos. As cadeias de gelatina são compostas por 18 aminoácidos. Glicina (Gly), prolina (Pro) e hidroxiprolina (Hyp) são os aminoácidos mais dominantes e representam quase dois terços do total de aminoácidos constituintes. A gelatina tem atraído muita atenção como um material plástico alternativo devido à sua abundância, baixo custo, biodegradabilidade, excelentes propriedades de gelificação, capacidade de formar filmes e não toxicidade para aplicações em contato com alimentos.

Os filmes a base de gelatina podem ser feitos de uma variedade de matérias-primas, sendo as mais utilizadas em embalagens de alimentos as derivadas de tecidos suínos [88], peixes [89] e bovinos [90]. As propriedades físico-químicas dos filmes de gelatina dependem da fonte, das condições de produção do filme (concentração, solvente, pH, temperatura, tempo de secagem do filme, etc.) e do tipo e concentração dos aditivos empregados (plastificante, carga de reforço, agentes reticulantes, etc.).

Em geral, os filmes de gelatina são incolores e exibem alta transparência e excelentes propriedades de barreira na região do ultravioleta. Outra grande vantagem da gelatina como material de embalagem é sua excelente barreira contra dióxido de carbono e oxigênio, devido à sua natureza hidrofílica [115]. No entanto, a natureza higroscópica da gelatina também representa a sua principal desvantagem como filmes. Esses filmes são sensíveis à umidade e apresentam

baixas propriedades mecânicas e barreira ao vapor de água em altas umidades relativas [87]. Entretanto, essas desvantagens podem ser superadas pela incorporação de nanopartículas de reforço à matriz de gelatina, como por exemplo, os nanocristais de celulose (CNCs) [3,9–12].

CNCs são domínios cristalinos extraídos de várias fontes naturais, incluindo madeira, plantas, microorganismos e animais que contêm celulose. CNCs apresentam uma combinação adequada de propriedades, como biodegradabilidade, alta razão de aspecto (~ 10-70), baixa densidade (1,5 - 1,6 g/cm³), baixo coeficiente de expansão térmica e transparência [13,138,139]. Além disso, as dimensões bem definidas dos CNCs e sua alta cristalinidade (70-90%) induzem excelentes propriedades mecânicas, como alta rigidez axial (~ 150 GPa), alto módulo de elástico (20-50 GPa) [19] e alta resistência à tração (~ 7 GPa) [16].

Além disso, a superfície dos CNCs pode ser facilmente modificada devido à reatividade dos seus grupos hidroxilas, o que torna os CNCs uma plataforma versátil para diversos tipos de funcionalização de superfícies. Essa característica permite expandir as aplicações específicas dos CNCs, tornando-os excelentes candidatos para desenvolvimento de nanocompósitos de alto desempenho em diversas aplicações [169].

O que concerne ao processamento de filmes poliméricos para embalagens, a maioria dos estudos tem se concentrado em técnicas de processamento por extrusão, injeção ou moldagem por compressão a quente, devido às tecnologias já estabelecidas para polímeros à base de petróleo [23]. No entanto, o processamento utilizando essas técnicas para polímeros naturais como proteínas, tem se mostrado um desafio devido principalmente à instabilidade térmica dessas macromoléculas.

Recentemente, um método de *casting* contínuo foi proposto para a produção de filmes a base de biopolímeros em escala piloto. A produção de filmes por *casting* contínuo é realizada em uma linha de *coating*. Neste processo, as soluções filmogênicas são continuamente espalhadas sobre um substrato móvel, como poliéster ou papel revestido, com uma lâmina cuja altura pode ser ajustada para

controlar a espessura do filme. Após, o substrato revestido com a solução laminada passa por um estágio de pré-secagem com aquecedores infravermelho e em seguida por câmaras de secagem. No final, o filme seco é enrolado em um rolo enquanto ainda está aderido ao substrato [194].

A abordagem de *casting* contínua pode ser considerada uma ampliação do processamento por *casting* em bancada. A principal vantagem do *casting* contínuo consiste no fato deste método requerer tempos de secagem curtos, graças ao uso da radiação infravermelha na fase de pré-secagem, temperaturas muito mais elevadas e intensa circulação de ar. Outras vantagens são o alto controle de espessura do filme, não requer o uso de aditivo de processamento, permite o uso de soluções/dispersões aquosas e possui menor necessidade de espaço e mão de obra. Essas características tornam o *casting* contínuo um processo atraente para a produção em larga escala de filmes a base de polímeros naturais.

Em linha com este contexto, vários objetivos podem ser anunciados para este doutorado:

- i. Investigar os parâmetros reológicos necessários para produzir filmes de gelatina/CNCs em escala piloto usando o método de *casting* contínuo.
- ii. Caracterizar as propriedades morfológicas, térmicas, mecânicas e de barreiras dos filmes de gelatina/CNCs obtidos por *casting* contínuo
- iii. Funcionalizar a superfície dos CNCs com ativos naturais e produzir filmes ativos de gelatina e CNCs funcionalizados.

Para alcançar esses objetivos, foi desenvolvida uma parceria colaborativa durante os quatro anos com especialistas em produção e funcionalização de nanocelulose do Laboratório de Ciência da Celulose e Papel e Artes Gráficas (França) e, especialistas em produção de filmes de origem natural da Embrapa Instrumentação (Brasil). Portanto, este doutorado ocorreu em um contexto dinâmico e interdisciplinar.

Os resultados obtidos neste doutorado foram organizados em quatro capítulos. O **Capítulo I** apresentam uma revisão da literatura que descreve o contexto e os

objetivos deste doutorado, focando no potencial uso de gelatina e CNCs como embalagens sustentáveis. Além disso, é descrito um método de processamento em escala piloto para filmes biodegradáveis de fontes naturais. Conforme mencionado no início deste resumo.

O **capítulo II** descreve os parâmetros reológicos das soluções formadoras de filmes (SFF) necessário para produção de filmes de gelatina/CNCs por *casting* contínuo. O estudo das propriedades reológicas da SFF é de grande importância para a avaliação da capacidade de laminação e determinação da formulação mais adequada para produção de filmes por *casting* contínuo. Todas as soluções analisadas apresentaram comportamento pseudoplástico em função da taxa de cisalhamento aplicada (Figura 1.1). O comportamento pseudoplástico é considerado o mais adequado para produção de filmes por *casting* contínuo, uma vez que as SFF devem apresentar baixa viscosidade sobre cisalhamento, para garantir condições de fluxo apropriadas sob a lâmina, e viscosidades mais elevadas em baixas tensões de cisalhamento geradas imediatamente após a faca de *coating*, para minimizar fluxo indesejado e efeitos de sedimentação.

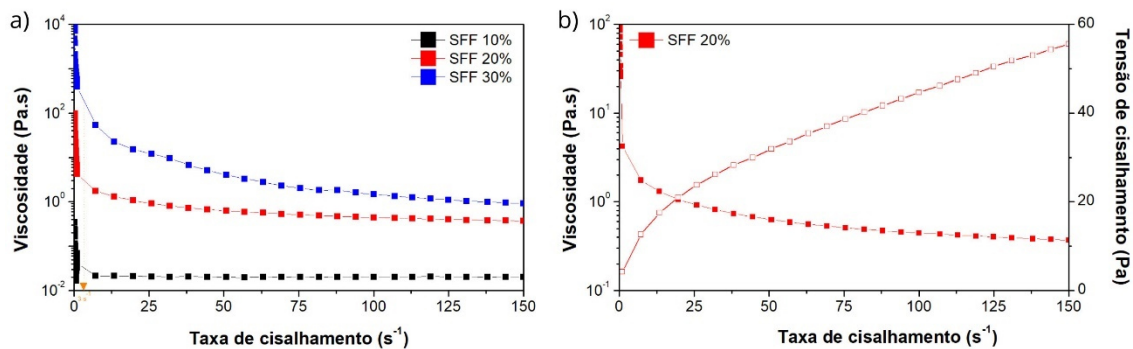


Figura 1.1 - Viscosidade em função da taxa de cisalhamento para (a) SFF com diferentes concentrações de gelatina e (b) viscosidade e tensão de cisalhamento em função taxa de cisalhamento para SFF 20%.

Filmes de gelatina obtidos por *casting* são produzidos geralmente usando-se SFF contendo $\leq 10\%$ em massa de gelatina [166,200,212]. No entanto, para a produção de filmes de gelatinas por *casting* contínuo, esta concentração não foi adequada, pois a suspensão apresentou viscosidade muito baixa (0.4 Pa.s) o

que favoreceu o escoamento da SFF para fora do substrato antes de ser laminada. Já SFF contendo 30% de gelatina apresentou viscosidade muito elevada, não sendo possível formar uma lâmina úmida homogênea, resultando em filmes descontínuos. SFF contendo 20% em massa de gelatina exibiu viscosidade (~ 100 Pa.s) e propriedades de fluxo adequadas e, puderam ser laminadas adequadamente sobre o suporte. Dessa forma, essa foi a formulação selecionada para avaliar a influência dos CNCs nas propriedades físicas dos filmes de gelatina/CNCs obtidos por *casting* contínuo.

A produção de filmes de gelatina/CNCs usando *casting* contínuo foi de 12 m de filme/h. A radiação infravermelha e as altas temperaturas de secagem aplicadas neste método promoveram forte interação intermolecular e intenso colapso estrutural, o que levou à formação de filmes densos. Filmes de gelatina com 4,0% de CNCs obtidos por *casting* contínuo apresentaram redução de 50% na permeabilidade ao vapor de água (PVA), alta resistência à tração (36 MPa) e módulo elástico (1,8 GPa), comparado com o mesmo filme obtido por *casting*. Portanto, o método de *casting* contínuo se mostrou vantajoso quando comparado ao *casting* de bancada, pois permitiu não somente aumentar a escala de produção de filmes à base de gelatina, bem como permitiu melhorar o desempenho desses filmes, sendo uma alternativa viável ao *casting* de bancada.

No **capítulo III** a influência do pH nas propriedades físicas dos filmes de gelatina/CNCs com diferentes concentrações de CNCs é investigada. As interações entre CNCs e gelatina foram estudadas avaliando-se o potencial- ζ de suspensões de gelatina e CNCs em condições ácida (pH 3) e alcalina (pH 8), e no ponto isoelétrico da gelatina (pI, pH 6). Em pH 3 ocorreu atração eletrostática, enquanto em pH 8 favoreceu a repulsão eletrostática no par gelatina-CNCs, aumentando a viscosidade das soluções em ambos os casos. A adição de 0,5% de CNCs em pH 3 e no pI diminuiu em 68% e 39% a PVA dos filmes, respectivamente. Já a adição de 5,0% de CNCs em pH 3 resultou na formação de coacervatos complexos, os quais contribuíram para diminuir as propriedades mecânicas e aumentar a PVA dos filmes.

O aumento do pH acima do pI da gelatina, aumentou notavelmente a formação de estruturas do tipo tripla hélice, o que se verificou ser chave para aumentar em

152% e 56% o módulo elástico e a resistência à tração, respectivamente, em filmes de gelatina com 0,5% de CNCs. Já o aumento da temperatura de secagem desses filmes teve um efeito inverso na formação da hélice tripla e, conseqüentemente, nas suas propriedades físicas. Essas descobertas podem ser exploradas para modular as propriedades físicas de filmes de gelatina com CNCs, de forma a adequá-los para uma variedade de aplicações, incluindo embalagens flexíveis para alimentos.

A primeira parte do **capítulo IV** descreve a funcionalização e caracterização da superfície de CNCs com rosina (r-CNCs) e dos filmes de gelatina/r-CNCs. Filmes de gelatina/r-CNCs (0,5 - 6% r-CNCs) obtidos por *casting*, exibiram transparência e altas propriedades de barreira ao UVA e UVB (mais de 95% para UVB e 59,0% para UVA), que foram superiores à plásticos convencionais utilizados em embalagem. Os filmes gelatina/r-CNCs apresentaram ainda PVA moderada (0,09 g mm/m² h kPa), alta resistência à tração (40 MPa) e módulo elástico (1,9 GPa). A graftização dos CNCs com rosina resultou em uma nanocelulose que inibe o crescimento de *Staphylococcus aureus* e *Escherichia coli*, inclusive quando incorporadas a matriz de gelatina, conforme demonstrado em experimentos de prova conceito para prevenção de deterioração microbiana em amostras de queijo muçarela. Esses resultados sugerem que, a incorporação de baixas quantidades de r-CNCs como agentes ativos em filmes de gelatina, pode ser altamente adequada para a produção de embalagens ativas antimicrobianas.

Finamente, a segunda parte do **Capítulo IV** os efeitos do ácido tânico não oxidado (TA), ácido tânico oxidado (OTA) e CNCs nas propriedades físicas, antioxidantes e antimicrobianas de filmes de gelatina foram investigados. QCM-D e medições reológicas confirmaram a interação da gelatina com TA e a formação de ligações de hidrogênio entre CNCs e gelatina. O efeito de reticulação nos filmes de gelatina com TA diminuiu em 17% em relação os filmes com OTA, resultando em 52% de aumento da capacidade antioxidante do filme. Isso também permitiu que os grupos de gelatina estivessem mais disponíveis para formarem interconectividades com CNCs, produzindo um aumento

substancial na viscosidade (410%) e estabilidade mecânica (G' 1697%) desses filmes.

Além disso, a adição de 6% de CNCs aos filmes de gelatina-TA levou a formação de filmes com estruturas mais densas e com baixas porosidades, conforme revelado por imagens de SEM, e filmes com menor PVA (67%) e maior resistência à tração (79%), em comparação com filme de gelatina com TA. Os filmes gelatina-TA-CNCs também demonstraram um efeito inibitório contra o crescimento de *Staphylococcus aureus* e *Escherichia coli*. Para aplicações em alimentos, principalmente quando a atividade antioxidante e antimicrobiana é importante, o uso desse tratamento é o mais adequado.

A Figura 1.2 - apresenta um resumo esquemático de todas as etapas desenvolvidas nesse trabalho, bem como os resultados mais relevantes encontrados em cada uma delas.

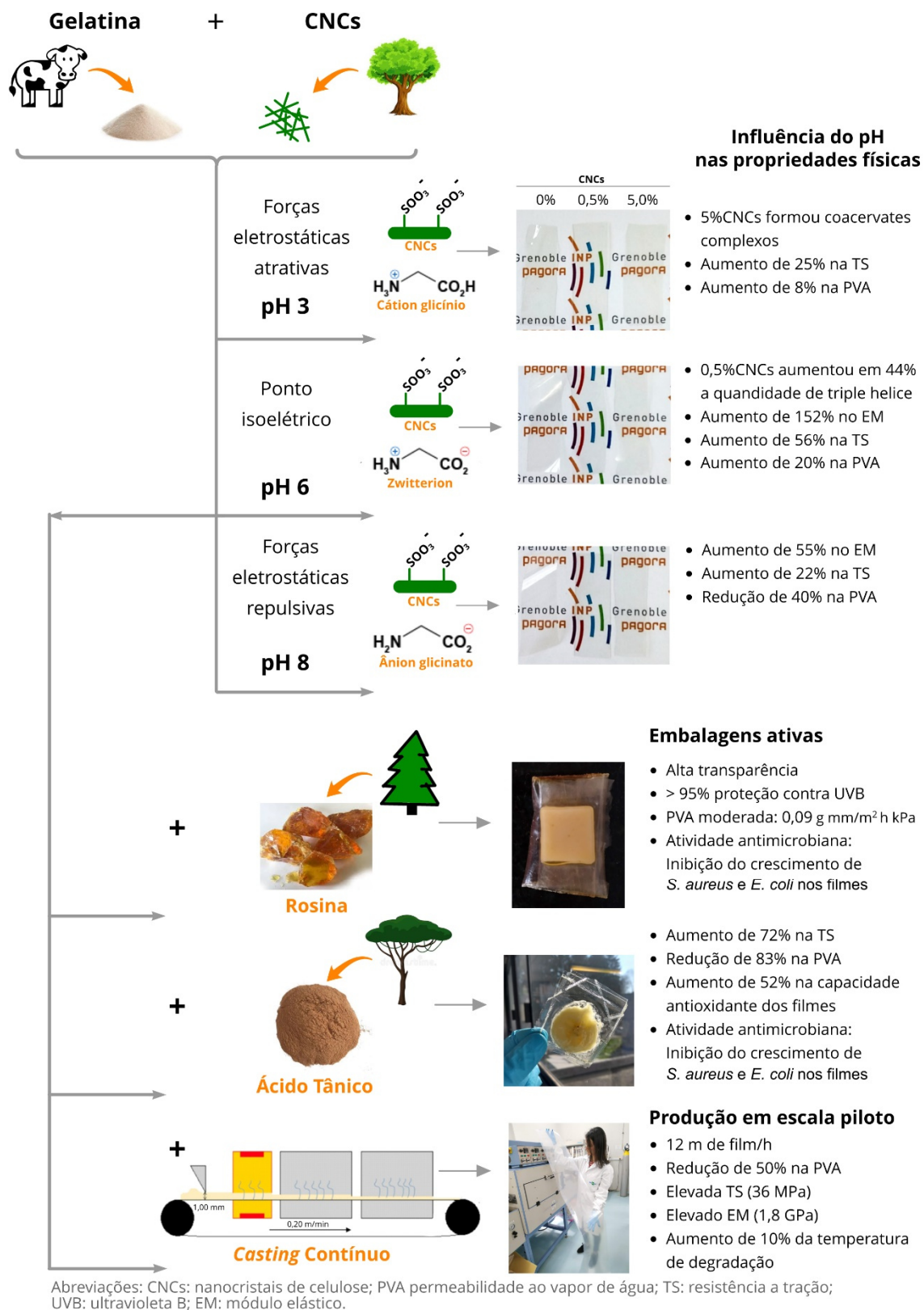


Figura 1.2 - Resumo esquemático dos resultados obtidos nesse trabalho de doutorado.

Os resultados apresentados nesse trabalho mostraram o uso promissor do método de *casting* contínuo para obtenção de filmes de gelatina com propriedades ópticas, mecânicas e térmicas interessantes para aplicações como embalagens. No entanto, investigações futuras ainda são necessárias para o uso desses materiais. Em relação às embalagens ativas, a investigação quantitativa da atividade antibacteriana ainda é necessária para comprovar a sua eficácia. Além disso, testes de vida-de-prateleira utilizando diferentes alimentos pode ampliar a aplicabilidade desses materiais. Posteriormente, esses filmes ativos também poderão ser produzidos e caracterizados por *casting* contínuo, utilizando os parâmetros para os filmes de gelatina/CNCs aqui descritos. Finalmente, embora todos os componentes usados para na produção dos filmes estudados nesse trabalho sejam sabidamente biodegradáveis, testes de biodegradação e compostagem devem ser realizados para provar sua eficácia.

Extended French Abstract
Résumé Français

Résumé Français

Extended French Abstract

La hausse de la production de plastique a conduit à une crise mondiale de l'élimination des déchets. À présent, les recherches sont concentrées pour résoudre ce problème grâce aux emballages biodégradables. Les biomatériaux, y compris les protéines et polysaccharides, sont les principales ressources naturelles utilisées pour développer les films biodégradables [1].

La gélatine est une protéine dérivée du collagène et soluble dans l'eau, elle est considérée comme l'une des plus abondantes protéines d'origine animale [68] [71]. Cette protéine se trouve dans la peau, les tendons, les os, le cartilage et dans la plupart des organes internes des animaux, et donne un support structural et mécanique. Les chaînes de gélatine sont composées de 18 acides aminés. La glycine (Gly), la proline (Pro) et l'hydroxyproline (Hyp) sont les acides aminés dominants et comptent pour presque deux tiers du total des acides aminés présents. La gélatine a attiré l'attention comme matériel plastique en raison de son abondance, son bas prix, sa biodégradabilité, ses propriétés gélifiantes, son habilité à former des films et sa non-toxicité en contact avec des aliments.

Les films à base de gélatine peuvent être composés d'une variété de matières premières, dont les tissus d'origine animale sont les plus utilisés [88], [89], [90]. Les propriétés physico-chimiques des films à base de gélatine dépendent de la source de gélatine, de la production du film (comprenant la concentration de gélatine, le solvant, le pH, la température, le séchage) et du type/concentration des additifs (plastifiant, charges renforçantes, agents de réticulation).

En général, les films à base de gélatine sont incolores, transparents, avec d'excellentes propriétés barrières contre la lumière UV. Par ailleurs, la gélatine présente d'excellentes propriétés barrières au dioxyde de carbone et à l'oxygène grâce à son caractère hydrophile [115]. Cependant, son caractère hygroscopique est considéré comme le principal inconvénient lorsqu'elle est utilisée pour les emballages, puisque les films sont sensibles à l'humidité et présentent des propriétés mécaniques et barrières faibles dans des conditions d'haute humidité

relative [87]. Cependant, ces inconvénients peuvent être maîtrisés par l'incorporation de nanoparticules renforçantes, comme par exemple, les nanocristaux de cellulose (CNCs), dans la matrice de gélatine [3,9–12].

Les CNCs sont des domaines cristallins extraits à partir de différentes sources naturelles, dont le bois, les plantes, les microorganismes et les animaux contenant de la cellulose. Les CNCs sont biodégradables, ils présentent un rapport longueur/diamètre élevé (environ 10-70), une faible densité (1,5-1,6 g/cm³), un faible coefficient de dilatation thermique et ils forment des films transparents [13,138,139]. De plus, les dimensions bien définies des CNCs et leur taux de cristallinité élevé (70-90 %) conduisent à d'excellentes propriétés mécaniques, comme une grande rigidité axiale (environ 150 GPa), un module de Young élevé (20-50 GPa) [19] et une résistance à la traction d'environ 7 GPa [16].

Par ailleurs, la surface des CNCs peut être modifiée grâce à la réactivité du groupe hydroxyle, ce qui rend les CNCs versatiles pour diverses possibilités de fonctionnalisation des surfaces. Cette caractéristique permet une augmentation des applications spécifiques des CNCs pour le développement des nanomatériaux haute performance avec applications diverses [169].

Concernant la mise en forme des films polymères pour les emballages, la plupart des études sont concentrées sur les techniques par extrusion, injection ou moulage par compression à chaud, en raison de la technologie bien définie pour les polymères à base du pétrole [23]. Cependant, l'utilisation de ces techniques appliquées aux polymères naturels, comme les protéines, sont considérées un vrai défi à cause de l'instabilité thermique de ces macromolécules.

Récemment, une méthode de *casting* continue a été proposée pour la production des films à base de biopolymères à l'échelle pilote. La production des films par *casting* continue est réalisée dans une ligne de *casting*. Dans ce processus, des solutions filmogènes sont disposées en continu sur un substrat mobile, par exemple polyester ou papier couché, avec une lame dont la hauteur est ajustée en fonction de l'épaisseur désirée. Ensuite, le substrat recouvert par la solution passe par une étape de pré-séchage par chauffage infrarouge puis par des

chambres de séchage. À la fin, le film sec est roulé alors qu'il est encore adhérent au substrat [194].

L'approche de la méthode de *casting* continue peut être considérée comme un élargissement du processus par *casting* traditionnel (normalement réalisé sur une paillasse de laboratoire). L'avantage principal du *casting* continue se compose du fait que cette méthode demande un temps de séchage plus court, grâce à l'utilisation du chauffage infrarouge dans la phase de pré-séchage, des températures plus élevées et une circulation d'air intense. D'autres avantages du *casting* continu sont le contrôle de l'épaisseur du film, l'absence d'additifs de traitement, l'utilisation de solutions/dispersions aqueuses et, la nécessité de moins d'espace et de personnel.

Dans ce contexte, les objectifs de ce travail de doctorat sont :

- i. Chercher les paramètres rhéologiques nécessaires pour la production des films à base de gélatine/CNCs à l'échelle pilote en utilisant la méthode de *casting* continu.
- ii. Caractériser les propriétés morphologiques, thermiques, mécaniques et barrières des films à base de gélatine/CNCs obtenus par la méthode de *casting* continue.
- iii. Fonctionnaliser la surface des CNCs par des actifs naturels et obtenir des films actifs à base de gélatine et CNCs fonctionnalisés.

Pour atteindre ces objectifs, une collaboration avec des spécialistes de la production et de la fonctionnalisation de nanocelluloses du Laboratoire de Génie des Procédés Papetiers (France) et des spécialistes de la production de films à base de sources naturelles à Embrapa Instrumentation (Brésil) a été développé au cours de ces quatre années de thèse. Ce doctorat s'est déroulé, par conséquent, dans un contexte dynamique et interdisciplinaire.

Les résultats obtenus pendant la préparation de cette thèse ont été organisés en quatre chapitres. Le **Chapitre I** présente une revue de la littérature et décrit le contexte et les objectifs de cette thèse, avec un intérêt particulier pour l'utilisation potentielle de la gélatine et des nanocristaux de cellulose (CNC) dans le domaine

des emballages écologiques. De plus, une méthodologie de mise en forme des films biodégradables et biosourcés à une échelle pilote est décrite.

Le **Chapitre II** décrit les propriétés rhéologiques des solutions filmogènes pour préparer les films (SF) à base de gélatine/CNCs en utilisant la méthode de *casting* continue. Cette étude est essentielle pour évaluer la capacité de lamination et déterminer la composition la plus appropriée pour la production des films en continu. Toutes les solutions analysées présentent un comportement pseudoplastique avec le taux de cisaillement appliqué (Figure 1.1). Ce comportement est considéré comme le plus convenable pour la production des films par la méthode de *casting* continu, une fois que les doivent posséder une faible viscosité lorsqu'un cisaillement est appliqué. Cette caractéristique permet d'assurer un écoulement approprié en dessous de la lame. Une haute viscosité dans les basses fréquences de cisaillement qui sont générées après le couteau d'écoulement est nécessaire pour minimiser l'écoulement non désiré et des effets de sédimentation.

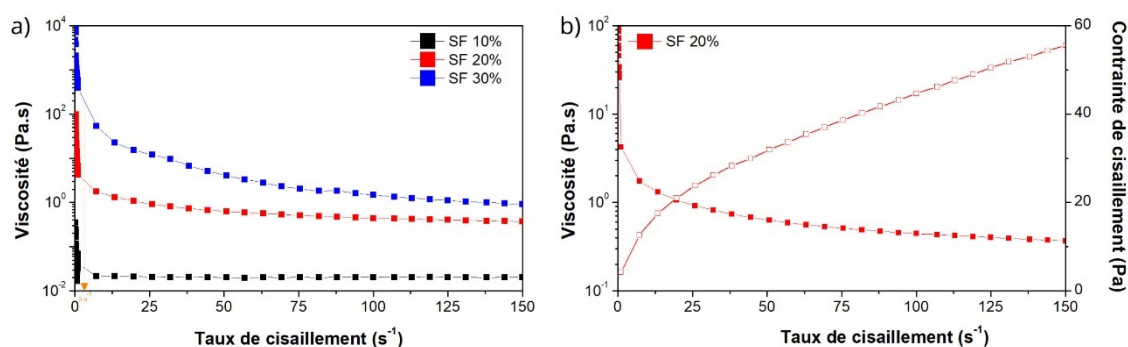


Figure 1.1 – Viscosité en fonction du taux de cisaillement pour (a) SF avec différentes concentrations de gélatine et (b) viscosité et contrainte de cisaillement en fonction du taux de cisaillement pour SF 20 %.

Généralement, les films à base de gélatine produits par la méthode de *casting* traditionnel utilisent SF avec une concentration massique de 10 % maximum de gélatine. Toutefois, cette concentration n'est pas appropriée pour la production des films de manière continue. En effet, les suspensions étudiées présentent une faible viscosité (0,4 Pa.s) ce qui a favorisé l'écoulement des solutions filmogènes

en dehors du substrat avant la lamination. D'autre part, les SF préparées avec 30 % de gélatine présentent des viscosités élevées au point où la formation d'une lame humide n'est pas possible résultant en la formation de films discontinus. Les préparées avec 20 % en masse de gélatine présentent une viscosité autour de 100 Pa.s et des propriétés d'écoulement appropriées à une lamination adaptée au moule. Par la suite, cette formulation a été choisie pour évaluer l'influence des CNCs dans les propriétés physiques des films à base de gélatine/CNC obtenus par *casting* continue.

La production de films à base de gélatine/CNCs par *casting* continu est de 12 mètres de matériel par heure. La radiation infrarouge et la température élevée utilisées dans cette méthode aboutissent à une forte interaction intermoléculaire et un à un effondrement structural, ce qui conduit à la formation de films de haute densité. Les films à base de gélatine préparés avec une concentration de 4,0 % de CNCs obtenus par *casting* continu présentent une perméabilité à la vapeur d'eau (PVE) réduite de 50 % comparé au film obtenu par *casting* traditionnel, une haute résistance à la traction (36 MPa) et un haut module d'élasticité (1,8 GPa). La méthode *casting* continu présente des avantages par rapport la méthode de *casting* traditionnel. Elle a permis d'augmenter l'échelle de production et la performance du film à base de gélatine, ce qui fait de la méthode de *casting* continu une alternative viable à la méthode traditionnelle.

Le **Chapitre III** présente l'étude de l'influence du pH sur les propriétés physiques des films de gélatine/CNCs avec différentes concentrations de CNCs. Les interactions entre les CNCs et la gélatine en suspension ont été étudiées par le potentiel ζ dans les conditions acide (pH 3), basique (pH 8) et au point isoélectrique de la gélatine (pI, pH 6). Une attraction électrostatique est observée à pH 3, alors qu'une répulsion est observée à pH 8, ce qui augmente la viscosité des solutions dans les deux situations. La PVE a été réduite de 68 % (pH 3) et de 39 % (pI) après l'addition de CNCs (0,5 % en masse) dans les films. D'autre part, la formation des coacervats complexes est observée avec l'addition de 5,0 % de CNCs dans une suspension acidifiée (pH 3). Ces coacervats contribuent à réduire les propriétés mécaniques et augmenter la PVE des films.

A pH supérieur au pl de la gélatine, la formation des structures en triple hélice augmente, ce qui est notamment la clé pour augmenter de 152 % les valeurs du module d'élasticité et de 56 % la résistance à la traction des films préparés avec une concentration de 0,5 % de CNCs. D'autre part, l'augmentation de la température de séchage des films a un impact contraire dans la formation des structures en triple hélice et, par conséquent, dans les propriétés physiques des films. Ces découvertes peuvent être explorées et les propriétés physiques des films à base de gélatine/CNCs adaptées dans différentes applications, y compris des emballages flexibles pour l'industrie alimentaire.

La première partie du **Chapitre IV** décrit la fonctionnalisation et la caractérisation de la surface des CNCs avec la rosine (r-CNCs) et des films à base de gélatine/r-CNCs. Les films (0,5 – 6 % de r-CNCs) obtenus par *casting* traditionnel, sont transparents et montrent des propriétés barrières aux rayons UVA (95 %) et UVB (59 %) élevées. Ces valeurs barrières sont plus élevées que celles normalement trouvées dans les emballages plastiques les plus utilisés. Les films à base de gélatine/r-CNCs démontrent une PVE modérée (0,09 g mm/m² h kPa), une résistance à la traction (40 MPa) et un module d'élasticité (1,9 GPa) élevés. Les nanocelluloses greffées (r-CNCs) peuvent inhiber la croissance des *Staphylococcus aureus* et *Escherichia coli*. Cet effet est observé même si la r-CNCs est ajoutée aux films, comme démontré par la preuve de concept de la prévention des dégradations microbiennes des fromages du genre mozzarella. Ces résultats suggèrent que l'incorporation de r-CNCs en faible quantité comme agents actifs dans les films à base de gélatine peut être appropriée pour la production des matériaux antimicrobiens pour des applications dans le domaine des emballages.

Finalement, la deuxième partie du **Chapitre IV** décrit les effets de l'acide tannique non oxydé (TA), de l'acide tannique oxydé (OTA) et des CNCs sur les propriétés physiques, antioxydantes et antimicrobiennes des films à base de gélatine. La technique de QCM-D et les mesures de rhéologie ont confirmé l'interaction de la gélatine avec le TA et la formation de liaisons d'hydrogène entre les CNCs et la gélatine. L'effet de réticulation a réduit de 17 % dans les films à base de gélatine préparés avec TA comparé aux films préparés avec OTA, ce qui résulte en une

augmentation de 52 % de la capacité antioxydante de ces films. Cela a également permis la disponibilité de la gélatine pour interagir avec les CNCs et, par conséquent, augmenter de manière significative la viscosité (410 %) et la stabilité mécanique (G' 1697 %) des films.

De plus, l'addition de CNC (6 %) aux films à base de gélatine-TA a conduit à la formation de matériaux plus denses avec une porosité réduite, observée par les images de microscopie électronique à balayage (MEB). Les films présentent une PVE réduite (67 %) et une résistance à la traction plus élevée (79 %). Les films à base de gélatine-TA-CNCs ont aussi démontré un effet inhibiteur à la croissance de *Staphylococcus aureus* et *Escherichia coli*.

La figure 1.2 présente un résumé schématique de toutes les étapes développées dans ce travail, ainsi que les résultats les plus pertinents de chacune d'elles.

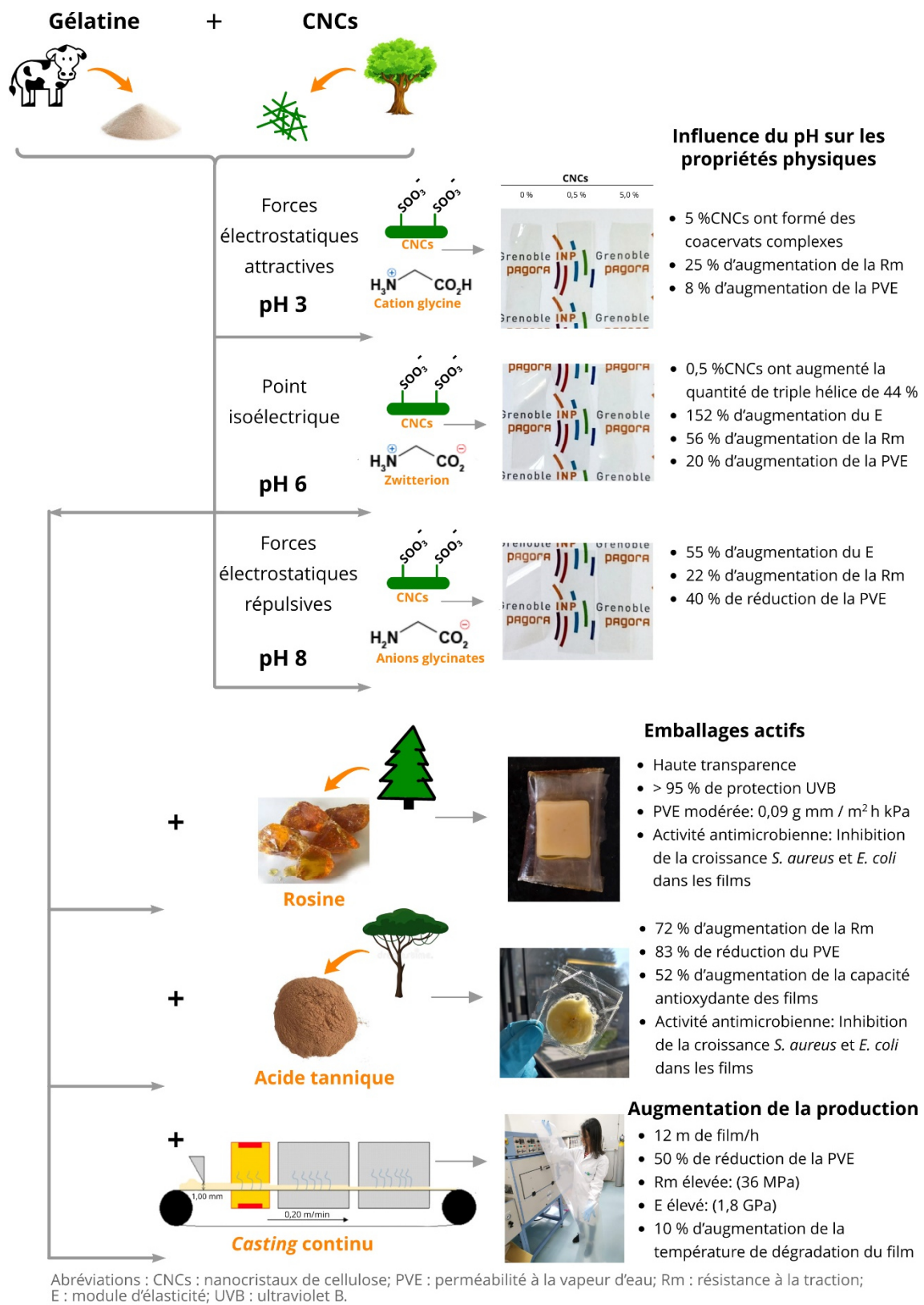


Figure 1.2 - Résumé schématique de tous les plus pertinents résultats et étapes développées dans ce travail.

Les résultats de ce travail ont montré que l'utilisation de la méthode de *casting* continue pour l'obtention des films à base de gélatine avec propriétés optiques, mécaniques et thermiques d'intérêt est prometteuse pour le développement des emballages. Cependant, des études supplémentaires sont encore nécessaires pour l'utilisation de ces matériaux. Concernant les emballages actifs, des études quantitatives de l'activité antibactérienne sont essentielles pour prouver son efficacité. De plus, des tests de durée de vie en utilisant des aliments différents peuvent étendre l'application de ces films. Des films actifs pourront ensuite être produits et caractérisés par *casting* continu, en utilisant les paramètres pour les films à base de gélatine/CNCs décrit dans ce travail. Enfin, malgré que tous les composants utilisés dans l'obtention des films étudiés au cours de ce projet soient reconnus comme des produits biodégradables, des tests de biodégradation et compostage sont nécessaires pour prouver leur efficacité.

REFERENCES

- [1] ESTEGHLAL, S.; NIAKOUSARI, M.; HOSSEINI, S. M. H. Physical and mechanical properties of gelatin-CMC composite films under the influence of electrostatic interactions. **International Journal of Biological Macromolecules**, v. 114, p. 1–9, Jul. 2018.
- [2] AL-TAYYAR, N. A.; YOUSSEF, A. M.; AL-HINDI, R. Antimicrobial food packaging based on sustainable Bio-based materials for reducing foodborne Pathogens: A review. **Food Chemistry**, v. 310, n. December 2019, p. 125915, Apr. 2020.
- [3] MOUSTAFA, H. et al. Eco-friendly polymer composites for green packaging: Future vision and challenges. **Composites Part B: Engineering**, v. 172, n. October 2018, p. 16–25, Sep. 2019.
- [4] LIU, X. et al. Chemical mapping analysis of compatibility in gelatin and hydroxypropyl methylcellulose blend films. **Food Hydrocolloids**, v. 104, n. December 2019, p. 105734, Jul. 2020.
- [5] WANG, Z. et al. The effects of ultrasonic/microwave assisted treatment on the water vapor barrier properties of soybean protein isolate-based oleic acid/stearic acid blend edible films. **Food Hydrocolloids**, v. 35, p. 51–58, 2014.
- [6] GÓMEZ-GUILLÉN, M. C. et al. Fish gelatin: a renewable material for developing active biodegradable films. **Trends in Food Science & Technology**, v. 20, n. 1, p. 3–16, Jan. 2009.
- [7] AZEREDO, H. M. C.; ROSA, M. F.; MATTOSO, L. H. C. Nanocellulose in bio-based food packaging applications. **Industrial Crops and Products**, v. 97, p. 664–671, Mar. 2017.
- [8] SIQUEIRA, G.; BRAS, J.; DUFRESNE, A. Cellulosic Bionanocomposites: A Review of Preparation, Properties and Applications. **Polymers**, v. 2, n. 4, p. 728–765, 13 Dec. 2010.
- [9] HOSSEINI, S. F.; GÓMEZ-GUILLÉN, M. C. A state-of-the-art review on the elaboration of fish gelatin as bioactive packaging: Special emphasis on nanotechnology-based approaches. **Trends in Food Science & Technology**, v. 79, n. July, p. 125–135, Sep. 2018.
- [10] AZEREDO, H. M. C. DE. Nanocomposites for food packaging applications.

Food Research International, v. 42, n. 9, p. 1240–1253, Nov. 2009.

[11] SQUINCA, P. et al. Nanocellulose production in future biorefineries: an integrated approach using tailor-made enzymes Nanocellulose production in future biorefineries : an integrated approach using tailor-made enzymes. **ACS Sustainable Chemistry & Engineering**, v. 8, n. 5, p. 2277–2286, 2020.

[12] THOMAS, B. et al. Nanocellulose, a versatile green platform: from biosources to materials and their applications. **Chemical reviews**, v. 118, n. 24, p. 11575–11625, 2018.

[13] HABIBI, Y.; LUCIA, L. A.; ROJAS, O. J. Cellulose Nanocrystals: Chemistry, Self-Assembly, and Applications. **Chemical Reviews**, v. 110, n. 6, p. 3479–3500, 9 Jun. 2010.

[14] DUFRESNE, A. Polysaccharide nanocrystal reinforced nanocomposites. **Canadian Journal Chemistry**, v. 86, p. 484–494, 2008.

[15] ZHUANG, C.; TAO, F.; CUI, Y. Eco-friendly biorefractory films of gelatin and TEMPO-oxidized cellulose ester for food packaging application. **Journal of the Science of Food and Agriculture**, v. 97, n. 10, p. 3384–3395, 2017.

[16] SUKYAI, P. et al. Effect of cellulose nanocrystals from sugarcane bagasse on whey protein isolate-based films. **Food Research International**, v. 107, n. February, p. 528–535, 2018.

[17] GEORGE, J.; SIDDARAMAIAH. High performance edible nanocomposite films containing bacterial cellulose nanocrystals. **Carbohydrate Polymers**, v. 87, n. 3, p. 2031–2037, Feb. 2012.

[18] LEITE, L. S. F. et al. Scaled-up production of gelatin-cellulose nanocrystal bionanocomposite films by continuous casting. **Carbohydrate Polymers**, v. 238, n. March, p. 116198, Jun. 2020.

[19] GARS, M. LE et al. Polymerization of glycidyl methacrylate from the surface of cellulose nanocrystals for the elaboration of PLA-based nanocomposites. **Carbohydrate Polymers**, v. 234, n. November 2019, p. 115899, Apr. 2020.

[20] TANG, J. et al. Functionalization of cellulose nanocrystals for advanced applications. **Journal of Colloid and Interface Science**, v. 494, p. 397–409, May 2017.

[21] ESPINO-PÉREZ, E. et al. Cellulose nanocrystal surface functionalization for

the controlled sorption of water and organic vapours. **Cellulose**, v. 23, n. 5, p. 2955–2970, 2016.

[22] KWAK, H. W. et al. Chemical and physical reinforcement of hydrophilic gelatin film with di-aldehyde nanocellulose. **International Journal of Biological Macromolecules**, v. 146, p. 332–342, Mar. 2020.

[23] REDDY, M. M. et al. Biobased plastics and bionanocomposites: Current status and future opportunities. **Progress in Polymer Science**, v. 38, n. 10–11, p. 1653–1689, Oct. 2013.

[24] ROBERTSON, G. L. History of food packaging. In: **Reference Module in Food Science**. Brisbane: Elsevier, 2019. p. 1–49.

[25] SMITH, J. P. Food packaging — Principles and practice. **Food Research International**, v. 26, n. 3, p. 233–234, Jan. 1993.

[26] LACKHART, H. E. A paradigm for packaging. **Packaging Technology and Science**, v. 10, p. 237–252, 1997.

[27] ANON. **Glossary of packaging terms**. Stamford, Connecticut: The packaging institute international, 1988.

[28] GUILLARD, V. et al. The Next Generation of Sustainable Food Packaging to Preserve Our Environment in a Circular Economy Context. **Frontiers in Nutrition**, v. 5, n. December, p. 1–13, 2018.

[29] YOUSSEF, A. M.; EL-SAYED, S. M. Bionanocomposites materials for food packaging applications: Concepts and future outlook. **Carbohydrate Polymers**, v. 193, n. February, p. 19–27, 2018.

[30] RHIM, J.-W.; PARK, H.-M.; HA, C.-S. Bio-nanocomposites for food packaging applications. **Progress in Polymer Science**, v. 38, n. 10–11, p. 1629–1652, Oct. 2013.

[31] BEITZEN-HEINEKE, E. F.; BALTA-OZKAN, N.; REEFKE, H. The prospects of zero-packaging grocery stores to improve the social and environmental impacts of the food supply chain. **Journal of Cleaner Production**, v. 140, n. February 2018, p. 1528–1541, Jan. 2017.

[32] HLPE. Food Losses and Waste in the Context of Sustainable Food Systems. **Hlpe Report**, n. June, p. 1–6, 2014.

[33] RIO+20, C. N. DE O. **Rio+20 conferência das Nações Unidas sobre**

- desenvolvimento sustentável.** Disponível em: <http://www.rio20.gov.br/sobre_a_rio_mais_20.html>. Acesso em: 14 aug. 2020.
- [34] EUROPEAN COMMISSION. **EU actions against food waste.** Disponível em: <https://ec.europa.eu/food/safety/food_waste/eu_actions_en>. Acesso em: 14 aug. 2020.
- [35] KOLTZENBURG, S. **Polymer chemistry.** [s.l.: s.n.].
- [36] GARDSIDE, M. **Global plastic production from 1950 to 2018 (in million metric tons).** Disponível em: <<https://www.statista.com/statistics/282732/global-production-of-plastics-since-1950/>>. Acesso em: 14 aug. 2020.
- [37] TAJEDDIN, B.; ARABKHEDRI, M. **Polymers and food packaging.** [s.l.] INC, 2020.
- [38] KIRWAN, M. J.; PLANT, S.; STRAWBRIDGE, J. W. **Plastics in Food Packaging.** In: **Food and Beverage Packaging Technology.** Oxford, UK: Wiley-Blackwell, 2011. p. 157–212.
- [39] PAYNE, A. **Key Debates in New Political Economy.** [s.l.] Routledge, 2006.
- [40] FERRARO, G.; FAILLER, P. Governing plastic pollution in the oceans: Institutional challenges and areas for action. **Environmental Science & Policy**, v. 112, n. April, p. 453–460, Oct. 2020.
- [41] UNEP. **Addressing Land-Based Pollution.** Disponível em: <<https://www.unenvironment.org/explore-topics/oceans-seas/what-we-do/addressing-land-based-pollution>>. Acesso em: 13 aug. 2020.
- [42] ROBAINA, M. et al. Circular economy in plastic waste - Efficiency analysis of European countries. **Science of The Total Environment**, v. 730, p. 139038, Aug. 2020.
- [43] EUROSTAT. **How much plastic packaging waste do we recycle?** Disponível em: <<https://ec.europa.eu/eurostat/web/products-eurostat-news/-/DDN-20191105-2>>. Acesso em: 14 aug. 2020.
- [44] WIT, W. DE et al. **Solucionar a poluição plástica: Transparência e responsabilização** WWF: Fundo Mundial para a Natureza. [s.l.: s.n.]. Disponível em: <https://jornalismosocioambiental.files.wordpress.com/2019/03/plastic_report_02-2019.pdf>.

- [45] THOMPSON, R. C. et al. Plastics, the environment and human health: current consensus and future trends. **Philosophical Transactions of the Royal Society B: Biological Sciences**, v. 364, n. 1526, p. 2153–2166, 27 Jul. 2009.
- [46] SIRACUSA, V. Food packaging permeability behaviour: A report. **International Journal of Polymer Science**, v. 2012, n. i, 2012.
- [47] FIGURA, L. O.; TEIXEIRA, A. A. **Food physics: physical properties - measurement and application**. 1 st ed ed. Berlin: Springer, 2007.
- [48] WANG, J. et al. Moisture and Oxygen Barrier Properties of Cellulose Nanomaterial-Based Films. **ACS Sustainable Chemistry and Engineering**, v. 6, n. 1, p. 49–70, 2018.
- [49] CLARKE, D. et al. Incorporation of commercially-derived antimicrobials into gelatin-based films and assessment of their antimicrobial activity and impact on physical film properties. **Food Control**, v. 64, p. 202–211, Jun. 2016.
- [50] BIDEAU, B. et al. Polypyrrole/nanocellulose composite for food preservation: Barrier and antioxidant characterization. **Food Packaging and Shelf Life**, v. 12, p. 1–8, 2017.
- [51] SCHMID, M. **Whey protein based barrier coatings**. Forum Wissenschaft TWB. **Anais...**2012
- [52] RAHMAN, R.; PUTRA, S. Z. F. S. **Tensile properties of natural and synthetic fiber-reinforced polymer composites**. [s.l.] Elsevier Ltd, 2018.
- [53] SHIKU, Y.; HAMAGUCHI, P. Y.; TANAKA, M. Effect of pH on the preparation of edible films based on fish myofibrillar proteins. **Fisheries science**, v. 69, p. 1026–1032, 2003.
- [54] KWON, S. et al. A Short Review of Light Barrier Materials for Food and Beverage Packaging. **Korean Journal of packaging and Science and Technology**, v. 24, n. 3, p. 141–148, 31 Dec. 2018.
- [55] HAN, J. W. et al. Food Packaging: A Comprehensive Review and Future Trends. **Comprehensive Reviews in Food Science and Food Safety**, v. 17, n. 4, p. 860–877, 2018.
- [56] E.V., E. B. **European bioplastics**. Disponível em: <<http://www.european-bioplastics.org/>>. Acesso em: 17 aug. 2020.
- [57] VERT, M. et al. Terminology for biorelated polymers and applications (IUPAC

Recommendations 2012). **Pure and Applied Chemistry**, v. 84, n. 2, p. 377–410, 11 Jan. 2012.

[58] KALE, G. et al. Compostability of Bioplastic Packaging Materials: An Overview. **Macromolecular Bioscience**, v. 7, n. 3, p. 255–277, 8 Mar. 2007.

[59] LICCIARDELLO, F.; PIERGIOVANNI, L. Packaging and food sustainability. In: **The Interaction of Food Industry and Environment**. [s.l.] Elsevier, 2021. p. 191–222.

[60] VROMAN, I.; TIGHZERT, L. Biodegradable Polymers. **Materials**, v. 2, n. 2, p. 307–344, 1 Apr. 2009.

[61] FALGUERA, V. et al. Edible films and coatings: Structures, active functions and trends in their use. **Trends in Food Science and Technology**, v. 22, n. 6, p. 292–303, 2011.

[62] MOHAMED, S. A. A.; EL-SAKHAWY, M.; EL-SAKHAWY, M. A.-M. Polysaccharides, Protein and Lipid-Based Natural Edible Films in Food Packaging: A Review. **Carbohydrate Polymers**, v. 238, n. March, p. 116178, Jun. 2020.

[63] PEELMAN, N. et al. Application of bioplastics for food packaging. **Trends in Food Science and Technology**, v. 32, n. 2, p. 128–141, 2013.

[64] RAMOS, M. et al. **Gelatin-based films and coatings for food packaging applications**. [s.l.] Elsevier, 2016. v. 6

[65] LUMDUBWONG, N. **Applications of Starch-Based Films in Food Packaging**. [s.l.] Elsevier, 2019.

[66] SILVA, N. H. C. S. et al. Protein-based materials: from sources to innovative sustainable materials for biomedical applications. **Journal of Materials Chemistry B**, v. 2, n. 24, p. 3715–3740, 2014.

[67] SILVA, N. H. C. S. et al. Protein-based materials: from sources to innovative sustainable materials for biomedical applications. **Journal of Materials Chemistry B**, v. 2, n. 24, p. 3715, 2014.

[68] CUQ, B.; GONTARD, N.; GUILBERT, S. Proteins as Agricultural Polymers for Packaging Production. **Cereal Chemistry Journal**, v. 75, n. 1, p. 1–9, Jan. 1998.

[69] ZHANG, L.; ZENG, M. Proteins as Sources of Materials. **Proteins as**

Sources of Materials, p. 479–493, [s.d.].

[70] CALVA-ESTRADA, S. J.; JIMÉNEZ-FERNÁNDEZ, M.; LUGO-CERVANTES, E. Protein-Based Films: Advances in the Development of Biomaterials Applicable to Food Packaging. **Food Engineering Reviews**, v. 11, n. 2, p. 78–92, 18 Jun. 2019.

[71] SHANKAR, S.; JAISWAL, L.; RHIM, J.-W. Gelatin-based nanocomposite films. In: **Antimicrobial Food Packaging**. [s.l.] Elsevier, 2016. p. 339–348.

[72] HARRINGTON, W. F.; HIPPEL, P. H. VON. The Structure Of Collagen And Gelatin. In: **Advances in Protein Chemistry**. [s.l.: s.n.]. v. 16p. 1–138.

[73] NUNES, Y. L. **Preparação E Caracterização De Bioblendas Poliméricas a Partir De Gelatina Bovina E De Tilápia Com Amido De Milho**. 2014. 1–113 f. Universidade Federal do Rio Grande do Norte. 2014.

[74] CAMPIGLIO, C. E. et al. Cross-linking strategies for electrospun gelatin scaffolds. **Materials**, v. 12, n. 15, 2019.

[75] HUANG, T. et al. Fish gelatin modifications: A comprehensive review. **Trends in Food Science & Technology**, v. 86, n. August 2018, p. 260–269, Apr. 2019.

[76] ABEDINIA, A. et al. Extraction and characterization of gelatin from the feet of Pekin duck (*Anas platyrhynchos domestica*) as affected by acid, alkaline, and enzyme pretreatment. **International Journal of Biological Macromolecules**, v. 98, p. 586–594, 2017.

[77] ZHOU, P.; MULVANEY, S. J.; REGENSTEIN, J. M. Properties of Alaska pollock skin gelatin: A comparison with tilapia and pork skin gelatins. **Journal of Food Science**, v. 71, n. 6, 2006.

[78] SARABIA, A. I.; GÓMEZ-GUILLÉN, M. C.; MONTERO, P. The effect of added salts on the viscoelastic properties of fish skin gelatin. **Food Chemistry**, v. 70, n. 1, p. 71–76, 2000.

[79] GOMEZ-GUILLEN, M. C. et al. Functional and bioactive properties of collagen and gelatin from alternative sources: A review. **Food Hydrocolloids**, v. 25, n. 8, p. 1813–1827, 2011.

[80] AHMED, J. Rheological Properties of Gelatin and Advances in Measurement. In: **Advances in Food Rheology and Its Applications**. [s.l.]

Elsevier, 2017. p. 377–404.

[81] KEMPKA, A. P. et al. Influence of bloom number and plastifiers on gelatin matrices produced for enzyme immobilization. **Brazilian Journal of Chemical Engineering**, v. 31, n. 1, p. 95–108, Mar. 2014.

[82] OSORIO, F. A. et al. Effects of concentration, bloom degree, and pH on gelatin melting and gelling temperatures using small amplitude oscillatory rheology. **International Journal of Food Properties**, v. 10, n. 4, p. 841–851, 2007.

[83] AGROPECUÁRIO, P. DO C. **Brasil inicia exportação de gelatina**. Disponível em: <https://www.agrolink.com.br/noticias/brasil-inicia-exportacao-de-gelatina_29770.html>. Acesso em: 29 aug. 2020.

[84] MORDOR INTELLIGENCE MARKET RESEARCH COMPANY. **Food grade gelatin market - growth, trends, and forecasts (2020-2025)**. Disponível em: <<https://www.mordorintelligence.com/industry-reports/food-grade-gelatin-market>>. Acesso em: 29 aug. 2020.

[85] GRAND VIEW RESEARCH. **Gelatin Market Size, Share & Trends Analysis Report By Raw Material (Pig Skin, Bovine Hides, Cattle Bones), By Function (Thickener, Stabilizer, Gelling Agent), By Application, By Region, And Segment Forecasts, 2020 - 2027**. Disponível em: <<https://www.grandviewresearch.com/industry-analysis/gelatin-market-analysis>>. Acesso em: 29 aug. 2020.

[86] VIEIRA, M. G. A. et al. Natural-based plasticizers and biopolymer films: A review. **European Polymer Journal**, v. 47, n. 3, p. 254–263, 2011.

[87] SUDERMAN, N.; ISA, M. I. N.; SARBON, N. M. The effect of plasticizers on the functional properties of biodegradable gelatin-based film: A review. **Food Bioscience**, v. 24, n. June, p. 111–119, 2018.

[88] K, J. et al. Fabrication of cationized gelatin nanofibers by electrospinning for tissue regeneration. **RSC Adv.**, v. 5, n. 109, p. 89521–89530, 2015.

[89] HANANI, Z. A. N.; YEE, F. C.; NOR-KHAIZURA, M. A. R. Effect of pomegranate (*Punica granatum* L.) peel powder on the antioxidant and antimicrobial properties of fish gelatin films as active packaging. **Food Hydrocolloids**, v. 89, n. October 2018, p. 253–259, Apr. 2019.

- [90] QUERO, F. et al. Stress transfer and matrix-cohesive fracture mechanism in microfibrillated cellulose-gelatin nanocomposite films. **Carbohydrate Polymers**, v. 195, n. January, p. 89–98, 2018.
- [91] CHIOU, B. et al. Effects of drying temperature on barrier and mechanical properties of cold-water fish gelatin films. **Journal of Food Engineering**, v. 95, n. 2, p. 327–331, Nov. 2009.
- [92] FAKHOURI, F. M. et al. Edible films and coatings based on starch/gelatin: Film properties and effect of coatings on quality of refrigerated Red Crimson grapes. **Postharvest Biology and Technology**, v. 109, p. 57–64, 2015.
- [93] MOHAJER, S.; REZAEI, M.; HOSSEINI, S. F. Physico-chemical and microstructural properties of fish gelatin/agar bio-based blend films. **Carbohydrate Polymers**, v. 157, p. 784–793, 2017.
- [94] NAGARAJAN, M. et al. Characteristics of bio-nanocomposite films from tilapia skin gelatin incorporated with hydrophilic and hydrophobic nanoclays. **Journal of Food Engineering**, v. 143, p. 195–204, Dec. 2014.
- [95] FLAKER, C. H. C. et al. Gelatin-based nanocomposite films: A study on montmorillonite dispersion methods and concentration. **Journal of Food Engineering**, v. 167, p. 65–70, Dec. 2015.
- [96] CHUAYNUKUL, K. et al. Comparative Characterization of Bovine and Fish Gelatin Films Fabricated by Compression Molding and Solution Casting Methods. **Journal of Polymers and the Environment**, v. 26, n. 3, p. 1239–1252, 16 Mar. 2018.
- [97] TAO, F.; SHI, C.; CUI, Y. Preparation and physicochemistry properties of smart edible films based on gelatin–starch nanoparticles. **Journal of the Science of Food and Agriculture**, v. 98, n. 14, p. 5470–5478, 2018.
- [98] URANGA, J. et al. Cross-linking of fish gelatins to develop sustainable films with enhanced properties. **European Polymer Journal**, v. 78, p. 82–90, May 2016.
- [99] IAHNKE, A. O. E S. et al. Gelatin capsule residue-based films crosslinked with the natural agent genipin. **Packaging Technology and Science**, v. 33, n. 1, p. 15–26, 3 Jan. 2020.
- [100] SANTOS, J. P. et al. Crosslinking agents effect on gelatins from carp and

tilapia skins and in their biopolymeric films. **Colloids and Surfaces A: Physicochemical and Engineering Aspects**, v. 539, p. 184–191, Feb. 2018.

[101] LIN, J. et al. The modification of gelatin films: Based on various cross-linking mechanism of glutaraldehyde at acidic and alkaline conditions. **Food Science & Nutrition**, v. 7, n. 12, p. 4140–4146, 19 Dec. 2019.

[102] MENEZES, M. DO L. L. R. et al. Effect of tannic acid as crosslinking agent on fish skin gelatin-silver nanocomposite film. **Food Packaging and Shelf Life**, v. 19, n. March 2018, p. 7–15, 2019.

[103] VOON, H. C. et al. Effect of Addition of Halloysite Nanoclay and SiO₂ Nanoparticles on Barrier and Mechanical Properties of Bovine Gelatin Films. **Food and Bioprocess Technology**, v. 5, n. 5, p. 1766–1774, 12 Jul. 2012.

[104] MARVIZADEH, M. M. et al. Preparation and characterization of bionanocomposite film based on tapioca starch/bovine gelatin/nanorod zinc oxide. **International Journal of Biological Macromolecules**, v. 99, p. 1–7, 2017.

[105] MUSSO, Y. S.; SALGADO, P. R.; MAURI, A. N. Smart edible films based on gelatin and curcumin. **Food Hydrocolloids**, v. 66, p. 8–15, 2017.

[106] JANG, S.-A.; LIM, G.-O.; SONG, K. BIN. Original article: Use of nano-clay (Cloisite Na⁺) improves tensile strength and vapour permeability in agar rich red algae (*Gelidium corneum*)-gelatin composite films. **International Journal of Food Science & Technology**, v. 45, n. 9, p. 1883–1888, Sep. 2010.

[107] HOSSEINI, S. F. et al. Preparation and functional properties of fish gelatin–chitosan blend edible films. **Food Chemistry**, v. 136, n. 3–4, p. 1490–1495, Feb. 2013.

[108] ZHANG, X. et al. Chemical modification of gelatin by a natural phenolic cross-linker, tannic acid. **Journal of Agricultural and Food Chemistry**, v. 58, n. 11, p. 6809–6815, 9 Jun. 2010.

[109] HALIM, A. L. A.; KAMARI, A.; PHILLIP, E. Chitosan, gelatin and methylcellulose films incorporated with tannic acid for food packaging. **International Journal of Biological Macromolecules**, v. 120, p. 1119–1126, Dec. 2018.

[110] KAVOOSI, G. et al. Antioxidant and Antibacterial Properties of Gelatin Films

Incorporated with Carvacrol. **Journal of Food Safety**, v. 33, n. 4, p. 423–432, Nov. 2013.

[111] SAHRAEE, S. et al. Effect of corn oil on physical, thermal, and antifungal properties of gelatin-based nanocomposite films containing nano chitin. **LWT - Food Science and Technology**, v. 76, p. 33–39, Mar. 2017.

[112] PELISSARI, F. M. et al. **Starch-based edible films and coatings: An eco-friendly alternative for food packaging**. [s.l.] Elsevier Inc., 2018.

[113] KAEWPRACHU, P. et al. Properties of fish myofibrillar protein film incorporated with catechin-Kradon extract. **Food Packaging and Shelf Life**, v. 13, n. August, p. 56–65, 2017.

[114] KAEWPRACHU, P. et al. Biodegradable Protein-based Films and Their Properties: A Comparative Study. **Packaging Technology and Science**, v. 29, n. 2, p. 77–90, Feb. 2016.

[115] AVENA-BUSTILLOS, R. J. et al. Gelation, oxygen permeability, and mechanical properties of mammalian and fish gelatin films. **Journal of Food Science**, v. 76, n. 7, p. 519–524, 2011.

[116] CAO, N.; FU, Y.; HE, J. Preparation and physical properties of soy protein isolate and gelatin composite films. **Food Hydrocolloids**, v. 21, n. 7, p. 1153–1162, 2007.

[117] MUHOZA, B.; XIA, S.; ZHANG, X. Gelatin and high methyl pectin coacervates crosslinked with tannic acid: The characterization, rheological properties, and application for peppermint oil microencapsulation. **Food Hydrocolloids**, v. 97, n. June, p. 105174, 2019.

[118] KUIJPERS, A. J. et al. Cross-linking and characterisation of gelatin matrices for biomedical applications. **Journal of Biomaterials Science, Polymer Edition**, v. 11, n. 3, p. 225–243, 2 Jan. 2000.

[119] SUNG, H.-W. et al. Evaluation of gelatin hydrogel crosslinked with various crosslinking agents as bioadhesives: In vitro study. **Journal of Biomedical Materials Research**, v. 46, n. 4, p. 520–530, 15 Sep. 1999.

[120] OKSMAN, K. et al. Manufacturing process of cellulose whiskers/poly(lactic acid) nanocomposites. **Composites Science and Technology**, v. 66, n. 15, p. 2776–2784, 2006.

- [121] URRUZOLA, I. et al. Nanopaper from almond (*Prunus dulcis*) shell. **Cellulose**, v. 21, p. 1619–1629, 2014.
- [122] PAYEN, A. Comptes rendus de l'academie des sciences serie lii - science de la vie. **Life Science**, v. 7, p. 1052, 1838.
- [123] HAWORTH, W. N.; HIRST, E. L.; THOMAS, H. A. The existence of the cellobiose residue in cellulose. **Nature**, v. 126, p. 438, 1930.
- [124] MOON, R. J. et al. Cellulose nanomaterials review: structure, properties and nanocomposites. **Chemical Society Reviews**, v. 40, n. 7, p. 3941–3994, Jul. 2011.
- [125] MARIANO, M.; KISSI, N. EL; DUFRESNE, A. Cellulose nanocrystals and related nanocomposites: Review of some properties and challenges. **Journal of Polymer Science, Part B: Polymer Physics**, v. 52, n. 12, p. 791–806, 2014.
- [126] RÅNBY, B. G.; RIBI, E. Über den feinaufbau der zellulose. **Experienta**, v. 6, p. 12–14, 1950.
- [127] TAIPINA, M. O.; FAVARO, M. M.; GONÇALVES, M. C. Morphological evolution of curauá fibers under acid hydrolysis. **Cellulose**, v. 19, n. 4, p. 1199–1207, 8 May 2012.
- [128] TAIPINA, M. O. et al. Surface modification of cotton nanocrystals with a silane agent. **Cellulose**, v. 20, n. 1, p. 217–226, 11 Nov. 2012.
- [129] YANG, Z.-Y. et al. **The transparency and mechanical properties of cellulose acetate nanocomposites using cellulose nanowhiskers as fillers** **Cellulose**, 17 Oct. 2013. Disponível em: <<http://www.springerlink.com/index/10.1007/s10570-012-9796-z>>. Acesso em: 14 mar. 2013
- [130] SOUZA LIMA, M. M. DE; BORSALI, R. Rodlike Cellulose Microcrystals: Structure, Properties, and Applications. **Macromolecular Rapid Communications**, v. 25, n. 7, p. 771–787, Apr. 2004.
- [131] LU, P.; HSIEH, Y. LO. Preparation and properties of cellulose nanocrystals: Rods, spheres, and network. **Carbohydrate Polymers**, v. 82, n. 2, p. 329–336, 2010.
- [132] DUFRESNE, A. Nanocellulose: a new ageless bionanomaterial. **Materials Today**, v. 16, n. 6, p. 220–227, Jun. 2013.

- [133] DUFRESNE, A. Cellulose nanomaterials as green nanoreinforcements for polymer nanocomposites. **Philosophical Transactions of the Royal Society A: Mathematical, Physical and Engineering Sciences**, v. 376, n. 2112, p. 20170040, 13 Feb. 2018.
- [134] ARAKI, J. et al. Flow properties of microcrystalline cellulose suspension prepared by acid treatment of native cellulose. **Colloids and Surfaces A: Physicochemical and Engineering Aspects**, v. 142, n. 1, p. 75–82, Nov. 1998.
- [135] ESPINOSA, S. C. et al. Isolation of thermally stable cellulose nanocrystals by phosphoric acid hydrolysis. **Biomacromolecules**, v. 14, n. 4, p. 1223–1230, 8 Apr. 2013.
- [136] SADEGHIFAR, H. et al. Production of cellulose nanocrystals using hydrobromic acid and click reactions on their surface. **Journal of Materials Science**, v. 46, n. 22, p. 7344–7355, 2011.
- [137] REID, M. S.; VILLALOBOS, M.; CRANSTON, E. D. Benchmarking cellulose nanocrystals: from the laboratory to industrial production. **Langmuir**, v. 33, n. 7, p. 1583–1598, 2017.
- [138] HUBER, T. et al. A critical review of all-cellulose composites. **Journal of Materials Science**, v. 47, n. 3, p. 1171–1186, 21 Jul. 2011.
- [139] LAGERWALL, J. P. F. et al. Cellulose nanocrystal-based materials: from liquid crystal self-assembly and glass formation to multifunctional thin films. **NPG Asia Materials**, v. 6, n. 1, p. e80–e80, 10 Jan. 2014.
- [140] PANDEY, J. K.; NAKAGAITO, A. N.; TAKAGI, H. Fabrication and applications of cellulose nanoparticle-based polymer composites. **Polymer Engineering and Science**, v. 53, n. 1, p. 1–8, 2013.
- [141] ZHANG, Y. P.; KIRK, V. P. C. A. G.; ANDREWS, M. P. Nanocrystalline cellulose for covert optical encryption. **Journal of Nanophotonics**, v. 6, n. 1, p. 063516, 2012.
- [142] HOENG, F.; DENNEULIN, A.; BRAS, J. Use of nanocellulose in printed electronics: A review. **Nanoscale**, v. 8, n. 27, p. 13131–13154, 2016.
- [143] CARPENTER, A. W.; LANNOY, C. F. DE; WIESNER, M. R. Cellulose nanomaterials in water treatment technologies. **Environmental Science and Technology**, v. 49, n. 9, p. 5277–5287, 2015.

- [144] ZHOU, C. et al. Electrospun bio-nanocomposite scaffolds for bone tissue engineering by cellulose nanocrystals reinforcing maleic anhydride grafted PLA. **ACS Applied Materials and Interfaces**, v. 5, n. 9, p. 3847–3854, 2013.
- [145] RAFIEIAN, F. et al. Mechanical, thermal and barrier properties of nano-biocomposite based on gluten and carboxylated cellulose nanocrystals. **Industrial Crops and Products**, v. 53, p. 282–288, 2014.
- [146] CRIADO, P. et al. Cellulose Nanocrystals in Food Packaging. In: **Reference Module in Food Science**. [s.l.] Elsevier, 2019. p. 1–13.
- [147] HALPIN, J. C.; KARDOS, J. L. Moduli of crystalline polymers employing composite theory. **Journal of Applied Physics**, v. 43, n. 5, p. 2235–2241, 1972.
- [148] SAMIR, A. S. A.; ALLOIN, F.; DUFRESNE, A. Review of recent research into cellulosic whiskers, their properties and their application in nanocomposite field. **Biomacromolecules**, v. 6, n. 2, p. 612–626, 2005.
- [149] FERREIRA, F. V. et al. Cellulose nanocrystal-based poly(butylene adipate-co-terephthalate) nanocomposites covered with antimicrobial silver thin films. **Polymer Engineering & Science**, v. 59, n. s2, p. pen.25066, 6 Feb. 2019.
- [150] GOFFIN, A. L. et al. Poly(ϵ -caprolactone) based nanocomposites reinforced by surface-grafted cellulose nanowhiskers via extrusion processing: Morphology, rheology, and thermo-mechanical properties. **Polymer**, v. 52, n. 7, p. 1532–1538, 2011.
- [151] LIN, N.; BRUZZESE, C.; DUFRESNE, A. TEMPO-Oxidized Nanocellulose Participating as Crosslinking Aid for Alginate-Based Sponges. **ACS Applied Materials & Interfaces**, v. 4, n. 9, p. 4948–4959, 26 Sep. 2012.
- [152] WEI, L.; MCDONALD, A. G.; STARK, N. M. Grafting of Bacterial Polyhydroxybutyrate (PHB) onto Cellulose via In Situ Reactive Extrusion with Dicumyl Peroxide. **Biomacromolecules**, v. 16, n. 3, p. 1040–1049, 2015.
- [153] VUILLEMIN, M. E. et al. Gum Arabic and chitosan self-assembly: Thermodynamic and mechanism aspects. **Food Hydrocolloids**, v. 96, n. May, p. 463–474, 2019.
- [154] KOFINAS, P.; COHEN, R. E.; HALASA, A. F. Gas permeability of polyethylene/poly(ethylene-propylene) semicrystalline diblock copolymers. **Polymer**, v. 35, n. 6, p. 1229–1235, 1994.

- [155] GARCÍA, M. et al. Hybrid organic inorganic nylon-6/SiO₂ nanocomposites: Transport properties. **Polymer Engineering & Science**, v. 44, n. 7, p. 1240–1246, Jul. 2004.
- [156] DUFRESNE, A. **Nanocellulose: From nature to high performance tailored materials**. second ed. ed. Berlin: De Gruyter, 2012.
- [157] LUZI, F. et al. Production and characterization of PLA_PBS biodegradable blends reinforced with cellulose nanocrystals extracted from hemp fibres. **Industrial Crops and Products**, v. 93, p. 276–289, 2016.
- [158] LI, F. et al. Tunable green oxygen barrier through layer-by-layer self-assembly of chitosan and cellulose nanocrystals. **Carbohydrate Polymers**, v. 92, n. 2, p. 2128–2134, 2013.
- [159] HERRERA, M. A.; MATHEW, A. P.; OKSMAN, K. Gas permeability and selectivity of cellulose nanocrystals films (layers) deposited by spin coating. **Carbohydrate Polymers**, v. 112, p. 494–501, 2014.
- [160] SILVA, A. P. M. et al. Mango kernel starch films as affected by starch nanocrystals and cellulose nanocrystals. **Carbohydrate Polymers**, v. 211, p. 209–216, May 2019.
- [161] PEREIRA, P. H. F. et al. Wheat straw hemicelluloses added with cellulose nanocrystals and citric acid. Effect on film physical properties. **Carbohydrate Polymers**, v. 164, p. 317–324, 2017.
- [162] KUMAR, R. et al. Effect of nano-cellulosic fiber on mechanical and barrier properties of polylactic acid (PLA) green nanocomposite film. **Materials Research Express**, v. 6, n. 12, p. 125108, 22 Nov. 2019.
- [163] PARALIKAR, S. A.; SIMONSEN, J.; LOMBARDI, J. Poly(vinyl alcohol)/cellulose nanocrystal barrier membranes. **Journal of Membrane Science**, v. 320, n. 1–2, p. 248–258, Jul. 2008.
- [164] ALVES, J. S. et al. Effect of cellulose nanocrystals and gelatin in corn starch plasticized films. **Carbohydrate Polymers**, v. 115, p. 215–222, Jan. 2015.
- [165] SANTOS, T. M. et al. Fish gelatin films as affected by cellulose whiskers and sonication. **Food Hydrocolloids**, v. 41, p. 113–118, Dec. 2014.
- [166] MONDRAGON, G. et al. Bionanocomposites based on gelatin matrix and nanocellulose. **European Polymer Journal**, v. 62, p. 1–9, Jan. 2015.

[167] YANG, S.; LI, H.; SUN, H. Preparation of gelatin-based films modified with nanocrystalline cellulose. **Iranian Polymer Journal (English Edition)**, v. 27, n. 9, p. 645–652, 2018.

[168] KARGARZADEH, H. et al. **Advances in cellulose nanomaterials**. [s.l.] Springer Netherlands, 2018. v. 25

[169] HABIBI, Y. Key advances in the chemical modification of nanocelluloses. **Chemical Society Reviews**, v. 43, n. 5, p. 1519–1542, 2014.

[170] TAIPINA, M. DE O. **Nanocristais de celulose: obtenção, caracterização e modificação de superfície**. 2012. 1–89 f. Universidade Estadual de Campinas. 2012.

[171] GOUSSE, C. et al. Stable suspensions of partially silylated cellulose whiskers dispersed in organic solvents. **Polymer**, v. 43, p. 2645–2651, 2002.

[172] SIQUEIRA, G.; MATHEW, A. P.; OKSMAN, K. Processing of cellulose nanowhiskers/cellulose acetate butyrate nanocomposites using sol–gel process to facilitate dispersion. **Composites Science and Technology**, v. 71, n. 16, p. 1886–1892, Nov. 2011.

[173] SIQUEIRA, G.; BRAS, J.; DUFRESNE, A. New Process of Chemical Grafting of Cellulose Nanoparticles with a Long Chain Isocyanate. **Langmuir**, v. 26, n. 1, p. 402–411, 5 Jan. 2010.

[174] JEAN, B. et al. Structural details of cellulose nanocrystals/polyelectrolytes multilayers probed by neutron reflectivity and AFM. **Langmuir**, v. 24, n. 7, p. 3452–3458, Apr. 2008.

[175] SOBKOWICZ, M. J.; BRAUN, B.; DORGAN, J. R. Decorating in green: surface esterification of carbon and cellulosic nanoparticles. **Green Chemistry**, v. 11, n. 5, p. 680, 2009.

[176] SASSI, J.-F.; CHANZY, H. Ultrastructural aspects of the acetylation of cellulose. **Cellulose**, v. 2, n. 2, p. 111–127, 1995.

[177] MISSOUM, K. et al. Nanofibrillated cellulose surface grafting in ionic liquid. **Soft Matter**, v. 8, n. 32, p. 8338, 2012.

[178] HATTON, F. L. et al. Xyloglucan-Functional Latex Particles via RAFT-Mediated Emulsion Polymerization for the Biomimetic Modification of Cellulose. **Biomacromolecules**, v. 17, n. 4, p. 1414–1424, 2016.

- [179] KEDZIOR, S. A. et al. Recent advances and an industrial perspective of cellulose nanocrystal functionalization through polymer grafting. **Current Opinion in Solid State and Materials Science**, v. 23, n. 2, p. 74–91, Apr. 2019.
- [180] YILDIRIM, S. et al. Active Packaging Applications for Food. **Comprehensive Reviews in Food Science and Food Safety**, v. 17, n. 1, p. 165–199, 2018.
- [181] BRAS, J.; SAINI, S. Nanocellulose in functional packaging. In: **Cellulose-Reinforced Nanofibre Composites**. [s.l.] Elsevier, 2017. v. 12p. 175–213.
- [182] SHARMA, R.; JAFARI, S. M.; SHARMA, S. Antimicrobial bio-nanocomposites and their potential applications in food packaging. **Food Control**, v. 112, n. September 2019, p. 107086, Jun. 2020.
- [183] VILARINHO, F. et al. Nanocellulose in green food packaging. **Critical Reviews in Food Science and Nutrition**, v. 58, n. 9, p. 1526–1537, 13 Jun. 2018.
- [184] DOBRE, L. M. et al. Modelling of sorbic acid diffusion through bacterial cellulose-based antimicrobial films. **Chemical Papers**, v. 66, n. 2, p. 144–151, 2012.
- [185] KHAN, A. et al. Mechanical and barrier properties of nanocrystalline cellulose reinforced chitosan based nanocomposite films. **Carbohydrate Polymers**, v. 90, n. 4, p. 1601–1608, 2012.
- [186] LI, J. et al. Nanocellulose-Based Antibacterial Materials. **Advanced Healthcare Materials**, v. 7, n. 20, p. 1800334, Oct. 2018.
- [187] VENTURA, C. et al. **On the toxicity of cellulose nanocrystals and nanofibrils in animal and cellular models**. [s.l.: s.n.]. v. 27
- [188] ROMAN, M. Toxicity of Cellulose Nanocrystals: A Review. **Industrial Biotechnology**, v. 11, n. 1, p. 25–33, Feb. 2015.
- [189] HARPER, B. J. et al. Impacts of chemical modification on the toxicity of diverse nanocellulose materials to developing zebrafish. **Cellulose**, v. 23, n. 3, p. 1763–1775, 2016.
- [190] KRISHNA, M.; NINDO, C. I.; MIN, S. C. Development of fish gelatin edible films using extrusion and compression molding. **Journal of Food Engineering**, v. 108, n. 2, p. 337–344, 2012.

- [191] SALGADO, P. R. et al. Edible films and coatings containing bioactives. **Current Opinion in Food Science**, v. 5, p. 86–92, 2015.
- [192] KOSHY, R. R. et al. Environment friendly green composites based on soy protein isolate – A review. **Food Hydrocolloids**, v. 50, p. 174–192, Aug. 2015.
- [193] MORAES, J. O. DE et al. Scale-up of the production of cassava starch based films using tape-casting. **Journal of Food Engineering**, v. 119, n. 4, p. 800–808, 2013.
- [194] OTONI, C. G. et al. Recent Advances on Edible Films Based on Fruits and Vegetables-A Review. **Comprehensive Reviews in Food Science and Food Safety**, v. 16, n. 5, p. 1151–1169, Sep. 2017.
- [195] SUHAG, R. et al. Film formation and deposition methods of edible coating on food products: A review. **Food Research International**, v. 136, n. July, p. 109582, Oct. 2020.
- [196] DU, W. X. et al. Antibacterial activity against E. coli O157:H7, physical properties, and storage stability of novel carvacrol-containing edible tomato films. **Journal of Food Science**, v. 73, n. 7, 2008.
- [197] DU, W. X. et al. Storage stability and antibacterial activity against Escherichia coli O157:H7 of carvacrol in edible apple films made by two different casting methods. **Journal of Agricultural and Food Chemistry**, v. 56, n. 9, p. 3082–3088, 2008.
- [198] MUNHOZ, D. R. et al. Sustainable Production and in vitro Biodegradability of Edible Films from Yellow Passion Fruit Coproducts via Continuous Casting. **ACS Sustainable Chemistry and Engineering**, v. 6, n. 8, p. 9883–9892, 2018.
- [199] SHIT, S. C.; SHAH, P. M. Edible polymers: challenges and opportunities. **Journal of Polymers**, v. 2014, p. 1–13, 2014.
- [200] BHOWMIK, S. et al. Reinforcement of gelatin-based nanofilled polymer biocomposite by crystalline cellulose from cotton for advanced wound dressing applications. **Polymers**, v. 9, n. 12, p. 222, 13 Jun. 2017.
- [201] GONZÁLEZ, A.; ALVAREZ IGARZABAL, C. I. Nanocrystal-reinforced soy protein films and their application as active packaging. **Food Hydrocolloids**, v. 43, p. 777–784, Jan. 2015.
- [202] CASTRO, R. J. S. DE et al. Whey protein as a key component in food

systems: Physicochemical properties, production technologies and applications.

Food Structure, v. 14, n. April, p. 17–29, Oct. 2017.

[203] NOORBAKSH-SOLTANI, S. M.; ZERAFAT, M. M.; SABBAGHI, S. A comparative study of gelatin and starch-based nano-composite films modified by nano-cellulose and chitosan for food packaging applications. **Carbohydrate Polymers**, v. 189, p. 48–55, Jun. 2018.

[204] ORTIZ, C. M. et al. Scale-up of the production of soy (*Glycine max* L.) protein films using tape casting: Formulation of film-forming suspension and drying conditions. **Food Hydrocolloids**, v. 66, p. 110–117, May 2017.

[205] GENNADIOS, A. et al. Mechanical and barrier properties of egg albumen films. **Journal of Food Science**, v. 61, n. 3, p. 585–589, May 1996.

[206] HAN, J. H.; FLOROS, J. D. Casting antimicrobial packaging films and measuring their physical properties and antimicrobial activity. **Journal of Plastic Film & Sheeting**, v. 13, n. 4, p. 287–298, 19 Oct. 1997.

[207] TONOLI, G. H. D. et al. Cellulose micro/nanofibres from Eucalyptus kraft pulp: preparation and properties. **Carbohydrate Polymers**, v. 89, n. 1, p. 80–88, Jun. 2012.

[208] ANIL KUMAR ANAL (ED.). **Food Processing By-Products and their Utilization**. New York, United States: John Wiley & Sons Inc, 2017.

[209] CORRÊA, A. C. et al. Cellulose nanofibers from curaua fibers. **Cellulose**, v. 17, n. 6, p. 1183–1192, 22 Dec. 2010.

[210] QIAO, C. et al. Structure and rheological properties of cellulose nanocrystals suspension. **Food Hydrocolloids**, v. 55, p. 19–25, Apr. 2016.

[211] LI, Y. et al. Investigation on complex coacervation between fish skin gelatin from cold-water fish and gum arabic: Phase behavior, thermodynamic, and structural properties. **Food Research International**, v. 107, n. 1, p. 596–604, May 2018.

[212] NING, N. et al. Enhanced electromechanical performance of bio-based gelatin/glycerin dielectric elastomer by cellulose nanocrystals. **Carbohydrate Polymers**, v. 130, p. 262–267, Oct. 2015.

[213] FADEL, S. M.; HASSAN, M. L.; OKSMAN, K. Improving tensile strength and moisture barrier properties of gelatin using microfibrillated cellulose. **Journal**

of Composite Materials, v. 47, n. 16, p. 1977–1985, 13 Jul. 2013.

[214] PASCHOALICK, T. M. et al. Characterization of some functional properties of edible films based on muscle proteins of Nile Tilapia. **Food Hydrocolloids**, v. 17, n. 4, p. 419–427, Jul. 2003.

[215] CHIOU, B.-S. et al. Cold water fish gelatin films: Effects of cross-linking on thermal, mechanical, barrier, and biodegradation properties. **European Polymer Journal**, v. 44, n. 11, p. 3748–3753, Nov. 2008.

[216] BAGHERIASL, D. et al. Shear rheology of polylactide (PLA)–cellulose nanocrystal (CNC) nanocomposites. **Cellulose**, v. 23, n. 3, p. 1885–1897, 21 Jun. 2016.

[217] LIU, P. et al. Rheological properties of soy protein isolate solution for fibers and films. **Food Hydrocolloids**, v. 64, p. 149–156, Mar. 2017.

[218] WANG, W. et al. Mechanical reinforcement of gelatin hydrogel with nanofiber cellulose as a function of percolation concentration. **International Journal of Biological Macromolecules**, v. 103, p. 226–233, Oct. 2017.

[219] MUKHERJEE, I.; ROSOLEN, M. Thermal transitions of gelatin evaluated using DSC sample pans of various seal integrities. **Journal of Thermal Analysis and Calorimetry**, v. 114, n. 3, p. 1161–1166, 23 Dec. 2013.

[220] CHING, Y. C. et al. Rheological properties of cellulose nanocrystal-embedded polymer composites: a review. **Cellulose**, v. 23, n. 2, p. 1011–1030, 12 Apr. 2016.

[221] YADAV, M.; CHIU, F. Cellulose nanocrystals reinforced κ-carrageenan based UV resistant transparent bionanocomposite films for sustainable packaging applications. **Carbohydrate Polymers**, v. 211, p. 181–194, May 2019.

[222] YU, Z. et al. Development of multifunctional nanocomposites containing cellulose nanofibrils and soy proteins as food packaging materials. **Food Packaging and Shelf Life**, v. 21, p. 100366, Sep. 2019.

[223] SHANKAR, S.; WANG, L.-F.; RHIM, J.-W. Effect of melanin nanoparticles on the mechanical, water vapor barrier, and antioxidant properties of gelatin-based films for food packaging application. **Food Packaging and Shelf Life**, v. 21, n. April, p. 100363, Sep. 2019.

[224] LEITE, L. S. F. et al. Morphological investigation of cellulose

acetate/cellulose nanocrystal composites obtained by melt extrusion. **Journal of Applied Polymer Science**, v. 133, n. 44, p. 1–10, 20 Nov. 2016.

[225] SCHMITT, C.; ABERKANE, L.; SANCHEZ, C. Protein–polysaccharide complexes and coacervates. In: **Handbook of Hydrocolloids**. [s.l.] Elsevier, 2009. v. 12p. 420–476.

[226] CAO, Y. et al. The relationship between cellulose nanocrystal dispersion and strength. **Construction and Building Materials**, v. 119, p. 71–79, 2016.

[227] OKSMAN, K. et al. Review of the recent developments in cellulose nanocomposite processing. **Composites Part A: Applied Science and Manufacturing**, v. 83, p. 2–18, Apr. 2016.

[228] KHOSHKAVA, V.; KAMAL, M. R. Effect of drying conditions on cellulose nanocrystal (CNC) agglomerate porosity and dispersibility in polymer nanocomposites. **Powder Technology**, v. 261, p. 288–298, Jul. 2014.

[229] SEGAL, L. et al. An Empirical Method for Estimating the Degree of Crystallinity of Native Cellulose Using the X-Ray Diffractometer. **Textil Research Journal**, v. 29, n. 10, p. 786–794, 1959.

[230] DÍAZ-CALDERÓN, P. et al. Influence of extraction variables on the structure and physical properties of salmon gelatin. **Food Hydrocolloids**, v. 71, p. 118–128, Oct. 2017.

[231] DEEPA, B. et al. Nanofibrils vs nanocrystals bio-nanocomposites based on sodium alginate matrix: An improved-performance study. **Heliyon**, v. 6, n. 2, 2020.

[232] LECORRE, D. et al. All starch nanocomposite coating for barrier material. **Journal of Applied Polymer Science**, v. 131, n. 3, p. 1–7, 2014.

[233] SALGADO, P. R. et al. Biodegradable sunflower protein films naturally activated with antioxidant compounds. **Food Hydrocolloids**, v. 24, n. 5, p. 525–533, 2010.

[234] FAVIER, V. et al. Mechanical Percolation in Cellulose Whisker. **Polymer Engineering and Science**, v. 37, n. 10, p. 1732–1739, 1997.

[235] BIGI, A.; PANZAVOLTA, S.; RUBINNI, K. Relationship between triple-helix content and mechanical properties of gelatin films. **Biomaterials**, v. 25, n. 25, p. 5675–5680, Nov. 2004.

- [236] BADII, F. et al. The Effect of Drying Temperature on Physical Properties of Thin Gelatin Films. **Drying Technology**, v. 32, n. 1, p. 30–38, 2 Jan. 2014.
- [237] YAKIMETS, I. et al. Mechanical properties with respect to water content of gelatin films in glassy state. **Polymer**, v. 46, n. 26, p. 12577–12585, 2005.
- [238] LEITE, L. S. F. et al. Morphological investigation of cellulose acetate/cellulose nanocrystal composites obtained by melt extrusion. **Journal of Applied Polymer Science**, v. 133, n. 44, 20 Nov. 2016.
- [239] SLAVUTSKY, A. M.; BERTUZZI, M. A. Water barrier properties of starch films reinforced with cellulose nanocrystals obtained from sugarcane bagasse. **Carbohydrate Polymers**, v. 110, p. 53–61, 2014.
- [240] FERNÁNDEZ-PAN, I. et al. Effect of drying conditions on the mechanical and barrier properties of films based on Chitosan. **Drying Technology**, v. 28, n. 12, p. 1350–1358, 2010.
- [241] CHEN, Y. et al. Superhydrophobic coatings on gelatin-based films: Fabrication, characterization and cytotoxicity studies. **RSC Advances**, v. 8, n. 42, p. 23712–23719, 2018.
- [242] SYAHIDA, N. et al. Effects of palm wax on the physical, mechanical and water barrier properties of fish gelatin films for food packaging application. **Food Packaging and Shelf Life**, v. 23, n. November 2019, p. 100437, 2020.
- [243] BIAŁOPIOTROWICZ, T.; JAŃCZUK, B. The changes of the surface free energy of the adsorptive gelatin films. **European Polymer Journal**, v. 37, n. 5, p. 1047–1051, May 2001.
- [244] DERKACH, S. R. et al. Polyelectrolyte Polysaccharide–Gelatin Complexes: Rheology and Structure. **Polymers**, v. 12, n. 2, p. 266, 26 Jan. 2020.
- [245] ZHAO, L.; SKWARCZYNSKI, M.; TOTH, I. Polyelectrolyte-based platforms for the delivery of peptides and proteins. **ACS Biomaterials Science & Engineering**, v. 5, n. 10, p. 4937–4950, 14 Oct. 2019.
- [246] SILVA, C. E. P. DA et al. Physical chemical study of zein and arabinogalactans or glucuronomannans polyelectrolyte complexes and their film-forming properties. **Food Hydrocolloids**, v. 100, n. September 2019, p. 105394, Mar. 2020.
- [247] HOSSEINI, S. F. et al. Fabrication of bio-nanocomposite films based on fish

gelatin reinforced with chitosan nanoparticles. **Food Hydrocolloids**, v. 44, p. 172–182, Feb. 2015.

[248] JOSHI, N.; RAWAT, K.; BOHIDAR, H. B. pH and ionic strength induced complex coacervation of Pectin and Gelatin A. **Food Hydrocolloids**, v. 74, p. 132–138, Jan. 2018.

[249] GIOFFRÈ, M. et al. Role of pH on stability and mechanical properties of gelatin films. **Journal of Bioactive and Compatible Polymers**, v. 27, n. 1, p. 67–77, 18 Jan. 2012.

[250] HOSSEINI, S. F.; GÓMEZ-GUILLÉN, M. C. A state-of-the-art review on the elaboration of fish gelatin as bioactive packaging: Special emphasis on nanotechnology-based approaches. **Trends in Food Science & Technology**, v. 79, n. January 2017, p. 125–135, Sep. 2018.

[251] LIN, L.; GU, Y.; CUI, H. Moringa oil/chitosan nanoparticles embedded gelatin nanofibers for food packaging against *Listeria monocytogenes* and *Staphylococcus aureus* on cheese. **Food Packaging and Shelf Life**, v. 19, n. November 2018, p. 86–93, 2019.

[252] BEHROUZAIN, F.; RAZAVI, S. M. A.; JOYNER, H. Mechanisms of whey protein isolate interaction with basil seed gum: Influence of pH and protein-polysaccharide ratio. **Carbohydrate Polymers**, v. 232, n. December 2019, p. 115775, Mar. 2020.

[253] VORON'KO, N. G. et al. The chitosan-gelatin (bio)polyelectrolyte complexes formation in an acidic medium. **Carbohydrate Polymers**, v. 138, p. 265–272, 2016.

[254] RAZZAK, M. A.; KIM, M.; CHUNG, D. Elucidation of aqueous interactions between fish gelatin and sodium alginate. **Carbohydrate Polymers**, v. 148, p. 181–188, 2016.

[255] BEHROUZAIN, F.; RAZAVI, S. M. A. Steady shear rheological properties of emerging hydrocolloids. In: **Emerging Natural Hydrocolloids**. Chichester, UK: John Wiley & Sons, Ltd, 2018. p. 81–100.

[256] JORGE, M. F. C. et al. Viscoelastic and rheological properties of nanocomposite-forming solutions based on gelatin and montmorillonite. **Journal of Food Engineering**, v. 120, p. 81–87, Jan. 2014.

[257] ALEXANDRE, E. M. C. et al. Gelatin-based films reinforced with montmorillonite and activated with nanoemulsion of ginger essential oil for food packaging applications. **Food Packaging and Shelf Life**, v. 10, p. 87–96, Dec. 2016.

[258] AHSAN, S. M.; RAO, C. M. Structural studies on aqueous gelatin solutions: Implications in designing a thermo-responsive nanoparticulate formulation. **International Journal of Biological Macromolecules**, v. 95, p. 1126–1134, Feb. 2017.

[259] CELEBI, H.; KURT, A. Effects of processing on the properties of chitosan/cellulose nanocrystal films. **Carbohydrate Polymers**, v. 133, p. 284–293, Nov. 2015.

[260] GENNADIOS, A. et al. Effect of pH on properties of wheat gluten and soy protein isolate films. **Journal of Agricultural and Food Chemistry**, v. 41, n. 11, p. 1835–1839, Nov. 1993.

[261] QIAO, C. et al. Viscosity properties of gelatin in solutions of monovalent and divalent salts. **Korea-Australia Rheology Journal**, v. 25, n. 4, p. 227–231, 24 Nov. 2013.

[262] DÍAZ, O.; CANDIA, D.; COBOS, Á. Whey protein film properties as affected by ultraviolet treatment under alkaline conditions. **International Dairy Journal**, v. 73, p. 84–91, Oct. 2017.

[263] YIN, Y. et al. A preliminary study on chitosan/gelatin polyelectrolyte complex. **Journal of Materials S**, v. 40, p. 4646–4652, 2005.

[264] ALBERTO, M.; GABRIELA, M. Hydrodynamic Properties of Gelatin - Studies from Intrinsic Viscosity Measurements. In: **Products and Applications of Biopolymers**. [s.l.] InTech, 2012. p. 85–116.

[265] SHANKAR, S. et al. Preparation, characterization, and antimicrobial activity of gelatin/ZnO nanocomposite films. **Food Hydrocolloids**, v. 45, p. 264–271, Mar. 2015.

[266] GARAVAND, F. et al. Improving the integrity of natural biopolymer films used in food packaging by crosslinking approach: A review. **International Journal of Biological Macromolecules**, v. 104, p. 687–707, Nov. 2017.

[267] HASSAN, B. et al. Recent advances on polysaccharides, lipids and protein

based edible films and coatings: A review. **International Journal of Biological Macromolecules**, v. 109, p. 1095–1107, Apr. 2018.

[268] SIVAKANTHAN, S. et al. Antioxidant and antimicrobial applications of biopolymers: A review. **Food Research International**, v. 136, n. October 2019, 2020.

[269] GÓMEZ-ESTACA, J. et al. Advances in antioxidant active food packaging. **Trends in Food Science and Technology**, v. 35, n. 1, p. 42–51, 2014.

[270] WANG, J. et al. Decrease of microbial community diversity, biogenic amines formation, and lipid oxidation by phloretin in Atlantic salmon fillets. **Lwt**, v. 101, n. June 2018, p. 419–426, 2019.

[271] ZHENG, Y. et al. Well-defined renewable polymers derived from gum rosin. **Macromolecules communication to the editor**, v. 43, p. 5922–5924, 2010.

[272] KUGLER, S. et al. Advances in rosin-based chemicals: The latest recipes, applications and future trends. **Molecules**, v. 24, n. 9, p. 1651–1703, 2019.

[273] LIU, X.; XIN, W.; ZHANG, J. Rosin-based acid anhydrides as alternatives to petrochemical curing agents. **Green Chemistry**, v. 11, p. 1018–1025, 2009.

[274] NARAYANAN, M. et al. UV protective poly(lactic acid)/rosin films for sustainable packaging. **International Journal of Biological Macromolecules**, v. 99, p. 37–45, 2017.

[275] CASTRO, D. O. DE et al. Surface grafting of cellulose nanocrystals with natural antimicrobial rosin mixture using a green process. **Carbohydrate Polymers**, v. 137, p. 1–8, Feb. 2016.

[276] LI, F. et al. Bifunctional Reinforcement of Green Biopolymer Packaging Nanocomposites with Natural Cellulose Nanocrystal–Rosin Hybrids. **ACS Applied Bio Materials**, v. 3, n. 4, p. 1944–1954, 20 Apr. 2020.

[277] NIU, X. et al. Rosin modified cellulose nanofiber as a reinforcing and co-antimicrobial agents in polylactic acid/chitosan composite film for food packaging. **Carbohydrate Polymers**, v. 183, p. 102–109, Mar. 2018.

[278] PAUDYAL, N. et al. Microbiology prevalence of foodborne pathogens in food from selected African countries – a meta-analysis. **International Journal of Food Microbiology**, v. 249, p. 35–43, 2017.

[279] FERRARIO, C. et al. Microbiology next generation sequencing-based

multigene panel for high throughput detection of food-borne pathogens.

International Journal of Food Microbiology, v. 256, n. May, p. 20–29, 2017.

[280] LY, E. HADJI B. et al. Surface functionalization of cellulose by grafting oligoether chains. **Materials Chemistry and Physics**, v. 120, n. 2–3, p. 438–445, Apr. 2010.

[281] RAMOS, Ó. L. et al. Edible Films and Coatings from Whey Proteins: A Review on Formulation, and on Mechanical and Bioactive Properties. **Critical Reviews in Food Science and Nutrition**, v. 52, n. 6, p. 533–552, Jun. 2012.

[282] OOI, S. Y.; AHMAD, I.; AMIN, M. C. I. M. Cellulose nanocrystals extracted from rice husks as a reinforcing material in gelatin hydrogels for use in controlled drug delivery systems. **Industrial Crops and Products**, v. 93, p. 227–234, 2016.

[283] SANTOS, M. R. E. et al. Recent developments in antimicrobial polymers: A review. **Materials**, v. 9, n. 7, 2016.

[284] AHMAD, M. et al. Physico-mechanical and antimicrobial properties of gelatin film from the skin of unicorn leatherjacket incorporated with essential oils. **Food Hydrocolloids**, v. 28, n. 1, p. 189–199, 2012.

[285] WANG, J. et al. Robust antimicrobial compounds and polymers derived from natural resin acids. **Chemical Communications**, v. 48, n. 6, p. 916–918, 2012.

[286] CAGRI, A.; USTUNOL, Z.; RYSER, E. T. Antimicrobial, mechanical, and moisture barrier properties of low pH whey protein-based edible films containing p-aminobenzoic or sorbic acids. **Journal of Food Science**, v. 66, n. 6, p. 865–870, Aug. 2001.

[287] VILELA, C. et al. A concise guide to active agents for active food packaging. **Trends in Food Science & Technology**, v. 80, n. July, p. 212–222, Oct. 2018.

[288] CHOLLAKUP, R. et al. Antioxidant and antibacterial activities of cassava starch and whey protein blend films containing rambutan peel extract and cinnamon oil for active packaging. **Lwt**, v. 130, n. May, p. 109573, 2020.

[289] ZHANG, X. et al. Plant extracts such as pine nut shell, peanut shell and jujube leaf improved the antioxidant ability and gas permeability of chitosan films. **International Journal of Biological Macromolecules**, v. 148, p. 1242–1250, 2020.

- [290] GÜLÇİN, I. et al. Radical scavenging and antioxidant activity of tannic acid. **Arabian Journal of Chemistry**, v. 3, n. 1, p. 43–53, 2010.
- [291] CHEN, S. C.; CHUNG, K. T. Mutagenicity and antimutagenicity studies of tannic acid and its related compounds. **Food and Chemical Toxicology**, v. 38, n. 1, p. 1–5, 2000.
- [292] GUO, J. et al. Development of tannin-inspired antimicrobial bioadhesives. **Acta Biomaterialia**, v. 72, p. 35–44, 2018.
- [293] AEWSIRI, T. et al. Antioxidative activity and emulsifying properties of cuttlefish skin gelatin-tannic acid complex as influenced by types of interaction. **Innovative Food Science and Emerging Technologies**, v. 11, n. 4, p. 712–720, 2010.
- [294] PARK, K. et al. Developing regulatory property of gelatin-tannic acid multilayer films for coating-based nitric oxide gas delivery system. **Scientific Reports**, v. 9, n. 1, p. 8308, 5 Dec. 2019.
- [295] CHOI, I. et al. Effect of oxidized phenolic compounds on cross-linking and properties of biodegradable active packaging film composed of turmeric and gelatin. **LWT - Food Science and Technology**, v. 93, p. 427–433, Jul. 2018.
- [296] HU, Z. et al. Tuning cellulose nanocrystal gelation with polysaccharides and surfactants. v. 30, p. 2684–2692, 2014.
- [297] BENSELFELT, T. et al. Adsorption of Xyloglucan onto Cellulose Surfaces of Different Morphologies: An Entropy-Driven Process. **Biomacromolecules**, v. 17, n. 9, p. 2801–2811, 2016.
- [298] PICCHIO, M. L. et al. Casein films crosslinked by tannic acid for food packaging applications. **Food Hydrocolloids**, v. 84, n. April, p. 424–434, 2018.
- [299] HU, Z. et al. One-Pot Water-Based Hydrophobic Surface Modification of Cellulose Nanocrystals Using Plant Polyphenols. **ACS Sustainable Chemistry & Engineering**, v. 5, n. 6, p. 5018–5026, 5 Jun. 2017.
- [300] RODAHL, M. et al. Quartz crystal microbalance setup for frequency and Q-factor measurements in gaseous and liquid environments. **Review of Scientific Instruments**, v. 66, n. 7, p. 3924–3930, 1995.
- [301] PALANGE, C. et al. The effect of the dispersion of microfibrillated cellulose on the mechanical properties of melt-compounded polypropylene–polyethylene

copolymer. **Cellulose**, v. 26, n. 18, p. 9645–9659, 2019.

[302] ANVARI, M.; CHUNG, D. Dynamic rheological and structural characterization of fish gelatin – Gum arabic coacervate gels cross-linked by tannic acid. **Food Hydrocolloids**, v. 60, p. 516–524, Oct. 2016.

[303] RIVERO, S.; GARCÍA, M. A.; PINOTTI, A. Crosslinking capacity of tannic acid in plasticized chitosan films. **Carbohydrate Polymers**, v. 82, n. 2, p. 270–276, Sep. 2010.

[304] SANTOS, T. M. et al. Zein films with unoxidized or oxidized tannic acid. **Journal of the Science of Food and Agriculture**, v. 97, n. 13, p. 4580–4587, Oct. 2017.

[305] SUN, B.; ZHANG, M.; NI, Y. Use of sulfated cellulose nanocrystals towards stability enhancement of gelatin-encapsulated tea polyphenols. **Cellulose**, v. 25, n. 9, p. 5157–5173, 3 Sep. 2018.

[306] ORTIZ-ZARAMA, M. A. et al. Rheological characterization of solutions of gelatin with bentonite and tannic acid. **Revista Mexicana de Ingeniera Quimica**, v. 15, n. 3, p. 819–830, 2016.

[307] RUBENTHEREN, V. et al. Physical and chemical reinforcement of chitosan film using nanocrystalline cellulose and tannic acid. **Cellulose**, v. 22, n. 4, p. 2529–2541, 9 Aug. 2015.

[308] PEREDA, M. et al. Polyelectrolyte films based on chitosan/olive oil and reinforced with cellulose nanocrystals. **Carbohydrate Polymers**, v. 101, n. 1, p. 1018–1026, 2014.

[309] DASH, R.; FOSTON, M.; RAGAUSKAS, A. J. Improving the mechanical and thermal properties of gelatin hydrogels cross-linked by cellulose nanowhiskers. **Carbohydrate Polymers**, v. 91, n. 2, p. 638–645, Jan. 2013.

[310] BERTOLO, M. R. V. et al. Rheological and antioxidant properties of chitosan/gelatin-based materials functionalized by pomegranate peel extract. **Carbohydrate Polymers**, v. 228, n. July 2019, p. 115386, 2020.

[311] COLLAZO-BIGLIARDI, S.; ORTEGA-TORO, R.; CHIRALT, A. Improving properties of thermoplastic starch films by incorporating active extracts and cellulose fibres isolated from rice or coffee husk. **Food Packaging and Shelf Life**, v. 22, n. November 2018, 2019.

- [312] RODRIGUES, A. P. H. et al. Control of properties of nanocomposites bio-based collagen and cellulose nanocrystals. **Cellulose**, v. 24, n. 4, p. 1731–1744, 22 Apr. 2017.
- [313] NAZMI, N. N.; ISA, M. I. N.; SARBON, N. M. Preparation and characterization of chicken skin gelatin/CMC composite film as compared to bovine gelatin film. **Food Bioscience**, v. 19, n. July, p. 149–155, 2017.
- [314] CARVALHO, R. A.; GROSSO, C. R. F.; SOBRAL, P. J. A. Effect of chemical treatment on the mechanical properties, water vapour permeability and sorption isotherms of gelatin-based films. **Packaging Technology and Science**, v. 21, n. 3, p. 165–169, Apr. 2008.
- [315] GUIL-GUERRERO, J. L. et al. Antimicrobial activity of plant-food by-products: A review focusing on the tropics. **Livestock Science**, v. 189, p. 32–49, 2016.
- [316] VILLANUEVA, M. E. et al. Chitin nanowhiskers as alternative antimicrobial controlled release carriers. **New Journal of Chemistry**, v. 39, n. 1, p. 614–620, 2015.